NOMENCLATURE FOR PYROLYSIS EXPERIMENTS INVOLVING H_2O

M. D. Lewan
U.S. Geological Survey
Box 25046, MS 977
Denver Federal Center
Denver, CO 80225

The importance of H_2O in laboratory pyrolysis experiments designed to simulate natural processes is well documented in studies of coalification (Berl and Schmidt, 1932; Schuhmacher et al., 1960) and petroleum formation (Jurg and Eisma, 1964; Lewan et al., 1979). Industrial pyrolysis processes also benefit from the presence of H_2O as demonstrated in oil-shale retorting (Gavin, 1922, p. 181), conversion of coal to oil (Fischer, 1925, p. 180), heavy oil upgrading (McCollum and Quick, 1976a and b), and conversion of organic refuse to oil (Appell et al., 1971 and 1975). As experimental work continues to indicate that the phase as well as the presence of H_2O are important in natural and industrial processes, a nomenclature for pyrolysis experiments involving different H_2O phases is needed to improve interlaboratory communication and comparison of results. The following nomenclature is proposed to meet this need.

Hydrous pyrolysis as originally defined by Lewan and others (1979) denotes experiments in which a sample is pyrolyzed in contact with H_2O liquid. This condition best represents subsiding sedimentary basins in which the pores and fractures in sedimentary rocks are usually filled with water. As shown in Figure 1, the upper temperature limit for pure H_2O in this type of pyrolysis is 374°C, but higher temperature limits in excess of 600°C may be obtained by the addition of soluble salts (i.e., NaCl). H_2O in hydrous pyrolysis experiments typically occurs as both liquid and vapor, unless pressure regulators are employed to maintain only a liquid phase. It is important in the vapor/liquid H_2O system to optimize the amount of water used for specific reactor and sample volumes to insure that the sample is completely submerged in the liquid phase during pyrolysis (Lewan, 1993).

Supercritical H_2O pyrolysis denotes experiments in which a sample is pyrolyzed in contact with a supercritical fluid containing more than 50 mole % H_2O. Although the lower temperature limit for pure water in this type of pyrolysis is 374°C, this critical temperature may be lowered below 300°C with the addition of CO_2 to the system (Figure 1). Supercritical H_2O pyrolysis represents deep crustal regimes where metamorphic grades in excess of greenschist facies occur.

Steam pyrolysis is more difficult to define because sedimentary organic matter and its accompanying rock usually generate or liberate minor amounts of H_2O during experiments commonly referred to as **dry** or **anhydrous pyrolysis**. The headspace in these experiments is typically sufficient for the minor amounts of

evolved H_2O to occur as vapor at a partial pressure dictated by the available volume and experimental temperature. As an operational definition, it is suggested that steam pyrolysis denotes experiments in which a sample is pyrolyzed in contact with H_2O vapor at partial pressures in excess of 20 percent of its saturated vapor pressure at experimental temperatures. Steam pyrolysis represents localized near-surface conditions where geothermal vents or subaerial volcanoes are active.

Hydrous, supercritical H_2O, and steam pyrolysis may be collectively referred to as **hydrothermal pyrolysis** or **aquathermolysis** (e.g. Siskin et al., 1990). These collective names are particularly useful for referring to pyrolysis experiments in which insufficient information is given to assess the H_2O phases present or the phase in which a reaction has occurred at experimental conditions.

REFERENCES

Appell, H. R., Fu, Y. C., Illig, E. G., Steffgen, F. W., and Miller, R. D., 1975, Conversion of cellulosic wastes to oil: U.S. Dept. of Interior, Bur. Mines Rept. Invest. 8013.

Appell, H. R., Fu, Y. C., Friedman, S., Yavorsky, P. M., and Wender, I., 1971, Converting organic wastes to oil: A replenishable energy source: U.S. Dept. of Interior, Bur. Mines Rept. Invest. 7560.

Berl, E., and Schmidt, A., 1932, Über die Entstehung der Kohlen, II. Die Inkohlung von Cellulose and Lignin in neutralem Medium: A. der Chemie 493:97.

Fischer, F., 1925, The Conversion of Coal into Oils, Ernest Benn Ltd., London.

Gavin, M. J., 1922, Oil-Shale: An historical, technical, and economic study: Dept. of Interior, Bur. Mines Bulletin 210, Bradford-Robinson, Denver.

Haas, J. L, Jr., 1976, Thermodynamical properties of the coexisting phases and thermochemical properties of the NaCl component in boiling NaCl solutions: U.S. Geol. Surv. Bull. 1421-B.

Jurg, J. W., and Eisma, E., 1964, Petroleum Hydrocarbons: Generation from fatty acid: *Science* 144:1451.

Lewan, M. D., 1993, Labortory simultion of petroleum formation: Hydrous pyrolysis, in *Organic Geochemistry* (M. H. Engel and S. A. Macko, eds.), Plenum, New York (in press).

Lewan, M. D., Winters, J. C., and McDonald, J. H., 1979, Generation of oil-like pyrolyzates from organic-rich shales. *Science* 203:897.

McCollum, J. D., and Quick, L. M., 1976a, Process for upgrading a hydrocarbon fraction: U.S. Patent 3, 960:708.

McCollum, J. D., and Quick, L. M., 1976b, Process for upgrading a hydrocarbon fraction: U.S. Patent 3, 989, 618.

Schuhmacher, J. P., Huntjens, F. J., and van Krevelen, D. W., 1960, Chemical structure and properties of coal XXVI. Studies on artificial coalification: *Fuel* 39:223.

Siskin, M., Brons, G., Katritzky, A. R., and Balasubramanian, 1990, Aqueous Organic Chemistry 1. Aquathermolysis: Comparison with thermolysis in the reactivity of aliphatic compounds: *Energy & Fuels* 4:475.

Sourirajan, S., and Kennedy, G. C., 1962, The system H_2O-NaCl at elevated temperatures and pressures: *Am. Jour. Sci.*, 260:115.
Takenouchi, S., and Kennedy, G. C., 1964, The binary system H_2O-CO_2 at high temperatures and pressures: *Am. Jour. Sci.* 262:1055.

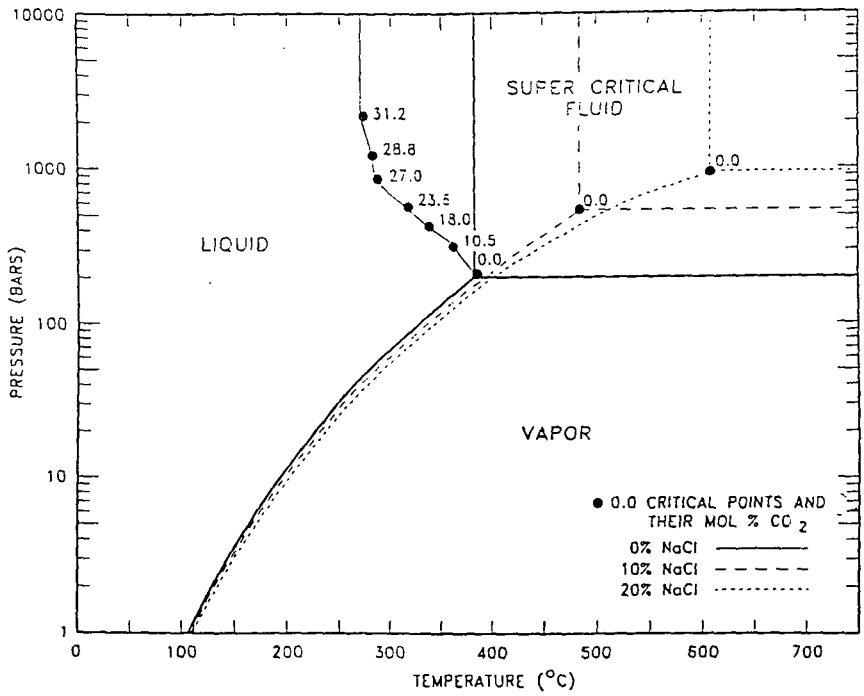

Figure 1. Pressure-temperature diagram showing phase relations and critical points for pure H_2O (heavy solid lines), CO_2 in solution with H_2O (solid circles on light solid line refer to critical points at denoted CO_2 mole fractions), 10 wt% NaCl solution with H_2O (dashed lines), and 20 wt% NaCl solution with H_2O (dotted lines). Diagram is based on experimental data reported by Haas (1976), Sourirajan and Kennedy (1962), and Takenouchi and Kennedy (1964).

LASER MICROPYROLYSIS/GAS CHROMATOGRAPHY MASS SPECTROMETRY: A USEFUL TECHNIQUE FOR THE STUDY OF COAL MACERALS?

Paul F. Greenwood, Etuan Zhang, Patrick G. Hatcher, Frank Vastola and Alan Davis,
The Pennsylvania State University, University Park, PA 16802

INTRODUCTION

Structural information regarding the microscopic composition of heterocyclic, polymaceralic materials such as coal and kerogens has proved elusive. The primary reason for this is the limited number of techniques which can analytically probe involatile, thermally labile materials.

Pyrolysis (i.e., thermal degradation) of coal and other organic materials is one technique to show much promise.[1,2] Conventional methods of coal pyrolysis include slow pyrolysis (heating rate between 25 °C/sec) and flash/fast pyrolysis (10,000 °C/sec). The pyrolysis of coal produces many gaseous fragments which can be analysed by mass spectrometry. The detected pyrolysates often reveal much structural information which can be related to the macroscopic composition of the parent coal.

The rapid heating from lasers has also been used to effectively induce coal pyrolysis.[3,4] Laser pyrolysis offers the unique advantage of micro-selective *in situ* sampling. Since readily available optics can focus the laser output to very small areas, it is possible to analyse very small components within complex mixtures such as coal. Several independent groups, some using the commercially available LAMMA instrument,[5] have demonstrated how individual components of coals and oil shales can be selectively irradiated with microscopic optics.[6-16]

Previous efforts to study individual maceral types involved the physical isolation of the selected macerals. This was performed either via hand-picked techniques[17] or density-gradient centrifugation.[18-20] The severe and time consuming sample pre-treatment requirements associated with these techniques is not present with the *in situ* analysis of the micropyrolysis technique.

The majority of the coal micro-pyrolysis studies to date have been concerned only with the laser techniques which produce charged particles. Many more neutrals than ions are produced during any laser ablation process so the detection sensitivity of pyrolysis products will be significantly reduced when limiting the analysis to ionic species. Other studies, by one of us, have revealed that carbon clusters tend to dominate the charged population produced from the laser ablation of coals.[21] This suggests analysis of directly produced ionic pyrolysates may not be an appropriate method to study the structural fragments from coal macerals.

In this paper we present a novel laser pyrolysis/GC-MS study using an instrument recently assembled in our laboratory. This apparatus includes a microscope to selectively pyrolyse individual coal macerals. The entire pyrolysate population, including neutrals, is subjected to the process of trapping (with a N_2 cold trap), separated by gas chromatography and analysed by electron impact mass spectrometry. In general, the product distribution from laser pyrolysis closely resembles that observed for flash pyrolysis. This exceptionally encouraging result suggests that laser micro-pyrolysis has

tremendous potential for the study of individual components not only within coals, but also other heterogeneous solids.

INSTRUMENTATION

The main components of the micropyrolysis apparatus used in this study include a laser, microscope, pyrolysis chamber and Kratos MS-80 GC-MS. A schematic illustration of the assembled system is shown in Figure 1.

Details of the laser (a pulsed ruby variety) and microscope can be found elsewhere.[3] In brief, the visible output of the laser has a wavelength of 694.3 nm and a maximum energy of 0.1 Joule. The microscope is equipped for reflected light illumination and long working distance objectives to enable the sample chamber to be mounted directly on the microscope substage. The laser beam is focused by the 4x objective of the microscope onto the surface of a polished coal sample mounted in the pyrolysis chamber. Focussing the laser pulse to very small sizes ensures that the very high irradiances necessary for pyrolysis are reached. The microscope also allows close visual examination of the coal sample so that particular macerals can be selected.

The pyrolysis chamber, developed in this laboratory, was designed to meet the requirements of the pyrolysis/GC-MS experiment. The sample port was kept to a small size (ID 7 mm, depth 10 mm) to reduce the amount of dead volume. A silica glass window on the the top allowed microscopic observation and laser penetration. The chamber was constructed of stainless steel and included a bore into which a thermocouple and heating element could be placed so as to heat the chamber (typically to 180 - 220 °C). Inlet and outlet carrier gas ports were also included. The pyrolysis chamber was connected to the column of the GC via (1/16") metal lined tubing (ID = 0.5 mm). A cold trap consisting simply of a loop of the column submerged in a liquid nitrogen bath is located in the oven of the GC. Heating ribbons were used to heat the transfer tubing as well as to pre-heat the helium carrier gas.

The Kratos MS-80 interfaces a Carlo-Erba GC with a scanning magnetic sector mass spectrometer. The GC is fitted with a fused-silica capillary column (30m x 0.25 mm ID) with stationary phase consisting of 50% phenylmethyl polysiloxane (J&W, DB-17). The column was temperature programmed from 40 to 280 °C at 4 °C/min. Mass spectra were obtained under EI conditions at 70 eV, a scan rate of 1500 m/z s^{-1} and an m/z 40 to 500 mass range. The individual peaks were identified by comparison of mass spectra to published spectra.

EXPERIMENTAL

Two coal samples were selected for analysis from the Penn. State Coal Sample Bank. These comprised a subbituminous humic coal (PSOC-1532) with a maximum vitrinite reflectance of 0.33% and a high volatile C bituminous cannel coal (PSOC-1109) with a vitrinite reflectance value of 0.44%. These particular coals were selected to examine the ability of this technique to differentiate the different types of macerals.

Sample pretreatment included: cutting the sample to small block sizes which could be accommodated by the sample port of the pyrolysis chamber; polishing by hand with grinding and polishing wheels according to conventional methods; and heating for considerable time (i.e., > 24 hrs) in an inert atmosphere (i.e., He) to remove absorbed volatiles.

The procedure for the pyrolysis experiments of this study is briefly as follows. Pyrolysis is induced by the focussed laser output. The microscope used to focus the laser

also allows particular coal surface sites to be selectively irradiated. The pyrolysed craters from the laser beam can be varied by altering the degree of focussing to between 10 to 250 μm in diameter. These craters can be 5 to 10 μm in depth. The actual depth is also dependent upon the size of the irradiated area as well as the energy setting of the laser. Throughout pyrolysis the volatile products are swept by He gas through the heated transfer line to the column and trapped in the liquid N_2 bath. The transfer efficiency of the volatiles being dependent on the temperature of the transfer line. This relationship between transfer efficiency and temperature is also observed to be mass discriminate with higher molecular weight species being filtered out by lower temperatures. Once the volatiles from a number of laser pulses (typically 10 - 20) have been collected, the oven of the GC is heated (at 4 ^{o}C/min from 40 ^{o}C to 280 ^{o}C) effectively releasing and separating them according to size as they pass through the column.

The separated samples are continually analysed by electron impact mass spectrometry as they emerge from the column.

RESULTS

Laser parameters such as duration of irradiation, wavelength, power density, and size of the irradiated area have been identified from the previous laser pyrolysis studies of coal[3]. Optimum spectral conditions are also investigated for the present experiments. A sufficient number of volatiles were produced from 20 laser shots at different surface sites. It was necessary to investigate fresh surfaces with each pulse so that char produced from a previous pulse is not subsequently analysed. The coal samples were successfully pyrolysed with tightly focussed (i.e., high energy) pulses. Different products were obtained by varying the laser power either through defocusing the microscope or using a neutral density filter control.

The volume of volatiles produced by the laser proved insufficient in itself to facilitate continual signal detection by the Kratos MS-80 mass spectrometer. Because of this it was necessary to extend the mass range to m/z 40 - 600 so that CO_2 (i.e., m/z = 44) contributes to the background ion signal. The signal from CO_2 is much larger than the signal from the pyrolysis volatiles which often remain hidden in the baseline (i.e., CO_2 signal) of the total ion chromatogram (TIC). A large signal present in all laser pyrolysis TIC's at a retention time of ~ 3 - 4 minutes can also be assigned to CO_2. This result is consistent with many of the earlier studies in which CO_2 was observed to be the most dominant pyrolysis product. Other low abundant pyrolysis products may only be successfully revealed by individual and summed ion chromatograms.

Summed ion chromatograms for the subbituminous coal and high volatile C bituminous cannel coal are shown in Figures 2 and 3, respectively. Ions of mass 108, 122 and 136 are summed in the case of the subbituminous coal to reveal the pyrolysis production of alkyl phenols. The 108 ion identifies cresol (i.e. C_1-phenol), the 122 ion C_2-phenol and the 136 ion C_3-phenol. Such products, previously observed from flash pyrolysis,[22] are thought to dominate the vitrinite component of these coals. The resolution of ortho-Cresol isomer from the para and meta isomers was also observed from flash pyrolysis. The detection of these known pyrolysis products highlights the suitability of the laser as a pyrolysis source. Other species identified from the laser pyrolysis TIC include C_n-benzenes ($n \leq 2$), phenol, indene and naphthalene. Although low molecular weight alkyl - aromatics such as these are typically produced from coal pyrolysis some of these products may arise from simple evaporation from the coal surface at the high temperatures (180 - 220) of the pyrolysis chamber. Studies are presently under way to determine which species do arise from simple evaporation.

All ions from 46 - 600 contribute to the summed chromatogram associated with the high volatile coal (i.e., Fig. 3) This trace effectively reflects the CO_2 subtracted TIC. Low molecular weight products such as alkyl benzenes, toluene, indene and naphthalene are again observed. In addition, a prominent homologous series of dominant n-alkanes which range to above n-C_{29} are observed. This distribution of n-aliphatic hydrocarbons is typical of immature, lignite-rich terrestrial organic matter.[23] The biomarker 17β(H)-22,29,30-trisnorhopane is also detected at a retention time of ~ 70 minutes. The production and detection of this species is particularly encouraging since pentacyclic triterpenoids with the hopane type skeleton are a widely utilized group of biomarkers found in organic geochemical materials.[24] The detection of these large molecular weight products indicates the successful transfer, trapping and column separation of high molecular weight species by this technique. It is likely that these alkanes and biomarkers are released from the coal not as pyrolysis fragments but as trapped molecules released during laser heating.

Interpretation of the different mass spectra does suggest that there exists a fundamental difference between the chemical and structural compositions of the two coals.

CONCLUSIONS

The initial results presented in this paper demonstrate that coal macerals can be successfully investigated by laser micropyrolysis. The energy from the focussed laser beam was sufficient to induce coal pyrolysis and the microscope offers the added advantage of irradiating specific areas of the coal surface. Heating the pyrolysis chamber and transfer line prevents condensation of the laser emitted volatiles which are successfully flushed into the column of the GC by the pre-heated He carrier gas.

Products typical of coal pyrolysis were detected from the two samples. The different results for the respective samples reflects the contrasting maceral components of the coals and the ability of this technique to differentiate these differences is established The investigation of individual components within a whole range of heterogeneous geochemical materials should now be possible with this technique.

REFERENCES

1 T. I. Elington, S. R. Larter and J. J. Boon, J. Anal. Appl. Pyrolysis, 20, 20 (1991).

2. B. Horsfield, Geochimica. et. cosmochimica. acta, 53, 891 (1989).

3. a) F. J. Vastola and L. J. McGahon, Fuel, 66, 886 (1987).

   b) F. J. Vastola and A. J. Parone, Am. Chem. Soc. Div. Fuel Chem., Prepr., 10, 53 (1966).

   c) F. J. Vastola, A. J. Parone, P. H. Given and R. R. Dutcher, "Spectrometry of Fuels", Plenum Press, N. Y., (1970), p29.6.

4. a) S. A. Stout and K. Hall, J. Anal. Appl. Pyrolysis, 21, 195 (1991).

   b) S. A. Stout and R. Lui, Org. Geochem., In Press (1992).

5. D. M. Hercules, R. J. Day, K. Balasanmugam, T. A. Dang and C. P. Li, Anal. Chem., 54, 280A (1982).

6. J. J. Morelli, D. M. Hercules, P. C. Lyons, C. A. Palmer and J. D. Fletcher, Mikrochim. Acta [Wien], 111, 105 (1988)

7. A. F. Gaines and F. M. Page, Fuel, 62, 1041 (1983).
8. P. K. Dutta and Y. Talmi, Fuel, 61, 1241 (1982).
9. F. S. Karn, R. A. Friedal and A. G. Sharkey, Carbon, 5, 25 (1967).
10. F. S. Karn, A. G. Sharkey, A. F. Logar and R. A. Friedal, US Bur. Mines Rep. Invest. 7328, 32 (1970).
11. W. H. Joy, W. R. Ladner, and E. Pritchard, Fuel, 19, 26 (1968).
12. J. P. Biscar, J. Chromatogr., 56, 348 (1971).
13. R. L. Hanson, N. E. Vanderborgh and D. G. Brookins, Anal. Chem., 47, 335, (1975).
14. R. L. Hanson, D. G. Brookins and N. E. Vanderborgh, Anal. Chem., 48, 2210, (1976).
15. R. L. Hanson, N. E. Vanderborgh and D. G. Brookins, Anal. Chem., 49, 390, (1977).
16. N. E. Vanderborgh, W. J. Verzino, M. A. Fletcher and B. A. Nichols, J. Anal. Appl. Pyrolysis, 4, 21 (1982).
17. D. R. Dyrkacz, C. A. A. Bloomquist and L. Rusic, Fuel, 63, 1367 (1984).
18. N. Bostick and B. Alpern, J. Microscopy, 109, 41 (1971).
19. P. Robert in "Organic Metamorphism and Geothermal History: Microscopic Study Organic Matter and Thermal Evolution of sedimentary basins", D. Reidel Publishing Comp., Boston, 1988, p311
20. M. Nip, J. W. deLeeuw, and J. C. Crelling, Energy and Fuels, 6, 125 (1991).
21. P. F. Greenwood, M. G. Strachan, G. D. Willett and M. A. Wilson, Org. Mass Spectrom., (1991).
22. P. G. Hatcher, H. E. Lerch, III, R. K. Kotra and V. T. Vincent, Fuel, 67, 1069 (1988).
23. S. R. Larter in "Analytical Pyrolysis, Techniques and Applications", Ed. K. J. Voorhees, Butterworths, Boston, 1984, pp 212 - 275.
24. G. Ourisson, P. Albrecht and M. Rohmer, Sci. American, 251, 44 (1984).

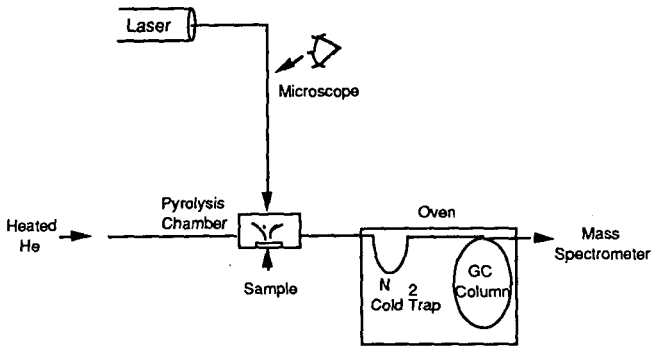

Figure 1 Assembly of Apparatus Used in the Micropyrolysis Experiment.

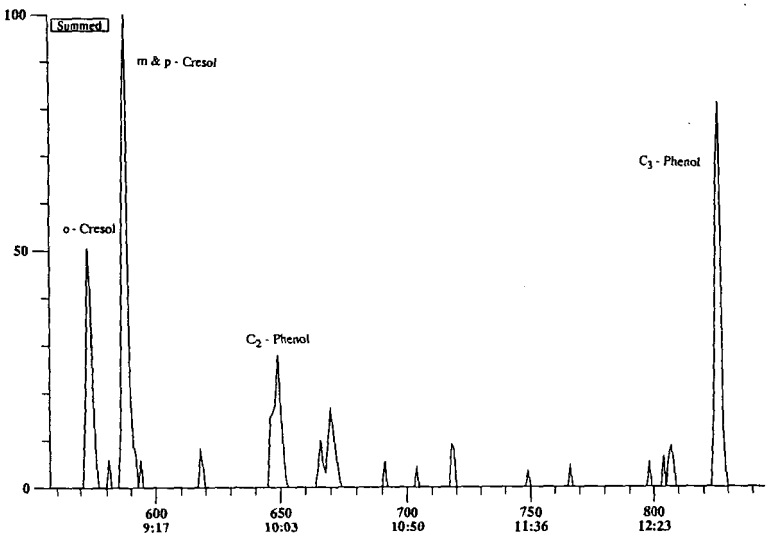

Figure 2 Summed chromatogram of the m/z 108, 122, 136 ions from the laser pyrolysis of a subbituminous coal.

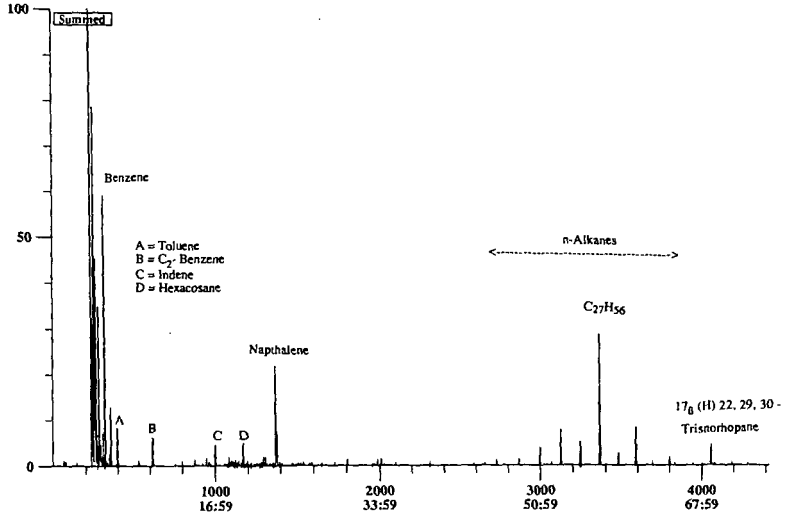

Figure 3 Summed chromatogram of all m/z 46 - 600 ions from the laser pyrolysis of a high volatile C bituminous cannel coal.

HYDROTHERMAL MEDIA, OIL SHALE, AND COAL

David S. Ross
SRI International
Menlo Park, CA 94025 USA

Keywords: hydrous pyrolysis, Wyodak, hydrothermal

INTRODUCTION

Hydrous pyrolysis has proved to be useful tool for the study of accelerated petroleum generation in source rocks. The techniques uses liquid water as a medium at thermolytic conditions in the 290°-360°C range (Lewan et al., 1979; 1981). Dry pyrolysis provides olefins in the pyrolysate, but with the addition of water the olefin yield is reduced and n-alkanes resembling those in petroleum emerge. Hoering (1984) extended the work using D_2O, developing results discussed below. The claim that hydrous pyrolysis mimics the natural process has been questioned recently (Monthioux et al., 1985; Tannenbaum and Kaplan, 1985; Comet et al., 1986). Nonetheless there is little question that the chemistry operating at hydropyrolysis conditions generates alkanes and other hydrocarbons from the immature source material.

The lack of understanding of the chemistry at hydrothermal conditions is underscored by a several observations. For example highly condensed polynuclear aromatic hydrocarbons (PAHs) including pyrene, benzpyrenes, and coronene are found in hydrothermal vent petroleums (Simoneit, 1985a; 1988). These compounds are commonly observed as products of hydrocarbon pyrolysis above 550°C, and coronene itself is not generated in pyrolyses at temperatures below 650°C (Commins, 1969). However it is difficult to explain their presence in the vent zones where temperatures are considerably lower.

Another curious point is the unusually high rate of epimerization of biological markers in hydrous pryolysis. Although cationic centers generated on highly acidic clay surfaces could be responsible (Alexander et al., 1984), the acidity of the clay sites is substantially reduced in an aqueous environment (Tannenbaum and Kaplan, 1985), and the high acidities required for epimerization at the rates observed cannot be present. The activity of acid clay sites can be questioned further because of the presence of normal alkanes, whereas acid-promoted cationic chemistry should produce highly branched alkanes. Calcium carbonate has also been suggested as significant to the isomerization (Eglinton et al., 1986), but the mechanistic aspects of that process are not apparent.

The role of water in the maturation process has not been clearly defined. It has been suggested that water transfers hydrogen to organic free radicals in the reaction mixture (Monthioux et al., 1985: Hoering, 1984; Comet et al., 1986).

$$R\cdot + H_2O \longrightarrow HO\cdot + R\text{-}H$$

However this reaction is endothermic by 25-30 kcal/mol and should not be significant at hydrous pyrolysis temperatures.

In the discussion here we seek to develop some understanding of the chemical processes in hydrous pyrolysis by first modeling the results of Hoering in D_2O. Some of that work has been recently reviewed (Ross, 1992), and the results are summarized here. We then seek to extend this view to the chemistry of coal, discussing our findings in studies of Argonne samples of

Wyodak coal in hydrothermal media (Ross, et al., 1990a,b). We begin with a summary of the nature of the medium at hydrous pyrolysis conditions.

RESULTS AND DISCUSSION

The Nature of the Hydrothermal Medium

Under common conditions, water is a highly polar, fluid medium accommodating ionic salts and having a modest capacity for dissolving some gases and polar organic compounds. However, liquid water near its critical point (374°C/220 atm) becomes a very different medium. The shifts in the key physical properties of liquid water up to its critical temperature are presented in Figure 1, with the shaded portion representing the region where hydrous pyrolysis is commonly conducted. The figure shows that while the density of the medium stays in the liquid-like region (> 0.3 g/mL) over most of the subcritical regime, the viscosity falls early to very low, almost gas-like, values. The net result is an interesting region where the medium has a liquid-like solvent capacity combined with a very high gas-like diffusivity. The mobilities of both neutral and charged solutes are much higher than they are in normal liquids, overcoming what could be mass transfer limitations at more conventional conditions.

The dielectric constant falls to levels like that of organic solvents, dramatically affecting the solubilities of organic materials. Thus naphthalene, virtually insoluble in water at ambient conditions, it is miscible in all proportions in liquid water at temperatures as low as 300°C (Jockers and Schneider 1978). Fully homogeneous combinations of ionic salts and nonpolar organics, which might not be feasible at common conditions, can easily be established at these conditions (Alwani and Schneider, 1969).

Hydrous Pyrolysis with D_2O -- The Results of Hoering

Hoering's data on the D-content in the n-alkanes from the treatment of preextracted Messel shale with D_2O at 330°C/3 days (1984) have been used to model the process (Ross, 1992). The profiles for the heptadecane recovered from the treatment are shown in Figure 2. The figure also shows the results of control experiments in which heptadecane was purposely added to the treatment mixture, and for heptadecane recovered from work in which heptadecene was initially added. In the latter, 60% of the added olefin was recovered as alkane, a remarkable result reflecting a considerable reducing potential in the reaction mixture, and requiring an explanation.

The added alkane does not undergo much exchange, and the fact that the kerogen-generated alkane is very highly exchanged rules out preexisting alkane as the source. The olefin-generated alkane contains considerable deuterium, but the distribution pattern is very different from that for the kerogen-derived material.

A process reconciling these facts is shown as Scheme I. The scheme features the view that water is significant to the reduction of olefins generated pyrolytically from the kerogen. The general arrangement was confirmed in modeling work done employing an integration routine based on the Gear algorithm (Moore and Pearson, 1981) and operated on a VAX 11/750 computer. The fit, shown in Figure 3, was generated for a reaction rates alignment in which reduction >> pyrolysis and exchange $\approx$ 2 x pyrolysis. It is emphasized that for the fit, it is necessary that reduction requires water, but produces *protio* alkane. The alkane then exchanges with the medium, presumably likely on the mineral surface.

A key question concerns the reduction step; there are no obvious reducing species introduced into the reaction. A clue to that chemistry may lie in the results of Amin, who studied the

pyrolysis of glucose in water at its critical point (1975). Data from the study in Table I show that the pyrolysis yields char, an oil, and gases including CO, CO_2, H_2, and CH_4.

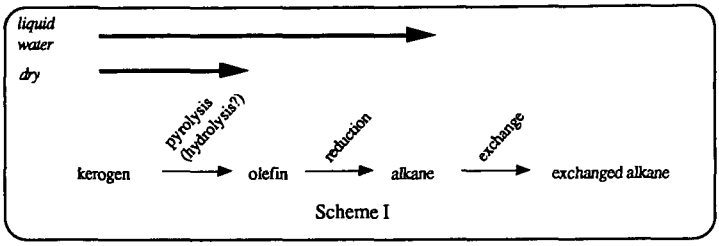

Scheme I

Significantly, however, as the density of the medium is increased from a gas-like value to one more liquid-like, the quantity of gas and oil increase substantially with a corresponding decrease in the char yield. Factors associated with the increased density that appear to promote reduction of the starting glucose and formation of simple gases.

Hoogwater reports similar findings in the pyrolysis a series of haloorganic compounds in supercritical water at liquid densities (1991). The results for trichloroethane are shown in Figure 4. These experiments, conducted in sealed quartz tubes and therefore eliminating metal wall-promoted reactions, yielded surprisingly large quantities of CO, CO_2, H_2, and a collection of hydrocarbons including alkanes and benzene.

These data suggest that liquid water in the near critical region or supercritical water at liquid densities promotes gasification reactions. Such conversions are essentially the water-promoted disproportionation of carbon, i.e.

modestly oxidized organics	➛ **highly reduced products**	+ **highly oxidized products**
e.g. olefins, phenols	alkanes, H_2	PAHs, CO, CO_2

They could be the basis of alkane production in petroleum genesis. We are unaware of studies confirming such chemistry, and submit that this area is an important one for development.

Hydrous Pyrolysis of Wyodak Coal

Our earlier accounts of this work described the effects of the treatment of Argonne samples of Wyodak coal with liquid water (hydrothermal) and with no medium (under N_2/thermal) at 250°-350°C for periods of 30 min and 5 hr (Ross, et al, 1990a). Much of the data were developed using thermal gravimetric analysis (TGA) and SRI's field ionization mass spectrometer (FIMS), both operating from ambient to 500°C at 2.5°C/min. A later report included additional results from studies in which water was replaced by n-undecane, a hydrocarbon with a critical temperature (363°C, estimated by the method of Lydersen, 1955) near that of water (374°C), and expected to be chemically unreactive over at least the 30-min heating period (Ross, et al., 1990b).

A tar representing 5-7% of the starting coal was consistently deposited on the quartz insert walls solely at the hydrothermal conditions. There was no evidence of tar in the thermal and undecane runs. In all cases the coal lost oxygen, with O-losses falling in the order:

hydrothermal (5 hr) > [hydrothermal (30 min) ≈ thermal (30 min) ≈ thermal (5 hr)] > undecane (30 min)

Some properties of the recovered coal and the tars are presented in Table II.

Our earlier accounts discussed these data; however there are two features of specific interest here. The first is the fact that the hydrothermally-promoted tars are at the same time more volatile and of a greater molecular weight than the FIMS-volatile products from the recovered coals. They are also considerably richer in hydrogen. They are thus substantially less polar, and it is tempting to view these results as parallel to those for hydrocarbon production in the hydrous pyrolysis of petroleum source rock and due to water-promoted reduction chemistry.

The second are the volatility changes shown in Figure 5, which displays the total FIMS ion count *vs* evaporation temperature for samples for both 30 min and 5 hr treatments. The profile for the untreated coal is also presented for comparison. (FIMS mass analysis begins at m/e 48, and so the profiles are independent of the evolution of water and carbon dioxide. They reflect solely organic volatiles.) For the 30 min treatment the undecane result is little different from that for the untreated coals. The thermally pretreated sample shows the presence of volatiles beginning to emerge at around 100°C; however these materials must be the thermolytically volatiles generated during the pretreatment. They are deposited on the coal, and then evaporated into the instrument during the FIMS heating.

The aqueous pretreatment, however, clearly has produced new material. It is emphasized that the ordinate in the figure is logarithmic and thus the absolute quantities of product are significantly greater than for the thermal case. This new material would seem to be the portion of the tar that condensed on the coal rather than on the insert walls.

For the 5-hr treatment little of the tar remains on the coal, and the hydrothermal and thermal results are similar. It is notable from Table II that the tar has become considerably more volatile with little change in the molecular weight. We found in addition by FIMS that the arenol content of the 30 min tar was less than 30% that of the treated coals. The arenols in the 5 hr tar were reduced yet further by another factor of 3.* Continued hydrothermal treatment appears to provide extended reduction and convert phenols to less polar material.

Remarkably, the undecane treatment has drastically reduced the volatility of the coal, essentially converting it to a char. The shaded portion of the figure reflects the loss in volatile material, those fractions becoming irreversibly reincorporated into the coal matrix.

CONCLUSIONS

The effects of water on the thermolysis of coal suggest a process similar to that in Scheme I for petroleum source rock (Scheme II). As in I, water promotes reduction of the initial pyrolytic products, and tar is the result. The scheme shows that extended hydrothermal treatment substantially increases the volatility of the tar.

In the absence of added water there is a pyrolytic release of material, including olefins and large quantities of phenolic material. These fragments will migrate to other regions of the coal and will probably tend to concentrate at the mineral sites due to acid/base interactions. At this point the recent results of Stein et al. can apply (1989). Their work showed that at 400°C dihydroxyben-zenes are very reactive and undergo acid catalyzed dehydroxylation and condensation. For coal, with distributions of clay and silica particles throughout the organic phase in sizes down perhaps to the nanometer level (Allen and VanderSande, 1984), we can expect significant degrees of such retrogressive chemistry.

For undecane the process is even more retrogressive. Neither water nor alkanes are good coal swelling media at ambient temperatures, the former because it is too polar, and the latter because

* The arenol content is the sum of the FIMS signals for phenol, dihydroxybenzene, and their respective C_1-, C_2-, and C_3- derivatives.

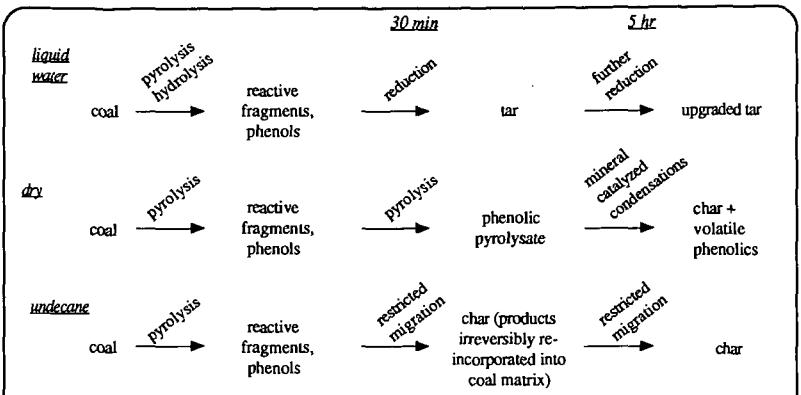

Scheme II

it is not polar enough. However water becomes increasingly more coal-accommodating in the hydrothermal region because its dielectric constant decreases to values like those for polar organic liquids (Schneider and Jockers, 1978). Undecane in contrast likely becomes an even poorer solvent, or in effect an antisolvent. In that medium coal should thus not swell but possibly collapse, a negative solvent action discussed for polymers by Magda et al. (1988). Such a tendency for the coal would trap otherwise volatile fractions, resulting ultimately in their irreversible reincorporation into the coal matrix, and the formation of char. As a consequence, the arenols will increasingly react within the cage.

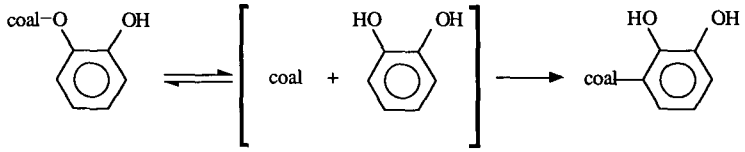

The essential component of this process is the replacement of labile, aryl ether links by stable, C-aryl bonds. That activity ultimately leads to the accumulation of structures that will tend to condense with further heating, and proceed to char. Such alkane-promoted condensation chemistry is clearly an undesirable component in conversion generally. Its regressive action, however, could be most seriously encountered in coprocessing, and additional studies in this area could prove profitable.

ACKNOWLEDGMENT

We acknowledge support of the US DOE for the coal-related portion of this work.

REFERENCES

Alexander, R, Kagi, R. I., and Larcher, A. V. (1984). Clay catalysis of alkyl hydrogen exchange reactions-reaction mechanisms. *Organic Geochemistry*, **6**, 755-760.

Allen, R. M., and VanderSande, J. B. (1984). Analysis of sub-micron mineral matter in coal via scanning transmission electron microscopy. *Fuel*, **63**, 24-29.

Alwani, Z. and Schneider, G. M. (1969). Phasengleichgewichte, kritische Erscheinungen und PVT-Daten in binären Mischungen von Wasser mit aromatischen Kohlenwasserstoffen bis 420°C und 2200 Bar. *Ber. Bunsenges.*, **73**, 294-301.

Amin, S. I. (1975). Reforming and decomposition of organics in water. Thesis prepared for M. Modell, MIT.

Comet, P. A., McEvoy, J., Giger, W., and Douglas, A. G. (1986). Hydrous and anhydrous pyrolysis of DSDP Leg 75 kerogens--a comparative study using a biological marker approach. *Organic Geochemistry*, **9**, 171-182.

Commins, B. T. (1969). Formation of polycyclic aromatic hydrocarbons during pyrolysis and combustion of hydrocarbons. *Atm. Env.* **3**, 565-572.

Eglinton, T. I., Rowland, S. J., Curtis C. D., and Douglas, A. G. (1986). Kerogen-mineral reactions at raised temperatures in the presence of water. *Organic Geochemistry*, **10**, 1041-1052.

Hoering, T. C. (1984). Thermal reactions of kerogen with added water, heavy water and pure organic substances, *Org. Geochem.* **5**, 267-278.

Hoogwater, S. (1991). High pressure hydrothermolysis of chlorinated hydrocarbons. Thesis prepared for J. M. L. Penninger, Eindhoven University of Technology.

Jockers, R. and Schneider, G. M. (1978). Fluid mixtures at high pressures--fluid phase equilibria in the systems fluorobenzene + water, 1,4-difluorobenzene + water, and 1,2,3,4-tetrahydronaphthalene + decahydronaphthalene (trans) + water up to 360 MPa. *Ber. Bunsenges. Phys. Chem.*, **82**, 576-582.

Lewan, M. D., Winters, J. C., and McDonald, J. H. (1979). Generation of oil-like pyrolysates from organic-rich shales, *Science*, **203**, 897-899.

Lewan, M. D., Winters, J. C., and Williams, J. A. (1981). A laboratory study of petroleum generation by hydrous pyrolysis, *Adv. in Organic Geochemistry 1979*, M. Bjorøy et al., eds., John Wiley and Sons, Ltd., Chichester, p. 524-533

Lydersen, A. L. (1955). Estimation of critical properties of organic compounds, College of Engineering, University of Wisconsin, *Eng. Expt. Sta. Rept.* **3**, Madison, WI.

Magda, J. J., Fredrickson, G. H., Larson, R., and Helfand, E. (1988). Dimensions of a polymer chain in a mixed solvent. *Macromolecules*, **21**, 726-732.

Monthioux, M., Laniais, P., and Monin, J-C. (1985). Comparison between natural and artificial maturation series of humic coals from the Mahakam delta, Indonesia. *Organic Geochemistry*, **8**, 275-292.

Moore, J., and Pearson, R. (1981). *Kinetics and Mechanism*, Third Edition, John Wiley and Sons, New York, 318-324.

Ross, D. S., Hirschon, A. S., Tse, D. S., and Loo, B. H. (1990a). The effects of hydrothermal treatment on Wyodak coal, *American Chemical Society Division of Fuel Chemistry Preprints* **35**, 352-363.

Ross, D. S., Loo, B. H., Tse, D. S., and Hirschon, A. S. (1990b). Hydrothermal treatment and the oxygen functionalities in Wyodak coal, *Fuel* **70**, 289-295.

Ross, D. S. (1992). Autoradiographic and hydrothermal probes of interfacial chemistry in oil shale and coal, *American Chemical Society Division of Fuel Chemistry Preprints* **37**, 375-384.

Simoneit, B.R.T. (1985a). Hydrothermal petroleum: Genesis, migration, and deposition in Guaymas Basin, Gulf of California. *Can. J. Earth Sci.* **22**, 1919-1929.

Simoneit, B.R.T. (1988). Petroleum generation in submarine hydrothermal systems: An update. *Can. Mineralogist* **26**, 827-840.

Stein, S. E., Wang, F., and Senthilnathan, V. P., 1989. Chemical Models for Regressive Reactions: I. Thermolysis of Dihydroxybenzenes, Proceedings of the 1989 International Conference of Coal Science, *International Energy Agency*, 165-168.

Tannenbaum, E. and Kaplan, I. R. (1985). Low-M_r hydrocarbons generated during hydrous pyrolysis and dry pryolysis of kerogen. *Nature*, **317**, 708-709.

Table I

PRODUCTS FROM THE PYROLYSIS OF GLUCOSE IN WATER (374°C/30 MIN)

Pressure (atm)	Density (g/Ml)	Fraction of Starting C (%)		
		Oil	Solid	Gas
152	0.07	27.8	68.9	3.4
220	0.32	60.4	8.5	9.5

Table II

Some Properties of the Recovered Coals and Tars

	Treatment Period	Starting coal	Hydrothermal	Thermal	Undecane
H/C					
		0.90			
	30 min	–	0.82	0.83	0.81
	5 hr	–	0.72 1.13 (tar)	0.76	0.75
O/C[a]					
		0.24			
	30 min	–	0.16	0.15	0.18
	5 hr	–	0.12 0.18 (tar)	0.16	–
$T_{1/2}$(°C)[b]					
	–	395-400	–	–	–
	30 min	–	340-350 200 (tar)	377-395	405
	5 hr	–	410 140 (tar)	425	465
$\bar{M}_w$[c]					
	–	403-411	–	–	–
	30 min	–	410-421 393 (tar)	329-380	373
	5 hr	–	332	308 432 (tar)	201

a. Oxygen determined by direct O-analysis.
b. The temperature at which one-half of the FIMS volatiles has passed into the instrument.
c. Weight average molecular weight.

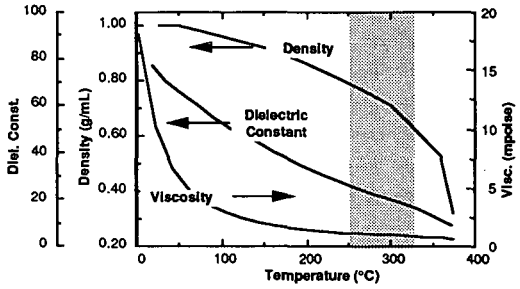

Figure 1. Some key properties of liquid water.

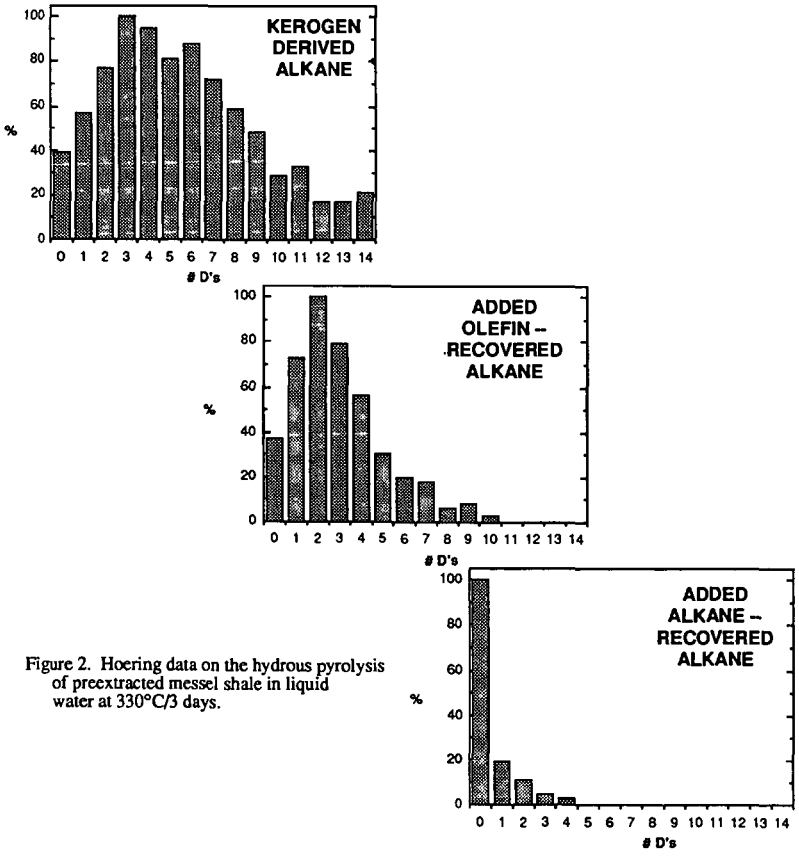

Figure 2. Hoering data on the hydrous pyrolysis of preextracted messel shale in liquid water at 330°C/3 days.

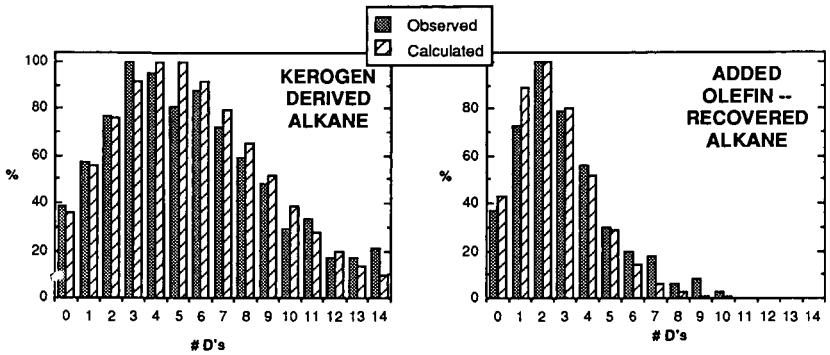

Figure 3. Hoering data and calculated profiles. The kinetic factors are reduction >> pyrolysis and exchange ≈ 2 x pyrolysis.

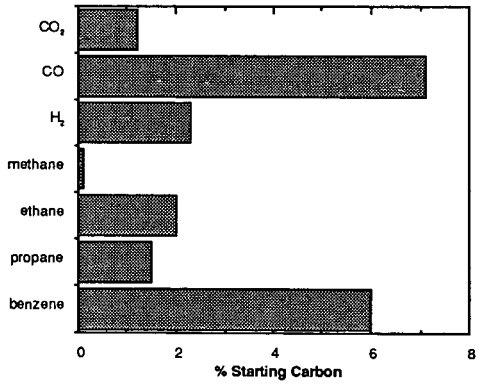

Figure 4. 1,1,2-trichloroethane conversion 428°C/ρ = 0.32mL/50 min.

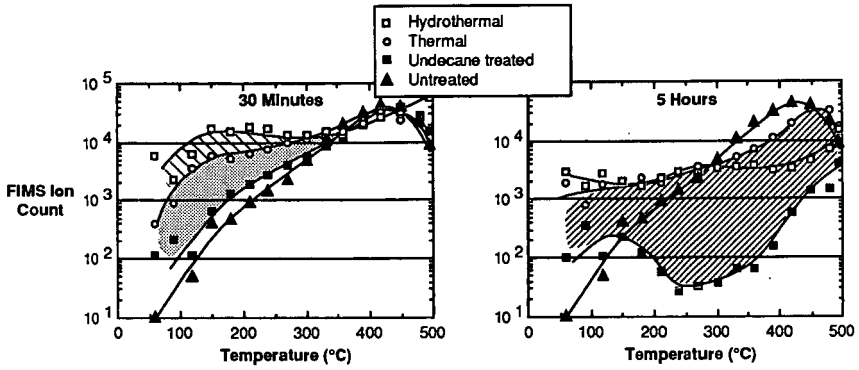

Figure 5. FIMS ion count values vs evaporation temperature for 30-min and 5-hr runs at 350°C.

Effects Of Transport Limitations On Pyrolysis Of Cellulosics

Ivan Milosavljevic and Eric M. Suuberg
Division of Engineering, Brown University
Providence, RI 02912

Keywords: Pyrolysis, Cellulosics, Heat Transfer, Mass Transfer

Introduction

The tendency of cellulosic materials to form chars during pyrolysis is well established. However the effects of sample density, size and grain orientation on char formation are not yet well established. In this work, the data obtained from different experimental systems are compared in order to deduce the effects of sample density, size and grain orientation on pyrolysis of cellulosics. It was noted that the overall pyrolysis process appears to be similar for a wide range of materials, sample densities and grain orientations, at least under high (fire-level) heat flux conditions.

Experimental

The pyrolysis behavior of purified cellulose (pressed to three different densities), white pine and oak were investigated in a large scale pyrolysis apparatus (designed to simulate fire conditions), a standard TGA, a standard tube furnace and a heated wire gauze reactor. This work was motivated by a desire to establish whether the kinetics of pyrolysis, measured in TGA-type devices can apply to room fire-type situations.

The large scale pyrolysis apparatus is shown schematically in Figure 1. A sample is heated by radiative heaters as it is positioned atop an electronic balance. The heat flux from the radiative heaters was 40 kW/m^2 in all tests reported here and all the tests were performed under nitrogen purge. It should be noted that not all of the incident heat flux was absorbed due to the heat losses from the surface (i.e. reflection, re-radiation and convection). Mass changes and/or temperatures within the sample were monitored continuously. Samples used in the large scale pyrolysis apparatus were cylindrical with diameter 38 mm and various thicknesses (typically about 10mm). Pressed cellulose samples had densities of 0.475±0.025 g/cm^3, 0.725±0.025 g/cm^3 and 1.000±0.090 g/cm^3, white pine a density of 0.377 g/cm^3 and oak a density of 0.734 g/cm^3. For tests with cellulose and white pine there were two different grain orientations with respect to the axis of incident radiative flux: parallel and perpendicular. For tests with oak only a "tangential" (with respect to growth rings) orientation was used.

In order to establish the difference in behavior between large samples (as used in a large scale pyrolysis apparatus) and small samples of purified cellulose, some tests were performed in a TGA/FTIR system using 3x3x3 mm cellulose samples of same densities as in a large scale pyrolysis apparatus. The atmosphere was helium and the heating rate was 60°C/min.
The wire gauze reactor was used in order to investigate the effect of grain orientation on the ultimate char yield. Samples for the wire gauze reactor were of 1.0 g/cm^3 density, 2.7x27 mm and different widths. The atmosphere was helium and the heating rate was 60°C/min.

Results and Discussion

Figures 2a and 2b show mass loss as a function of time for different initial sample densities for perpendicular (tangential for oak) and parallel grain orientation recorded in the large scale pyrolysis apparatus, respectively. Despite the diversity of materials and their densities, the behavior, with respect to mass loss, appears similar. There is some small amount of mass loss observed before the actual heating started. This is probably due to the sample drying, since the samples were handled in air without any drying prior to a run, and the atmosphere in the apparatus was dry nitrogen from the moment the sample was placed in the apparatus.

It can be seen from Figures 2a and 2b that the point of first significant mass loss is a function of density. Higher density samples tend to start to pyrolyze later than the lower density samples, independent of the grain orientation. The reason for such behavior is a difference in heat transport. The higher the density of the sample, the more efficiently it serves as a heat sink (since thermal conductivity varies with density), and the more slowly the temperature of the surface rises. Since it is the surface layer that begins the process of pyrolysis, it is the temperature of the surface that matters. This hypothesis is supported by the data of Figure 3, which shows the behavior of small samples of cellulose in a TGA device. In this case, the samples are uniformly heated over their surface and the gas phase temperature histories are identical, but there is a trend, again, towards "earlier" pyrolysis in the lower density samples. The process is undoubtedly external heat transfer controlled, since there is absolutely no reason to believe that pressing density affects kinetics (all samples were pressed from the same powder).

The pine samples of Figures 2a and 2b behave in a manner quite similar to that of pure cellulose. This cannot be said for the oak sample, perhaps because the pine is much more homogenous than the oak (there are clearly observable inhomogenities in the oak sample). The nature of sample inhomogeneity and its importance will be further discussed below.

It can be seen from Figures 2a and 2b that during the middle stage of pyrolysis mass loss is linear in time, as is often seen in the literature for this type of material [1, 2, 3, 4, 5]. The reason for such a behavior is that the process is heat conduction limited, with surface flux prescribed. The pyrolysis wave is "pushed" at constant velocity by the heat deposited on the surface at constant rate (vide infra).

Figure 2c depicts the temperature at the surface and at 10 mm from the surface for a 12.25 mm thick cellulose sample of 1.078 g/cm^3 density with perpendicular grain orientation, recorded in the large scale pyrolysis apparatus. The temperature profiles clearly establish that the pyrolysis process is heat transfer limited, in such a system. Note that the "kinks" in the profiles at between 300°C and 400°C are reproducible, and we believe indicate an endothermic step in the overall process (though not necessarily the main reaction process). This will be discussed elsewhere.

Figures 4a, 4b and 4c show cumulative amounts of carbon monoxide, carbon dioxide and methane, respectively from the TGA experiments of Figure 3. It is obvious that there is an effect of sample density. There is more gas evolved from higher density samples. This is probably due to the higher residence times of tars, such that there is a higher probability for their cracking to lighter gases prior to escape from the particles. By examining the starting point of gas evolution in these figures, it can be concluded that both carbon monoxide and carbon dioxide are the products of primary pyrolysis as well as of secondary cracking reactions whereas methane appears as a product of the secondary reactions alone (otherwise it should start to evolve immediately with the other gases).

Figure 5 shows the final char yield for the three different sample densities, examined in the TGA and large scale pyrolysis apparatus. Obviously the TGA data support the notion that with increasing density, there is an increasing tendency towards cracking reactions of tars, which leave behind a char product as well. The effect, while measurable, certainly cannot be termed large, over the range of densities explored. Thus for pyrolysis of cellulose in woody materials, there is a suggestion that density alone is not a key factor in determining pyrolysis char yields. The data from the large scale apparatus requires consideration of other factors, discussed below.

Figure 6 presents mass loss rates (averaged over the linear portions of mass loss curves only) as a function of initial sample density for cellulose samples with perpendicular and parallel grain orientation from experiments in the large scale pyrolysis apparatus and from the experiments in the TGA. The samples used for a TGA should not be affected by a grain orientation due to the uniform heating of the samples from all sides. The mass loss rate follows the same trend for both grain orientations used in the large pyrolysis apparatus. The rate of mass loss is linear in density. The actual mass loss rates are shown in Table I as the parameter B, where the relationship between sample mass M and time t is roughly:

$$M = M_0 - Bt$$

Again, this holds approximately over a large fraction of the sample's pyrolysis history. The fact that Figure 6 shows B to be linear in density (ρ) suggests that the ratio (B/ρ) is constant, and these values are also shown in Table I. For a sample of constant cross-sectional area, (B/ρ) is proportional to the linear propagation velocity of a pyrolysis wave through the sample, viz:

$$(B/\rho) = V\,A$$

where V is the velocity and A is the cross-sectional (1134 mm^2). Thus it may be seen that the average propagation velocity is $9.8 \times 10^{-3}/1.134 \approx 8.6 \times 10^{-3}$ cm/s or about 0.5 cm/min. It can be seen from Table I that the pyrolysis wave speed is fairly independent of density. All (B/ρ) values fall within the standard deviation of the mean (i.e. $\pm 3 \times 10^{-3}$ cm^3/s). No clear trends are established by the limited data available. Again, the constancy of (B/ρ) is expected, if thermal conductivity is linear in density.

Mass loss rates (averaged over the linear portions of mass loss curves only), obtained in the TGA experiments are also shown in Figure 6. The effect of density is not pronounced but is certainly observable. These data show the opposite trend from the data recorded in the large scale pyrolysis apparatus. Of course there is a significant difference between the two situations. Consider the locus of resistance to heat transfer in the two cases. There is little doubt that in the large-scale pyrolysis system, the process is conduction-limited. A sample that is partially pyrolyzed and sectioned shows a sharp pyrolysis front separating a black char from a relatively white unpyrolyzed zone. In the case of the samples in the TGA, the process is not conduction limited within the sample. This may be easily shown by considering the Biot number for the sample $Bi = hr/k_s$, where h is the heat transfer coefficient, r is the radius of the sample (treated as an effective sphere) and k_s is its thermal conductivity. Taking h to be governed by the conduction limit, $Nu = hd/k_g = 2$, where d is the diameter of a particle and thus $Bi = k_g/k_s$. Since $k_g \cong 0.2 W/mK$ for helium near 500K, and since k_s for woods (cellulosics) is of the same order of magnitude, then clearly the influence of external heat transfer cannot be neglected since Bi is of order unity. With a few particles in a sample pan, the system is not as well-defined, but the conclusion that external heat transfer limitations can influence results still stands, and a clear relationship between density and rate should not be expected, as was seen in the conduction limited case.

Figures 5 and 6 clearly reveal effects of sample orientation in the bulk samples used in the large scale pyrolysis apparatus. The bulk samples all have a distinctly anisotropic appearance, despite the fact that they are produced by pressing from fine powder. Bands run across the entire diameter of the sample, in a direction perpendicular to the direction from which pressing force is exerted. The band structure reveals itself during pyrolysis as well. When samples are pyrolyzed in which the bands are perpendicular to the incident radiative flux, the samples tend to crack or split in a direction parallel to the bands. In the case in which incident flux is parallel to the bands the cracking is also in a direction parallel to the bands.

Given the anisotropy of the samples there is little surprise then that pyrolysis is affected to some extent by band orientation. As Figure 5 reveals, char yield correlates with band orientation as well as with density in the bulk samples. Care must be exercised in interpreting these results, because what is termed "char" in these experiments in fact includes partially pyrolyzed material, due to existence of heat losses at the back face of the sample. But for present purposes, it is significant that when the volatiles must cross the pressing bands to escape the front surface of the sample, a higher amount of secondary reactions occur than when the volatiles can move parallel to the bands (the secondary reactions, again, are believed to deposit extra char). Note that the volatiles must escape the front face of the sample because the back and sides are enclosed in a ceramic cup.

The effect of band orientation relative to a surface flux is probably somewhat analogous to wood grain orientation to a surface flux. The ultimate effect of such a choice of orientation does not

appear to be very large, in terms of char yield - a percent or two at most in Figure 5. Again, mass transfer effects are seen, but they are not large, just as in the case of the density effect seen with the small samples examined in the TGA. The density effect on char yield appears to be large in the case of the large samples of Figure 5, but again this is probably in large part an artifact induced by the differences in temperature profiles for samples of different density.

The mass loss rate data of Figure 6 suggest that the samples with band structures parallel and perpendicular to the incident flux have roughly comparable mass loss rates at low density ($<0.5 g/cm^3$). Upon increasing the density above 0.7 g/cm^3, there begins to be apparent a slight tendency towards higher rates when the volatiles can move parallel the band structure. As was seen in Table I, the trend towards faster mass loss in parallel samples is not particularly pronounced, so that roughly comparable mass loss rates give rise to the conclusion of roughly comparable rates of thermal wave propagation, irrespective of orientation. The trend is nevertheless consistent with a slight retardation of volatiles escape from samples in which volatiles have to cross the bands.

The importance of with- and cross-band transport was explored in one further experiment. Figure 7 presents the variation of the ultimate char yield with sample width, obtained from thin samples pyrolyzed in a wire gauze reactor. These samples all had a thickness of 2.7 mm and a length of 27 mm, and all had a density of around 1 g/cm^3. The samples were heated at a rate of 60°C/min up to 600°C. The samples were thus thin rectangular parallelopipeds, and had been pressed in the direction of 2.7mm thickness. The pressing direction is again significant, as the work with the larger samples has revealed. There would be expected a slight difference in rates of escape of volatiles in a direction parallel to the main faces of the parallelopiped vs across the faces.

The results of Figure 7 were surprising in the magnitude of the effect they revealed. The work with the narrowest samples (2.3 mm) gave a char yield of just over 5.5%, perfectly consistent with the TGA results shown in Figure 5. Increasing the sample width (while keeping thickness constant at 2.7 mm and length constant at 27 mm) had a surprisingly large effect on char yield. These results strongly suggest that the volatiles in fact have a great deal of difficulty moving cross-band and must move parallel to the band to escape (otherwise the fact that the shortest dimension remained 2.7 mm should have dictated that there be little effect on yield). It should also be remembered that in these experiments the samples were heated from all sides, so a pathway to a cooler zone was not available, as it might be in larger samples.

Thus it must be concluded that the concept of "ultimate char yield" is somewhat meaningless, when applied to samples of characteristic dimensions more than a few millimeters, in view of the results of Figures 5 and 7.

Conclusions

The behaviors of three different materials (purified cellulose, white pine and oak) with different grain orientations and different densities were investigated using different experimental approaches. The behavior of white pine and oak are seen to be quite similar to pure high density cellulose under heat-transfer controlled, fire-like conditions. The role of density is seen in its effect on heat transfer; higher density samples conduct better, and if the process is conduction limited, will pyrolyze faster. The density also affects the ability of volatiles to escape pyrolyzing samples, and this affects both char yields and volatile yields. These effects are considerably less important than the effect of density on heat transfer.

Sample band, or grain, structure also has some small effect on volatiles escape, but again, the effect is small. Sample particle size is seen to be important in several respects, as it influences both heat and mass transfer measurably, even when particles are a few millimeters in size. Applications of TGA data to modeling of fire situations must involve cognizance of such issues.

Acknowledgments

The support from the Center for Fire Research of NIST under grant 60NANB0D1042 is gratefully

acknowledged. Authors deeply appreciate the contribution of Dr H. Teng who performed the TGA/FTIR experiments.

References

1. Lee, C. K., Chaiken, R. F. and Singer, J. M. XVI Symp. (Int) on Combustion, 1976
2. Julien, S., Chornet, E., Tiwari, P. K. and Overend, R. P. Journal of Analytical and Applied Pyrolysis, **19**, 81, 1991
3. Radlein, D., Piskorz, J. and Scott, D. S. Journal of Analytical and Applied Pyrolysis, **19**, 41, 1991
4. Lipowicz, P. J. and Rothenberg, S. J. Combustion and Flame, **75**, 217, 1989
5. Raissi, A. T., Mok, W. S. L. and Antal, M. J. Ind. Eng. Chem. Res., **28**, 856, 1989

Table I: Pyrolysis Wave Speed in Large Scale Apparatus, 40 kW/m^2 flux, as a function of sample density and orientation for Cellulose, Oak and Pine

Orientation	Density (g/cc)	B (g/s)x10^3	B/ρ (cc/s)x10^3
Perpendicular	0.47	5.0	10.6
Perpendicular	0.46	5.3	11.5
Perpendicular	0.70	6.5	9.8
Perpendicular	0.73	7.1	9.7
Perpendicular	1.06	8.0	7.5
Perpendicular	1.06	8.9	8.4
Parallel	0.49	4.7	9.6
Parallel	0.72	8.0	11.1
Parallel	0.72	7.8	10.8
Parallel	0.93	8.3	8.9
Parallel	0.97	9.2	9.5
Perpendicular (Oak)	0.73	7.2	9.9
Perpendicular (Pine)	0.38	2.9	7.6
Parallel (Pine)	0.38	4.9	12.9
			9.8

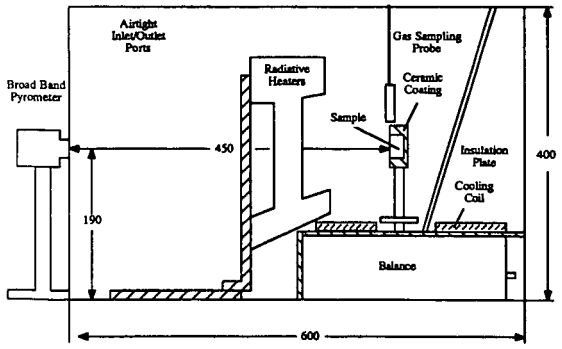

FIGURE 1: LARGE SCALE PYROLYSIS APPARATUS
(All measures in millimeters)

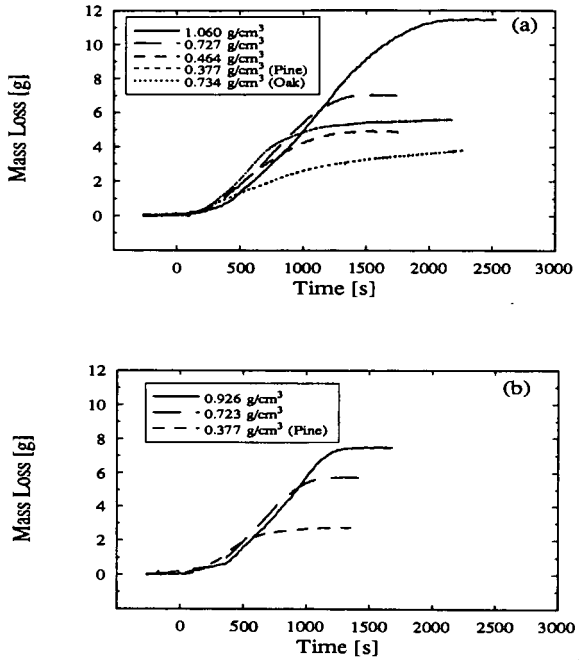

Figure 2: Mass loss as a function of time for (a)-perpendicular and (b)-parallel grain orientation from the large scale apparatus (flux was 40 kW/m^2)

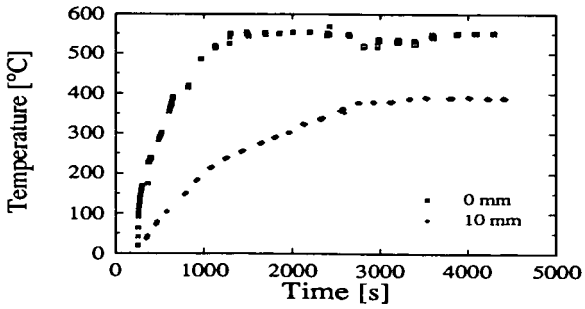

Figure 2c: Typical temperature profiles in a sample pyrolyzed in the large scale apparatus

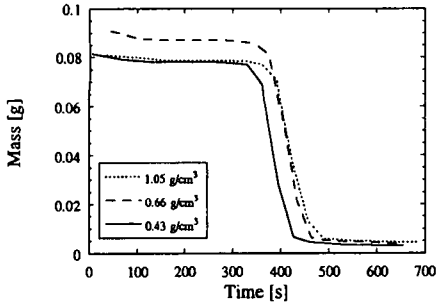

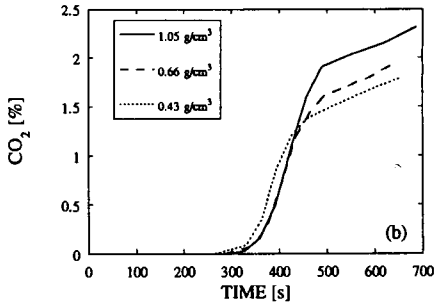

Figure 3: Mass loss as a function of time from the TGA (heating rate was 60°C/min)

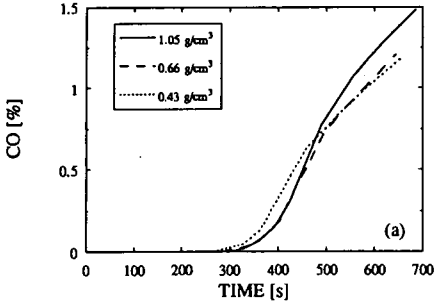

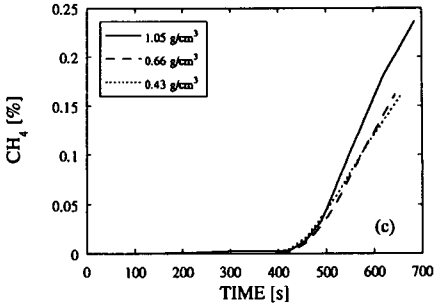

Figure 4: Cumulative amounts of a-CO, b-CO2 and c-CH4 as functions of time from the TGA (heating rate was 60°C/min)

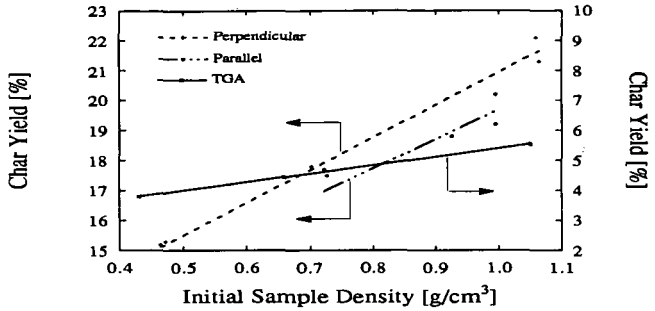

Figure 5: Cellulose char yield as a function of initial sample density for perpendicular and parallel grain orientation from the large scale apparatus and from the TGA

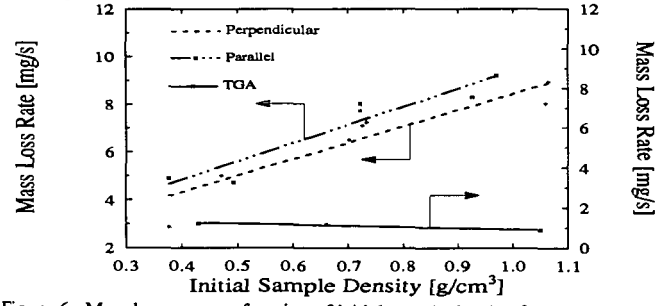

Figure 6: Mass loss rate as a function of initial sample density for perpendicular and parallel grain orientation from the large scale apparatus and from the TGA

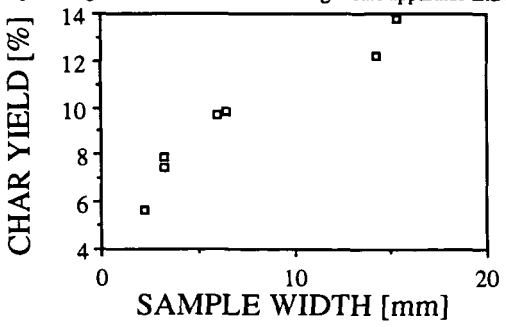

Figure 7: Cellulose char yield as a function of sample width from wire gauze reactor

FLASH HYDROPYROLYSIS OF THE COAL SUPPORTING A CATALYST THROUGH SOLVENT SWELLING

Kouichi Miura, Kazuhiro Mae, Hiroshi Morikawa and Kenji Hashimoto*
Research Laboratory of Carbonaceous Resources Conversion Technology
*)Department of Chemical Engineering
Kyoto University, Kyoto 606, Japan

Key words: Catalytic Hydropyrolysis, Solvent Swelling of Coal, Hydrogen Bonding

INTRODUCTION

Flash hydropyrolysis of coal is expected as a means to recover a large amount of liquid products under rather milder conditions than direct coal liquefaction. However, total coal conversion does not increase even under 10 MPa of H_2 as compared with the pyrolysis in an inert atmosphere. This is because hydrogen does not contribute to the primary coal devolatilization but to the secondary gas phase reaction of primary tar vapors, resulting in the increase in CH_4 yield. Several attempts to increase the coal conversion by use of catalysts such as Ni, Mo, Co, and Fe have not succeeded so far. The catalysts contributed only to the secondary gas phase reaction[1,2]. On the other hand, catalysts such as Zn, Sn and Mo are reported to be very effective to increase both the coal conversion and the liquid yield significantly under slow pyrolysis conditions when the catalysts are in sulfide forms[3-5]. Since Zn, for example, is supported as $ZnCl_2$, it is transformed to ZnS during the slow pyrolysis[6]. However, $ZnCl_2$ can not be sulfided in such a short time during which the primary devolatilization is finished. Summarizing these researches suggests that two conditions must be satisfied for the catalyst to be active during the primary devolatilization of the flash hydropyrolysis of coal: the first one is that the catalyst must be activated or presulfided, and the other is that the catalyst must be in close contact with the functional groups which will be cleaved during the flash pyrolysis.

In this paper a new catalyst supporting method which satisfies the above conditions was presented. The method consists of two steps: the first step is the impregnation of $ZnCl_2$ or $SnCl_2$ from a methanol solution into the micropores of coal by utilizing the swelling of coal induced by methanol, and the second step is the sulfidation of $ZnCl_2$ or $SnCl_2$ in a gas stream containing 5 % of H_2S at room temperature. The coal supporting the catalyst was pyrolyzed by use of a high pressure Curie-point pyrolyzer to examine the validity of the presented supporting method. The coal supporting catalyst was further treated by tetralin at 100 °C to prepare the coal containing both catalyst and tetralin in the swollen coal. The coal treated by tetralin by the above procedure was also prepared. These samples were pyrolyzed to examine the roles of the catalyst and tetralin during the pyrolysis.

EXPERIMENTAL

Catalyst supporting method

An Australian brown coal, Morwell (Ultimate analysis (daf basis): C; 67.1%, H;4.9%, S+O;27.40%) was used as a raw coal. It was ground into the particles less than 70 μm in diameter and dried in vacuo at 110°C for 24 h before use. The catalyst was supported on the coal by the following method:

1. 1.0 g of coal particles were immersed in 0.9 ml of methanol dissolving 0.123 g of $ZnCl_2$ or 0.094 g of $SnCl_2$ at room temperature, and kept for 24 h, by which all the methanol including the metal chloride was incorporated into the coal by swelling it by 32% by volume.

2. Methanol was removed by the vacuum drying almost completely, remaining the metal chloride within the coal. The coal incorporating the metal chloride is still swelling. The sample of this stage is abbreviated to Zn-Swell or Sn-Swell.
3. The Zn-Swell or the Sn-Swell was treated by a N_2 stream containing 5 % of H_2S by volume for 1 h, and was purged by a pure nitrogen stream for 30 min. The sample thus prepared was abbreviated to Zn-S-Swell or Sn-S-Swell.
4. The Zn-S-Swell was further treated by tetralin at 100°C under 1 MPa of N_2, by which the sample was swollen by 35% by volume, and tetralin was incorporated within the sample. This sample was abbreviated to Zn-S-Swell-Tet .

The coal sample supporting Zn by a conventional method was also prepared for comparison. Namely, $ZnCl_2$ was supported on the coal from an aqueous $ZnCl_2$ solution, then the sample was treated by the H_2S containing gas stream as stated above. The sample prepared by this method is abbreviated to Zn-S-Impreg. The amount of catalyst (as metal) in the coal was adjusted to be around 5 wt% on the daf basis for all the samples except for the Zn-S-Swell. The coal sample swollen by tetralin by the procedure 4 was also prepared. It was abbreviated to Tet.

Flash hydropyrolysis

Figure 1 shows a schematic of the experimental setup used for the flash hydropyrolysis. The detail of the high-pressure Curie-point pyrolyzer is shown in Figure 2. The quarts reactor (12 mm OD and 6.0 mm ID) was installed in the pressure vessel made of SUS-316. The inside of the reactor and the pressure vessel were pressurized using the same gas line, then experiments up to 10 MPa were possible in a flowing gas stream.

We have designed the apparatus so that the amount of hydrogen consumed (R_H) as well as each product yield can be measured during the pyrolysis. The procedure for the pyrolysis under 5 MPa of H_2, for example, is as follows: 2 to 3 mg of sample wrapped by a pyrofoil (an Ni-Fe alloy) which has a unique Curie-point temperature was placed in the reactor, and was pressurized up to 5 MPa by a He stream. Hydrogen containing 1 % of N_2 was stored at 5 MPa in a small gas holder (5.0 ml in volume), whose volume was adjusted to purge the reactor for 20 s. The hydrogen was pushed out by the He stream into the reactor by switching the 4-way valve 1. After the sample was exposed to the hydrogen for 5 s it was heated to the Curie-point temperature by the induction coil and kept there for 10 s to be pyrolyzed rapidly. The sample was exposed to the hydrogen for 5 more seconds. The primary tar vapors were all collected by the quarts wool placed just below the sample, because the vapors were cooled immediately by the gas stream. Gaseous products and the unreacted hydrogen were all stored in a product gas holder, and were analyzed to determine the amounts of inorganic gases (N_2, H_2, CO, CO_2 and H_2O) and hydrocarbon gases (CH_4, C_2H_4, C_2H_6, C_3H_6, C_3H_8, C_4H_8, C_4H_{10}, C_5, and C_6 gaseous compounds, benzene, toluene and xylene). The yields of char and tar were measured from the weight change of the sample in the pyrofoil and the reactor. From the analysis of N_2 and H_2 we can know both the hydrogen supplied and the amount of unreacted hydrogen, then we can calculate the amount of hydrogen consumed during the pyrolysis. The pyrolysis temperature was changed from 485 to 920°C by using the pyrofoils which have different Curie-point temperatures.

RESULTS AND DISCUSSION

Physical and chemical changes of coal through the catalyst support

Figure 3 shows the change in the volumetric swelling ratio and the micro pore volume of the Zn-Swell with the increase of the catalyst loading. The micrpore volume corresponding to

0.33 to 1.0 nm in pore diameter was calculated from the CO_2 adsorption isotherm measured at 25°C. Both the swelling ratio and the micropore volume increased with the increase of Zn loading. No such a change was observed for the Zn-S-Impreg. F.T.i.r. measurement of the Zn-Swell showed the increase in the intensity associated with free -OH groups as compared with the raw coal. Methanol is known to break the hydrogen bonds in the coal to produce free -OH groups and swell the coal. Therefore, $ZnCl_2$ in the Zn-Swell is probably retained between the free -OH functional groups which formed hydrogen bondings in the raw coal, which increased the micropore volume and the swelling ratio.

We are expecting that the Zn in the Zn-S-Swell or the Sn in the Sn-S-Swell is transformed into the sulfide by the treatment with H_2S at room temperature, but we could not prove it in spite of several chemical analyses performed. However, we can safely say ZnS is formed judging from the fact that $Zn(OH)_2$ is easily transformed into ZnS by the treatment with H_2S, because $ZnCl_2$ in the Zn-Swell is well expected to be less stable than $Zn(OH)_2$.

Effect of the catalyst supporting method on the pyrolysis yield

Figure 4 shows the product yields obtained by pyrolyzing the samples prepared above at 764°C under 5 MPa of H_2. Although each yield obtained from the Zn-Swell was almost similar as that obtained from the raw coal, the total volatile matter (TVM), the tar yield and the hydrocarbon gas yield of the Zn-S-Swell and Sn-S-Swell were significantly larger than those obtained from the raw coal. Significant decreases in the water yield were found for these two samples. The amount of hydrogen consumed, R_H, of the Zn-S-Swell and Sn-S-Swell were also larger than that of the raw coal. These results indicate clearly that Zn and Sn supported utilizing the solvent swelling and sulfided by H_2S at room temperature contribute to the primary devolatilization reaction. On the other hand, in case of the Zn-S-Impreg, where Zn is sulfided but the coal is not swelling, only the tar yield and the R_H value were slightly larger than those of the raw coal. Therefore, close contact of the catalyst with the coal matrix such as -OH functional groups, which is realized through the solvent swelling, is essential in addition to the sulfidation for the catalyst to contribute the primary devolatilization reaction.

Pyrolysis of the Zn-S-Swell

To examine how the catalyst contributes to the primary devolatilization reaction, the pyrolysis yields of the Zn-S-Swell obtained at different temperatures were compared with those of the raw coal in Figure 5. Within the temperature range where both samples were pyrolyzed, the total volatile matter, the tar yield, the hydrocarbon gas yield of the Zn-S-Swell were larger than those of the raw coal. On the other hand, the yield of water of the Zn-S-Swell was smaller than that of the raw coal. Significant difference was found in the R_H value as shown in the bottom figure. The gaseous hydrogen started to be utilized from around 600°C for the Zn-S-Swell, whereas from around 700°C for the raw coal. These results indicate that the total volatile matter of the Zn-S-Swell was increased by at least two mechanisms. The first mechanism is the acceleration of the hydrogen transfer from the gas phase as clearly shown in the R_H value, and the other is the suppression of the water forming cross-linking reaction, resulting in the increase of the tar yield through the suppression of the condensation reaction.

Roles of the catalyst, hydrogen and tetralin during the primary devolatilization

We have presented a novel flash pyrolysis method in which the coal swollen by a hydrogen donor such as tetralin was pyrolyzed in an atmospheric pressure of N_2[7,8]. Both the coal

conversion and the liquid yield were increased significantly by the method. This was because hydrogen radicals were effectively transferred from/via tetralin to coal fragments, and because the water forming cross-linking reaction was suppressed by the tetralin molecules retained within micropores. In this study we have clarified that hydrogen radicals were effectively transferred from gaseous hydrogen to coal fragments via catalyst if the catalyst was supported properly. Now, we have two hydrogen radical suppliers, hydrogen and tetralin, and two hydrogen radical transfer promoters, the catalyst and tetralin. Therefore, we can expect at least five hydrogen radical transfer paths as shown in Figure 6: (1) from gaseous hydrogen, (2) from tetralin, (3) from gaseous hydrogen via catalyst, (4) from gaseous hydrogen via tetralin, and (5) from tetralin via catalyst. Then we tried to examine the relative magnitude of the five hydrogen radical transfer paths.

Figure 7 shows the pyrolysis yields and the R_H values for 4 samples, the raw coal, the Tet, the Zn-S-Swell and the Zn-S-Tet, pyrolyzed at 764°C under 5MPa of H_2 or He. Helium was used as an inert carrier gas when gaseous hydrogen was not necessary. We will examine the relative magnitude of the 5 paths based on the value of the coal conversion (char yield) first. Three experiments from the left were performed to examine the separate effect of gaseous hydrogen and tetralin. These experiments showed that tetralin and gaseous hydrogen have similar effects. The next three experiments were related to the combined effect of the hydrogen radical supplier and the radical transfer promoter. The relative magnitudes of the paths (3), (4) and (5) are judged to be (5)>(4)>(3) from these experiments. It is interesting to note that the contribution of the path (4) is larger than that of the path (3). The last experiment was performed including the catalyst, tetralin and gaseous hydrogen. From the last four experiments we can judge the path (5) is the most effective to increase the coal conversion. Summarizing the above results, we can say that the order of the relative magnitudes of the 5 paths can be written as

$$(5) > (4) > (3) > (2) \cong (1)$$

Next, we focused our attention on the product distribution and the amount of hydrogen consumed. Hydrogen radicals supplied from tetralin tended to increase the tar yield preferentially, whereas those supplied from gaseous hydrogen increased the hydrocarbon gas yield also as clearly shown in the product distributions. This suggests that the rate and/or the mechanism of the hydrogen radical transfer is different among the gaseous hydrogen and tetralin. The R_H values could be measured for only the experiments performed in H_2 atmosphere. It is clearly shown that the amount of hydrogen consumed increases for the samples supporting the catalyst and/or incorporating tetralin within the coal, indicating that the increases in the coal conversion were realized through the increase in the amount of hydrogen transfer. However, we can not discuss the contribution of tetralin now from the view point of the amount of hydrogen transferred, since we could not measure the amount of radicals transferred from/via tetralin.

CONCLUSIONS

A new catalyst supporting method which enhances the primary reaction of the flash pyrolysis of coal was presented, in which $ZnCl_2$ or $SnCl_2$ was supported from a methanol solution and the chloride was sulfided (activated) by a gas containing H_2S. The catalyst thus prepared enhanced the hydrogen radical transfer from gaseous hydrogen and from tetralin incorporated within micropores of coal, resulting in the increase of the coal conversion and the liquid yield. The relative magnitude of the hydrogen radical transfer paths during the flash pyrolysis was also examined.

REFERENCES

1. Asami, K., Tani, H., Ohtsuka, Y. and Nishiyama, Y., Proceed. of the 26th Conf. on Coal Sci. (Japan), p.220(1989).

2. Yamashita, H., Jinoka, T., Shrotri, Y., Hajima, M., Xu, W.-C. and Tomita, A., Proceed. of the 26th Conf. on Coal Sci. (Japan), p.252(1989).

3. Sulimma, A., Leonhard, P., van Heek, K.H. and Juntgen, H., *Fuel*, **65**, 1457(1986).

4. Bolton, C., Riemer, C., Snape, C.E., Derburshire, F.J. and Terrer, M.T., *Fuel*, **67**, 901 (1988).

5. Snape, C.E., Bolton, C., Dosch, R.G. and Stephens, H.P., *Energy & Fuels*, **3**, 421(1989).

6. Jolly, R., Charcosset, H., Boudou, J.P. and Guet, J.M., *Fuel Process. Techn.*, **20**, 51(1988).

7. Miura, K., Mae, K., Asaoka, S., Yoshimura, T. and Hashimoto, K., *Energy & Fuels*, **5**, 340(1991).

8. Miura, K., Mae, K., Yoshimura, T., Masuda, K. and Hashimoto, K., *Energy & Fuels*, **5**, 803(1991).

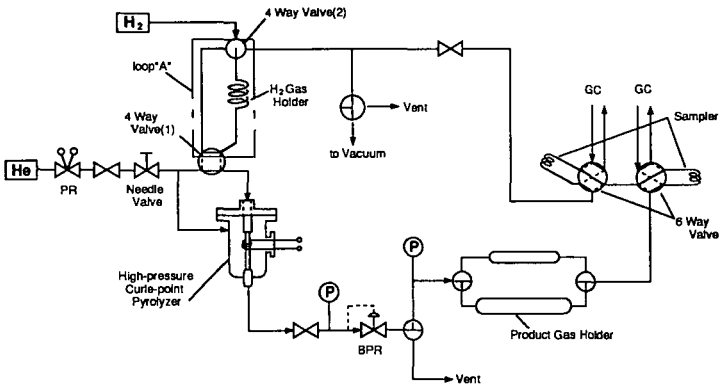

Figure 1 Schematic diagram of experimetnal apparatus

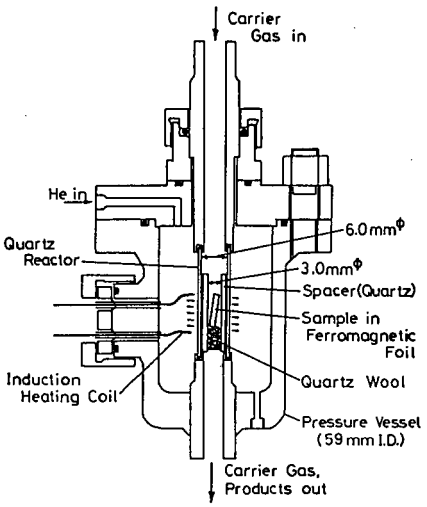

Figure 2 Detail of the high-pressure Curie-point pyrolyzer

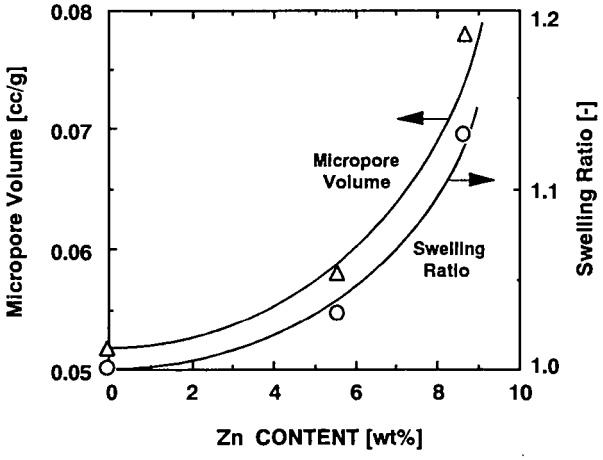

Figure 3 Change in the swelling ratio and the micropore volume with theincrease of the catalyst loading for the Zn-Swell

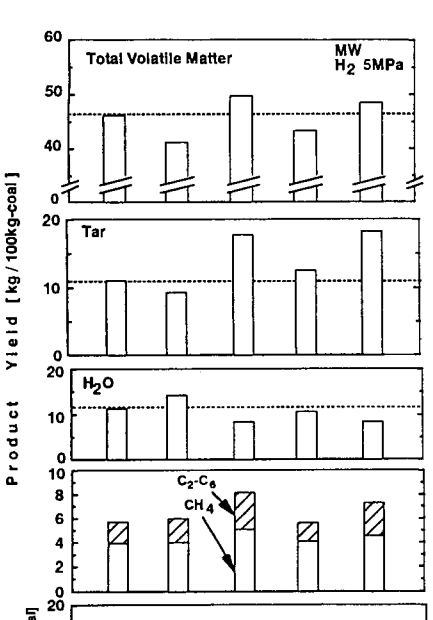

Figure 4 Effect of the catalyst supporting method on the product yield

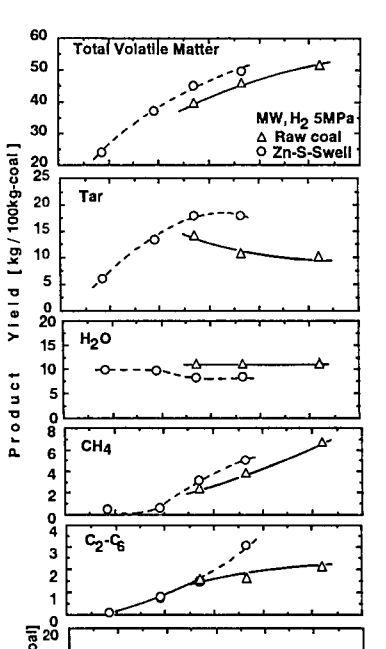

Figure 5 Comparison of the product yields between the raw coal and the Zn-S-Swell at different pyrolysis temperatures

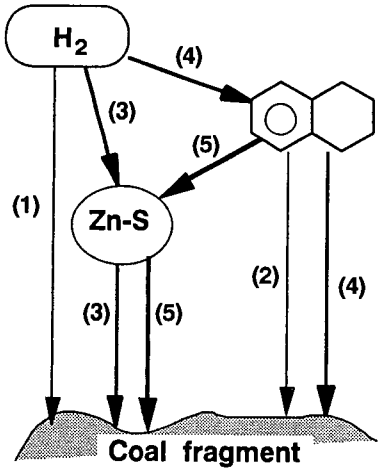

Figure 6 Possible hydrogen radical transfer paths during the flash pyrolysis

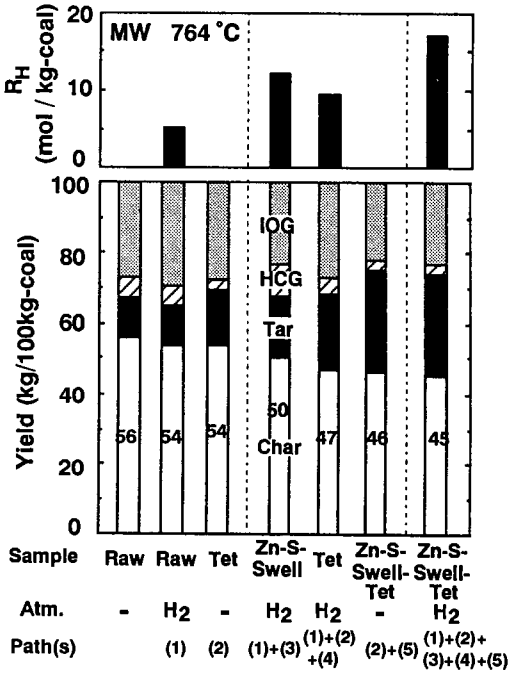

Figure 7 The product yields and the amount of hydrogen consumed for 7 experiments performed for examining relative importance of the gaseous hydrogen, tetralin and the catalyst

EVIDENCE FOR MACERAL SYNERGISM IN CATALYTIC HYDROPYROLYSIS AND HYDROGENATION OF A SUB-BITUMINOUS COAL

Stuart Mitchell[1], Carol McArthur[1], Colin E. Snape[1], Darrell Taulbee[2] and James C. Hower[2]

[1] University of Strathclyde, Dept. of Pure & Applied Chemistry, Glasgow G1 1XL, UK.
[2] University of Kentucky, Centre for Applied Energy Research, 3572 Iron Works Pike, Lexington, KY 40511-8433 ,USA.

Keywords: Maceral concentrates, liquefaction, hydropyrolysis, hydrogenation

ABSTRACT

In order to investigate the possible synergistic effect of exinite on vitrinite conversion in both hydropyrolysis and batchwise (solvent-free) hydrogenation, experiments with and without a sulphided molybdenum catalyst have been conducted on maceral concentrates separated by density gradient centrifugation (DGC) from an Indonesian sub-bituminous coal. As anticipated, the conversions achieved with virtually pure exinite in both catalytic hydropyrolysis (520°C, 150 bar) and hydrogenation (400°C, 70 bar) are close to 100% daf coal. Without catalyst, there is no evidence of synergism in hydropyrolysis. However, with catalyst, the conversions achieved in both regimes with the fractions and blends containing between 25 and 50% exinite are higher than the predicted values (both pyridine and dichloromethane-solubles in hydrogenation).

INTRODUCTION

Although it is now generally recognised that oil yields broadly increase with decreasing rank especially when retrogressive reactions for low-rank coals are avoided by having good contact between coal and solvent [1,2], these ideal circumstances are not realised under other conversion regimes. For example, in hydropyrolysis where there is no vehicle solvent to aid conversion, dispersed catalysts are much less effective for lignites and sub-bituminous coals [3] than for bituminous coals. In such instances, hydrogen transfer within the coal is going to be the crucial factor and, intuitively, this is going to be aided by having a high degree of fluidity and sufficient hydrogen-rich exinite. Indeed, it has been recognised that synergistic effects involving macerals may be evident in coal liquefaction and this has prompted a number of studies on maceral concentrates [4-6]. Care is required in interpreting results since fine grinding normally required to prepare high purity maceral concentrates may induce oxidation. Nonetheless, as anticipated, conversions for exinite concentrates are generally much higher than those for vitrinite [4-6], but appreciable conversions to pyridine and THF-soluble material have been found for inertinite fractions, especially those rich in semi-fusinite [4,5]. Further, conversions for whole coals have been found to be higher than those predicted from individual maceral yields suggesting that synergism occurs from the maceral associations within the coals [4,5]. Indeed, the liquefaction residue from the vitrinite of one of these coals comprised mainly vitroplast which was not evident for the whole coal [4].

Although the above evidence strongly suggests that synergism between macerals can occur at a microscopic scale within coals, there is little information thus far on the influence of liquefaction conditions on the extent to which this phenomenon occurs. However, hydropyrolysis tests on handpicked durain and fusain samples from a UK bituminous coal have indicated that exinite only promotes vitrinite conversion in the presence of catalyst [3]. In order to investigate this aspect further in both hydropyrolysis and batchwise (solvent-free) hydrogenation, experiments with and without a sulphided molybdenum (Mo) catalyst have been conducted on maceral concentrates separated by density gradient centrifugation (DGC) from an Eocene sub-bituminous coal from Indonesia. This coal has a high exinite and low inertinite content which facilitated the separation of relatively pure exinite and vitrinite fractions with + 400 mesh particles size required for hydropyrolysis to prevent the fixed-bed reactor plugging.

EXPERIMENTAL

The Indonesian sub-bituminous coal was obtained from the US Geological Survey. The coal was crushed to -100 mesh, demineralised with hydrofluoric and boric acids [7] and dry screened to + 400 mesh. Maceral separation was based on the density gradient centrifugation (DGC) method developed by Dyrkacz and co-workers [8] with certain modifications [7]. Briefly, the DGC separation involves forming forming a cesium chloride density gradient within a spinning, high capacity (2 dm^3) centrifuge rotor. A demineralised coal/surfactant slurry is then dispersed across this gradient at forces ranging from 7,000 to 25,000 gravity. The procedure can be repeated numerous times with the corresponding fractions from repeat runs being combined to provide sufficient sample. In this study, two preliminary DGC runs were carried out on 16.2 g of sample. This provided a density profile curve to design a more efficient larger scale separation which was conducted on 225.1 g of coal in a series of 15 DGC runs, the recovery being 98.5%. The rotor effluent was divided into 12 density fractions plus the remaining sink fraction. The results of chemical and petrographic analysis on the initial coal and the fractions actually used in the hydropyrolysis and hydrogenation experiments are listed in Table 1.

For the hydrogenation and hydropyrolysis experiments with the sulphided Mo catalyst, the maceral concentrates and their blends were impregnated with ammonium dioxydithiomolybdate in methanol solution to give a Mo loading of 1%. The fixed-bed hydropyrolysis apparatus in which the reactor tube is heated resistively has been described previously [3, 9,]. A temperature of 520°C and a pressure of 150 bar were chosen as the standard test conditions to optimise both the tar yield and selectivity (% tar/% gas) in catalytic hydropyrolysis [3,9]. To simplify the mass balances, dried coals were used (50°C *in vacuo* for 1 hr.). Tests were carried out on 2-5 g of sample which was mixed with of sand (1:2 mass ratio) to prevent blockages and to enable the reactor tube to be emptied easily. The reactor were heated at 5°C s^{-1} and held at 520°C for 10 minutes with a hydrogen flow rate of 10 dm^3 min^{-1} (measured at atmospheric pressure and ambient temperature) which was sufficient to overcome mass transfer. Char yields were determined from the weight loss of the reactor tube and tar yields from the weight gain of the dry-ice cooled trap. Tar was recovered for analysis by washing the trap thoroughly with dichloromethane (DCM).

The hydrogenation experiments were carried out in a 9/16" O.D. microautoclaves (*ca* 10 cm^3 internal volume) constructed of Autoclave Engineer high pressure fittings. 0.3 g of sample was loaded into the microautoclave which was pressurised to 70 bar with hydrogen. The sandbath at 400°C was raised to fully submerge the microautoclave for 60 min., the heat-up period being *ca* 5

min. After reaction, the microreactor was cooled in dry-ice before de-pressurising. The reactor contents were then recovered by filling the microreactor with dichloromethane (DCM) and placing it in an ultrasonic bath. The DCM washings were refluxed for *ca* 5 hours, filtered through phase separating paper and then the DCM-solubles were recovered by evaporating the filtrate to dryness. The DCM-insolubles were weighed after drying *in vacuo* and were then refluxed in pyridine for *ca* 5 hours and filtered to determine the yield of pyridine-insolubles.

RESULTS AND DISCUSSION

Hydropyrolysis

Figure 1 shows the effect of exinite concentration on conversion in hydropyrolysis with and without catalyst for the maceral concentrates and one of their blends. As anticipated, the conversion achieved with virtually pure exinite (fraction 1) in catalytic hydropyrolysis is close to 100% daf coal. Without catalyst, there is no evidence of synergism with the conversions lying close to the predicted values from those obtained with virtually pure exinite and the concentrates containing 90% vitrinite (fractions 5 and 6, Figure 1). However, with catalyst, the conversions achieved with the fractions containing between 25 and 50% exinite generally appear to be higher than the predicted values; above 50% exinite, the experimental error of ± 1-2% is greater than the differences anticipated making synergistic effects more difficult to identify. Since the two fractions, 5 and 6 which both contain *ca* 90% vitrinite give conversions differing by 5 % daf coal, it is difficult to deduce a baseline conversion for vitrinite. Further, synergism may be evident within these fractions as they contain 10% exinite (Table 1). However, the fact that the conversion with catalyst for the 50:50 blend of fractions 1 and 6 is higher by 5% daf coal than that predicted from the individual conversions confirms that the effect is real.

Hydrogenation

Figure 2 presents the yields of DCM-soluble product and pyridine-insolubles obtained in catalytic hydrogenation using essentially the same fractions and, again, there is clear evidence of synergism. The fact that it is evident in both the yields of DCM-soluble oil and pyridine-insolubles indicates that both the inital dissolution process and subsequent hydrocracking of the primary dissolution product are affected. Indeed, the synergistic effect is somewhat more pronouced than in catalytic hydropyrolysis possibly due to the longer residence time and the more effective contact between exinite and vitrinite in catalytic hydrogenation.

General discussion

The synergistic effects reported here are perhaps more evident than in hydroliquefaction where the presence of a vehicle solvent aids hydrogen transfer. Clearly, in both batchwise hydrogenation and hydropyrolysis, the exinite plays a crucial role in transferring hydrogen atoms from the catalyst sites to the depolymerising coal probably because it forms a fluid pyrobitumen in the early stages of conversion. For hydropyrolysis, the general trends found here are the same as those reported previously for a UK bituminous coal containing 87% dmmf C [3]. However, the reasons why lower conversions than anticipated are obtained in catalytic hydropyrolysis for the higher rank bituminous coals and most of the low-rank coals investigated thus far [3] are somewhat different. The low-rank coals do not soften to an appreciable extent and there is probably insufficient pyrobitumen generated in the early stages of conversion to prevent retrogressive reactions occurring which probably involve dihydric phenolic moieties. For the bituminous coals containing more than *ca* 84% dmmf C, the hydrogen requirement required for hydrogenating the aromatic structures is likely to be higher than for their lower rank counterparts and, despite the development

of plasticity at some stage during conversion, there is still insufficient hydrogen transfer capability to prevent retrogressive condensation reactions occurring.

ACKNOWLEDGEMENTS

The authors thank the European Community (Contract No. EN3V-0048-UK(H)), the US Department of Energy and Commonwealth of Kentucky for financial support.

REFERENCES

1. C.E. Snape, *Fuel Process. Technol.*, **15**, 257.(1987).
2. R.M. Baldwin, *Prepr. Am. Chem. Soc. Div. Fuel Chem.*, **34(3)**, 787.(1989).
3. C.E. Snape and C.J. Lafferty, *Prepr. Am. Chem. Soc. Div. Fuel Chem.*, **35(1)**, 1 (1990).
4. R.A. Keogh, B. Chawla, D. Taulbee and B.H. Davis, *Proc. 1989 Int. Conf. on Coal Sci.*, 683.
5. S. Parkash, K. Lali, M. Holuszko and M.P. Du Plessis, *Liquid Fuels Technol.*, **3(3)**, 345 (1985).
6. J. Pajek, *Fuel Process. Technol.*, **21**, 245 (1989).
7. D.N. Taulbee, S.H. Poe, T.L. Robl and B. Keogh, *Energy & Fuels*, **3(6)**, 662 (1989).
8. G.R. Dyrkacz and E.P. Horwitz, *Fuel*, **61**, 3 (1982).
9. C.E. Snape, C.J. Lafferty, S. Mitchell, F. Donald, C. A. McArthur, G. Eglinton, N. Robinson and R. Collier, *Final Report, EC Project EN3V-0048-UK(H)* (1991).

Table 1 Elemental, proximate and petrographic analysis of maceral concentrates

		Parent coal	Maceral fraction 1	2	3	4	5	6
Density range, g cm^{-3}			1.12-1.15	1.15-1.18	1.20-1.25	1.25-1.26	1.26-1.27	1.27-1.28
% moisture		1.5	0.6	0.9	1.5	1.8	2.3	1.9
% ash, dry basis		0.4	1.4	1.2	0.7	1.0	0.6	1.3
% V.M., daf basis		58.9	67.0	65.0	55.9	51.0	49.6	48.3
% dmmf	C	79.2	80.1	80.2	78.5	77.0	76.5	76.6
	H	7.2	8.2	7.9	6.8	6.4	6.1	6.0
	N	0.6	0.6	0.9	0.6	0.7	0.7	0.7
% dmmf	Exinite	39.8	97.8	95.2	52.6	22.4	10.0	9.8
	Vitrinite	54.4	1.8	3.4	46.8	77.2	89.4	89.0
	Inertinite	5.6	0.4	1.2	0.6	0.4	0.6	1.2

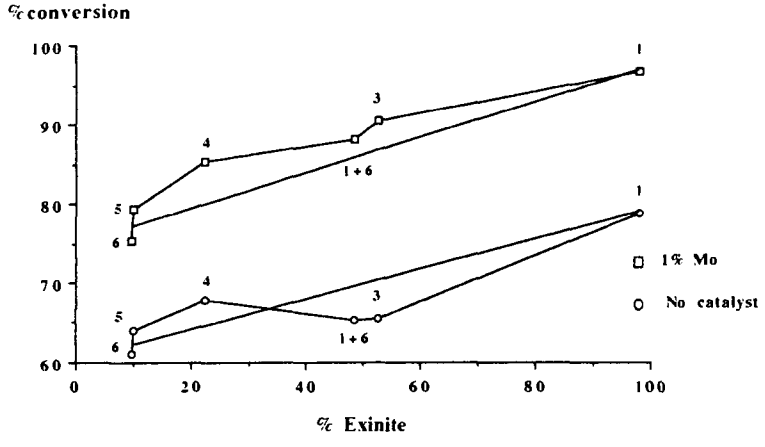

Figure 1. Effect of exinite concentration on hydropyrolysis conversions using maceral concentrates

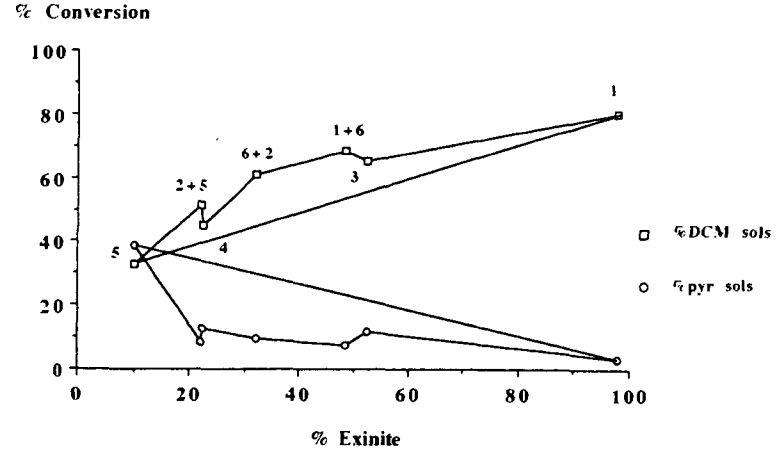

Figure 2. Effect of exinite on catalytic hydrogenation yields using maceral concentrates

EVALUATION OF FACTORS INFLUENCING THE THERMAL MATURATION OF ORGANIC MATTER DURING CONFINED PYROLYSIS EXPERIMENTS.

Raymond MICHELS, Patrick LANDAIS,
Marcel ELIE, Laurence GERARD and Laurence MANSUY.

CNRS-CREGU - BP 23, 54501 Vandoeuvre Cedex. FRANCE.

Key Words : Pyrolysis, Water, Pressure

INTRODUCTION

Pyrolysis of organic matter can be dedicated either to investigate its chemical structure or to mimic the transformations induced by subsidence in sedimentary basins i.e. thermal maturation. Reproducing natural geological conditions has been for a long time strictly considered as a matter of time and temperature. More recently, the roles of water, pressure, mineral content and type of autoclave have been investigated. However, few studies offered the opportunity to adjust and control these different parameters in order to evaluate their respective influence on the thermal maturation of kerogens and source-rocks. The present paper summarizes the results of confined and hydrous pyrolysis experiments dedicated to re-evaluate the validity of the technique and determine the influence of the experimental conditions.

EXPERIMENTAL

Confined Pyrolysis : 200 mg of kerogen or 1-1.5 g of source-rock are introduced in gold tubes (ø = 0.5 or 1 cm; L = 5 cm) under argon atmosphere. The sealed gold tubes are placed in stainless steel autoclaves and isothermally heated at temperatures ranging between 250 and 400 °C for 72 hours under pressures ranging between 300 and 1300 bars (1). At the end of each run, gold tubes are pierced and their organic content washed and extracted with chloroform.

Hydrous Pyrolysis : about 400 mg of rock are isothermally heated for 72 hours in a stainless steel autoclave in the presence of an excess of liquid water. The rock sample is covered by pure liquid water and the headspace is filled with helium (2). The pressure inside the autoclave is due to the expansion of water and to the generation of oil and gas but rarely exceeds 330 bars. The theoretical maximum pyrolysis temperature is limited by the supercritical temperature of pure water (374 °C) and generally set to 350 °C because of the generation of CO_2 and hydrocarbons. At the end of each run, the autoclave is cooled, gases are collected, floating oil (expelled oil) recovered and rock chips collected for subsequent extraction.

High Pressure Hydrous Pyrolysis : Because in conventional hydrous pyrolysis devices, internal pressure depends on the initial filling of the autoclave (water + rock) and on the temperature, high pressure hydrous pyrolysis runs were performed in order to test the effect of increasing pressures on the hydrocarbons expulsion and generation. The use of a high pressure system (pump + autoclave) allows water to be injected inside the autoclave as soon as the isothermal stage is reached and to adjust the pressure to the desired value (300, 700 and 1300 bars in the present work). The recovery of oil and gas is similar to that described for conventional hydrous pyrolysis.

TEMPERATURE CHOICE

Most of the artificial maturation series are generated using temperature steps of 30 to 50 °C. Nevertheless, in order to describe the complete thermal evolution of an immature organic matter, it can be necessary to perform more pyrolysis runs (3). For example, the different maturation stages of a Mahakam coal were fully evidenced only when using a 10 °C pyrolysis step. The maximum generation of polar compounds, aromatics and saturates occuring at 320, 330 and 340 °C respectively. Similarly, this was the only way to define the chronology of the transformations affecting both the solid residue and the soluble fraction.

CHOICE OF THE TIME-TEMPERATURE PAIR

In order to compensate geological times, pyrolysis experiments use higher temperatures than those noticed in natural environments. Several hours to several years experimentations have been carried out and generally show that long term experiments improve the quality of the simulation. On the other hand, comparison of the analytical data derived from 5 hours to 100 days experiments on an immature Mahakam coal has evidenced the influence of time-temperature pairs on the composition of both solid residues and $CHCl_3$ extracts. It is shown that saturates content increases with experimentation time (4). As far as $CHCl_3$ extract / TOC ratios are similar for a given Time Temperature Index (Arrhenius TTI), such evolution evidences the increasing effect of secondary cracking in long term experiments. Furthermore, the expulsion of oil from source-rock is enhanced in long term experiments (Paris Basin shale).

KEROGEN vs. WHOLE ROCK

Heating experiments can be performed either on whole rock or on kerogen concentrates. While kerogen pyrolysis allows more structural parameters to be investigated and catalytic effects to be ignored, whole rock pyrolysis takes into account the transformation of all the rock components

(organic + mineral) (5, 6). However, kinetics of clay minerals transformations cannot generally be extrapolated to temperatures higher than 300 °C and organo-mineral interactions are not easily duplicated. Then, the extent of the modifications of the maturation process related to the behaviour of the mineral matrix cannot be accurately determined. Results from confined-pyrolysis experiments on the Woodford shale have shown that the peak generation of hydrocarbons as well as the onset of the petroleum potential decrease always occur earlier for kerogen than for whole rock (Figure 1).

EFFECTS OF PRESSURE

The role of pressure in the simulation of organic matter thermal maturation has not been widely investigated. However, recent results have demonstrated that the rates of hydrocarbon cracking (7) as well as the activation energy (8) were pressure dependant. It is generally accepted that increasing pressures induce a delay in oil genesis and in kerogen transformation (9). In the present work the role of pressure has been studied in both confined and hydrous pyrolysis systems.

The effects of pressure on isolated kerogen or coal transformation are minor and necessitate a careful control of temperature (± 1°C) to be shown. No clear variations in the extract yield or in the Rock-Eval HI and Tmax have been noticed. However, a bimodal distribution of n-alcanes has been observed on GC traces for low pressure experiments (300 bars) on a type II kerogen. Furthermore the pristane/phytane ratios are systematically lower in high pressure experiments (1300 bars) whereas the evolutions of the Pr/nC17 and Ph/nC18 ratios are not pressure dependant. Similar results have been obtained when increasing the dead volume in gold tubes by decreasing the amount of kerogen (Mahakam coal) to be pyrolyzed from 200 mg to 50 mg. Spectroscopic studies of total extracts (^{1}H NMR, ^{13}C NMR, IR and synchronous UV fluorescence) also allowed pressure-dependant structural parameters to be recognized.

High pressure hydrous pyrolysis experiments on whole rock (Woodford shale) revealed that amounts of expelled oil and total yield (expelled + extracted) were highly dependant on pressure. Figure 2 confirms that high water pressure delays and hinders the genesis and expulsion of hydrocarbons. On the other hand, results from confined pyrolysis did not reveal an important control of pressure neither on the genesis nor on the expulsion of oil. The total yields maxima are similar but can be shifted of 50 °C (Figure 3) while expulsion maxima occur at the same temperature (330°C).

EFFECT OF WATER

The effect of water on the artificial maturation of organic matter is still a subject of controversy. Addition of water in confined experiments on Mahakam coals did not seem to give detectable effects (10). On the other hand, the role of water during organic compounds pyrolysis has been frequently emphasized (11).

Such situation can probably be related to the unavailability of analytical data derived from hydrous and confined pyrolysis experiments performed on the same rock and in the same P-T-t conditions. Furthermore the analytical procedures for oil and gas recovery as well as shale extraction cannot be identical for both types of pyrolysis. For example, the "expelled fractions" corresponding to floating oil and to cold chloroform washing in hydrous and confined pyrolysis respectively cannot be simply compared.

As far as pressure can be controled, experiments conducted in a high pressure hydrous pyrolysis system can be compared to those performed in confined pyrolysis. On Figure 4 are reported the expelled/washed as well as extracted fractions obtained on hydrous and confined Woodford shale pyrolyzates at 700 bars. Despite some discrepancies concerning the maximum temperature for extract yield, a general agreement can be noticed in the trends as well as in the amounts of generated and expelled hydrocarbons. Similarly, the addition of water in gold tubes (10, 50 and 100 wt % of shale) did not significantly modify the oil expulsion rate. However, when hydrous pyrolysis experiments are carried out in low pressure conditions (P<200 bars), the total oil yield is much more important than in confined and high pressure hydrous pyrolysis systems (see Figure 2, open circles).

SUMMARY

The examination of various sets of data deduced from organic matter pyrolysis in closed systems (confined and hydrous) revealed that experimental conditions must be carefully defined:

- A wide range of temperatures can be useful in order to determine the various stages of hydrocarbons generation and kerogen transformations.
- Long term experiments induce secondary cracking reactions that chiefly affect polar compounds.
- Pressure effects on oil generation and expulsion in confined pyrolysis system are not as determinative as in hydrous pyrolysis. However, variations of external pressure as well as effluents pressure can significantly modify the distribution of the generated hydrocarbons.
- In order to evaluate the role of water in organic matter maturation, hydrous and anhydrous pyrolysis must be conducted in the same experimental conditions (temperature, pressure, time).
- When performed in the same T-P-t conditions, confined and high pressure hydrous pyrolysis can generate and expell similar amonts of hydrocarbons.

These observations strongly suggest to take into account other experimental parameters than time and temperature when simulating organic matter thermal maturation. They also support further work on the comparison of the different pressurized pyrolysis systems used to reproduce the natural transformations of organic matter.

Anowledgements

The present work has benefited from the financial and technical supports of the Oklahoma University (USA), AMOCO (USA), CNRS (France) and DBT program 91/ATP/645.

REFERENCES

1. Landais P., Michels R., Poty B. and Monthioux M. J. Anal. Appl. Pyrol., 16, 1989, pp 103-115.
2. Lewan M.D., Winters J.C. and MCDonald J.H. Science, 203, 1979, pp 897-899.
3. Wenger L.M. and Price L.C. In "Organic geochemistry, advances and applications in the natural environment", 1991, D.A.C. Manning ed., Manchester University Press, pp 335-339.
4. Landais P. Org. Geochem., 17, 1991, pp 705-710.
5. Horsfield B. and Douglas A.G. Geochim. Cosmochim. Acta, 44, 1980, pp 1119-1131.
6. Huizinga B.J., Tannenbaum E. and Kaplan I.R. Org. Geochem., 50, 1987, pp 591-604.
7. Dominé F., Maquaire P., Muller C. and Côme G. Energy and Fuels, 4, pp 2-10.
8. Carr A.D. In "Organic geochemistry, advances and applications in the natural environment", 1991, D.A.C. Manning ed., Manchester University Press, pp 285-287.
9. McTavish R.A. Nature, 271, 1978, pp 648-650.
10. Monthioux M., Landais P. and Durand B. Org. Geochem., 10, 1985, pp 299-311.
11. Siskin M. and Katritzky A.R. Science, 254, 1991, pp 231-237.

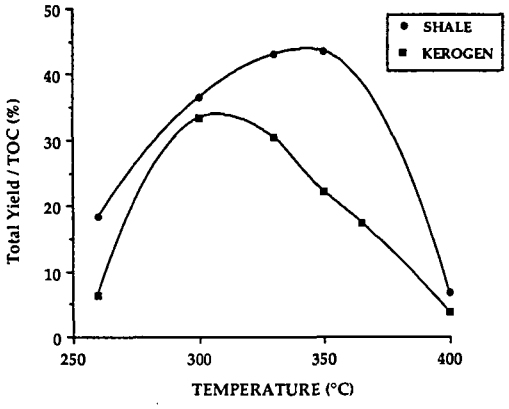

Figure 1: Comparison of the total yield evolution during the confined pyrolysis of type II shale and extracted kerogen

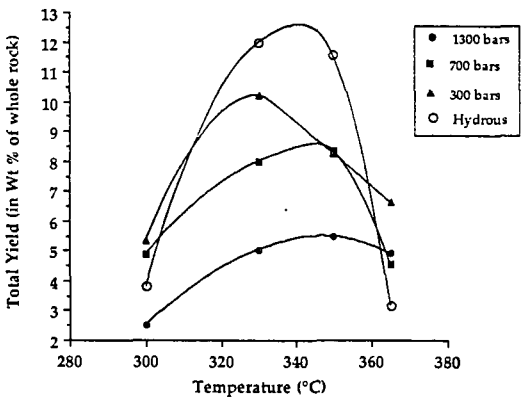

Figure 2: Effect of pressure on oil generation during hydrous and high pressure hydrous pyrolysis of a Woodford shale.

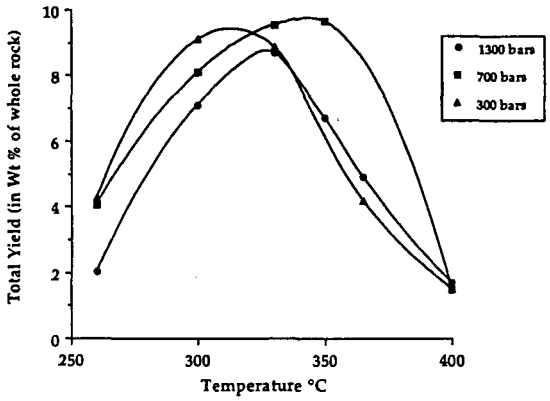

Figure 3 : Effect of pressure on the generation of hydrocarbons during the confined pyrolysis of a Woodford shale.

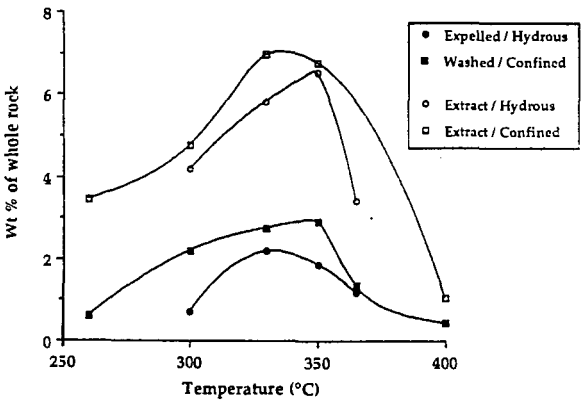

Figure 4: Comparison of the evolution of generated and expelled fractions during the high pressure hydrous and confined pyrolysis at 700 bars.

ARTIFICIAL MATURATION OF COAL AND MACERAL CONCENTRATES: SATURATE AND POLYAROMATIC MOLECULAR MARKERS

Michael A. Kruge[1] and Patrick Landais[2]

[1]Department of Geology, Southern Illinois University, Carbondale, IL 62901, USA
[2]GS CNRS-CREGU, BP 23, 54501 Vandoeuvre-lès-Nancy cedex, France

Keywords: Coal macerals, pyrolysis, polyaromatic hydrocarbons

ABSTRACT

A sample from the "Simon" coal bed (Lorraine Basin, France) was separated into its constituent macerals vitrinite, exinite and inertinite by density gradient centrifugation. Aliquots of the macerals and whole coal were sealed in gold tubes with no added water and pyrolyzed separately at 350, 375, 400 and 450 °C for 24 hr at 100 MPa. The distributions of *n*-alkanes in the pyrolyzates are profoundly affected by pyrolysis temperature and sample type, but hopane and sterane distributions show little variation. The classic maturity parameters based on sterane isomerization are particularly ineffective. In contrast, distributions of polyaromatic hydrocarbons (PAH) change dramatically as a function of pyrolysis temperature. A variety of maturity-sensitive ratios are shown to be efficacious, including those employing dimethylphenanthrenes and methylpyrenes. These PAH ratios work particularly well for vitrinite pyrolyzates. For exinite pyrolyzates, the PAH ratios consistently show little change between 350 and 375°, but by 400° the ratios operate effectively.

INTRODUCTION

Slow, confined pyrolysis is often called upon for laboratory simulation of the thermal maturation of organic matter. The chief variables in confined pyrolysis experiments include temperature, duration of heating, the use of isolated kerogen *vs.* a kerogen/mineral mixture (natural or artificial), hydrous *vs.* anhydrous conditions, and the use of metal *vs.* glass reactors[1-7]. Confined pyrolysis provides a better simulation of natural petroleum generation in that its products lack the *n*-alkenes characteristic of open pyrolysis methods. While several studies have used open pyrolysis techniques in the characterization of isolated coal macerals[8-10], the present work is an attempt at confined pyrolysis of macerals, with the objective of observing of the effects of temperature and starting material type on distributions of saturate and, especially, aromatic hydrocarbons.

METHODS

The sample employed in the study is from the "Simon" coal bed (Lorraine Basin, France), petrographically determined to be 74% vitrinite, 13.2% inertinite, 5.5% exinite and 7.3% mineral matter[11]. Maceral separation by density gradient centrifugation[12] was performed on hand-picked lithotype concentrates. The resulting isolated macerals were vitrinite, inertinite (predominantly semifusinite and fusinite), and exinite (mainly sporinite and resinite). The pyrolytic and liquid chromatographic techniques used in this study have been previously described[11,13]. In brief, isothermal confined pyrolysis experiments in sealed, thin-walled gold tubes were run on 150 mg aliquots of the raw coal and of each of the three isolated macerals at temperatures of 350, 375, 400 and 450 °C for 24 hours at 100 MPa. The saturate and aromatic fractions of the pyrolyzates were analyzed by a Hewlett Packard 5890A gas chromatograph, coupled to an HP 5970B Mass Selective Detector (GCMS). The GC was held

initially at 100° C for 10 min., then raised to 300° at 3°/min., where it was held for 21 min. (saturates) or 5 minutes (aromatics). A 25 m OV-1 column with 0.2 mm inside diameter and 0.33 μm film thickness was employed. The mass spectrometer, using an ionization energy of 70 eV, was run in selective ion monitoring mode, collecting data on the principal fragment ions of biological marker compounds and on the molecular ions of the polyaromatic compounds.

RESULTS AND DISCUSSION

The normal alkane distributions vary considerably as a function of starting material and pyrolysis temperature. The 350° pyrolyzate of the whole coal shows a broad maximum in the C_{22} to C_{27} region, with a slight odd carbon number preference. There is a increasingly severe depletion of higher molecular weight *n*-alkanes as one progresses to the 375° and on to the 400° runs. The *n*-alkane concentrations in the 450° pyrolyzate are extremely low. The exinite *n*-alkane distributions for both the 350 and 375° runs are essentially the same and are very similar to the 350° whole coal run, except that they lack the odd carbon number preference. By 400° however, the exinite pyrolyzate shows a marked shift towards lower carbon numbers, roughly comparable to the 375° coal. Normal alkane distributions in the 350 and 375° vitrinites are also very similar to one another, having a maximum at C_{19}. They bear a strong resemblance to the 375° coal. By 400°, the overall concentration of *n*-alkanes decreases. The *n*-alkane distributions in the 350 and 375° inertinite pyrolyzates are very similar to one another, with a maximum at C_{21} and a slight odd carbon predominance. When compared to other samples, they most closely resemble the 400° vitrinite. The high temperature destruction of *n*-alkanes sets in at 400° for the inertinite. The yields of the 450° inertinite experiment were too low for analysis. Overall, there is a loss of higher molecular weight *n*-alkanes as pyrolysis temperatures increase. As higher temperatures ($\geq$ 400°) are reached, general destruction of *n*-alkanes occurs. 400° exinite resembles 375° coal and vitrinite. In turn, 400° vitrinite bears similarities to 350 and 375° inertinites. Thus, those samples richer in pyrolyzable and extractable organic matter lag behind the leaner in thermal alteration effects.

The hopane distributions show little variation among the samples, either as a function of temperature or starting material type. Lack of difference in hopane distributions in pyrolyzates of the macerals from a single coal is expected, because their bacterial precursors would have inhabited all macerals in the freshly deposited peat[14]. The steranes are a relatively minor component of the pyrolyzate saturate fractions. The sterane distributions within one sample vary even less than those of the hopanes as a function of organic matter type and level of thermal alteration. Consequently, the standard sterane maturation parameters[15] are ineffective, with the partial exception of the C_{29} ($\alpha\beta\beta/(\alpha\alpha\alpha + \alpha\beta\beta)$) ratio for exinite.

A wide variety of polyaromatic molecular marker compounds are readily detectable in the aromatic fractions of the pyrolyzates, by setting the GCMS to monitor their molecular ions, which are often the strongest peaks in their mass spectra. These compounds include homologues and isomers of naphthalene, phenanthrene, dibenzothiophene, pyrene, fluoranthene and chrysene, as well as several pentaaromatic hydrocarbons. The distributions of these compounds exhibit profound changes due to thermal alteration. Aromatic steroids are among the most frequently employed aromatic molecular markers[16]. However, in this study they are not discussed, as C_{26}-C_{28} triaromatic steroids were detected in only 4 samples and monoaromatics were not detected at all. For the sake of brevity, only two groups of compounds are covered in this paper — the dimethylphenanthrenes and methylpyrenes, along with their isomers. A fuller discussion will be presented elsewhere[17].

Figure 1a presents an example of a partial m/z 206 mass chromatogram showing the distribution of dimethylphenanthrenes, ethylphenanthrenes and dimethylanthracenes, identified and, for simplicity, labelled as peaks 206a through 206j. In figure 1b, the quantitation results from the m/z 206 data for each of the vitrinite and exinite experiments are presented.

Excluding the ethylphenanthrene and dimethylanthracene peaks 206a, b and e, it can be seen that dimethylphenanthrene peaks 206c and d increase with pyrolysis temperature, while peaks 206f, g, h and i decrease. This phenomenon is shown in ratio form (fig. 1c), in which the ratio increases smoothly with temperature for vitrinite. There is little increase in the exinite ratio between 350 and 375°, but by 400°, the exinite value has nearly overtaken the vitrinite. The exinite ratio shows little further increase at 450°. The behavior of this ratio is in strong contrast to the commonly employed methylphenanthrene index[18], which increases from 350 to 400° for these samples, but drops sharply by 450°. Similar dimethylphenanthrene ratios have previously been employed[19,20].

The data from the m/z 216 partial mass chromatograms, showing distributions of methylpyrenes and methylfluoranthenes, are presented in figure 2 in a fashion analogous to that of figure 1, except that specific isomer assignments were not possible, due to the lack of standards and published identifications. Peak 216b increases with pyrolysis temperature, while peaks 216e and f decrease markedly. The resulting ratio (fig. 2c) increases nicely for vitrinite over the entire 350 to 450° temperature range. In contrast, the increase in the exinite ratio is delayed until temperatures climb above 375°, giving a curve very similar to the dimethylphenanthrene ratio (fig. 1c). Methylpyrenes have been previously used as thermal alteration indicators, but employing Shpol'skii spectral data, rather than GCMS[21].

Among the differences between vitrinite and exinite, the most profound is the delay in maturation response of the exinite between 350 and 375°, corresponding to the temperatures at which it is generating the most pyrolyzate[11]. This phenomenon is consistently detected by both Rock Eval and molecular parameters. The recognition of maturity-independent molecular characteristics is also desirable, but difficult in this case, since the range of thermal alteration levels is so great, and the effects of temperature so all-pervasive. However, some success may be expected in differentiating exinite and vitrinite, since their macromolecular structures are so dissimilar. Very little difference is apparent among saturate biomarkers, either due to maturity or organic matter type. For polyaromatic compounds, subtle features which differentiate the vitrinite and exinite pyrolyzates are worthy of note. Peak 206h (1,7-dimethylphenanthrene, also known as pimanthrene) appears relatively stronger in exinite than in vitrinite (fig. 1b). Among methylpyrenes and methylfluoranthenes, peak 216c is also stronger in exinite than in vitrinite pyrolyzates (fig. 2b). Peaks 206h and 216c are minor features on their respective mass chromatograms and the differences tend to be lost by 450°. It would be of interest to examine a greater variety of maceral types from other coals and kerogens by the same methods, to determine if PAH distributions have greater potential for organic matter type differentiation than is apparent in this study.

CONCLUSIONS

1) The distributions of *n*-alkanes in the pyrolyzates are profoundly affected by pyrolysis temperature and sample type, but hopane and sterane distributions show little variation. The classic maturity parameters based on sterane isomerization are particularly ineffective.
2) Distributions of polyaromatic hydrocarbons change dramatically as a function of pyrolysis temperature. A variety of maturity-sensitive ratios are shown to be efficacious, including those employing dimethylphenanthrenes and methylpyrenes.
3) The aromatic ratios work particularly well for vitrinite pyrolyzates. For exinite pyrolyzates, these ratios consistently show little change between 350 and 375°, but by 400° the ratios operate effectively. For exinite, 350-375° is also the temperature range in which maximum generation of pyrolyzate occurs.
4) Vitrinite and exinite may be distinguished by subtle, temperature-independent features among the aromatic data.

REFERENCES

1. Comet P. A., McEvoy J., Giger W. and Douglas A.G., *Org. Geochem.* **9**, 171-182 (1986).
2. Rohrback B.G., Peters K.E. and Kaplan I.R., *AAPG Bull.* **68**, 961-970 (1984).
3. Lewan M.D., Winters J.C. and McDonald J.H., *Science* **203**, 897-899 (1979).
4. Lewan M.D., *Phil. Trans. R. Soc. Lond.* A **315**, 123-134 (1985).
5. Lewan M.D., Bjøroy M. and Dolcater D.L., *Geochim. Cosmochim. Acta* **50**, 1977-1987 (1986).
6. Tannenbaum E., Ruth E. and Kaplan I.R., *Geochim. Cosmochim. Acta* **50**, 805-812 (1986).
7. Saxby J.D., Bennett A.J.R., Corcoran J.F., Lambert D.E. and Riley K.W., *Org. Geochem.* **9**, 69-81 (1986).
8. Nip M., de Leeuw J.W. and Schenk P.A., *Geochim. Cosmochim. Acta* **52**, 637-648 (1988).
9. Nip M., de Leeuw J.W., Schenk P.A., Windig W., Meuzelaar H.L.C. and Crelling J.C., *Geochim. Cosmochim. Acta* **53**, 671-683 (1989).
10. Nip M., de Leeuw J.W. and Crelling J.C., *Energy & Fuels* **6**, 125-136 (1992).
11. Landais P., Zaugg P., Monin J.-C., Kister J. and Muller J.-F., *Bull. Soc. géol. France* **162**, 211-217 (1991).
12. Crelling J.C., *Am. Chem. Soc. Div. Fuel Chem. Prepr.* **34** (1), 249-255 (1989).
13. Monthioux M., Landais P. and Monin J.-C., *Org. Geochem.* **8**, 275-292 (1985).
14. Kruge M.A., Crelling J.C., Hippo E.J. and Palmer S.R., *Org. Geochem.* **17**, 193-204 (1991).
15. Mackenzie A.S., Patience R.L., Maxwell J.R., Vandenbroucke M. and Durand B., *Geochim. Cosmochim. Acta* **44**, 1709-1721 (1980).
16. Mackenzie A.S., Disko U. and Rullkötter J., *Org. Geochem.* **5**, 57-63 (1983).
17. Kruge M.A. and Landais P., in prep.
18. Radke M. and Welte D.H., *Adv. in Org. Geochem. 1981*, 504-512 (1983).
19. Radke M., *Advances in Petroleum Chemistry, Vol. 2* (eds. J. Brooks and D.H. Welte), 141-207, Academic Press, London (1987).
20. Garrigues P., Oudin J.L., Parlanti E., Monin J.C., Robcis S. and Bellocq J., *Adv. in Org. Geochem. 1989*, 167-173 (1990).
21. Garrigues P., De Sury R., Angelin M.L., Bellocq J., Oudin J.L. and Ewald M., *Geochim. Cosmochim. Acta* **52**, 375-384 (1988).
22. Budzinski H., Garrigues P., Connan J., Lee M.L., Andersson J. and Bellocq J., *Organic Geochemistry: Advances and Applications in the Natural Environment*, (ed. D.A.C. Manning) Manchester University Press, Manchester, p. 619-623 (1991).

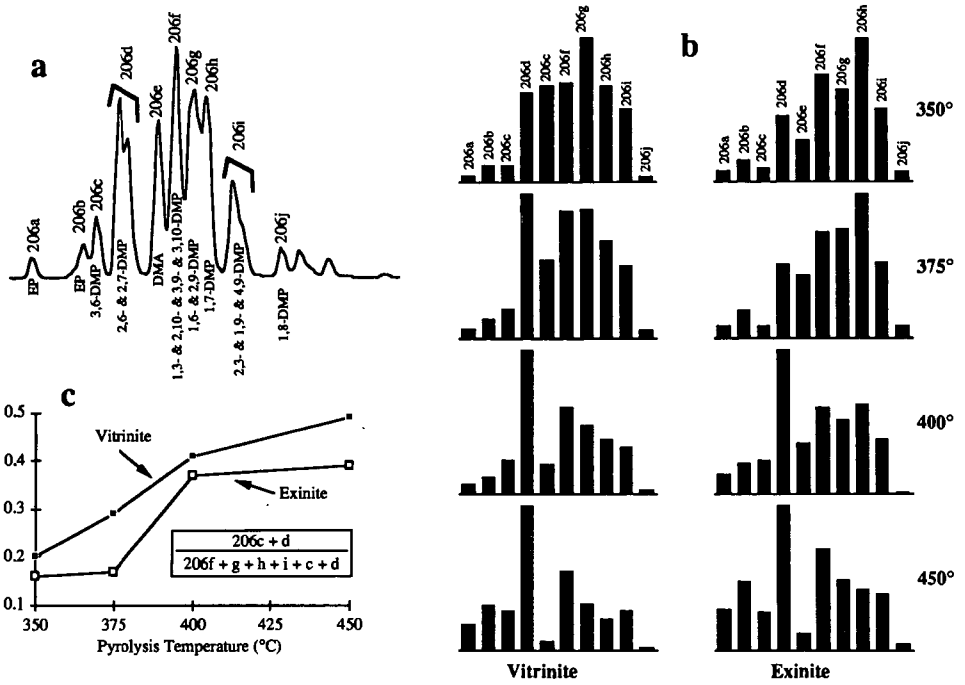

Figure 1 — Data from m/z 206 mass chromatograms of pyrolyzate aromatic fractions. 1a) Example of mass chromatogram (375° vitrinite). DMP peak identifications after Budzinski et al.[22]. EP: ethylphenanthrene, DMA: dimethylanthracene, DMP: dimethylphenanthrene. 1b) Peak distributions as a function of pyrolysis temperature and maceral type. 1c) Dimethylphenanthrene isomer ratio showing effects of thermal alteration.

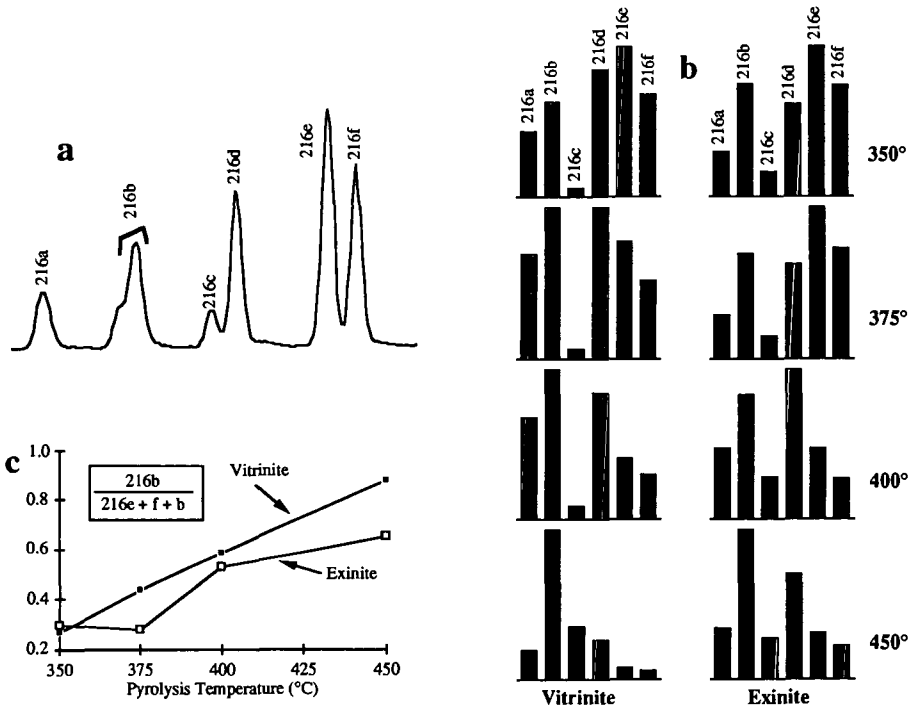

Figure 2 — Data from m/z 216 mass chromatograms of pyrolyzate aromatic fractions. 2a) Example of mass chromatogram (375° exinite), showing methylpyrene and methylfluoranthene isomers. 2b) Peak distributions as a function of pyrolysis temperature and maceral type. 2c) Isomer ratio showing effects of thermal alteration.

A comparison of maturity dependent chemical trends in samples from hydrous pyrolysis and naturally matured samples.

Tanja Barth*, Marit Seim and Kristin Skadsem
Department of Chemistry, University of Bergen
Allegt. 41, N-5007 Bergen, Norway

Keywords: Hydrous pyrolysis, asphaltenes, aromatic fraction

Introduction

Hydrous pyrolysis is the method most often used for simulated maturation of source rocks when the aim is to experimentally reproduce the chemical processes of organic matter maturation and petroleum generation as closely as possible. The procedure has been set up so the laboratory conditions correspond to the natural process within the limitations implicit in short-term experiments that do not require sophisticated equipment (1). However, the high temperature/short time procedure (e.g. 250-365°C for 72 hours) compared to the natural situation (80-120°C over millions of years) involve a risk of changes in reaction mechanisms or a decrease in importance of finely balanced energy relationships. The pyrolysis system has a high level of thermal energy which increases the probability of kinetic control of product composition, while thermodynamic control is more probable in the slow processes of the natural low-energy reaction systems.

A major part of petroleum generation consists of the irreversible breaking of carbon-carbon bonds during thermal decomposition of organic matter. Reproducing such processes at increased temperatures and short times should be possible with a reasonable correspondence to the naturally occurring chemical reactions. However, the detailed composition of the products, e.g. isomer composition, homolog distribution etc., should be more liable to be dependent on the reaction rates and temperature levels. Since hydrous pyrolysis is used as a method for chemical reproduction of the natural processes it is important to establish to what compositional levels the simulation is accurate. The molecular maturity markers are good test cases since they often are based on the relative amounts of isomeric forms of the same molecular skeleton. For such compounds there are only small variations in energy levels, and they can be expected to be especially sensitive to artificial effects.

We have compared the patterns of maturity induced change in the chemical composition of two sub-fractions of bitumen in samples from artificially matured source rocks and naturally matured coals. Asphalt fractions are analyzed by FT-IR (Fourier transform infrared) spectroscopy and the maturity related trends are extracted from the spectra by multivariate data analysis. The aromatic fractions of the same samples are analyzed by GC and phenanthrene isomer based maturity parameters are calculated. Multivariate analysis of a larger set of the aromatic components has also been performed.

Experimental

Hydrous pyrolysis: Samples from four immature source rock were artificially matured by hydrous pyrolysis in home-made stainless steel reactors by standard procedures (2). A fixed time of 72 hours and variable temperatures from 250°C to 365°C were used. This gave sets of samples covering the oil generation stage and the start of oil-to gas cracking. A summary of the source rock characteristics is given in Table 1.

The generated bitumen was Soxhlet extracted from the solid residue with dichloromethane (DCM). The extract was combined with the expelled oil collected from the water and reactor surfaces and deasphalted with 40 volumes of hexane. The deasphalted extract was separated into saturate, aromatic and polar fractions by MPLC on a silica column. The aromatic fractions were separated by ring size by HPLC. The maturity of the samples was measured on the residues as vitrinite reflectance, $\%R_o$, when possible and by Rock-Eval T_{max}.

Natural samples: A set of 56 coal samples from different sources with $\%R_o$ ranging from 0.38 to 2.62 (donated by Norsk Hydro, Bergen, Norway) were extracted and fractionated as described for the hydrous pyrolysis samples. The resulting fractions comprise the naturally matured reference set. Asphaltene spectra were recorded from all samples, and the aromatic fractions from 35 samples were also analyzed by GC.

Analytical procedures, asphalt fractions: Diffuse reflectance IR-spectra were recorded using a Perkin Elmer 1720x FTIR-spectrometer interfaced to a Vax computer. 10 µl of a 5 mg/ml solution of asphaltenes in DCM was deposited as a thin film on a KBr surface, and the solvent evaporated at room temperature. The spectra were analyzed in Kubelka-Munk form. The spectra initially had 3401 data points, but were reduced to 750 variables by a maximum entropy procedure (3). The resulting "condensed" spectra together with maturity measures or hydrous pyrolysis temperature comprise the matrices for multivariate data analysis of maturation trends.

Analytical procedures, aromatics: Aromatic fractions from Series I and II and the coal samples were analyzed. Both the whole aromatic fractions and the isolated three-ring fractions were analyzed by GC on a 50 m CP-Sil-5-CB column with FID-detection. The resulting chromatogram was directly registered in a VG Multichrom laboratory data system. The identification of specific components were based on retention times and comparisons with standards, and confirmed by GC-MS. As concentration measures, both peak heights and areas from the automatic integration were used together with manually measured peak heights. The methylphenanthrene parameters F_1 and F_2 (4) were calculated from the phenanthrene isomer ratios and used as maturity parameters. 30 peaks over the whole range of components were selected for multivariate analysis.

Data analysis: Multivariate analysis to establish patterns of chemical change calibrated to maturity measurements were performed by PLS (Projection to Latent Structures) using the Sirius program for chemometric multivariate analysis (5). Target rotated components were used to visualise the sum of maturity dependent changes in the spectra or chromatograms.

Results

FTIR of asphaltenes: Visual inspection of the IR-spectra to some degree shows the expected maturity trends in all sample sets, with increase in C-H and C=C aromatic stretching and decrease in C=O stretch, but the trends are difficult to quantify directly. However, the maturity components of the spectra extracted with multivariate analysis by PLS describe more than 90 % of the variation in all sample sets, and give well-fitted models. Fig.1 gives an overview of the results for source rock III, a Brent coal, with representative spectra after variable reduction, the target projected maturity component and the fit of the calibration model to the data points. Fig.2 gives an equivalent presentation of the naturally matured samples. Table 2 gives a qualitative summary of the maturity dependent changes for all the data sets. Clear similarities in the maturity dependent trends are observed. Series I shows most deviation. This can be caused by the initially very immature state of the brown coal sample, which gives a different range of maturation than the other series.

However, quantitative comparisons of the different series of hydrous pyrolysis samples and the naturally matured samples is not successful. The multivariate calibration models cannot be used to predict pyrolysis temperatures or maturity parameters for samples from other sets. The model based on the spectra of the naturally matured samples does not correctly predict maturity from the spectra of the artificially matured samples. The similarities in the asphaltene IR spectra thus reflect similar chemical trends with maturity, but the correspondence is not sufficient to be a basis for quantitative measurements or an universal calibration model.

GC of aromatics: The indices gave a reasonably good linearity with measured vitrinite reflectance for the naturally natured coals, as shown in Fig.3a. For the hydrous pyrolysis samples no trend was observed for either of the data sets analyzed. Series I is shown for comparison in Fig 3b. The multivariate analysis for maturity dependent trends is shown in Fig. 3c and d, where the naturally matured samples give inverse isomer loadings, i.e. negative correlations between the amounts of α and β isomers. The hydrous pyrolysis samples only give a negative correlation of the more volatile components with the less volatile components, and no isomer separation in either of the hydrous pyrolysis series.

Conclusion

The standard hydrous pyrolysis procedure which is used for simulating the chemical processes of organic matter maturation can reproduce overall chemical changes in a qualitative manner, as observed in IR-spectra of asphaltenes. The detailed isomer distributions between single components in the aromatic fraction is not reproduced. This indicates that hydrous pyrolysis should be used with caution as a method for simulating natural processes on a molecular level.

References

1: Winters, J.C; Williams, J.A.;Lewan, M.D. Adv. in Organic Geochemistry 1981, 1983, 524-533
2. Barth, T.; Borgund, A.E. and Hopland, A.L. Org. Geochem. 1989, 14, 69-76
3. Karstang, T.V. and Eastgate, R.J. Chemolab. 1987, 209-219
4. Kvalheim, O.M.; Christy, A.A.; Telnæs, N.; Bjørseth, A. Geochim.Cosmochim.Acta, 1987, 51, 1183-1888.
5. Kvalheim, O.M. Chemolab. 1988, 4, 11-25.

TABLES:

Table 1: Source rocks for hydrous pyrolysis.

Source rock	Initial maturity	TOC %	S_2 mg/g	Max.final maturity	No. of exp.
I: Brown coal	0.25 $\%R_o$	53.3	58.1	1.53 $\%R_o$	10
II: Kimmeridge	0.29 $\%R_o$	51.3	333	T_{max} 513	11
III: Brent	T_{max} 428	39.6	32.8	T_{Max} 525	8
IV: Heather	T_{max} 424	5.03	22.1	T_{Max} 536	7

Table 2: Maturity trends in IR-spectra of asphalt fractions.

Sample	O-H	C-H aro.	C-H ali.	C=O	C=C	C=O acid	C-H ali.	-O- eth.	C-H aro
	ca cm^{-1}								
	3700-3100	3100-3000	3000-2850	1765-1690	1630	1575-1520	1450-1380	1400-1050	880-700
I	-	+	+	-	+	-	+	-	
II	+	+	-	-	+				+
III		+	-		+				+
IV	+	+	-						+
V[1]		+	-	-	+		+		+

1: Naturally matured samples

Figure 1.
IR-spectra, target component
and fit of model for series I
Brent coal pyrolysis samples.

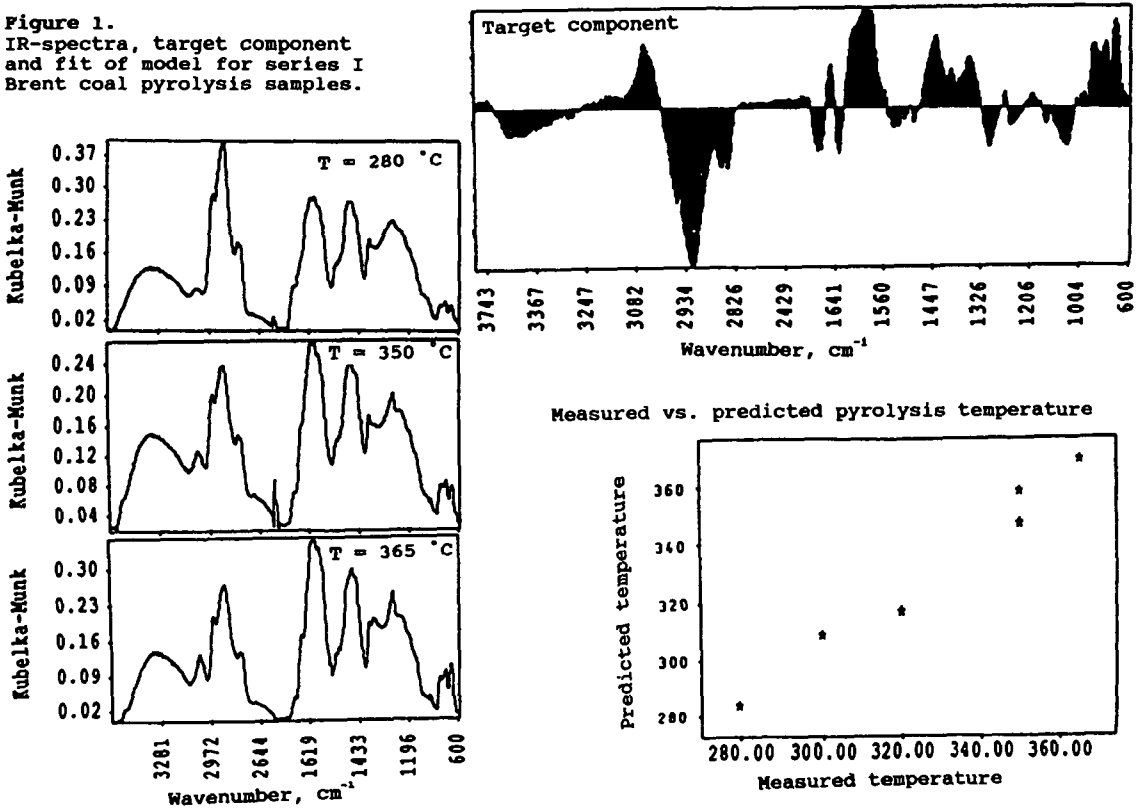

Figure 2.
IR-spectra, target component and fit of model for series V naturally matured coals.

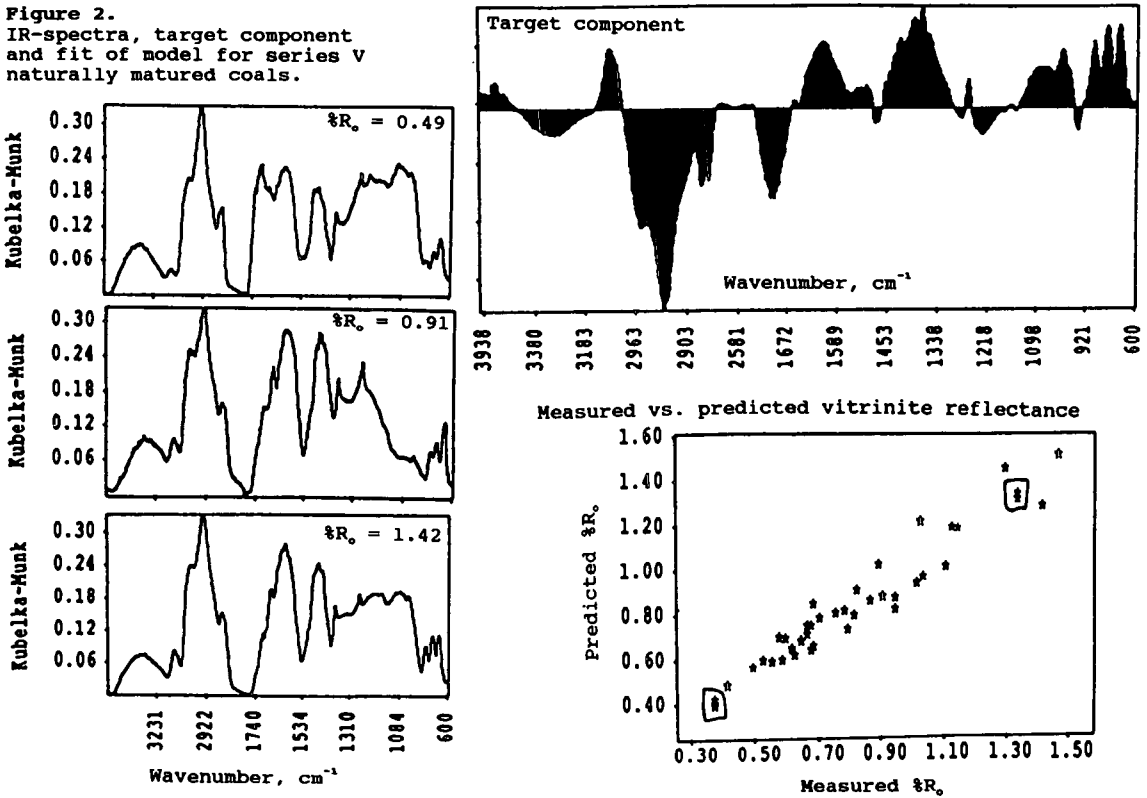

Figure 3.
Methylphenanthrene indices and maturity components
for V - coal samples and I- pyrolyzed brown coal.

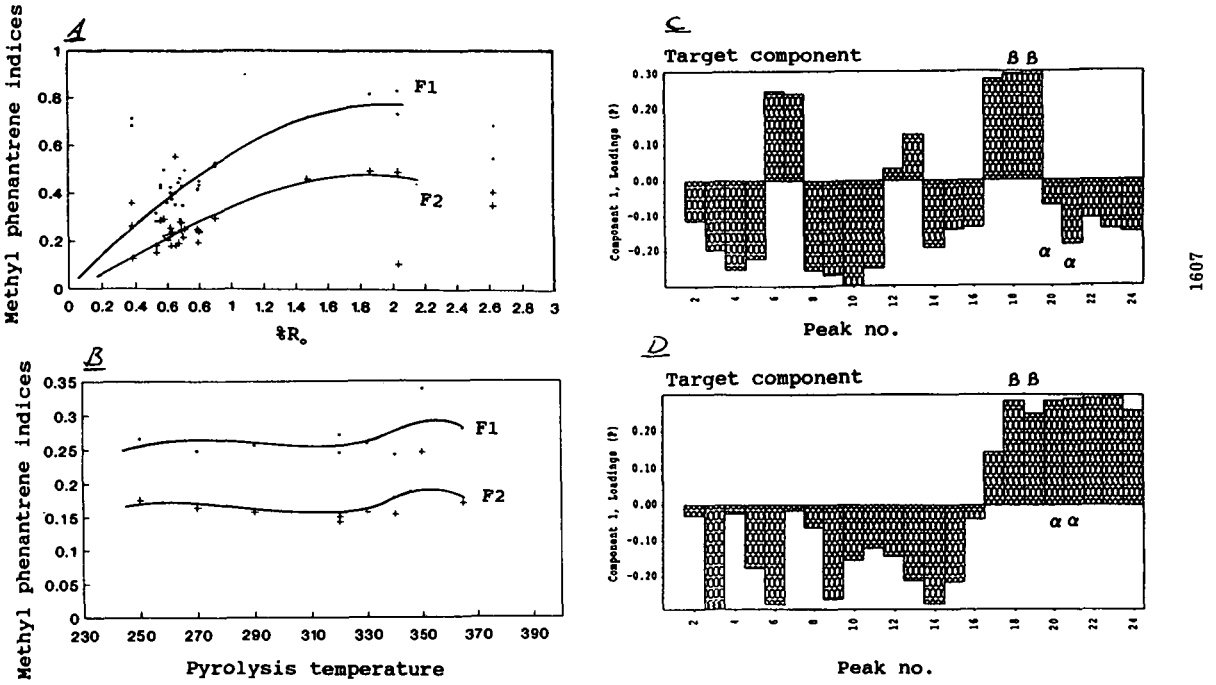

THE OFF-LINE AND ON-LINE ANALYSIS OF EFFLUENTS GENERATED DURING CONFINED PYROLYSIS OF ORGANIC MATTER

Patrick LANDAIS
Laurence GERARD and Laurence MANSUY
CNRS-CREGU - BP 23 Vandoeuvre Cedex. FRANCE

Keywords: artificial maturation, confined pyrolysis, multidimensional GC.

INTRODUCTION

Confined system pyrolysis using gold tubes in cold-sealed pressurized autoclaves has proven his efficiency for simulating the main transformations of organic matter during thermal maturation (1), (2). However, these pressurized experimental systems are still poorly adapted to the quantitative analysis of effluents generated during pyrolysis. Indeed, until now, the acquisition of mass balances required fractionations of effluents into several classes and frequently induced the evaporation losses of volatile components.

In order to overcome such analytical problems, two new techniques have been designed and developped. The off-line analysis is a thermodesorption-multidimensional gas chromatograph which allows quantitative evaluation, in a single injection, of the amounts of CO_2, CO, N_2, H_2S, H_2O, C_1-C_{30} hydrocarbons after gold-tube piercing. The on-line technique couples confined pyrolysis and analytical devices by means of a dual-oven allowing effluents pressure recording and continuous analysis of effluents by GC or GC-IR-MS during thermal maturation.

Description and applications of these two techniques are presented in this paper.

THERMODESORPTION-MULTIDIMENSIONAL GAS CHROMATOGRAPHY

This analytical system is constituted by a thermodesorption oven connected to a multidimensional gas chromatograph (Figure 1). The thermodesorption system is composed of a specially designed piercing device connected to a high temperature Valco C6UWT gas sampling valve via a series of valves which allow the sampling system to be evacuated and calibration gases or calibration liquid hydrocarbons mixtures to be injected. This sampling part is placed into a thermostated oven providing a homogeneous temperature of 250°C. A pressure transducer connected to a -1/0 bar vacuummeter measures the vacuum level in the sampling zone before piercing. A high temperature pressure transducer connected to a 0/16 bar manometer measures the effluent pressure in the sampling zone after piercing and before injection. The 0.5 ml injection loop of the Valco valve is connected to the chromatograph by a capillary fused silica transfer line heated at 280°C (carrier gas: H_2).

The two ovens of the Siemens Sichromat 2-8 multidimensional GC have their own temperature control and program which facilitate the installation of two capillary columns (oven 1: OV1, 50 m • 0,32 mm; oven 2: paraplot Q, 23 m • 0,32 mm) connected together by a pneumatic live switching system. A selected portion of the column 1 effluent containing partially resolved components (Ar, CO_2, CO, H_2S, H_2O, N_2, C_1-C_6) is transferred to column 2 for a complete separation and detection by a TCD. Other components (C_7-C_{30}) are separated by column 1 and directly transferred to a FID. Chromatographic data are recorded and processed by a ChemStation HP3365 software running on a HP Vectra computer.

The 5 cm long gold tube in which the kerogen has been pyrolysed is introduced in the piercing device. The sampling system is closed, evacuated and heated to 250°C before the gold tube is pierced. The thermovaporizable content of the tube expands into the evacuated sampling system and fills the sample loop. After an equilibration time of 30 min, the pressure is recorded by the manometer and the sample is injected into the chromatograph system. After each run, the gold tube is collected and weighed in order to determine the total weight loss. Calibration of H_2O and C_7-C_{30} hydrocarbons is performed by injection of calibrated mixtures with a syringe. Gases are calibrated by direct injection of a calibration mixture into the sampling system.

Series of artificially matured kerogens from the Paris basin, the Mahakam Delta and the Woodford Shale have been obtained by confined pyrolysis at 250, 300, 350, 375, 400°C, 100M Pa in experiments lasting 24 and 72 hours. The pyrolyzates have been analyzed by TD-MDGC and subsequently $CHCl_3$ extracted.

On Figures 2a and 2b are represented the TD-MDGC FID and TCD traces of the 350°C pyrolyzate of an immature kerogen from Toarcian of the Paris Basin. The use of the selective transfer technique with columns of different polarity allows a good separation of the gases (TCD, b) and of the higher molecular weight hydrocarbons (FID, a).

Several results from TD-MDGC have been compared with data obtained by LC-GC of the high molecular weight components. Chromatographic distribution of *n*-alkanes as well as pristane/nC_{17} ratios are similar. However, more accurate quantitative information is obtained on the C_7-C_{12} and C_1-C_6 fractions. A complete mass balance for a series of artificially matured kerogens from the Toarcian of the Paris Basin is presented on Figure 3. The quantitative evolution of the different classes contribution relative to the initial organic matter weight clearly evidences the different phases of thermal maturation.

Comparison of TD-MDGC analysis of type II and type III series of maturation demonstrates their different behaviour especially when considering the amounts of CO_2, H_2O and gasolines generated during maturation. For example, late generation of CO_2 has been evidenced during the catagenetic phase of a type II kerogen.

Source-rocks pyrolyzates can also be directly analyzed by this technique.

PRESSURE RECORDING AND EFFLUENT SAMPLING DURING ARTIFICIAL MATURATION

Until now, the only pressure variations in the gold tube could be indirectly but continuously recorded. Preliminary results indicate a close correlation between effluents generation (gas + oil) and pressure variations. Furthermore, it is still impossible to differenciate the effects of secondary cracking from those of primary cracking.

So, a new pyrolysis system has been designed, allowing pressure recording and effluent sampling while preserving the characteristics of confined systems.

This device includes two separate ovens (Figure 4). The first one contains a 50 cc autoclave and a high temperature pressure transducer connected to a pressure recorder. The gold bag containing kerogen or source-rock (up to 10 g) is placed in the autoclave. An external pressure ranging between 0 to 100 MPa is applied on the bag through an argon pressurized line connected to an air-driven pump. A perfect gas-tight is assumed between the autoclave cell and the inside of the bag. This allows an absolute pressure record of the effluents released during pyrolysis. A micro-metering valve in the oven 1 and a pressure regulation valve in the oven 2 allows the transfer of an effluent aliquot toward the oven 2. In this second oven, a high temperature pressure transducer connected to a pressure recorder measures the effluent pressure in the 5 cc steel cell where the effluent are collected or in the sampling loop of the Valco C6UWT valve if the system is connected to a GC or a GC-IR-MS by a capillary fused silica transfer line heated at 360°C. In each oven, a blow-pipe valve connected to a vacuum pump allows the venting of the effluents at the beginning of the experiments and after each effluent sampling. The temperature is controled by four K-thermocouples located in each oven, in the autoclave and in the furnace. The temperatures in the two thermostated ovens and in the furnace are regulated independently with a precision of ± 1°C by an electronic system. The temperature is assumed to be homogeneous in the whole system. The effluent pressure variations are plotted against time by a graphic recorder.

The kerogen or the source-rock is placed in the gold bag and compacted. The bag is fixed to the autoclave and the external argon pressure is applied (0-100 MPa). The heating rate up to the isotherm temperature depends on the final temperature and range between 5 and 10 °C/mn. The generated effluents are released in the pipe of the oven 1 and the pressure evolution is recorded. Aliquots are sampled at different time intervals: each 2 hours during the first day of pyrolysis and then at longer time intervals. For each sampling, the aliquots are evacuated toward the oven 2 whose temperature is the same as oven 1 in order to avoid any condensation. A constant volume of effluents is injected toward a GC by the Valco valve after measuring the pressure. The chromatograph analyses H_2O, CO, CO_2, H_2S, N_2 and C_1-C_{40} hydrocarbons in one single injection. The connection with an IR-MS will allow the precise typing of oxygenated functions, cyclic and aromatic compounds. After each sampling, the

residual effluents of the oven 2 are vented by opening the blow-pipe valve connected to the vacuum pump.

This new technique makes possible new experiments in confined medium:

- the large volume of the gold bag (ø = 1,5 cm, L = 5 cm) facilitates source-rock pyrolysis and studies of organic/mineral interactions
- the sampling and venting facilities allow the studies of the expelled fraction in source-rock pyrolysis
- the differentiation between primary and secondary reactions can be done by venting the oven 1 after each sampling. So, the only effluents generated between two samplings are analysed and only primary cracking is considered. The secondary cracking can be studied by thermal maturation of the aliquot in the oven 2 (independant regulation) after each sampling.

Acknowledgements - This work has been supported by the CPM (France), SNEA(P) and INSU (n° 91/ATP/645).

REFERENCES

(1) Monthioux M., Landais P. and Monin J.C. (1985) Comparison between natural and artificial maturation series of humic coals from the Mahakam Delta, Indonesia. *Org. Geochem.*, 8, 275-292.

(2) Landais P., Michels R., Poty B. and Monthioux M. (1989) Pyrolysis of organic matter in cold-seal pressure autoclaves. Experimental approach and applications. *J. Appl. and Anal. Pyrol.*, 16, 103-115.

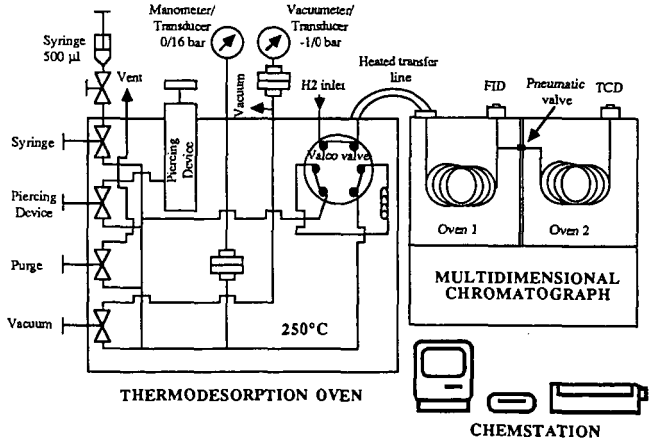

Fig.1. Scheme of the thermodesorption-multidimensional gas chromatography system

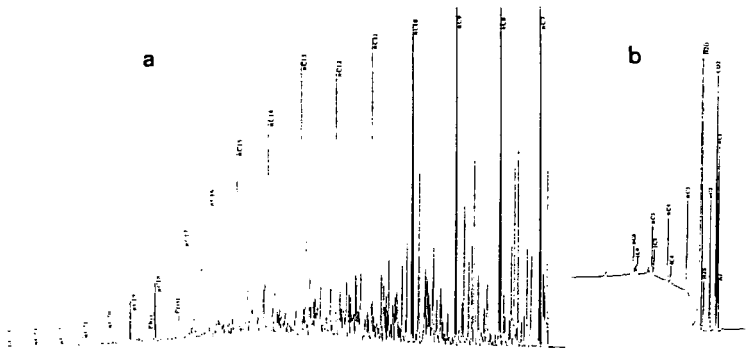

Fig. 2. TD-MDGC FID (a) and TCD (b) traces of the 350°C pyrolyzate of a Paris Basin kerogen.

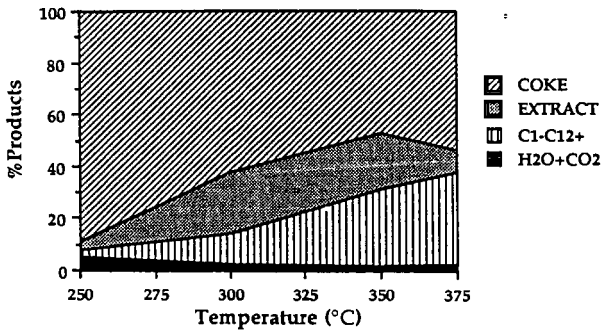

Fig. 3. Mass balance of a series of artificially maturated kerogens from the Paris Basin.

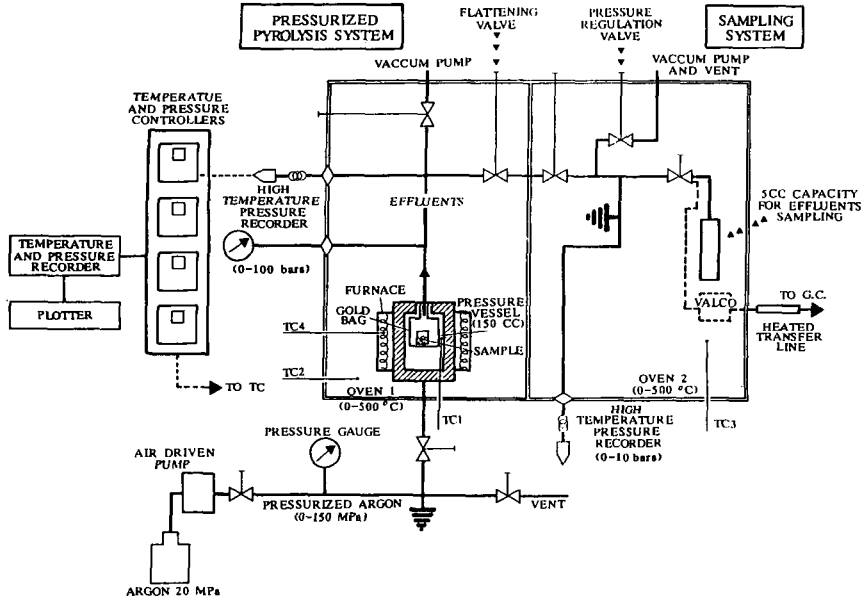

Fig. 4. Scheme of the pyrolysis and sampling systems in the new pressurized confined-pyrolysis device.

MEASUREMENT OF PRESSURE EFFECTS ON N-HEXADECANE CRACKING RATES

Kenneth J. Jackson, Alan K. Burnham, Robert L. Braun, and Kevin G. Knauss
L-202, Earth Sciences Dept.
Lawrence Livermore National Laboratory
Livermore, CA 94550

Keywords: Hexadecane, cracking rates, pressure effects

ABSTRACT

Experiments designed to determine the possible role of pressure in governing the kinetics of n-hexadecane (n-C_{16}) cracking reactions were conducted in Dickson-type autoclaves at temperatures from 300 to 370 °C and pressures from 150 to 600 bars. Good agreement with published reaction kinetics was obtained at temperatures ≥350 °C. Values determined at lower temperatures indicate slower rates than predicted from earlier experiments and show a distinct induction period at 300 °C. The activation energy determined for this reaction is about 60 kcal/mole at T > 330 °C, but it may exceed 70 kcal/mole at lower temperatures. Product hydrocarbon compounds lighter than n-C_{16} seem to follow the single, first order reaction kinetics shown by the disappearance of n-C_{16}. Hydrocarbons larger than n-C_{16}, however, seem to follow a serial reaction of generation and subsequent destruction (including conversion to solid products) at high percentage conversion. Limited data suggest that the cracking rate of n-C_{16} may have a small dependence on pressure.

EXPERIMENTAL PROCEDURES

The high temperature/pressure cracking experiments were run in Dickson-type, gold bag autoclaves (Seyfried et al., 1987). In this apparatus, the reaction vessel comprises an approximately 250 ml capacity gold bag which is capped with a commercially pure titanium head. The Ti head is fitted with a Ti or Au capillary-lined stainless steel sampling tube that allows the experiment to be sampled periodically during the course of a run at *in situ* conditions. During the runs, the samples contact only Au and carefully passivated Ti. The Au bag assembly is inserted into a stainless steel pressure cell filled with de-ionized water that serves as the pressure medium. In

turn, this assembly is fitted into a furnace assembly, as described by Seyfried et al. (1987).

Starting materials for all runs were 98.75 wt % n-C_{16} spiked with small amounts of naphthalene and phenanthrene (approximately 1.0 and 0.25 wt. %, respectively), which served as internal standards. Before the samples were loaded into the Au bags, high purity N_2 gas was bubbled through them for at least 30 minutes to remove any reactive gases (e.g., O_2) that might be dissolved in the starting materials. The Au bag was partially filled with about 70 g of the hexadecane solution. The remaining space was filled with N_2 gas after emplacing the Ti head assembly. After the vessel was loaded, pressure was gradually increased. This collapsed the Au bag and expelled the N_2 gas in the head space; leaving only the hexadecane solution in the reaction vessel.

SAMPLING PROCEDURES

During the course of the run, the solution was periodically sampled by bleeding off a small amount (usually 1-2 g) of the experimental charge into gas-tight glass syringes. The initial samples were a single liquid phase, but later samples yielded two phases because a gas phase separated from the liquid as the sample cooled. The gas was stripped from the liquid phase using a He gas extraction method, and the two fractions were analyzed separately. Liquid samples were diluted in CS_2 and analyzed by gas chromatography. Fig. 1 shows a sample analysis of the reaction products obtained from Run 1 at 353 °C and 300 bars after 169.3 hours of reaction. Gas samples were injected directly into a gas chromatograph, and checked for air contamination using mass spectrographic analyses.

RESULTS

The matrix of experimental conditions investigated in this work is shown in Table 1. Temperatures ranged from 300 to 370 °C and pressures ranged from 150 bars to 600 bars. Within this range of physical conditions, the disappearance of n-C_{16} was measured as a function of time (e.g., Fig. 2a). Exponential rates of disappearance of n-C_{16} are consistent with a single first order reaction and yield rate parameters consistent with published values (see below). An exception to this is the significant induction period exhibited by the 300 °C experiment (Fig. 2b). In addition to the disappearance of n-C_{16}, the rate of production of various classes of product phases was determined. For convenience in interpreting the data, the product

phases were separated into methane and four additional groups determined by their carbon numbers. These groups are arbitrarily defined as: C2-C4, C5-C9 C10-C15, and everything larger than C16. Fig. 3 shows that the rate of appearance of these products, when plotted as a function of the percent of hexadecane remaining in the solution, is essentially identical for all seven runs.

Rate constants for the reaction of hexadecane shown in Fig. 4 and 5 were determined using the KINETICS code of Braun and Burnham (1990). Based on results from these experiments, the cracking rate of n-C_{16} may have a small dependence on pressure (Fig. 5). It is not possible to quantitatively assess the size of this effect based on results from these experiments, because there are only a limited number of runs at a single temperature and different pressures. The activation energy for this reaction is 60 kcal/mole at T> 330 ^{o}C, but it appears to be increasing at lower T. However, this proposed decrease in activation energy is based on a single experiment at 300 ^{o}C in which there is some evidence of a distinct induction period, as shown in Fig. 2b. The significant induction period may influence interpretation of previous kinetic studies based on low-temperature, low-conversion data (e.g., Domine, 1991).

The kinetics of the production of the C1, C2-C4, C5-C9 and C10-C15 groups of product compounds seem to follow the same single, first order reaction kinetics exhibited by the disappearance of the hexadecane. However, the > C16 products follow a serial reaction of generation and subsequent destruction at high percent conversion.

REFERENCES

Braun, R. L. and A. K. Burnham (1990) KINETICS: A computer program to analyze chemical reaction data. UCID-21588 Rev. 1, Lawrence Livermore National Laboratory, Livermore, CA, 11 p.

Domine, F. (1991) *Organic Geochemistry* 17, 619-634.

Doue, F. and G. Guiochon (1968) *J. Chim. Phys -Chim. Biol.* 64, 395.

Doue, F. and G. Guiochon (1969) *Can. J. Chem.* 47, 3477.

Fabuss, B. M., J. O. Smith, R. I. Lait, A. S. Borsanyi, and C. N. Satterfield (1962) *Ind. Eng. Chem. Process Des. Dev.* 1, 293.

Fabuss, B. M., J. O. Smith, and C N. Satterfield, (1964) *Adv. Pet. Chem. Refin.* 9, 179.

Ford T. J. (1986) *Ind. Eng. Chem. Fundam.* 25, 240-243.

Groenendyk, H., E. J. Levy, and S. F. Sarner (1970) *J. Chromatogr. Sci.* 8, 115.

Panchenkov, G. M., V. Ya. Baranov (1958) *Izv. Vyssh. Uchebn. Zaved., Neft Gaz.* **1**, 703.
Tilcheev, M. D. and K. I. Zimina (1956) *Khim. Tekhnol. Topl.* **8**, 23.
Voge, H. H. and G. M. Good (1949) *J. Am. Chem. Soc.* **71**, 593.
Seyfried, W. E., D. R. Janecky and M. E. Berndt (1987) Rocking autoclaves for hydrothermal experiments II. The flexible reaction-cell system. In *Hydrothermal Experimental Techniques* (G. C. Ulmer and H. L. Barnes, eds.) Wiley-Interscience, 216-237.

Run Number	T (°C)	P (bars)	Maximum Conv. (%)	Duration (hr)
1	353	300	77.3	764
2	330	150	22.8	1052
3	300	300	1.1	5615
4	329	480	5.4	1027
5	333	600	28.1	2397
6	369	250*	89.3	433
7	371	300*	88.7	315

Table 1. Experimental conditions, extent of reaction, and run duration for the seven experiments described in this work. *Near the end of Runs 6 and 7, pressure increased to 283 and 343 bars, respectively.

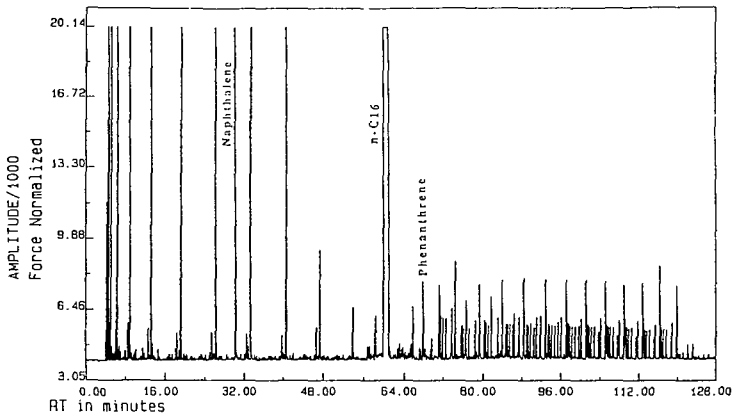

Figure 1. Sample gas chromatography trace showing the composition of the liquid phase in Run 1 (353 °C and 300 bars) at 169.3 hr elapsed time.

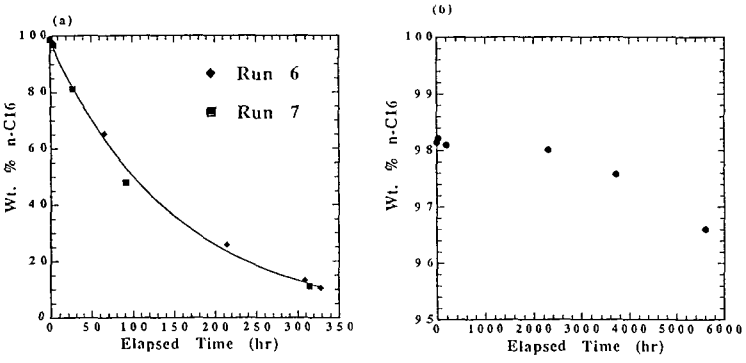

Figure 2. The disappearance of n-C_{16} as a function of elapsed time (a) in Runs 6 and 7 (370 °C) and (b) in Run 3 (300 °C). The symbols are experimental values, and the curve represents an exponential curve fit through the points.

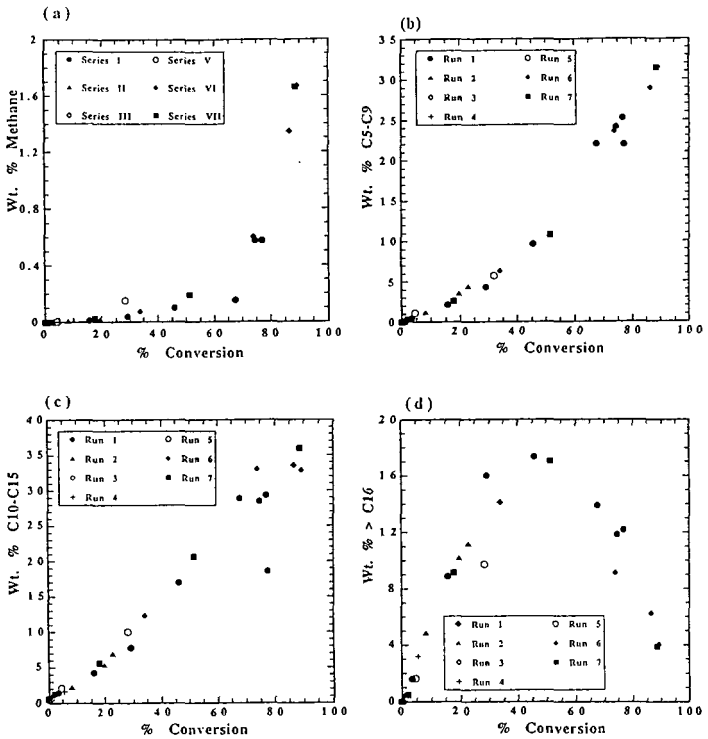

Figure 3. The appearance of product phases for all seven experiments as a function of % conversion of n-C_{16}: (a) the appearance of methane, (b) the appearance of the C5 to C9 fraction, (c) the appearance of the C10 to C15 fraction, and (d) the appearance and subsequent disappearance of the > C16 fraction.

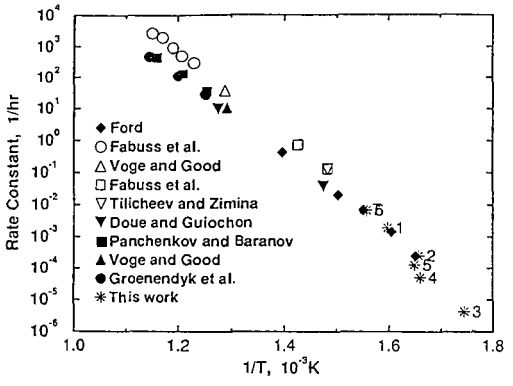

Figure 4. Comparison of hexadecane cracking rates compiled by Ford (1986) with values determined in this study. The numbered points correspond to run numbers listed in Table 1.

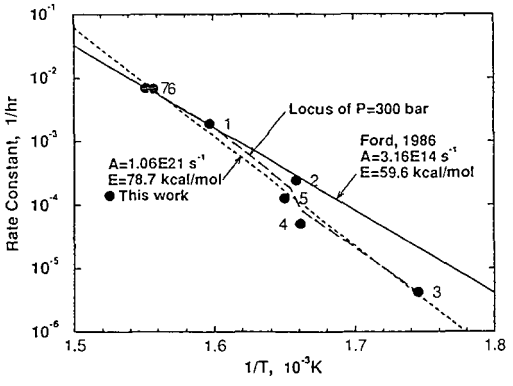

Figure 5. An enlargement of the lower right hand portion of Figure 4. The solid line shows an extrapolation of the activation energy and frequency factors determined by Ford (1986). The dotted line is a linear least squares fit through the rate constants determined in this work. The dashed line defines a locus of points consistent with the trace of a 300 bar isobar suggested by the data in this study.

HYDROUS PYROLYSIS OF NEW ALBANY AND PHOPHORIA SHALES: EFFECTS OF TEMPERATURE AND PRESSURE ON THE KINETICS OF PRODUCTION OF CARBOXYLIC ACIDS AND LIGHT HYDROCARBONS

Kevin G. Knauss, Sally A. Copenhaver, Robert L. Braun and Alan K. Burnham
Earth Sciences Department
Lawrence Livermore National Laboratory
Livermore, CA 94550

Keywords: Hydrous pyrolysis, Carboxylic acid, Kinetics

ABSTRACT

We used hydrous pyrolysis to determine the production kinetics of carboxylic acids and light hydrocarbons over the temperature interval 200° to 330°C at 300 and 600 bar pressure. We used Dickson-type, gold-bag autoclaves (1) allowing us to acquire multiple fluid and gas samples under *in situ* conditions throughout the runs, each lasting from 60 to 120 days, depending on temperature. During the runs and while sampling, fluids were exposed to only non-reactive materials (gold, passivated titanium and glass gas-tight syringes). Gases were extracted into He and analyzed using GC and MS. The aqueous samples were analyzed for carboxylic acids using IC, for inorganic cations using ICP-ES and for inorganic anions using IC. Carbon disulfide extractions were made on some aqueous fluids allowing GC analyses for heavier hydrocarbons.

The kerogen pyrolysis produced significant amounts of the monocarboxylic acids (acetic > propionic > butyric). Formic acid was present only briefly at the start of runs and little, if any, of the dicarboxylic acids were produced. The gases were dominated by CO_2 and methane, in that order, and progressively smaller amounts of the alkanes (ethane > propane > butane > pentane). Preliminary kinetic analyses of production rates suggest activation energies (E) ranging from 50 to 60 kcal/mol for both the light hydrocarbons and acids. Pressure had little effect on measured rates for the New Albany Shale.

INTRODUCTION

The potential importance of the carboxylic acids in generating reservoir porosity and controlling aqueous fluid chemistry (2) has resulted in considerable interest in knowing their rate of production and thermal stability (3), although not without some controversy (4). The recognition of the reactivity of organic compounds in aqueous solutions at high temperature (5) has argued for the use of hydrous pyrolysis as a particularly appropriate method of investigation (6). Unfortunately, experimental artifacts, like catalysis by the reaction vessel (6), and inappropriate kinetic analyses (7) have sometimes conspired to complicate progress in understanding the processes and rates.

We are studying the pyrolysis of oil shales and the generation of carboxylic acids and light hydrocarbons using chemically inert (Au and Ti) hydrothermal reaction vessels specifically designed to allow sampling of fluids under *in situ* condi-

tions. In this way we hope to avoid many of the complications noted by others. In addition, we are using a variety of approaches to kinetic analyses in determining kinetic parameters.

EXPERIMENTAL AND ANALYTICAL TECHNIQUES

The term hydrous pyrolysis has been used by some workers (8) to mean a relatively specific, restrictive experimental approach. Although useful for comparison between samples of the "potential for generating oil-like pyrolysate", this approach may not be ideally suited to studies aimed at mechanisms and kinetics of processes. We use the term more loosely to imply simply the pyrolysis (cracking) of kerogen in the presence of liquid water. Our lowest pressure (300 bar) was sufficiently high to keep the aqueous system single phase throughout each run. The use of a flexible gold bag allows us to control pressure (e.g., isobaric) through significant degrees of maturation. This approach has been used to advantage by others (9). Our apparatus differs from that of these earlier workers, however, in that we may withdraw multiple samples from each run while maturation continues uninterrupted. Concentration *vs.* time data are adjusted to compensate for the change in area/mass ratio caused by sampling.

Runs were isothermal (after a heating period lasting a few hours) and isobaric. All runs used 30 g of shale and an appropriate volume of de-oxygenated (purged using N_2 gas) distilled water to just fill the gold bag at run conditions. The headspace was further swept with N_2 gas prior to collapsing the gold bag before heating and pressurizing the vessel. Each run lasted from 2 to 4 months, depending on temperature. At the highest temperature, this allowed us to follow both the production and subsequent destruction (through decarboxylation) of the organic acids. A total of five runs were made with the New Albany Shale: 200°, 270° and 330°C at 300 bars pressure, 270° at 500 bars pressure, and 330°C at 600 bars pressure. Two runs are still in progress with the Phosphoria Shale at 330°C at 300 and 600 bars pressure. The Phosphoria Shale runs will not be dealt with here.

The shale samples were coarsely crushed (2 to 4 mm) and then washed ultrasonically in distilled water to remove adhering fine particles. We were faced with the usual conundrum of deciding whether or not to pre-extract the samples prior to hydrous pyrolysis. If we pre-extracted, we ran the risk of performing the hydrous pyrolysis on material unrepresentative of natural kerogen. If we didn't pre-extract, we would need to account for any light hydrocarbons or carboxylic acids released immediately upon heating that were the product of natural maturation and not the artificial maturation taking place as a result of the hydrous pyrolysis. We elected not to pre-extract, because we felt that the water washing would remove some of the acids already present, and because we could correct for the initial acid input, since we would take closely spaced samples early in each run.

During the runs and while sampling, fluids were exposed to only non-reactive materials (gold, passivated titanium and glass gas-tight syringes). Gases were extracted into He and analyzed using GC and MS. The aqueous samples were analyzed for carboxylic acids using IC, for inorganic cations using ICP-ES and for inorganic anions using IC. Carbon disulfide extractions were made on some aqueous fluids allowing GC analyses for heavier hydrocarbons. At the conclusion of each run the vessels were quenched to room temperature and pressure and the solids and remaining liquids recovered and sampled. Although the gas and liquid analyses are essentially complete for the five runs, the solid phase analyses continue. These will include XRD, SEM/electron microprobe, and pyrolysis-MS analyses.

Initial TOC analyses made post-run suggest that significant degrees of artificial maturation were achieved. For example, the 270°C and 300 bar run achieved 30% conversion (based on kerogen loss) during the two months of artificial maturation.

RESULTS

Carboxylic acids

The kerogen pyrolysis produced significant amounts of the monocarboxylic acids (acetic > propionic > butyric). Formic acid was present only briefly at the start of runs. No dicarboxylic acid anions were unequivocally identified in any samples, suggesting that *if* they are produced at *all* under any of the conditions that we investigated, their production rate is very small. Figure 1 illustrates typical results for the carboxylic acids produced at 270°C. Note that at all temperatures there was an initial rapid release of carboxylic acid anions to the aqueous phase upon heating. In the subsequent kinetic analyses we have corrected the results for this initial pulse of released carboxylic acid. At 270°C, following the initial pulse, carboxylic acid concentrations continue to increase throughout the runs.

Figure 2 illustrates typical results for the carboxylic acids produced at 330°C. At this temperature the production rate of the carboxylic acids is much higher than at 270°C, however, within a few days the rates of production and destruction *via* decarboxylation are about equal. Within two weeks the rate of decarboxylation exceeds the rate of production and there is a continuous decrease in carboxylic acid concentration throughout the remainder of the runs. It is very likely that both the processes of production and decarboxylation are catalyzed by the mineral phases in the shale and, although our experimental apparatus is unlikely to have catalyzed processes, any rates that we measure are specific to these shales.

Light hydrocarbons

Unlike the carboxylic acids, the light hydrocarbons (<C7) and CO_2 were not rapidly released upon initial heating in water, implying that such compounds produced as a result of natural maturation are rapidly lost from the kerogen. The gases were dominated by CO_2 and methane, in that order, and progressively smaller amounts of the alkanes (ethane > propane > butane > pentane). Figure 3 illustrates typical results for these compounds at 270°C. Gas concentration continues to increase throughout the runs.

Effect of pressure

Pressure (300 *vs.* 600 bars) had little effect on the production of either the carboxylic acids or the light hydrocarbons produced from the pyrolysis of kerogen contained in the New Albany Shale. As an illustration, Figure 4 compares the 330°C carboxylic acid results obtained at the two pressures.

KINETIC ANALYSES

The concentration data were used to calculate fraction reacted on an absolute scale, based on the maximum concentration measured for each compound during the period of production. We then used the KINETICS code (10) to analyze the data acquired from the hydrous pyrolysis experiments. Table 1 summarizes the kinetic analyses.

For the gases, the data acquired at all three temperatures were used in the kinetic analyses. At 200°C over a 4 month period, little if any carboxylic acid was

produced by the artificial maturation. All of the carboxylic acid present at this temperature was that produced naturally and rapidly released to the aqueous phase upon heating. For this reason, the kinetic analyses of the carboxylic acid data are based only on the results from the 270° and 330°C runs.

In order to test our assumption that the reactions producing the carboxylic acids and light hydrocarbons were first order, we first made a kinetic analysis based on a Gaussian distribution of activation energies with all terms (the pre-exponential (A), activation energy (E), Gaussian distribution parameter (S), and reaction order (N)) calculated by fit, rather than being fixed. The mean calculated N for the gases was 0.98 ± 0.12 and for the carboxylic acids was 0.87 ± 0.10. The results suggested that for all compounds the production reaction may be assumed to be approximately first order, although a spread in calculated activation energies resulted from the sparseness of the data. Pyrolysis kinetics determined using a Pyromat II instrument suggested that an appropriate pre-exponential factor, A, for the production of volatile hydrocarbons from the New Albany Shale was $2x10^{14}$ (11). The kinetics analyses summarized in Table 1 used this value.

The kinetic analyses suggest that the activation energies for the production of both the light hydrocarbons and the carboxylic acids from the hydrous pyrolysis of kerogen contained in the New Albany Shale are within the range of 50 to 60 kcal/mole.

CONCLUSION

We have demonstrated the use of a new type of hydrothermal apparatus in determining the production kinetics of light hydrocarbons and carboxylic acids from kerogen pyrolysis. It is ideally suited to determine the effects of temperature and pressure on production kinetics, free of the experimental artifacts frequently encountered using other types of apparatus.

In this paper we have only presented preliminary results from the organic analyses of fluids and gases. We are continuing to analyze the data from solid phase analyses and from the inorganic fluid chemistry analyses. We intend to try to understand the interaction between the inorganic and organic chemical systems. We are especially interested in the effectiveness of carboxylic acids in complexing the cations released as a result of mineral dissolution, i.e., the increase in "solubility", and the impact of the carboxylic acids on the solution pH. We are utilizing the geochemical modeling code EQ3/6 (12) in this effort.

REFERENCES

(1) Seyfried, W.E., Janecky, D.R. and Berndt, M.E., in Hydrothermal Experimental Techniques, edited by G.C. Ulmer and H.L. Barnes (John Wiley and Sons, N.Y., 1987), p. 216.

(2) Lundegard, P.D. and Kharaka, Y.K., in Chemical Modeling in Aqueous Systems II, edited by D.C. Melchior and R.L. Bassett (Amer. Chem. Soc. Symposium Series 416, 1990) p. 169.

(3) Crossey, L.J., Geochim Cosmochim. Acta 55, 1515 (1991).

(4) Stoessel, R.K. and Pittman, E.D., Am. Assoc. Petrol. Geol. 74, 1795 (1990).

(5) Sisken, M. and Katritzky, A.R., Science 254, 231 (1991).

(6) Lundegard, P.D. and Senftle, J.T., Appl. Geochem. 2, 605 (1987).

(7) Burnham, A.K., Braun, R.L. and Samoun, A.M., Org. Geochem. 13, 839 (1988).

(8) Lewan, M.D., Winters, J.C. and McDonald, J.H., Science 203, 897 (1979).
(9) Monthioux, M., Landais, P. and Monin, J.-C., Org. Geochem. 4, 275 (1985).
(10) Braun, R.L. and Burnham, A.K., Lawrence Livermore National Laboratory Report UCID-21588, Rev. 1 (1990).
(11) Braun, R.L., Burnham, A.K., Reynolds, J.G. and Clarkson, J.E., Ener. & Fuels 5, 192 (1991).
(12) Wolery, T.J., Jackson, K.J., Bourcier, W.L., Bruton, C.J., Viani, B.E., Knauss, K.G., and Delany, J.M., in Chemical Modeling in Aqueous Systems II, edited by D.C. Melchior and R.L. Bassett (Amer. Chem. Soc. Symposium Series 416, 1990) p. 104.

TABLE 1

KINETIC ANALYSES OF PRODUCTION RATE DATA

Compound	Pressure (bar)	E (kcal/mol)	A (s^{-1})	S (%E)	N
methane	300	55.3	2e14	3.46	1
	600	55.2	"	3.06	"
ethane	300	55.1	"	3.73	"
	600	54.9	"	1.71	"
propane	300	55.6	"	4.16	"
	600	54.9	"	0.57	"
butane	300	55.5	"	4.25	"
	600	55.7	"	1.49	"
acetate	300	52.6	"	0.77	"
	600	52.6	"	0.84	"
propionate	300	52.5	"	1.44	"
	600	51.6	"	2.49	"
butyrate	300	52.9	"	0.09	"

Figure 1. NA-1 (270°C, 300 bar)

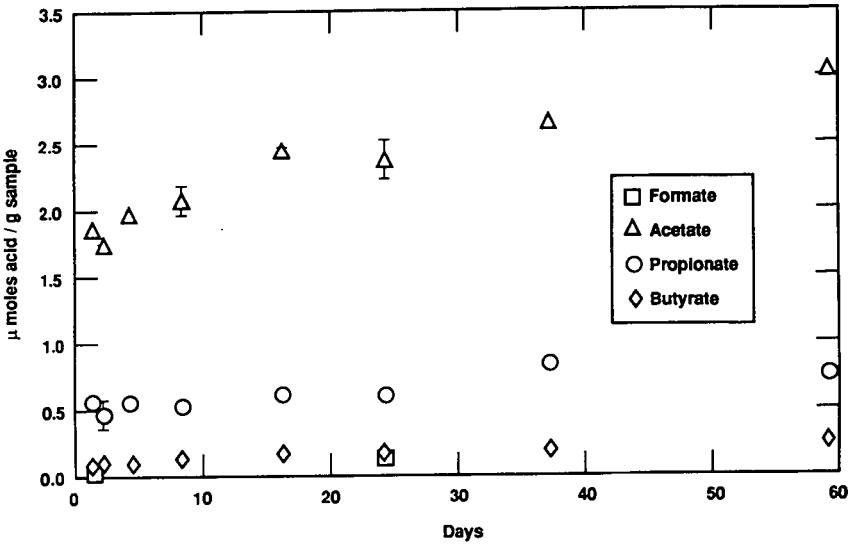

Figure 2. NA-7 (330°C, 600 bar)

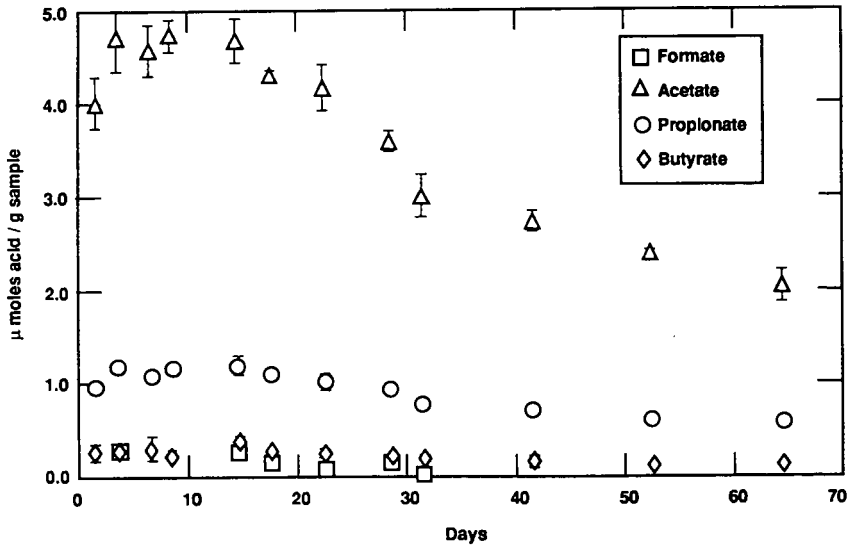

ES-05/22/92-KK#4-01 & 02

Figure 3. NA-4 gasses (270°C, 500 bar)

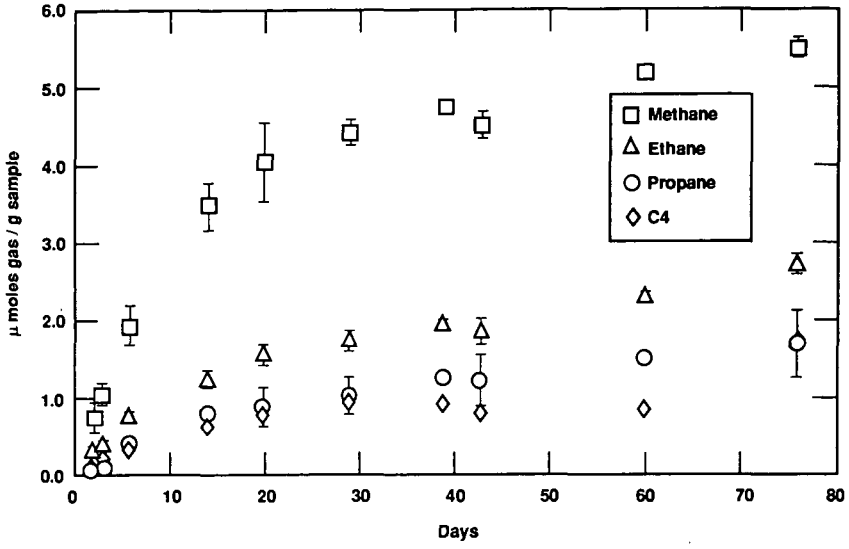

Figure 4. New Albany Shale at (330°C and 300 or 600 bar)

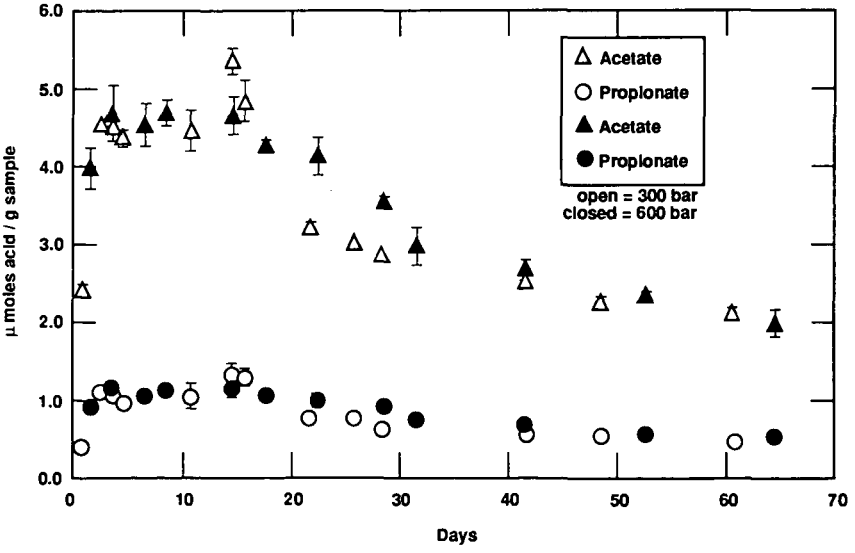

ES-05/28/92-KK#4-03 & 04

The Effect Of Pressure On The Kinetics Of Kerogen Pyrolysis

H. Freund, J. A. Clouse, G. A. Otten
Exxon Production Research Co.
P. O. Box 2189
Houston, TX 77252

Keywords: activated volume, pyrolysis kinetics, kerogen maturation,

Introduction

The determination of the kinetics of oil generation is usually done in the laboratory using shales of interest and subjecting the material to high temperatures to accelerate the conversion. Kinetics are determined at these high temperatures, low pressures and extrapolated back to the geological conditions believed to exist at the time of generation. The validity of the extrapolation of these rate constants over a wide range of temperatures[1,2] and pressures[2] has recently been studied.

Other authors have addressed the issue of pressure. Teichmuller and Teichmuller[3] have suggested that high pressure retards the coalification process based on field measurements of vitrinite reflectance. Also using vitrinite reflectance measurements from the offshore of northwestern Europe, McTavish developed a correlation quantitatively relating pressure to vitrinite reflectance.[4] More recently, Sajgo et al [5] compressed alginite and lignite into disks and determined the effect of pressure on their thermal alteration. They observed significant retardation at 1 kbar equivalent to about 50°C (i.e., the high pressure case had to be raised 50° to obtain the same extent of conversion). Price and Wenger have performed aqueous pyrolysis experiments on Phosphoria shale and report a similar retardation.[6]

The role of pressure in the generation of hydrocarbons has also been addressed theoretically by Perlovsky and Vinkovetsky[7] who presented a treatment involving an activated volume to suggest that increased pressure will retard the hydrocarbon generation reactions. In another theoretical paper, Neto[8] hypothesized that reactions only occur when reactants are within a critical distance between each other. He predicted a pressure dependence on the kinetics but did not quantify it.

Monthioux et al[9] studied the effect of reactor configuration, water, and pressure in the artificial maturation of coal. He found the effect of pressure (as well as water) to be minimal if the experiments were done in a confined system, with the pressure provided externally.

In an effort to elucidate the role of pressure in oil generation, we have done experiments to quantify the effect of pressure on the kinetics of maturation. Our approach was to quantify the pressure effect by determining an activated volume. We examined two shales: Bakken, a type II marine shale and Monterey, a type IIS

marine shale.

Experimental/Analytical

The samples to be heated were prepared in small gold tubes (~25mm long x 4mm O.D.) welded at one end before adding sample. Typically, 200 mg of ground shale were loaded into the tubes along with 25 mg sea water. The tubes were then welded shut under an argon atmosphere. The tubes were inserted into a pressure vessel and placed in a furnace. A thermocouple inserted in the end of the pressure vessel measured the temperature of the sample. It had been previously calibrated against a thermocouple inserted down the inside of the vessel. The vessel was then pressurized with argon causing the gold tube to collapse tightly around its contents. Experiments for a given shale were done varying the time, temperature, and pressure to which the sample was subjected. After heating, the samples were removed and the gold tubes punctured. The shale was removed and typically allowed to air dry, removing water and light hydrocarbons. The shale was then extracted using dichloromethane until the extract was visually colorless.

Conversion was defined based on Rock-Eval S_2 data:

$$\text{Conversion} = 1 - (S_2 \text{ (sample)} / S_2\text{(raw)})$$

The Rock-Eval parameters for the raw (initial, unheated) sample were also done on rock extracted by the above procedure.

Results

Bakken data

The results of a series of runs with the gold tubes at different pressures are shown in Figure 1, plotting S_2 and conversion versus pressure. The line is a quadratic best fit to the data.

In order to quantify the effect of pressure, we needed to put the data on a consistent kinetic basis. We chose to use a distributed, Gaussian activation energy functional form to fit the data. Data at 4000 psi were input to the Lawrence Livermore KINETICS[10] program. Figure 2 shows the fit obtained at 4000 psi allowing the program to optimize A, E, and s. Because we wanted to compare parameters as a function of pressure, the input values for the A factor and the breadth (standard deviation) of the distribution, s, were then fixed and not allowed to vary during subsequent optimizations at different pressures. Hence, we obtained as a function of pressure different activation energies. Figure 3 is a plot at high pressure showing an example of the fit obtained. Also included in Figure 3 is the sensitivity to a change in activation energy of 200 cal/mole. A total of more than 60 runs were made with the Bakken shale.

To quantify the effect of pressure for a reaction with rate constant k, one typically plots ln k versus PV_a/RT, where P is the system pressure, R the universal

gas constant and T is the absolute temperature.[11] The parameter V_a is the activated volume. It is the pressure analog to the Arrhenius activation energy and for simple or elementary reactions, represents the change in volume of the activated complex relative to the reactants. In more complex systems, as we have, the methodology is still valid but the activated volume is best thought of as a parameter which quantifies the pressure sensitivity of the system.

As we mentioned, we have reduced our kinetic data in the form of a distributed Gaussian activation energy. As the pressure is varied, we expect this distribution to shift, i.e., the center of the activation energy distribution, E, will vary with pressure. Because this activation energy tends to track ln k, we can relate E to the activated volume, V_a:

$$E = P V_a + E_o$$

where E is the center of the activation energy distribution determined from the kinetics program at a given pressure and E_o is the center of the distribution at very low pressures. Hence, we plot in Figure 4 the determined activation energy as a function of pressure. The solid line is a least squares fit through the Bakken data–the slope yields a value of 32.8 cc/mole for the activated volume of the Bakken.

What is conversion?

Conversion in these experiments is based on the S_2 peak in a Rock-Eval analysis after extraction. Hence, material which is very heavy yet soluble in methylene chloride is considered product and removed. This material would tend to increase S_2 if it weren't extracted. We did a series of experiments in which no extraction was done on the samples after reaction. In these experiments, we still define conversion as before, based on S_2, but now the reacted material contains those molecules (or pieces of kerogen) which have been released from the starting material but are very large, soluble molecules (as well as smaller product molecules which show up as S_1). During Rock-Eval, this material will decompose leading to a higher S_2 and hence lower calculated conversion. We constrain the data to have the same activation energy as the extracted case and determine a new A factor. The A factor for the unextracted runs at low pressure is 7.2×10^{15} sec^{-1} compared to the extracted case of 9.5×10^{16} sec^{-1}.

The effect of pressure for the unextracted case was examined at one high pressure (P = 25000 psi). Using the aforementioned methodology, we obtained an activated volume of 12.8 cc/mole.

Monterey data

To examine the dependence on kerogen type, we measured the pressure dependence of a high sulfur type IIS kerogen, a Monterey formation shale. The experiments were run as described earlier although only 14 runs were done and two

pressures were used. The KINETICS program determined the following parameters:

P= 2000 psi	P = 15000 psi
A =7.5 x 10^{15} sec^{-1}	
E = 54376 cal/mole	E = 54866 cal/mole
s = 3.46 %	

This led to an activated volume of 22.9 cc/mole as indicated in Figure 4.

Discussion

The activated volumes obtained in this work range from 13-33 cc/mole. Activated volumes are known for simple elementary free radical reactions, e.g., V_a for H-atom abstraction reactions range 10-20 cc/mole. For material as complex as kerogen, the authors are unaware of any measurements of activated volume for decomposition. Typical values for the activation volume in polymerization reactions are in the range – (15-25) cc/mole.[11] Because bonds are forming, the activation volumes are negative meaning the rates accelerate with increasing pressure. The polymerization reactions, however, are similar mechanistically in that they are free radical reactions involving initiation, propagation, and termination. It is reasonable to expect that the pyrolysis of kerogen (essentially a de-polymerization reaction) would have a similar, albeit positive, activation volume because of the similar kinds of reactions occurring. The activated volume we measured for the Bakken was 32.8 cc/mole and 22.8 cc/mole for the Monterey.

From Figure 4 for the Bakken, one can see that a pressure of 20000 psi would cause an activation energy increase of about 1 kcal/mole. If we assume that temperature would not effect the measured activated volume (determined around 300 °C) then it is valid to consider the effect of this on the maturation of kerogen at much lower temperatures. Figure 5 shows the effect a 1 kcal/mole difference between two kerogens would have under maturation conditions. We have taken the heating rate to be 1°/million years and have used the parameters obtained for the Bakken. At 50% conversion there is an offset of 7° between the two generation curves. This temperature offset is about the same as the extrapolation uncertainty from the determination of the high temperature rate constants. Hence the role of pressure is small. Note that Figure 1 indicates a significant change in S_2 as the pressure increases from 2000 to 30000psi. Although S_2, the amount of pyrolyzed volatiles expelled in Rock-Eval, increases over a factor of 2, the conversion only drops from around 80% to 58%. It is the conversion, not S_2, which is the important kinetic parameter. S_2 is a measure of what is still left behind unreacted and must be related to the initial or raw value to obtain the conversion.

The results of Sajgo et al and Price and Wenger would suggest an offset in

temperature of more than 35 ° when applied to a similar maturation situation. The discrepancy between these results and ours is disconcerting. We see a relatively minor effect with pressure whereas they see differences amounting to an increase of more than 5000 cal/mole in the activation energy at 15000 psi compared to 2000 psi. Sajgo et al examined lignite, a type III kerogen material whereas we have investigated types II and IIS. Price and Wenger examined the Phosphoria, a type IIS shale. We do not believe kerogen type is the cause of the differences. The reactor configuration used by Sajgo was quite different than our experimental apparatus. However, one set of our experiments was quite similar in configuration to that of Price and Wenger.

We have measured the activated volume for the pyrolysis of two shales We have done a large number of experiments in different configurations under a range of experimental conditions (in addition to those discussed here). Our results support our belief that pressures below 2 kbar (30000psi) play a minor role in kerogen pyrolysis.

References

1. Freund, H., Energy and Fuel, in press.
2. Dominé, F., Org. Geochem.,*1991*, v. 17, 619-634.
3. Teichmuller, M. and Teichmuller, R., in Coal and Coal-Bearing Strata, Murchison, D. and Westoll, T. S., editors, American Elsevier, New York, 1968.
4. McTavish, R. A., Nature, *1978*, v. 271,594-596.
5. Sajgo, C., McEvoy, J., Wolff, G. A., and Horvath, Z. A., Adv in Org. Geochem.,*1985*, v. 10, 331-337.
6. Price, L. C., and Wenger, L. M., Advances in Organic Geochemistry, *1991*, D. A. C. Manning, ed., 1992.
7. Perlovsky, L. I., and Vinkovetsky, Y. A., Bollettino di Geofisica Teorica ed Applicata, 1989, *v.* 31, 87-89.
8. Neto, C. C., Org. Geochem., *1991*, v. 17, 579-584.
9. Monthioux, M., Landais, P., and Monin, J., Org. Geochem., *1985*,, 275-292.
10. Braun, R. L. and Burnham, A.K., "Kinetics: A Computer Program to Analyze Chemical Reaction Data," Lawrence Livermore National Laboratory, Report UCID- 21588, Nov. 1988.
11. Isaacs, N. S., Liquid Phase High Pressure Chemistry, John Wiley & Sons, New York, 1981.

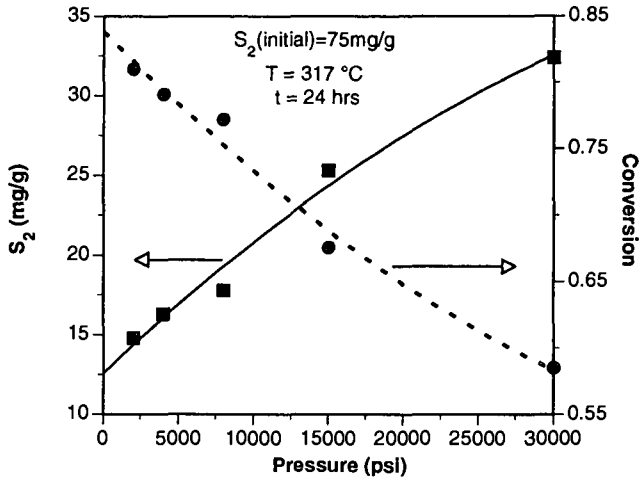

Figure 1. S_2 and conversion as a function of pressure.

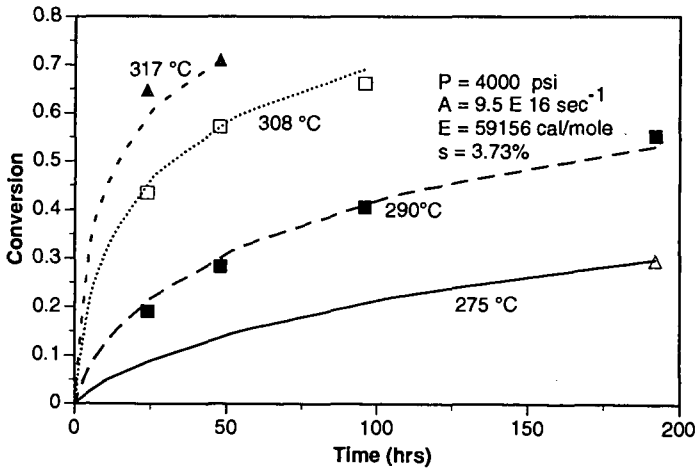

Figure 2. Determination of kinetic parameters using the KINETICS program. Curves are best fit to the experimental points by varying A, E, and s.

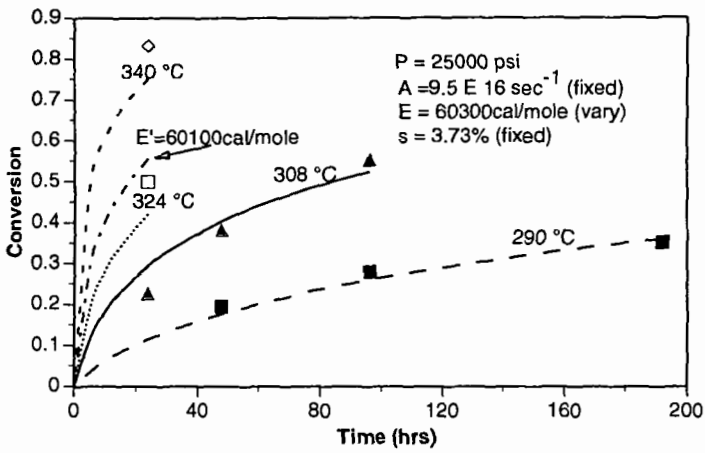

Figure 3. High pressure example of the fit obtained from the KINETICS program. Curves are fit to data varying only the activation energy. A and s are determined from the 4000 psi run. To get an idea of sensitivity, we also show for the 324°C case, a curve having the center of its activation energy distribution decreased by 200 cal/mole.

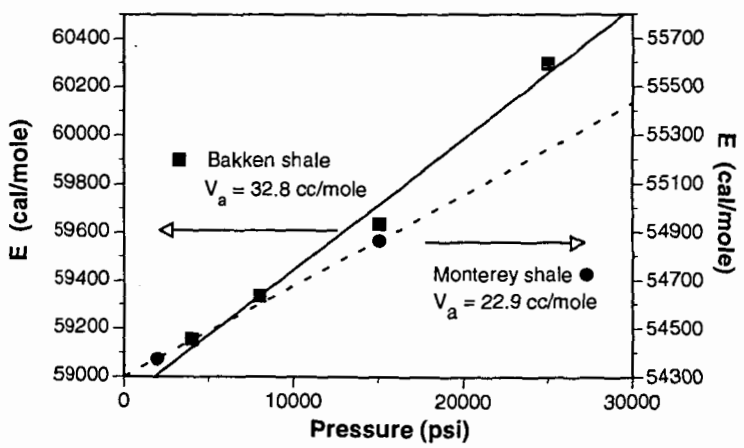

Figure 4. A plot of the center of the activation energy distribution, E, as a function of pressure. The temperature ranged from 250-360°C for the Bakken and from 270-300°C for the Monterey.

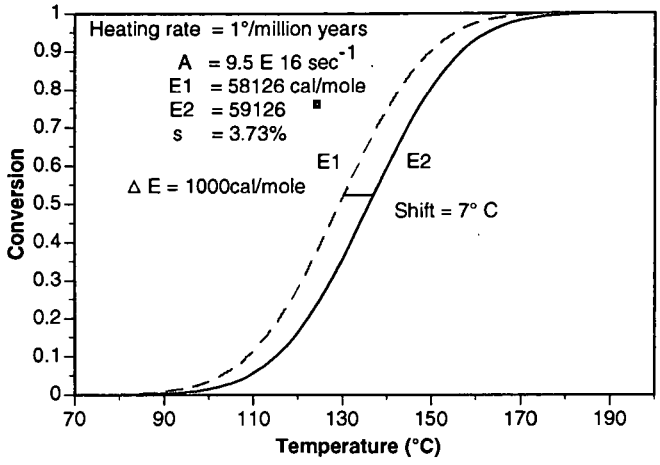

Figure 5. The effect of 1 kcal/mole on the kinetics of oil generation from kerogen.

BIARYL FORMATION AS A SOURCE OF HYDROGEN DURING PYROLYSIS OF RESID STRUCTURAL ELEMENTS

Donald F. McMillen, Jeffrey A. Manion, and Ripudaman Malhotra
Molecular Physics Laboratory, SRI International
333 Ravenswood Ave., Menlo Park, CA 94025-3493

Keywords: Coking, hydrous pyrolysis, PAH

ABSTRACT

The problems of formation of carbonaceous solids ("coke") during the processing of heavy petroleums and coal are clearly related to the formation of "excess" alkanes during hydrous or "confined" pyrolysis: in both cases the hydrogen needed to keep the ratio of alkanes/olefins high in the converted (i.e., volatile) aliphatic portions of the product streams must come primarily from the aromatic, or non-volatile, portions of the feed. In the first case, this transfer is undesirable because it forms coke; in the second case, it is (or "was") desirable because it increased the volatility and aliphatic nature of the petroleum pool during source rock maturation. In both cases, we have speculated that the formation of aryl-aryl coupling products is very likely a key step. In an effort to connect the dominant chemistry in these two contexts, we are performing experimental and mechanistic numerical model studies on selected structures as surrogates for the petroleum resid and kerogen components as well. One question of interest is how the presence of water in hydrous pyrolysis promotes the critical hydrogen transfer, particularly since the 118-kcal/mol O-H bond in water makes it very difficult for water to participate in any radical-chain hydrogen transfer pathways. Initial results are in accord with this reservation in that the presence of supercritical water, up to a fluid density of 0.4 g/cc, did not enhance the redistribution of hydrogen to produce more volatile alkanes.

INTRODUCTION

Hydrogen redistribution among feedstock components or structural elements is key to both the conversion of vacuum resids to distillate materials, and also to the formation of volatile fractions during hydrous pyrolysis. In the case of resid hydroprocessing, there is a well-appreciated tendency for some of the hydrogen required for bond scission and radical-capping to come from coke intermediates, thus propelling the formation of coke. This tendency toward disproportionation is well understood in thermodynamic terms, being due to the respective stabilities of methane and graphite. However, it is poorly understood in terms of the kinetic factors controlling its rate. The goal in catalytic hydroprocessing of resids is of course to ameliorate this tendency to the maximum extent practical through the use of catalysts and hydrogen pressure.

Hydrous pyrolysis of oil shale and other types of kerogen is presumably driven by a similar tendency for the kerogen structure to disproportionate into a hydrogen-rich volatile portion and a hydrogen-poor less-volatile portion. The presence of liquid phase (or dense supercritical fluid phase) water during the hydrous- or confined- pyrolysis is known to markedly increase the alkane/alkene ratio in the volatile products.[1-3] Since the evidence appears to indicate that water does not serve as the principal source of additional hydrogen in the volatile products, the additional hydrogen must be coming, as in the resid hydroprocessing case, from the organic matrix itself. Our basic premise is that the hydrogen-transfer chemistry in these two cases is closely related. Accepting that premise as a working hypothesis, the pertinent question then becomes, "From what structures and by what chemical mechanisms does this hydrogen come, and how might water influence that transfer?"

It is well known that petroleum residua consist basically of large polycyclic aromatic (PAH) clusters to which are attached a number of aliphatic chains. It is also generally appreciated that the problem of resid hydroprocessing is not primarily one of cracking off the alkyl chains, which occurs rather readily (even the absence of H_2 and a catalyst)[4-6], but one of doing so without having

the PAH form carbonaceous solids that foul the catalyst, coat reactor surfaces, and build aggregates that interfere with fluid bed operation. Nevertheless, prior to 1989, the open literature contained only one report[7] of the behavior of long-chain alkylaromatics other than of alkyl benzenes[8] or alkylpyridines.[9] On the basis of pyrolysis at high temperatures (ca. 800°C), Billaud et al. concluded that the pyrolysis pathways were independent of the number of rings in the PAH.[7] However, in work first reported in 1988, Savage and coworkers[10-12] showed that the conclusions of Billaud et al. definitely *do not* apply to pyrolysis at lower temperatures, particularly to the 350-450°C range relevant to resid hydroprocessing and hydrous- or confined- pyrolysis. Their experiments demonstrate very clearly that the ease of bond cleavage at the alkyl-aryl junction (i.e., ipso displacement) depends very markedly on the number and arrangement of rings in the PAH, ranging from extremely slow for alkylbenzenes to very fast for certain pyrenyl, anthryl, chrysyl, and perylenyl derivatives. For these PAH, the ispo displacement is so facile that it is often the dominant reaction in pyrolysis of the neat alkylaromatic (that is, even in the absence of a hydroaromatic or other "intended" hydrogen-transfer agent). The relative ease of this ipso-displacement is also completely consistent with findings on the relative ease of hydrogen transfer to these same categories of structures under donor-solvent coal liquefaction conditions.[13-15] The purpose of this presentation is to address the question of where the hydrogen comes from and how it arrives at the ipso position of these alkylaromatics.

EXPERIMENTAL

Procedures. Pyrolysis experiments were carried out in evacuated fused silica ampoules. The sealed tube and an appropriate quantity of solvent for pressure equalization was placed in an outer jacket of stainless steel tubing capped with compression fittings. The reaction vessel was then immersed in a temperature-controlled molten-salt bath for the desired time, the tube removed and quenched in water. After cooling in liquid nitrogen to condense CO_2 and volatile organics, the ampoule was opened and the sample removed by pipet and repeated washing of the tube with solvent. An internal standard was added and the sample analyzed by capillary gas chromatography with flame ionization and/or mass selective detection. Quantitation was obtained using the FID analyses with molar responses determined separately for those compounds for which we had authentic samples and estimated by comparison with similar species when no sample was available. Generally, at least three split injections of each sample were performed using an autoinjector. For most species the reproducibility was within ± 2% and we estimate the overall analytical accuracy to be within ± 5%. The reaction mixtures were also analyzed by field ionization mass spectrometry (FIMS), using SRI's magnetic sector FIMS instrument, in order to assess the polyaryls and other low volatility products.

Chemicals. n-Hexadecylpyrene (99+% by GC analysis), was obtained from Molecular Probes, Inc. of Eugene, Oregon. Biphenyl was obtained from Aldrich Chemical Co. Toluene used for GC analyses was Malinkrodt reagant grade. These materials were used without further purification. Tetrahydrofuran was used without stabilizer and distilled daily from sodium acetonylacetonate. The added-water pyrolyses employed deionized, low-conductivity water.

RESULTS

Initial pyrolysis experiments with n-hexadecylpyrene were conducted under conditions similar to those used by Savage and coworkers and the products analyzed by GC-MS and FIMS. Subsequently, we performed some experiments with added (supercritical) water. To facilitate comparison, Table 1 gives summary figures relating to the balance of hydrogen, and aromatic and aliphatic carbon for the pyrolysis of 1-dodecylpyrene calculated from the data of Savage and coworkers[11] along with findings from our study.

Perhaps the most striking observation in these and other data of Savage is the very high alkane/alkene ratio in the reported products, particularly at large extents of reaction. It is also clear from these data there is a shortage (in the GC-MS analyzable products) of pyrene rings and of

hydrogen-deficient materials. Evidently, non-volatile, hydrogen-deficient, pyrene-containing products (aka char) have been generated in the course of converting radicals and olefins (produced from ipso-displacement and Rice-Herzfeld alkyl chain scission) into alkanes. The high alkane/alkene ratio, in the absence of an external source of hydrogen, is strikingly reminiscent of the ratios reported by Lewan[1] and others for hydrous pyrolysis of shale kerogen.

Reaction Rates and Hydrogen Balance. The defined first order rate constant (for alkylpyrene disappearance) from the 90-minute quartz ampoule pyrolysis is only about 1/8 of that obtained by Savage[11] in a stainless steel reactor after reaction for the same time. The rate constant derived from the 513-minute run is about three times higher. This increase in first-order rate constant is consistent with the auotcatalysis described in reference 11, although it is difficult at this point to precisely compare the degree of autocatalysis in the two reactor types. The product distributions are quite similar, with there again being a marked excess of alkanes over alkenes and a substantial shortage of pyrene-containing products at higher extents of reaction. The extent of this excess and shortage are shown in Table 1. The mol % yield of alkanes is numerically equivalent to the mol % of "extra" hydrogen required to produce cleaved and reduced (non-olefinic) products. As the conversion of the alkyipyrenes approaches 90%, the yield of extra hydrogen in the reduced products can also approach 90%, meaning that out of every ten original alkylpyrenes that have disappeared, there have been nine chain cleavages that have utilized this extra hydrogen coming from somewhere. Savage and coworkers pointed out this hydrogen imbalance,[11] but were unable to address with GC-MS the nature of the incipient "char" that was presumably providing the hydrogen.

The last two columns in Table 1 show the products obtained when water was included in the reaction mixture along with the organic substrate (at ca. 0.1 and 0.4 g/cc supercritical fluid density). As indicated above, the question of interest here was whether the addition of water would accelerate the formation of those oxidized products whose generation supplies hydrogen (and therefore accelerates cleavage and reduction). The data in Columns 7 and 8 clearly indicate that this was *not* the case. In fact, there was a consistent and progressive *decrease* in the alkane/alkene ratios seen in the aliphatic products, as reflected by 45 and 80% drops in the overall alkane/alkene ratio shown for the two water runs in Table 1. Thus, the effect of water under these conditions has not only *not* been to increase cleavage and reduction, but to make the volatile products more oxidized (olefinic).

Assuming our originally postulated connection between alkylpyrene pyrolysis and hydrous pyrolysis really does exist, the reason why water failed to accelerate cleavage is likely that here there are virtually no ionic species, other than those provided by the autoionization of the water itself. There is neither the mineral matter, nor the organic heteroatom species, nor the stainless steel surfaces generally present in hydrous pyrolysis of oil shale and other kerogens. In fact, the pyrolysis of alkylpyrenes in fused silica ampoules represents the extreme in terms of a "kerogen surrogate" free from any ionic or polar species that may be contributing to the marked effects that water has in hydrous pyrolysis. It does make sense, after all, that if water as a polar medium and ionic reactant is to somehow help connect the ionic reaction manifold to the radical reaction manifold, this will likely require not only fluid densities approaching normal liquid densities[16] (i.e., above ca. 0.3 g/cc) but also the presence of polar species and redox agents. Accordingly, experiments are now underway to see if any of these factors will enable water to accelerate the redistribution of hydrogen and enhance the production of reduced ipso-displaced products during alkylpyrene pyrolysis.

Identity of the Sources of Extra Hydrogen. Savage describes an acetone-insoluble, toluene-soluble non-elutable "char" as the probable source of the hydrogen that produces high alkane/alkene product ratios. The major elutable unidentified product reported by these workers[11] was a material whose presumed molecular ion was reported as m/z 242. Based upon recent field ionization mass spectrometric analyses we have performed on Wilsonville coal liquefaction resids in conjunction with Consolidation Coal Co.[17], and also on earlier HPLC-FIMS analyses of petroleum-resid-derived vacuum gas oils reported by Sullivan et al.,[18] we can identify m/z 242 as the odd-carbon aromatic derived from pyrene by completion of a $-CH_2CH_2CH_2-$ bridge between

the 1- and the 10- positions.. As an analog of phenalene ($C_{13}H_{12}$) it is an odd-carbon molecule that would have to lose three hydrogens to be fully aromatic, it cannot form a closed shell fully aromatic PAH. However, the radical species formed when three hydrogens are lost is among the most stable of all radicals, and earlier esr studies have found it to be common in thermally processed petroleums *even at room temperature* .

m/z 242

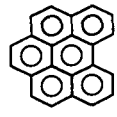

Benzo[ghi]perylene, m/z 276

From our recent analyses of Wilsonville coal-derived resids,[17] it is apparent that m/z 242 is a commonly recurring PAH structure that builds up during catalytic processing. How important it actually is as a step in the ring-growth processes that lead to still larger PAH and eventually char is a critical question, the answer to which has not yet appeared in the literature. However, a partial answer appears here in the form of a second important higher molecular weight product we have detected. At longer reaction times the molar yield of this product approaches 3%, and, from its apparent molecular ion at m/z 276, this product can be identified as benzo[ghi]perylene. Although not previously reported in alkyl pyrene pyrolysis,[10-12] this PAH has been found to be prominent in coal- and petroleum- derived resids and to be correlated with increased problems of coke formation.[18] Benzoperylene could conceivably be formed from the original 1-alkyl pyrene by two successive ring closures, as shown below, proceeding through an intermediate having the m/z 242 ring system.

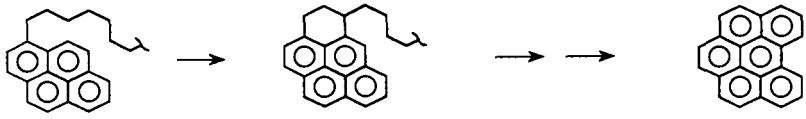

Thus it begins to appear that the phenalene-type structure represented by m/z 242 is in fact important in the ring-growth processes by which higher PAH and eventually char are produced. Benzoperylene (m/z 276) represents five degrees of unsaturation beyond pyrene. Taken together with cleavage of the residual alkyl chain, the net result is the freeing of four units of 2(H) for the production of reduced and cleaved products. For the 513 min run in Table 1, the formation of the single product at m/z 276 accounts for a significant minority of the extra hydrogen made available: the yield of benzo[ghi]perylene represents about 11 percentage points of the 85 mol% of 2(H) generated by "char-forming" reactions.

The operation of ring-growth mechanisms that involve attachment and cylization of alkyl fragments is of course not the only way of generating the larger PAH that eventually become char. The formation of biaryls and their ring-closure (e.g. naphthalene to binaphthyl to perylene) represents passing from pre-existing aromatics to much larger PAH in a minimum number of steps. Furthermore, given that biaryl bonds are the strongest C-C single bonds that can be formed in hydrocarbons, the formation of biaryls can be expected to be very facile *once* aryl radicals have been generated.[19] In contrast, one rather expects that alkylation and cyclization would become much more facile in the presence of acidic catalysts.[20] Hence, we expected in these pure hydrocarbon pyrolyses to find biaryls as the major oxidation products.

We subjected one of the product mixtures from ethylpyrene pyrolysis (supplied to us by Savage) to FIMS analysis to assess the formation of biaryls (which are not analyzable by capillary GC). The spectrum from this analysis is presented in Figure 1. Even though the extent of reaction in this case was only about 35% and the yield of pyrene is only about 5%, the peaks for dimers and

trimers of ethylpyrene are clearly visible. In contrast, the peak at m/z 242 is barely above background and there is no peak visible at m/z 276. Thus it would appear that under these nominally non-ionic conditions, biaryl formation is indeed a more important source of hydrogen than alkylation and ring-closure processes.

FIMS analysis of the 513-minute reaction product (sample from Row 6 in Table 1) does not show such clear presence of biaryls, presumably because rather than having dimer intensity primarily at three masses (2(230) - 2, 2(230) - 2 + 28, and 2(230) - 2 - 28) as in Figure 1, the class of dimers will be distributed over at least 32 different masses.(i.e., m/z = 2(426) - 2 and any mass containing from one to 32 fewer side chain carbons). However, the ring-building species at m/z 240, 242, and 276, and are clearly visible, together with modest amounts of the corresponding 276-alkylation products up to the C_{17} analog. These alkylation products of benzoperylene, in sum, essentially double to about 20 percentage points the extra hydrogen supplied through the formation of all benzo[ghi]perylene species. Thus, both biaryl formation and ring-building processes can each be seen, under different circumstances, to supply substantial percentages of the hydrogen used for ring closure and olefin reduction.

SUMMARY

Pyrolysis of long chain alkylpyrenes at 400°C in fused silica ampoules yields a product distribution and autocatalytic behavior very similar to that detailed by Savage for reaction in stainless steel microreactors, but at about an 8-fold lower rate. The hydrogen needed for the ipso-displacement bond cleavage and for reduction of olefinic products is indeed supplied by the generation of heavy materials. From GC-MS and FIMS analysis, we find both ring-growth and poly-aryl products to be significant sources of this "extra" hydrogen. Some of these ring-growth products, particularly the odd-carbon phenalene analog at m/z 242 and benzo(g,h,i)perylene at m/z 276 have been previously correlated with buildup of coke and refractory resids during catalytic hydrporcessing of heavy petroleums and coal-derived liquids. Somewhat surprisingly, we do *not* find that the addition of supercritical water, at least up to a fluid density of 0.4 g/cc, enhances the formation of biaryls and thereby enhances this supply of extra hydrogen. This observation leads to the tentative conclusion that the interaction of water and the organic matrix that commonly leads to an enrichment in volatile hydrocarbons during hydrous pyrolysis must depend upon the presence of ionic or polar species that are not present during pure hydrocarbon pyrolyses in fused silica. We anticipate that extension of these studies will yield important information on factors controlling coke formation during processing of residual oils as well as on the chemistry responsible for alkane enrichment during hydrous pyrolysis.

ACKNOWLEDGMENTS

The authors wish to acknowledge the Support of the U.S. Department of Energy under Contract No. DE-AC22-91PC91044 and also to thank Drs. Phillip E. Savage and C. Michael Smith for permission to publish the FIMS spectrum in Figure 1.

REFERENCES

1. Lewan, M. D., "Laboratory Simulation of Petroleum Formation: Hydrous Pyrolysis," *in Organic Geochemistry*, eds. M. H. Engel and S. A. Macko, Plenum Publishing Corp., New York, 1989.
2. Hoering, T. C. *Org. Geochem.*, **1984**, *5*, 267.
3. Larter, S. R.; Douglas, A. G. *J. Anal. Appl.Pyrolysis* **1982**, *4*, 1.
4. Khorasheh, F.; Rangwala, H. A.; Gray, M. R.; Dalla Lana, I. G., *Energy and Fuels*, **1989**, *3*, 716.
5. Savage, P. E.; Klein, M. T.; Kukes, S. G., *Energy and Fuels*, **1988**, *2*, 619.

6. Miki, Y.; Yamadaya, S.; Oba, M.; Sugimoto, Y., *J. Catal.*, **1983**, *83*, 371.
7. Billaud, F.; Chaverot, P.; Berthelin, M.; Freund, E. *Ind. Eng. Chem. Res.* **1988**, *27*, 1529.
8. Savage. P. E.; Klein, M. T. *Ind. Eng. Chem. Res.* **1987**, *26*, 488.
9. Mushrush, G. W.; Hazlett, R. N.*Ind. Eng. Chem. Fundam.* **1984**, *23*, 288.
10. Javanmardian, M.; Smith, P. J.; Savage, P. E. *Am. Chem. Soc. Div. Fuel Chem. Preprints* **1988**, *33*(2), 242.
11. Savage, P. E.; Jacobs, G. E.; Javanmardian, M. *Ind. Eng. Chem. Res.* **1989**, *28*, 645.
12. Smith, C. M.; Savage, P. E. *Ind. Eng. Chem. Res.* **1991**, *30*, 331, and other references cited therein.
13. McMillen, D. F.; Malhotra, R.; Chang, S. -J.; Fleming, R. H.; Ogier, W. C.; Nigenda, S. E., *Fuel* **1987**, *66*, 1611.
14. Malhotra, R.; McMillen, D. F. *Energy Fuels* **1990**, *4*, 184.
15. Futamura, S.; Koyanagi, S.; Kamiya, Y. *Fuel*, **1988**, *67*, 1436.
16. Penninger, J. M. L.; Kolmschate, J. M. M. "Chemistry of Methoxynaphthalene in Supercritical Water," in *Supercritical Fluid Science and Technology*, Am. Chem. Soc. Symposium Series, 242.
17. Malhotra, R.; McMillen, D. F.; Huestis, D. L. *Am. Chem. Soc. Div. Fuel Chem. Preprints* **1992**, *37*(2), 908.
18. Sullivan, R. F.; Boduszynski, M. M.; Fetzer, J. C.*Energy &Fuels* **1989** *3*, 603.
19. Fahr, A.; Stein, S. E., *J. Phys. Chem.* **1988**, *92*, 4951.
20. Langlois, G. E.; Sullivan, R. F.; "Chemistry of Hydrocracking," in *Refining Petroleum for Chemicals*, L. J. Spillane, H. P. Leftin, Eds.; Advances in Chemistry, 97; American Chemical Society, Washington, DC, 1970, p. 38.

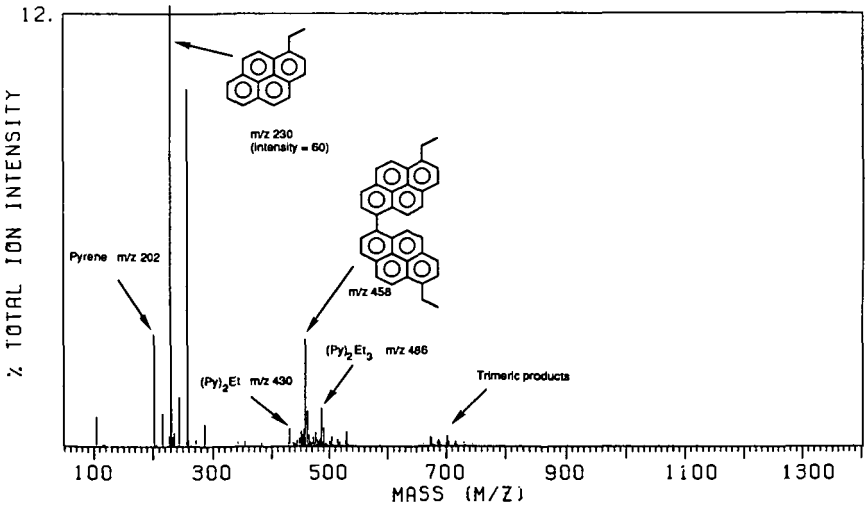

Figure 1. Mass spectrum of a moderate-conversion 1-ethylpyrene pyrolysis product mixture.

Table 1

Comparison of literature and current data on the pyrolysis of long chain alkylpyrenes.

	Literature Data[a]			Current Results[b]			
Time (min)	30	90	180	90	513	90	90
Water density (g/cc)	–	–	–	–	–	0.12	0.40
10^4 Defined k_1 (s^{-1})	1.39	1.84	2.62	0.24	0.60	0.25	0.31
Products (mol%)							
Pyrene	0.74	20.7	43.5	1.91	52.9	1.41	0.28
Me-Pyrene	2.86	6.62	8.38	5.47	9.64	6.04	6.19
Et-Pyrene	1.90	2.08	2.68	1.55	2.35	2.64	1.50
Vinyl-Pyrene	c	c	c	0.033	<0.02	0.14	1.96
Σ(Pyrenes)	82.6	71.9	65.8	Unk	Unk	Unk	Unk
Σ(Identified Pyrene Products)	4.8	34.8	59.9	11.9[d]	80.3[d]	12.4[d]	15.4[e]
Σ(Alkanes)[f,g]	>1.94	>23.5	>54.9	>6.49	>85.14	>5.34	>2.19
Σ(Alkenes)[f]	>2.37	4.60>	>2.61	>4.47	>0.66	>6.74	7.66
Alkanes/Alkenes	0.81	4.60	19.5	1.45	128	0.79	0.29
Excess mols of 2(H)[g]	1.0	24.0	52.3	3.5	77.7	1.9	1.14

a Pyrolysis of 1-dodecylpyrene/biphenyl mixtures at 400°C in stainless steel reactors, Ref. 11.

b Pyrolysis of 1-hexadecylpyrene/biphenyl mixtures at 400°C in quartz ampoules.

c Not reported but stated to be very small due to rapid hydrogenation to ethylpyrene.

d Includes pyrenes with alkyl chain lengths up to C_{12} and selected ring-closure products.

e Includes pyrenes with alkyl chain lengths up to C_{15} and selected ring-closure products.

f Includes aliphatic products from C_8 to C_{16}.

g The mol % yield of alkanes is numerically equivalent to the mol % of excess hydrogen required to produce cleaved non-olefinic products

WATER AS A SOURCE OF HYDROGEN AND OXYGEN IN PETROLEUM FORMATION BY HYDROUS PYROLYSIS

M. D. Lewan
U.S. Geological Survey
Box 25046, MS 977
Denver Federal Center
Denver, CO 80225

The importance of water in laboratory experiments designed to understand natural processes is well documented in the studies of granite melts (Goranson, 1932; Tuttle and Bowen, 1958), metamorphic reactions (Winkler, 1974, p. 15; Rumble et al., 1982; Ferry, 1983), coal formation (Berl and Schmidt, 1932; and Schuhmacher et al., 1960), and clay mineral diagenesis (Whitney, 1990). Prior to 1979, organic geochemists did not fully appreciate the ubiquity of water in sedimentary basins and its role in petroleum formation. A notable exception is the work by Jurg and Eisma (1964). Noting difference in the thermal decomposition of behenic acid in the presence and absence of liquid water, these investigators suggested that water played an important role in petroleum formation. Although a subsequent study in 1969 by Brooks and Smith employed water in laboratory simulations of petroleum generation from coals, laboratory experiments over the next decade did not consider the role of water in petroleum formation (e.g., Tissot et al., 1974; Larter et al., 1977, Harwood, 1977). Lewan and others (1979) reported that heating organic-rich rocks submerged in liquid water resulted in the generation and expulsion of a free-flowing oil that accumulated on the water surface above the submerged rock. Physically, chemically, and isotopically this expelled oil pyrolyzate was similar to natural crude oils. This experimental approach was referred to as hydrous pyrolysis. Although hydrous pyrolysis has since been shown to provide useful information on primary migration, stages and kinetics of petroleum generation, and thermal maturity indices (Lewan, 1983, 1985, 1987; Winters et all., 1983; Lewan et al., 1986), the actual role of water in petroleum formation has not been determined.

In order to better understand the role of water in petroleum formation, a series of pyrolysis experiments were conducted on aliquots of a sample of Woodford Shale under hydrous and anhydrous conditions. The experiments involved isothermally heating 400 g of thermally immature, gravel-sized (0.5-2.0 cm) rock in one-liter stainless steel-316 reactors at 300°, 330° and 350°C for 72 hours. Hydrous experiments included 320 g of deionized water and 241 kPa of helium in the headspace. No water was added to the anhydrous experiments and the head space was evacuated at the start of the experiment. The experiments were conducted at these three temperatures for 72 hours because previous experiments with Woodford Shale showed that the two overall reactions responsible for petroleum formation occur in part over these conditions. The first overall reaction occurs at temperatures below 330°C for 72-hour experiments, and involves the cleavage of

weak noncovalent bonds in the kerogen to form a soluble, high-molecular-weight tarry bitumen (kerogen to bitumen). This bitumen impregnates the ground mass of the rock to form a continuous organic network. The second overall reaction occurs at temperatures from 330°C to 350°C for 72-hour experiments, and involves the cleavage of covalent bonds in the bitumen to form an immiscible oil that is expelled from the organic network in the rock (bitumen to oil).

Pyrolyzate yields from these comparative experiments are given in Table 1 in terms of generated gas, expelled oil, bitumen extract, and total pyrolyzate (i.e., gas + oil + bitumen). The most obvious difference is the total lack of expelled oil in the anhydrous experiments, with no signs of oil droplets or an oily film on the surfaces of the rock chips. At 300°C for 72 hours, only a small amount of expelled oil is generated in the hydrous experiment and the amount of total pyrolyzate generated is essentially the same in the hydrous and anhydrous experiments. Partial decomposition of kerogen to bitumen predominates at this time-temperature condition and the presence of water appears to have no significant effect on this overall reaction. However, distinct differences in the amounts of total pyrolyzate are evident in the 330°C and 350°C experiments (Table 1), which represent conditions for the partial decomposition of bitumen to oil. Amounts of total pyrolysate and bitumen decrease significantly under anhydrous conditions, but the amount of bitumen decreases to a lesser extent and the amount of total pyrolyzate increases under hydrous conditions. These results indicate that bitumen degrades to an insoluble pyrobitumen under anhydrous conditions, while it decomposes to an expellable immiscible oil under hydrous conditions.

Another difference between the hydrous and anhydrous experiments is the significantly higher amounts of CO_2 generated by the former. Table 2 shows the total amount of aqueous and gaseous CO_2 to be one order of magnitude higher under hydrous conditions than under anhydrous conditions at 350°C for 72 hours. Mass balance calculations for the loss of oxygen from kerogen at 350°C for 72 hours indicate that under hydrous conditions the kerogen oxygen accounts for only 64 percent of the oxygen in the generated CO_2. The lack of carbonate minerals in the original rock implicates H_2O as the source of the excess oxygen in the generation of CO_2 under hydrous conditions. Several reactions, including gas-shift reactions, have been considered to explain this excess oxygen, and the most feasible reaction appears to be oxidation of carbonyl groups in the kerogen or bitumen by H_2O. A working hypothesis envisages formation of carboxylic intermediates that are decarboxylated with increasing thermal stress to generate CO_2.

Regardless of the specific mechanism responsible for H_2O to act as a source of the excess oxygen generated as CO_2, the remaining hydrogen from the reacted H_2O would be available for terminating free radical sites. This source of hydrogen is supported by a hydrous pyrolysis experiment that was conducted on the Woodford Shale at 330°C for 72 hours with D_2O instead of water. Deuterium-NMR analyses of the pyrolyzate products from this experiment showed that the expelled immiscible

oil as well as the bitumen and kerogen retained in the rock contained significant quantities of deuterium. Quantification of the deuterium content of the isolated kerogen was not performed, but the NMR spectrum was typical for powdered solids containing deuterium. Quantification of the deuterium content of the oil and bitumen was determined from the NMR analyses with an internal standard of deuterated dichloromethane. Assuming hydrogen contents of 13 wt. % for undeuterated oil and 10 wt. % for undeuterated bitumen, dueterium substitution for hydrogen is approximately 40% for the expelled oil and 33% for the extracted bitumen in the D_2O experiment. This high degree of deuterium substitution is interpreted to be the result of free radical sites being terminated by deuterium atoms derived from the oxidation of carbonyl groups by D_2O.

The ability of hydrous pyrolysis to generate an expelled oil while anhydrous pyrolysis generates a pyrobitumen may be explained by differences in the availability of hydrogen and type of free-radical terminations that occur during bitumen decomposition. Figure 1 diagramatically presents a working hypothesis for hydrous and anhydrous reaction pathways involving a hypothetical bitumen molecule (Figure 1a) subjected to a barrage of extraneous free radicals thermally generated from other bitumen molecules or the kerogen (Figure 1b). Under hydrous conditions, the free radical sites formed on the bitumen molecule by encounters with incoming free-radicals are frequently terminated with water derived hydrogen (Figure 1c) before β-sission in the molecule occurs. Free-radical fragments that do occur by the infrequent β-sissions are also frequently terminated by water-derived hydrogen (Figure 1d). As a result, a liquid oil is generated. H_2O in this reaction pathway occurs as a dissolved species in the bitumen that impregnates the rock. Although the solubility of hydrocarbons in water is low, the solubility of water in hydrocarbons is two orders of magnitude higher. This solubility is sufficient to supply H_2O for the proposed reactions within the bitumen impregnated rock (Lewan, 1992). Dissolved water in the bitumen network of the rock is maintained at a fully saturated level by the water surrounding the rock in the reactor. Lewan (1992) proposes that this H_2O-saturated bitumen is also responsible for the development of an oil that is immiscible in the bitumen network of the rock. Under anhydrous conditions, the lack of water-derived hydrogen for terminating free-radical sites that occur on the bitumen molecule results in frequent β-sissions (Figure 1e). The numerous free-radical fragments that consequently occur are also deprived of terminations by water-derived hydrogen, and resort to termination by recombination with other free radical sites on the bitumen molecule or on neighboring molecular fragments (1f). In a closed pyrolysis system, these carbon-carbon bond terminations result in the formation of pyrobitumen through the development of a highly cross-linked structure that aromatizes through disproportionation.

REFERENCES

Berl, E., and Schmidt, A., 1932, Über die Entstehung der Kohlen, II. Die Inkohlung von Cellulose and Lignin in neutralem Medium, *Ann. der Chemie* 493:97.

Brooks, J. D., and Smith, J. W., 1969, The diagenesis of plant lipids during the formtion of coal, petroleum, and natural gas - II. Coalification and the formation of oil and gas in the Gippsland Basin, *Geochim. Cosmochim. Acta* 33:1183.

Butler, J. N., 1982, *Carbon Dioxide Equilibria and Their Applications*, Addison-Wesley, London, 259p.

Ferry, J. M., 1983, Regional metamorphism of the Vassalboro Formation, south-central Maine, U.S.A.: A case study of the role of fluid in metamorphic petrogenesis. *J. Geol. Soc.* London 140-551.

Goranson, R. W., 1932, Some notes on the melting of granite, *Am. Jour. Sci.*, 23:227.

Harwood, R. J., 1977, Oil and gas generation by laboratory pyrolysis of kerogen. *Am. Assoc. Petrol. Geol. Bull.* 61:2082.

Jurg, J. W., and Eisma, E., 1964, Petroleum Hydrocarbons: Generation from fatty acid. *Science* 144:451.

Larter, S. R., Horsfield, B., and Douglas, A. G., 1977, Pyrolysis as a possible means of determining petroleum generating potential of sedimentary organic matter, *in*: *Analytical Pyrolysis*, (C. E. R. Jones and C. A. Cramers, eds.), Elsevier, Amsterdam, pp. 189-202.

Lewan, M. D., 1983, Effects of thermal maturation on stable organic carbon isotopes as determined by hydrous pyrolysis of Woodford Shale, *Geochim. Cosmochim. Acta* 47:1471.

Lewan, M. D., 1985, Evaluation of petroleum generation by hydrous pyrolysis experimentation, *Phil. Trans. Roy. Soc. Lond.* A315-123.

Lewan, M. D., 1987, Petrographic study of primary petroleum migration in the Woodford Shale and related rock units, *in*: *Migration of Hydrocarbons in Sedimentary Basins* (B. Doligez, ed.), Editions Technip. Páris, pp. 113-130.

Lewan, M. D., 1992, Primary oil migration and expulsion as determined by hydrous pyrolysis, *13th World Petroleum Congress Proceedings*, Topic 3 (in press).

Lewan, M. D., Bjorøy, M., and Dolcater, D. L., 1986, Effects of thermal maturation on steroid hydrocarbons as determined by hydrous pyrolysis of Phosphoria Retort Shale, *Geochim. Cosmochim. Acta* 50:1977.

Lewan, M. D., Winters, J. C., and McDonald, J. H., 1979, Generation of oil-like pyrolyzates from organic-rich shales, *Science* 203:897.

Rumble, D., III, Ferry, J. M., Hoering, T. C., and Boucot, A. J., 1982, Fluid flow during metamorphism at the Beaver Brook fossil locality, New Hampshire, *Am. Jour. Sci.* 292-886.

Schuhmacher, J. P., Huntjens, F. J., and van Krevelen, D. W., 1960, Chemical structure and properties of coal XXVI. Studies on artificial coalificaiton, *Fuel* 39:223.

Tissot, B., Durand, B., Espitalié, J., and Combaz, A., 1974, Influence of nature and diagenesis of organic matter in formation of petroleum, *Am. Assoc. Petrol. Geol.* 58:499.

Tuttle, O. F., and Bowen, N. L., 1958, Origin of granite in the light of experimental studies in the system $NaAlSi_3O_8$-$KAlSi_3O_8$-SiO_2-H_2O, *Geol. Soc. Am. Mem,*. 74.

Whitney, G., 1990, Role of water in the smectite-to-illite reaction, *Clays and Clay Minerals* 38:343.

Winkler,. G. F., 1974, *Petrogenesis of Metamorphic Rocks,* 3rd ed., Springer-Verlag, New York.

Winters, J. C., Williams, J. A., and Lewan, M. D., 1983, A laboratory study of petroleum generation by hydrous pyrolysis, *in: Advances in Organic Geochemistry, 1981* (M. Bjorøy, ed.) John Wiley & Sons, New York, pp. 524-533.

Table 1. Comparison of pyrolyzate yields from hydrous and anhydrous pyrolysis of crushed aliquots (0.5-2.0 cm) of an immature sample of Woodford Shale (WD-26). All of the experiments were conducted with 400g of rock in one-liter stainless steel-316 reactors.

Experimental Conditions (temp./time)	Generated Gas (wt. % of rock)	Expelled Oil (wt. % of rock)	Bitumen Extract (wt. % of rock)	Total Pyrolyzate[1] (wt. % of rock)
300°C/72 hr				
Hydrous[2]	**0.43**	**0.65**	**8.35**	**9.43**
Anhydrous3	0.78	0.00	8.66	9.44
Δ%	-81.4	+100.0	-3.7	-0.1
330°C/72 hr				
Hydrous[2]	**1.05**	**2.79**	**8.19**	**12.03**
Anhydrous3	1.74	0.00	6.62	8.36
Δ%	-65.7	+100.0	+19.2	+30.5
350°C/72 hr				
Hydrous[2]	**1.68**	**4.15**	**5.71**	**11.54**
Anhydrous[3]	2.40	0.00	3.30	5.70
Δ%	-42.9	+100.0	+42.2	+50.6

$$\Delta\% = [(\text{Hydrous-Anhydrous})/\text{Hydrous}] \times 100$$

[1]Total pyrolyzate = generated gas + expelled oil + bitumen extract.

[2]Crushed rock with 320g of deionized (ASTM type I) water under an initial He pressure of 241 kPa.

[3]Crushed rock initially in an evacuated reactor.

Table 2. Millimoles of headspace gas (g) and dissolved aqueous gas (aq) generated from 400 grams of Woodford Shale sample WD-26. Total gas quantities do not include species dissolved in expelled oil or bitumen.

EXPERIMENT CONDITIONS	300°C/72 h		330°C/72 h		350°C/72 h	
	Hydrous	Anhydrous	**Hydrous**	Anhydrous	**Hydrous**	Anhydrous
CO2 (g)	**20.07**	14.39	**31.17**	20.88	**44.01**	21.56
CO2 (aq)*	**15.06**	–	**49.12**	–	**196.14**	–
TOTAL CO2	**35.13**	14.39	**80.29**	20.88	**240.15**	21.56

*$CO_2(aq) = H_2CO_3 + HCO_3 + CO_3 = K_H\, PCO2\, \{1+(k_1/H^+)+(k_1k_2/(H^+)^2)\}$
where PCO_2 = partial pressure of CO_2 gas (atm), $K_H = 10^{-1.47}$ mol/l.atm (Butler, 1982), H^+ = hydrogen ion concentration (mol/l), k_1 = first disassociation constant ($10^{-6.352}$), and k_2 = second disassociation constant ($10^{-10.329}$).

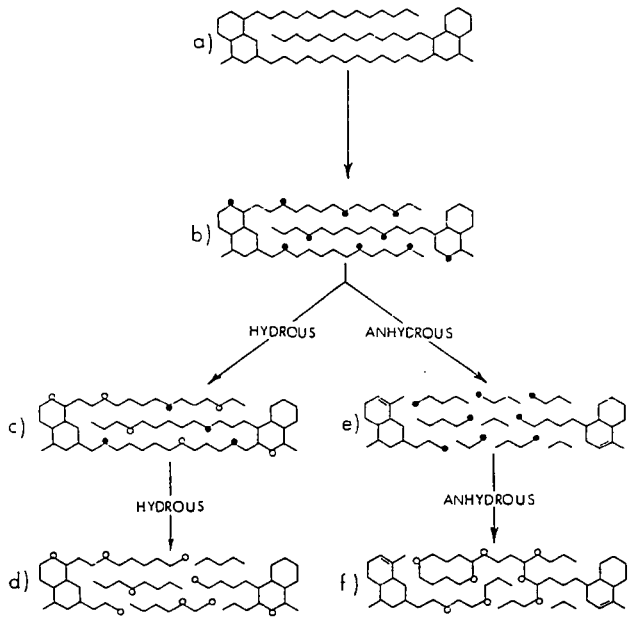

Figure 1. Reaction pathways suggested for thermal maturation of bitumen under hydrous and anhydrous closed-system pyrolysis. Solid circles denote free radicals formed by the loss of hydrogen atoms. Open circles denote terminated free radicals. a) Hypothetical molecule representing aliphatic component of bitumen. b) Molecule with free radical sites, after being subjected to a barrage of extraneous free radicals. c) Termination of free radical sites with water-derived hydrogen atoms before β-sission of chains and disproportionation of cyclics occurs. d) Termination of free-radical fragments with water-derived hydrogen atoms from dissolved water in bitumen. e) Free-radical fragments resulting from frequent β-sissions, which are infrequently terminated by hydrogen atoms due to the lack of dissolved water. f) Termination of free-radical fragments by recombination to form carbon-carbon bond cross linking in the absence of hydrogen atoms from dissolved water.

ALTERNATIVE MECHANISMS FOR RADICAL CATION BOND CLEAVAGE

John H. Penn,* Jin-hai Wang, and You-quan Liu
West Virginia University
Department of Chemistry
Morgantown, WV 26506

Keywords: radical cation, coal liquefaction, mechanism

INTRODUCTION

Recently, a new set of model compounds has been advocated for understanding the reactivity occurring under processing conditions of fossil fuel substrates. These compounds possess multiple functionality and high molecular weight in order to better simulate the reactions which occur in real fuel conversion processes.[1] Chief among these compounds are 4-(naphthylmethyl)bibenzyl, hereafter referred to as Model Compound I, and 4-(2-naphthylethyl)diphenylmethane, II (see structures below). These compounds contain a dicyclic aromatic compound in addition to the monocyclic phenyl groups. Chemical reactivity can then be inferred from the position of the cleavage of the linkages between the aryl groups.

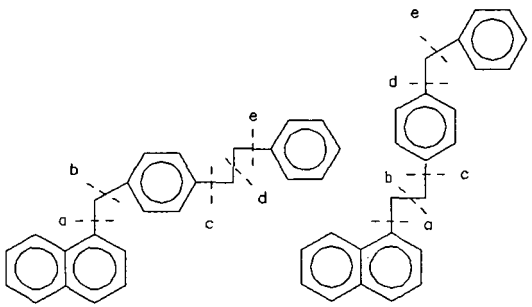

These compounds have been used to test the reactivity of various catalysts. For both compounds, these catalysts cleave bond *a*, *i.e.*, the bond next to the naphthyl ring. Radical cation reactivity has been implicated in these reactions because the naphthyl group is the moiety most likely to lose an electron in these compounds and because the catalytic behavior originates at temperatures in which the surface of the catalyst becomes charged.[2] Theoretical calculations have also been used to support radical cation cleavage of bond a in these compounds.[3]

This reactivity contrasts with the known radical cationic cleavage pathways of monocyclic arenes. For example, the radical cation of 1,1,2,2-tetraphenylethane (**TPE**) is known to cleave at bond *b*, as shown in eq (1).[4] The radical cation of bibenzyl also cleaves at bond *b*, albeit at a much slower rate. The slow cleavage of the radical cation of bibenzyl presumably results from loss of resonance stabilization in the incipient radical and cation formed in this reaction.

In order to distinguish between the contrasting reactivity patterns exhibited by the polycyclic aromatic radical cations and the monocyclic aromatic compounds, we have attempted to independently generate and observe the bond cleavage of the radical cations of naphthyl-containing compounds I, di-(1-naphthyl)methane (**DNM**), and 1,2-di(1-napthyl)ethane (**DNE**). Our strategy for these reactions was to use the photoinitiated electron transfer reactions from 9,10-dicyanoanthracene (**DCA**).[5] In these reactions, **DCA** absorbs a photon of light to produce an excited state of **DCA** (*i.e.*, **DCA***) which does a one-electron oxidation of compounds with oxidation potential $\leq$2.88 V *vs SCE*.[5] These reaction are usually performed in methanol or acetonitrile solutions to facilitate electron transfer and to trap the resulting cations which are expected to be produced in these reactions.

(1)

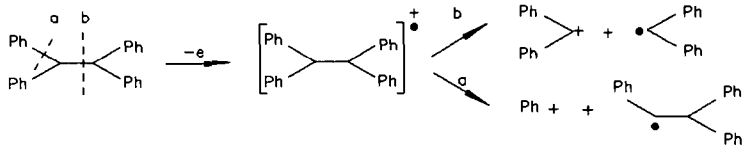

RESULTS AND DISCUSSION

Generation of the Radical Cation of I, DNM, and DNE Under Degassed Conditions: Irradiation of a freshly distilled acetonitrile solution of **I** (2.0 mM) and **DCA** (0.1 mM) using light of 350 nm from a Rayonet reactor for 96 h yielded no product when the reaction solution was degassed with N_2 for 15 min prior to the irradiation and then sealed with a latex septum. The lack of reaction was initially indicated by the lack of low molecular weight products by GC analysis of the reaction solution and was confirmed by the use of internal standards which were added prior to initiation of the reaction. The reactions of **DNM** and **DNE** were similar in that no reactions were detectable after 96 h of irradiation. Again the lack of reactivity was conclusively demonstrated by the use of internal standards.

Since the interpretation of negative results can be often ascribed to poor technique or the inability of a laboratory to reproduce other worker's results, we have generated the radical cation of **TPE** using this methodology. As expected, diphenylmethane and diphenylmethyl methyl ether were produced in quantitative yield in just 24 h of irradiation. These results are consistent with the results obtained in Reference 4 and demonstrate that the radical cations of these substrates are being generated under these conditions.

The significance of these results is that the radical cations of **DNM** and **DNE** do not cleave readily at room temperature. These results are analogous to those reported for bibenzyl (*i*.e., 1,2-diphenylethane)[6] in which a very low quantum efficiency for cleavage has been reported using the photoinitiated electron transfer methodology for radical cation generation. While the lack of bond cleavage from the radical cation of these 1,2-diarylethanes does not rule out the bond cleavage reactions of radical cations under catalytic conditions where higher temperatures may lead to faster reactions from these intermediates, the lack of bond cleavage suggests that these intermediates have higher energy bond dissociation energies which makes their intermediacy more difficult to postulate without further characterization of their reactivity.

Generation of the Radical Cation of I, DNM, and DNE With O_2 in the Solution: Similar experiments to those above were performed after bubbling of O_2 for 15 min prior to irradiation. In contrast to the lack of reactivity observed under degassed conditions, bond cleavage is observed for **I**, **DNM**, and **DNE** (Note Figure 1). In all cases, bond *a* cleavage is noted in addition to a variety of other products.

Complete interpretation of the reaction results is not possible since the mass balances in these reactions are poor at the present time. We speculate that secondary reactions involving O_2 and the $DCA^{\bullet-}$ (formed by electron transfer from the DCA^* and the aromatic moiety) to yield $O_2^{\bullet-}$, followed by a H^+ transfer to yield a pair of radicals which initiate a chain reaction may be responsible for the observed reactivity (Note Figure 2). However, definitive interpretation must await better mass balances and more detailed work to explore the bounds of this

reactivity.

ACKNOWLEDGEMENTS
This work was supported by the Consortium for Fossil Fuel Liquefaction Science under contract to the U.S. Department of Energy.

REFERENCES

1. Farcasiu, M.; Smith, C.M. Ladner, E.P.; Sylwester, A.P. *Prepr. Pap. Am. Chem. Soc. Div. Fuel Chem.*, **1991**, 36.

2. Farcasiu, M.; Smitth, C.M. *Energy Fuels*, **1991**, *5*, 83.

3. Ades, H.F.; Companion, A.L.; Subbaswamy, K.R. *J. Phys. Chem.*, **1991**, *95*, 2226, 6502.

4. Okamoto, A.; Snow, M.S.; Arnold, D.R. *Tetrahedron*, **1986**, *42*, 6175.

5. Mattes, S.L.; Farid, S. *Organic Photochemistry*, **1983**, *6*, 233.

6. Arnold, D.R.; Lamont, L.J. *Can. J. Chem.* **1989**, *67*, 2119.

FIGURES

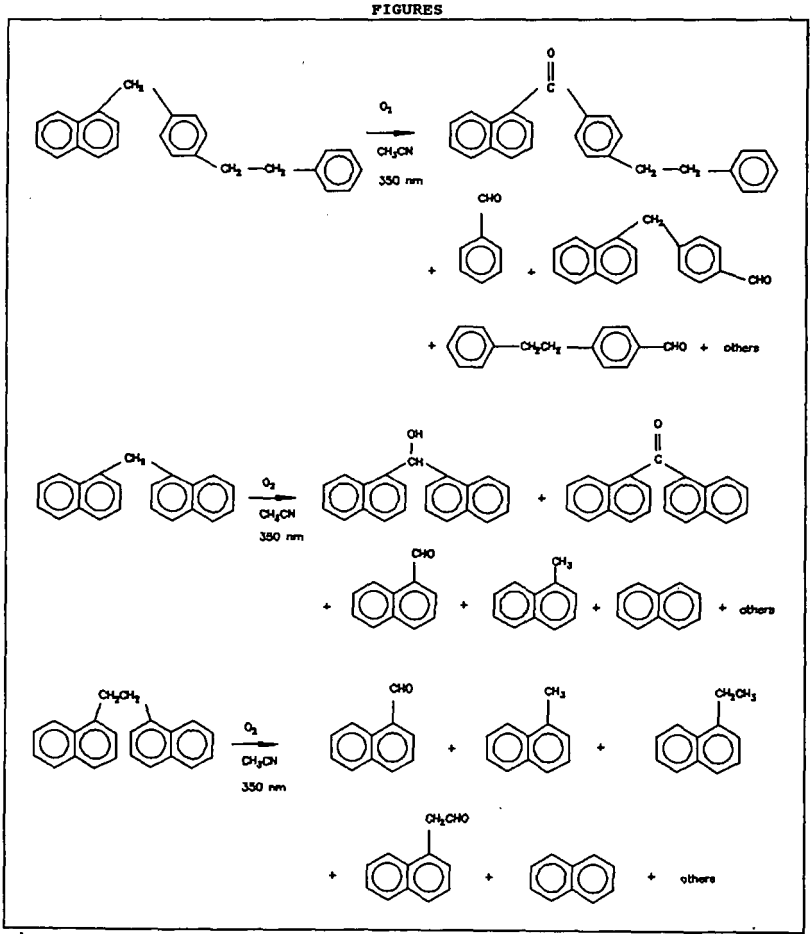

Figure 1. Change in reactivity influenced by O_2

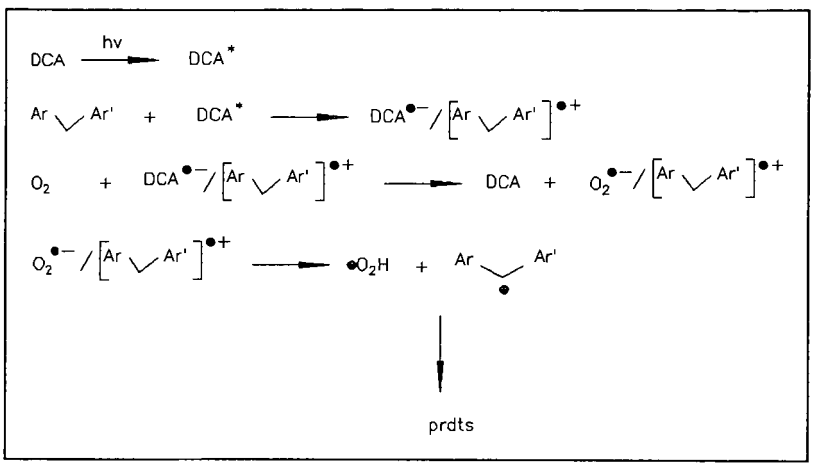

Figure 2. Partial Mechanism Explaining the Influence of O_2.

Hydrogen-Transferring Pyrolysis of Cyclic and Straight-Chain Hydrocarbons. Enhancing High Temperature Thermal Stability of Aviation Jet Fuels by H-Donors

Chunshan SONG*, Wei-Chuan LAI and Harold H. SCHOBERT

Fuel Science Program, Department of Materials Science and Engineering, 209 Academic Projects Building, The Pennsylvania State University, University Park, PA 16802

Keywords: Pyrolysis, Hydrogen-Transferring pyrolysis, Jet fuel, Thermal stability

INTRODUCTION

The present work is a fundamental study of condensed-phase pyrolysis of saturate hydrocarbons including alkylcyclohexanes, trans- and cis-steric isomers of decalin and straight-chain paraffins as well as hydroaromatics such as tetralin. This work is a part of an on-going research program for developing advanced jet fuels thermally stable at high temperatures. One of the critical problems in developing thermally stable jet fuels for high-Mach aircraft is the formation of solid from hydrocarbon fuels in pyrolytic regime (Roquemore et al., 1989; Hazlett, 1991). In studying the pyrolytic degradation of jet fuels, it occurred to us that hydrogen-transfer from H-donors, such as those present in coal-derived JP-8C jet fuel, could play an important role in suppressing thermal decomposition and solid formation (Song et al., 1991a, 1991b, 1992a, 1992b). The hydrogen-transferring pyrolysis described in this paper refers to the thermal decomposition of straight-chain and cyclic hydrocarbons in the presence of H-donors.

This paper reports on 1) pyrolytic degradation of the above-mentioned cyclic and straight-chain hydrocarbons; 2) inhibiting effects of H-donors on the decomposition and solid-forming tendency of n-tetradecane (n-C_{14}), n-butylcyclohexane (n-BCH), cis-decalin (cis-D) and n-butylbenzene (n-BB) as well as a petroleum-derived JP-8P jet fuel; and 3) the mechanisms of the pyrolysis and H-transferring pyrolysis. It should be noted that the experimental conditions used in this work are such that they are close to the high-temperature thermal environment of jet fuel in the future high-Mach aircraft under consideration. These conditions are characterized by condensed or supercritical phases, relatively high pressure, static reactor, and long residence time. Such conditions are distinctly different from those used in most previous paraffin pyrolysis work (vapor phase, low-pressure, flow reactor, short residence time).

EXPERIMENTAL

Reagent-grade n-C_{14}, n-BCH, ethylcyclohexane (ECH), trans-decalin (trans-D) and cis-decalin (cis-D), decalin, tetralin, n-butylbenzene (n-BB) from Aldrich and a petroleum-derived JP-8P jet fuel (Song et al., 1992a) were used. Several compounds including tetralin, decalin, cis-D and trans-D were also examined as H-donors. The pyrolysis was conducted at 450°C for 0-8 h under 0.69 MPa UHP-N_2 (cold) in 25 mL tubing bombs using 5 mL sample. A fluidized sandbath preheated to 450°C was used as heater. The products were identified by capillary GC-MS and quantified by GC. More experimental details may be found in a companion paper (Lai et al., 1992).

RESULTS AND DISCUSSION

I. Pyrolysis of Cyclic and Straight-Chain Hydrocarbons

We first conducted a comparative examination of thermal stability of several cyclic and straight-chain hydrocarbons, which are representative components in coal- and petroleum-derived jet fuels, respectively. Figure 1 shows the time-pressure profiles for the pyrolysis of these compounds. Since static reactor was used, the sample is always confined within the reactor. Therefore, the increase of system pressure after equilibrium boiling is indicative of the extent of thermal decomposition. As shown in Figure 1, when tetralin was heated under 0.69 MPa N_2 (cold) pressure, the system pressure increased to 3.4 MPa within 10 minutes, then the pressure maintained nearly constant. All the other compounds displayed more or less pressure increase. Their t-p profile patterns provide a convenient measure for the extent and rate of their thermal decomposition to form smaller molecules. It should also be noted from Figure 1 that the temperature of 450°C and pressures at 450°C ($\geq$ 3.5 MPa) are higher than the critical temperatures and critical pressures of all the compounds, suggesting the occurrence of supercritical-phase pyrolysis.

Figure 2 shows the conversion of several compounds versus residence time at 450°C for 0-8 h. The typical component of petroleum jet fuels, n-C14, exhibited the highest degree of decomposition, and its pyrolysis led to 50% conversion in just 30 min. For the cycloalkanes, the rate of *n*-BCH decomposition is faster than that of ECH, indicating that increasing the length of side chain on alkylcyclohexane decreases the thermal stability. Decalin appears to

be more stable than the other saturates (Eser et al., 1992, Song et al., 1992b) but it is originally a mixture of trans- and cis-D (see below). Tetralin was the most stable compound when stressed alone. Combination of the data in Figures 1 and 2 indicates that cycloalkanes are much more stable than the long-chain paraffins; the increase in the length of side-chain of alkylcycloalkanes or straight-chain paraffins decreases the stability and increases the decomposition rate.

Alkylcyclohexanes. Figure 3 shows the distribution of products from n-BCH as a function of conversion. At low conversion level of 11.8 mol%, the major products are cyclohexane (3.0, mol%), methylene-cyclohexane (2.3), methylcyclohexane (1.9) and cyclohexene (1.1). Scheme I shows the possible reaction mechanisms proposed based on the identified products. The initiation reaction of n-butylcyclohexane is likely the homolytic cleavage of the C-C bond between the ring and the side-chain to form cyclohexyl and 1-butyl radicals. The formation of the four predominant initial products can be rationalized by the radical reaction pathways I, II, III, and IV, respectively. After 1 h at 450°C, the yield of methylenecyclohexane begins to decrease with further increasing residence time, presumably due to hydrogenation to form methylcyclohexane.

In regard to the reaction mechanisms for alkylcyclohexane pyrolysis, there is little information in the literature except for the recent report of Savage and Klein (1988), who found that there are only two major pathways for pyrolysis of n-tridecylcyclohexane. The pathways I and II for n-BCH are also consistent with their observations. However, the present work reveals that other major pathways, III and IV, also exist for the alkylcyclohexanes with shorter side-chains, as shown in Scheme I. Interestingly, when the residence time was extended to 2.5 h and longer, cyclohexane and methylcyclohexane become the two most predominant products, and their yields were several times higher than those of all the other products. These results suggest that pathways I and III dominate in long-duration n-BCH pyrolysis.

Scheme I. Possible Mechanisms for Pyrolysis of n-Butylcyclohexane

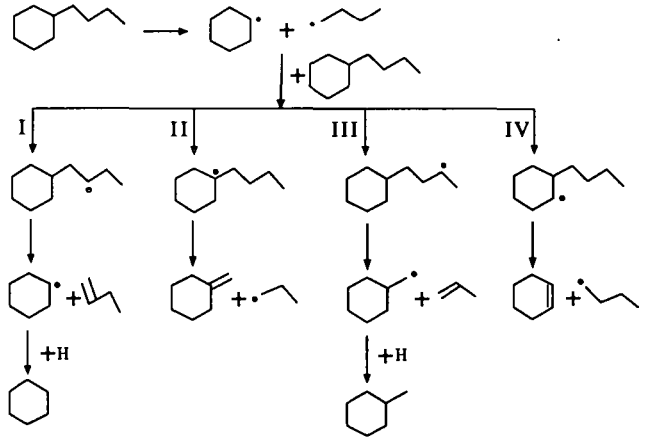

Figure 4 shows the distribution of products from ECH. At low conversion level (7.3 mol%), the major products from ECH are cyclohexene (1.50 mol%), methylcyclohexane (0.83 mol%), methylcyclohexene (0.87 mol%). The preference of cyclohexene formation indicates that the reaction via cyclohexyl radical is a major path, similar to path IV for n-BCH. However, methylenecyclohexane is a minor product in this case (0.17 mol%), indicating that one of the major pathways for n-BCH becomes a minor one for ECH. Another major difference between ECH and n-BCH is the higher yields of isomerization products from ECH pyrolysis, such as methylcyclopentane.

Decalin. Figure 5 shows the product distribution for pyrolysis of decalin, which was originally a mixture of nearly equivalent weights of trans- and cis-D. After decalin pyrolysis at 450°C, the yield of trans-D increased slightly and that of cis-D decreased monotonically with increasing time up to about 4 h. There are two possible reasons for such observations: isomerization of cis- to trans-D or decomposition of cis-D. To gain further insight, we performed the runs of pure trans-D and cis-D, as shown in Figure 6. It was found that cis-D is not stable and tends to isomerize into trans-D as outlined in Scheme II. Amount of trans-D formed from cis-D increased from 6% in 30 min to 41% after 4 h at 450°C. Roberts and Madison (1959) found that di-t-butylperoxide can initiate such an isomerization. Probably

this is initiated via H-abstraction by a radical from 9-position. On the other hand, trans-D is much more stable than cis-D. Its isomerization to cis-D also occurred but the extent was very limited, even after 8 h, as can be seen from Figure 6. In fact, trans-D was found to be one of the most stable components in coal-derived jet fuel JP-8C (Song et al., 1992a).

Scheme II. Isomerization of cis-Decalin to trans-Decalin

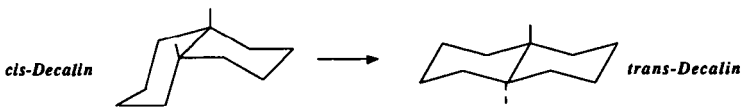

We also observed substantially higher gas yields from cis-D (5.4 wt% in 4 h) than from trans-D (0.8 wt% in 4h), showing higher degree of ring-opening cracking and subsequent dealkylation with cis-isomer. In the case of cis-D, 1-butylcyclohexene was also detected as a major cracking product (0.7 mol%) after 30 min at 450°C. It was formed probably via the 9-decyl radical and subsequent β-scission which caused the ring-openning cracking. The cracking via 9-decyl radical was also suggested for hydropyrolysis of decalin by Shabtai et al. (1979). Therefore, the ring-opening cracking and isomerization of cis-decalin may share the same initiation path, because the latter also involves 9-decyl radical formation as the first step. In summary, the steric conformation of cycloalkanes also affects their thermal stability, and for decalin, trans-isomer is much more stable.

n-Tetradecane Pyrolysis. Pyrolysis of n-tetradecane at 450°C for 0-8 h produced up to about 175 compounds, and the products ranged from lightest molecules such as hydrogen and methane to heavy polyaromatics such as pyrene and solid deposits. After 30 min at 450°C, 49% of n-C_{14} has been decomposed, and the main products are C_1-C_{13} alkanes and C_2-C_{13} 1-alkenes. Scheme III shows the possible reaction pathways for thermal cracking of long-chain n-alkanes such as n-tetradecane under the conditions employed. The first substrate radicals from n-C_{14} include both sec-$C_{14}H_{29}$• (eq.2) and 1-$C_{14}H_{29}$• (eq. 3). Formation of the primary radical requires higher activation energy than that of secondary radical, but the difference is not very large in H-abstraction reaction. For example, the activation energies for H-abstraction from n-butane to form 2-C_4H_9• and 1-C_4H_9• at 427°C are 10.4 and 12.3 kcal/mol, respectively (Allara and Shaw, 1980).

There are two extremes of the same fundamental mechanism for radical reactions: the Rice-Kossiakoff mechanism and the Fabuss-Smith-Satterfield mechanism (Fabuss et al., 1966; Poutsuma, 1990), which afford different product spectra. Pyrolysis of long-chain paraffins is still the subject of many investigations. Several recent papers reported the preferential formation of 1-alkenes from vapor-phase pyrolysis of long-chain paraffins (Zhou et al., 1987; Fairburn et al., 1990). In the present work, significant amounts of olefins, mainly 1-alkenes, were also detected, both in liquid and gaseous products. However, unlike the literature results for high temperature and short-residence time pyrolysis, the olefins are not dominant species for most product groups with the same carbon number under the present conditions, except the C_{12} group in which 1-dodecene yield was higher than dodecane for 30 min run.

Scheme III. Possible Mechanisms of Pyrolysis of n-Alkanes C_mH_{2m+2}

$$C_mH_{2m+2} \rightarrow 1\text{-}R^{\bullet} + 1\text{-}R^{\bullet} \quad 1)$$

$$1\text{-}R^{\bullet} + C_mH_{2m+2} \rightarrow \text{sec-}C_mH_{2m+1}{}^{\bullet} + RH \quad 2)$$

$$1\text{-}R^{\bullet} + C_mH_{2m+2} \rightarrow 1\text{-}C_mH_{2m+1}{}^{\bullet} + RH \quad 3)$$

$$\text{sec-}C_mH_{2m+1}{}^{\bullet} \rightarrow 1\text{-}C_{m-n}H_{2(m-n)+1}{}^{\bullet} + 1\text{-}C_nH_{2n} \quad 4)$$

$$1\text{-}C_mH_{2m+1}{}^{\bullet} \rightarrow 1\text{-}C_{m-n-2}H_{2(m-n-2)+1}{}^{\bullet} + C_2H_4 \quad 5)$$

$$1\text{-}C_{m-n}H_{2(m-n)+1}{}^{\bullet} + C_mH_{2m+2} \rightarrow C_{m-n}H_{2(m-n)+2} + \text{sec-}C_mH_{2m+1}{}^{\bullet} \quad 6)$$

$$C_mH_{2m+1}{}^{\bullet} + C_nH_{2n+1}{}^{\bullet} \rightarrow C_{m+n}H_{2(m+n)+2} \quad 7)$$

The differences between the present and literature results can be explained as follows. At high temperature (≥ 550°C)-low pressure-short residence time (< 1 min) conditions, as employed in most previous pyrolysis work, radicals tend to undergo β-scission, which leads to products rich in 1-alkene and ethylene. Analytical data show that pyrolysis under our conditions (about 3.4-8.9 MPa system pressures at 450°C for 0-4 h) leads to more alkanes, which can be rationalized based on the Fabuss-Smith-Satterfield mechanism. Under high-pressure conditions, which in general tend to enhance bimolecular reactions, β-scission (eqs. 4,5) will be in competition with hydrogen abstraction (eq.6). Because C_8-C_{12} alkanes and alkenes were still the major components in liquid products after 30 min at 450°C, it is likely that

the first radical formed by β-scission of $C_{14}H_{29}$• radicals (eqs. 4,5) will already prefer to undergo hydrogen-abstraction (eq. 6), which yield one 1-alkene molecule and one alkane molecule. The activation energy required for H-abstraction by a radical from a hydrocarbon or molecular H_2 is smaller than that required for β-scission of the same radical. For example, the energy for β-scission of 1-C_5H_{11}• to form 1-C_3H_7• plus C_2H_4 is 29 kcal/mol, while that for its H-abstraction from another hydrocarbon or H_2 is about 10-12 or 15-17 kcal/mol at 427°C (Allara and Shaw, 1980).

II. H-Transferring Pyrolysis and Inhibition of Solid Formation

The present work on H-transferring pyrolysis seeks to clarify whether and how the hydrogen-donors affect the pyrolytic degradation and solid-forming tendencies of jet fuel components. Figure 7 shows the inhibiting effect of tetralin on solid deposit formation from JP-8P fuel, n-C14, and n-BB, respectively, at 450°C for 4 h. In the absence of H-donor, the amounts of deposits formed were n-BB (5.6 wt%) > JP-8P (3.1 wt%) ≥ n-C14 (3.0 wt%). These figures are extremely large if one considers the deposit formation inside fuel lines in aircraft. It is clear from Figure 3 that adding a small amount of tetralin significantly reduced the deposit formation from all these compounds. As for the efficiency of H-donor, adding 10 vol% tetralin to JP-8, n-C_{14} and n-BB reduced the formation of deposits by 90% (from 3.1 to 0.3 wt%), 77% (from 3.0 to 0.7 wt%) and 54% (from 5.6 to 2.6 wt%), respectively. These results demonstrate that by means of H-transferring pyrolysis, hydrocarbon jet fuels can be used at high operating temperatures in pyrolytic regime with little or no solid deposition.

Multi-ring cyclic alkanes such as decalin can also serve as H-donors at high temperatures, although decalin is not as active as tetralin for inhibiting solid formation (Song et al., 1991c). Table 1 shows that decalin can also suppress the deposit formation from JP-8P jet fuel, n-C_{14} and n-BB. In fact, adding both trans- and cis-D by 50 vol % almost eliminated solid formation from n-C_{14}, JP-8P, and n-BB. Since decalin and n-C_{14} are also representative components of coal- and petroleum-derived jet fuels, respectively, their mixture can also be viewed as a fuel blend. These results also account for the fact observed in previous work that the presence of significant amounts of C_{12}-C_{18} in coal-derived JP-8C did not cause remarkable solid formation (Song et al., 1991b, 1992a).

Based on the foregoing, the reduced solid formation and the enhanced stability of hydrocarbons in H-transferring pyrolysis can be attributed to the stabilization of the reactive radicals via hydrogen-abstraction from tetralin or decalin type compounds, which contributes mainly to inhibiting the secondary radical reactions and suppressing solid formation, as shown in Scheme IV.

Scheme IV. Radical Stabilization via H-Transfer from Tetralin and Decalin

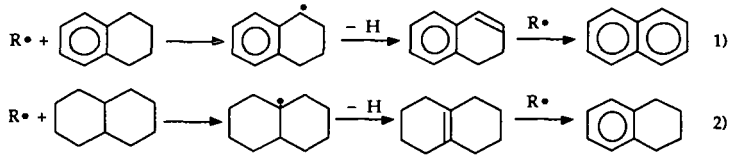

We further examined the effect of adding 10 vol% H-donor tetralin on pyrolysis of n-C_{14}, n-BB, n-BCH, and cis-D at 450°C for 0.5 h (Table 1). Adding tetralin significantly suppressed the n-C_{14} decomposition, and its conversion decreased from 49 to 37 mol%. Surprisingly, it was found that the yields of lower alkanes decreased more than those of corresponding 1-alkenes upon tetralin addition. For example, the ratio of 1-dodecene to n-dodecane increased from 1.6 to 2.6, and that of 1-undecene to undecane increased from 0.5 to 0.6 upon addition of 10 vol% tetralin. In long duration runs, the effect of tetralin in suppressing n-C_{14} decomposition becomes smaller. This is because H-donors inhibit the radical-induced reactions but do not suppress the homolytic C-C bond cleavage. After 4 h, the major effects of H-donor appear to be the inhibition of solid and C_1-C_4 gas formation, as can be seen from Table 1.

For 30 min run of n-BCH, adding tetralin decreased its conversion from about 12 to 6 mol%. In addition to the conversion decrease, the product distribution pattern changed upon tetralin addition. It was found that the decreasing extents in yields of cyclohexane, methyl- and ethylcyclohexane were higher than those for cyclohexene, methyl- and ethylcyclohexene. For cis-D, adding 10 vol% tetralin suppressed the isomerization and decomposition of cis-decalin: the conversion decreased from 12 to 8 mol%, and the cis-D/trans-D ratio increased from 14.2 to 18.9.

III. Reactions of H-donors in H-Transferring Pyrolysis

Tetralin is quite stable when stressed alone at 450°C. The major products from pyrolysis of pure tetralin are 1-

methylindan and naphthalene as well as a small amount of n-butylbenzene. Even after 8 h pyrolysis at 450°C, the total gas products were still within 1 wt%, indicating the ring-opening cracking and dealkylation reactions were very limited with tetralin. On the basis of the findings of Benjamin et al. (1979) and Franz et al. (1980), the isomerization proceeds through the 2-tetralyl radical to form 1-indanylmethyl radical, as shown in Scheme V.

Scheme V. Isomerization of Tetralin to 1-Methylindan

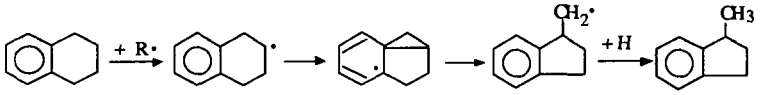

In the H-transferring pyrolysis of n-C_{14} and n-BB, the distribution of products from tetralin shows a significantly different pattern. n-BB is a reactive alkylbenzene (Peng et al., 1992) As shown in Scheme VI, in the presence of n-C_{14} or n-BB, tetralin mainly undergoes dehydrogenation reaction to form naphthalene. For the mixtures of 10 vol% tetralin with reactive compounds such as n-C_{14} or n-BB, the ring-contraction isomerization was enhanced slightly at 450°C for 30 min but further increasing residence time increased mainly dehydrogenation. After 4 h, more than 90% of tetralin has been dehydrogenated in the case of its mixture and its isomerization was reduced significantly as compared to the run of itself. For 30 min runs, the radicals from n-BB were more active in dehydrogenating tetralin, although n-BB conversion was lower than that of n-C_{14} under this condition. For the mixtures of 25 vol% tetralin with n-C14, however, the yield of 1-methylindan from tetralin increased significantly after 4 h run, the value of which is close to that from pure tetralin.

Scheme VI. Products from Tetralin in Pyrolysis & H-Transferring Pyrolysis

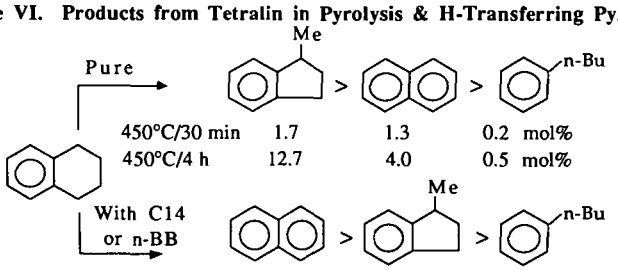

Taking into account the difference in reaction mechanisms of dehydrogenation (Scheme IV) and isomerization (Scheme V), our results show that when the H-donor concentration is relatively low, the radicals from n-C_{14} and n-BB mainly abstract benzylic hydrogen to yield 1-tetralyl radical. In such case, the formation of 2-tetralyl radical is very limited and hence the isomerization is not very important. This also confirms that the reactions via 1-tetralyl radical shown in Scheme IV are the major reactions. When tetralin is present at high levels, however, radicals from n-C_{14} abstract hydrogens from both 1- and 2-positions. As a result, n-C_{14} not only promotes tetralin dehydrogenation, but also enhances its isomerization to form 1-methylindan, although the former is still the dominant reaction. It is also interesting to note that the presence of 90 vol% n-BCH caused little increase in reactions of tetralin, neither dehydrogenation nor isomerization, although tetralin suppressed the n-BCH decomposition from 12 to 6 mol% at 450°C

for 0.5 h. On the contrary, adding 10 vol% tetralin to n-BB had little impact on n-BB conversion and gas formation at 450°C for 0.5 h, although tetralin dehydrogenation was more remarkable than in the case of n-BCH.

CONCLUSIONS

High temperature thermal stability of hydrocarbons depends mainly on their chemical structure, carbon number, length of main-chain or alkyl side-chain, and steric conformation (cis, trans). Cycloalkanes are more stable than long-chain paraffins. The stability of straight-chain paraffins decreases with increasing carbon number. Increasing the length of side-chain of alkylcyclohexanes decreases the thermal stability. Steric conformance also affects thermal reactivity, and it was found that trans-decalin is much more stable than cis-decalin.

Pyrolysis of n-tetradecane, a JP-8P jet fuel and n-butylbenzene at 450°C can result in significant amounts of solid deposits. Adding small amounts of H-donors such as tetralin and decalins was found to be effective for inhibiting fuel decomposition and solid formation at 450°C. By taking advantage of hydrogen-transferring pyrolysis reported in this work, hydrocarbon jet fuels can be used at high temperatures in pyrolytic regime with little or no solid deposition.

ACKNOWLEDGMENTS

This project was jointly supported by the U.S. Department of Energy, Pittsburgh Energy Technology Center and the Air Force WRDC/Aero Propulsion Laboratory. Funding was provided by the U.S. DOE at Sandia National Laboratories under contract DE-AC04-76DP00789. We are pleased to thank Drs. W.E. Harrison III and D.M. Storch of WRDC, E. Klavetter of SNL, and S. Rogers of PETC for their support and technical advice. We also wish to thank Dr. P.G. Hatcher of PSU for instrumental support to the maintenance of analytical equipments for the jet fuel project.

REFERENCES

Allara, D.L.; Shaw, R. J. Phys. Chem. Ref. Data, **1980**, 9 (3), 523-559.
Benjamin, B.M.; Hagaman, E.W.; Raaen, V.F.; Collins, C.J. Fuel, **1979**, 58, 386.
Eser, S.; Song, C.; Copenhaver, R., Parzynski, M., ACS Div. Petrol. Chem. Prepr., **1992**, 37 (2), 493-504.
Fabuss, B. M.; Smith, J.O.; Satterfield, C.N., Adv. Petrol. Chem. Refin., **1964**, 9, 158-201.
Fairburn, J.F.; Behie, L.A.; Svrcek, W.V., Fuel, **1990**, 69 (12), 1537-1545.
Franz, J.A.; Camaioni, D.M., J. Org. Chem., **1980**, 45, 5247-5245.
Hazlett, R.N., Thermal Oxidation Stability of Aviation Turbine Fuels, ASTM, 1991, and references cited therein.
Lai, W.-C.; Song, C.; Schobert, H.H.; Arumugam, R., Paper in this issue.
Peng, Y.; Schobert, H.H.; Song, C.; Hatcher, P.G., Paper in this issue.
Poutsma, M.L., Energy & Fuels, **1990**, 4 (2), 113-131.
Roberts, R.M.; Madison, J.J., J. Am. Chem. Soc., **1959**, 81, 5839.
Roquemore, W.M.; Pearce, J.A.; Harrison III, W.E.; Krazinski, J.L.; Vanka, S.P. ACS Div. Petrol. Chem. Prepr., **1989**, 34 (4), 841.
Savage, P.E.; Klein, M.T., Ind. Eng. Chem. Res., **1988**, 27, 1348-1356.
Shabtai, J.; Ramakrishnan, R.; Oblad, A.G., Adv. Chem. Ser., **1979**, 183, 297.
Song et al., Compositional Factors Affecting Thermal Degradation of Jet Fuels, Technical Progress Report for Period October 1990-January 1991, Air Force Aero Propulsion Laboratory, 42-3462-TPR-2, February, **1991a**.
Song et al., Advanced Thermally Stable Jet Fuel Development Program Annual Report, Vol. 2, Final Report for Period July 1990-July 1991, Air Force Aero Propulsion Laboratory, WL-TR-91-2117, Vol. II, August **1991b**.
Song, C.; Nihonmatsu, T.; Nomura, M., Ind. Eng. Chem. Res., **1991c**, 30 (8), 1726-1734.
Song, C.; Eser, S.; Schobert, H.H., Hatcher, P.G., ACS Div. Petrol. Chem. Prepr., **1992a**, 37 (2), 540-547.
Song, C.; Peng, Y.; Jiang, H.; Schobert, H.H., ACS Div. Petrol. Chem. Prepr., Vol. 37, **1992b**, 37 (2), 484-492.
Zhou, P.; Hollis, O.L.; Crynes, B.L., Ind. Eng. Chem. Res., **1987**, 26, 846-852.

Abbreviations

n-BB:	n-Butylbenzene
n-BCH:	n-Butylcyclohexane
n-C10:	n-Decane
n-C_{14}:	n-Tetradecane
cis-D:	cis-Decalin or cis-Decahydronaphthalene
trans-D:	trans-Decalin or trans-Decahydronaphthalene
ECH:	Ethylcyclohexane
JP-8P:	Petroleum-derived JP-8 jet fuel
JP-8C:	Coal-derived JP-8 jet fuel

Table 1. Deposit Formation and Liquid Depletion during H-Transferring Pyrolysis of Hydrocarbons and JP-8P Jet Fuel

Feedstocks		Condition		Products (wt%)			
Sample	+ vol% H-Donor	Temp, °C	Time, h	C1-C4 Gas	≥ C5 Liquid	Solid Deposit[a]	Recovered Deposit[b]
n-Tetradecane		450°C	4.0	38.3	58.8	3.0	1.9
Tetradecane	+ 50% cis-Decalin	"	"	19.5	80.3	0.1	0
Tetradecane	+ 50% trans-Decalin	"	"	18.2	81.7	0.1	0
Tetradecane	+ 10% Tetralin	"	"	27.3	72.0	0.7	0.2
Tetradecane	+ 50% Tetralin	"	"	9.1	90.8	0.1	0
cis-Decalin		"	"	5.4	94.6	0	0
trans-Decalin		"	"	0.8	99.2	0	0
Tetralin		"	"	0.7	99.4	0	0
n-Butylbenzene (n-BB)		"	"	17.2	77.2	5.6	5.0
n-BB	+ 50% cis-Decalin	"	"	14.3	85.9	0	0
n-BB	+ 50% trans-Decalin	"	"	12.1	87.9	0	0
n-BB	+ 10% Tetralin	"	"	15.4	82.0	2.6	2.5
n-BB	+ 50% Tetralin	"	"	9.8	90.2	0	0
JP-8P Jet Fuel		"	"	26.8	70.2	3.1	1.9
JP-8P	+ 50% trans-Decalin	"	"	13.3	86.6	0.1	0
JP-8P	+ 10% Tetralin	"	"	20.0	79.7	0.3	0.1
JP-8P	+ 50% Tetralin	"	"	7.9	92.0	0.1	0
n-Tetradecane		450	0.5	5.9	94.1	0	0
n-Tetradecane	+ 10% Tetralin	"	"	2.3	97.7	0	0
n-Butylbenzene		"	"	5.1	94.9	0	0
n-BB	+ 10% Tetralin	"	"	5.4	94.6	0	0
n-Butylcyclohexane		"	"	1.8	98.2	0	0
n-Butylcyclohexane	+ 10% Tetralin	"	"	0.7	99.3	0	0
cis-Decalin		"	"	0.3	99.7	0	0
cis-Decalin	+ 10% Tetralin	"	"	0.2	99.8	0	0
Tetralin		"	"	0.1	99.9	0	0

a) Solid deposit on the reactor wall determined by measuring weight gain of the microreactor after the stressing, pentane washing and drying; b) Solid deposit recovered from the reactor wall.

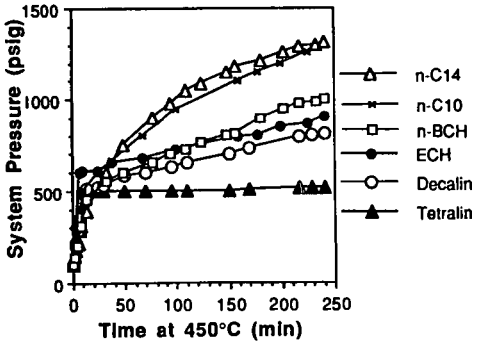

Fig.1. System t-p profiles for pyrolysis of model compounds

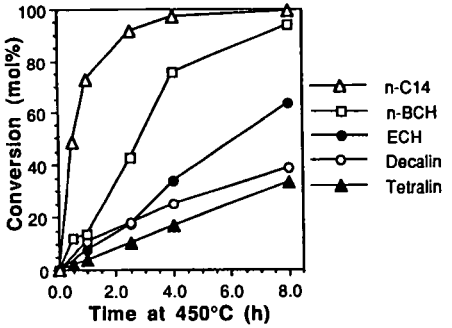

Fig.2. Conversion of model compounds in pyrolysis

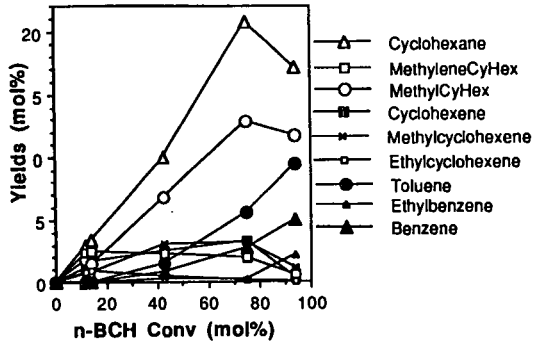

Fig.3. Product distribution for n-BCH pyrolysis

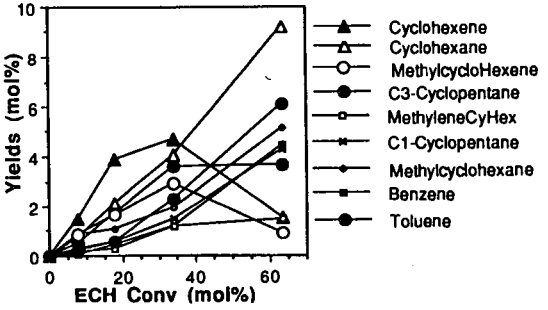

Fig.4. Product distribution for ECH pyrolysis

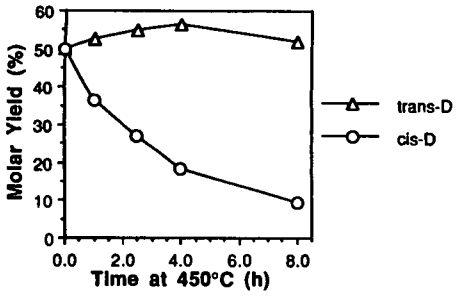

Fig.5. Compositional change during decalin pyrolysis

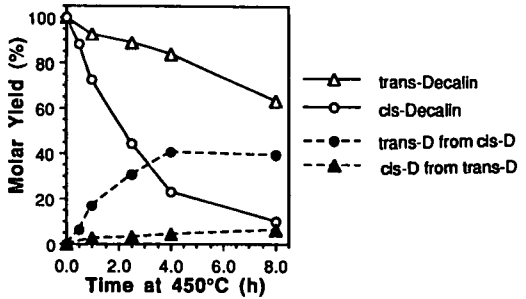

Fig.6. Conversion and isomerization during pyrolysis of pure cis-decalin and pure trans-decalin

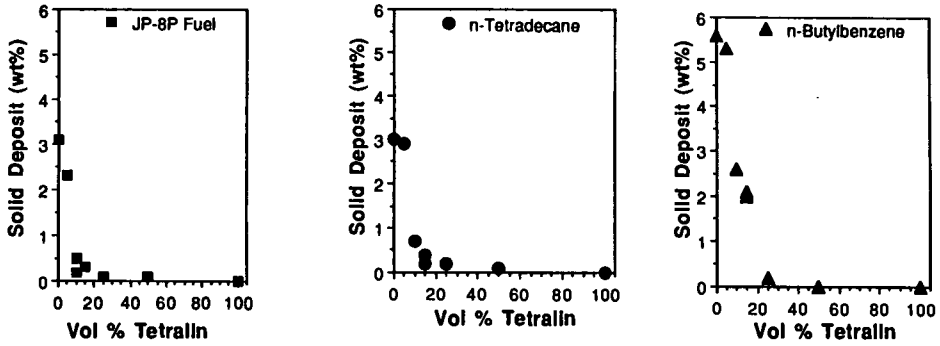

Fig.7. Inhibiting effect of H-donor tetralin on the solid formation from JP-8P, n-tetradecane and n-butylbenzene

POTENTIAL STABILIZERS FOR JET FUELS SUBJECTED TO THERMAL STRESS ABOVE 400°C: 2. NMR STUDIES.

Maria Sobkowiak, Leena Selvaraj, Emily Yoon and Michael M.Coleman*
Department of Materials Science and Engineering
The Pennsylvania State University
University Park, PA 16802

Keywords: Jet Fuels, Thermal Stabilizers, NMR

INTRODUCTION

We recently reported[1,2] the results of Fourier transform infrared (FTIR) and visual studies of Jet A-1 samples that had been subjected to thermal stresses for varying periods of time at a temperature of 425°C. FTIR spectroscopy was shown to be an excellent experimental method that has just about the right degree of sensitivity for our purposes, as it probes at the level of the functional group and is capable of unveiling the major reactions that lead to the formation of carbonaceous solids during thermal stressing at these high temperatures. From these leads we have been successful in identifying a number of additives, specifically benzyl alcohol and 1,4-benzene dimethanol, that appear to function as hydrogen donors and which perform well as thermal stabilizers, significantly retarding the onset of carbonaceous solid formation in jet fuels at temperatures in excess of 400°C.

Evidence obtained from the infrared studies performed to date suggests that the primary route to carbonaceous deposits at temperatures above 400°C may well be the formation of olefins, followed by cyclization and aromatization, similar to the mechanism suggested for the degradation of polyacrylonitrile copolymers used in the formation of carbon fibers[3]. The focus of our research thus turned to studying molecules that might act as hydrogen donors in the anticipation that they might resaturate the double bonds as they are produced and ultimately retard the subsequent reactions that result in the formation of carbonaceous solids. Hydrogenation agents employed in coal liquefaction, such as tetralin or tetrahydroquinoline, do act as thermal stabilizers and significantly retard the formation of carbonaceous solids.

Surprisingly, however, the best thermal stabilizers we found were methalol derivatives, such as benzyl alcohol and 1,4-benzene dimethanol[2]. From infrared studies of the Jet A-1 fuels containing these two alcohols we know that methalol groups *slowly* transform over a period of hours in the jet fuel to aldehydes. A simple mass balance indicates that this is achieved with the loss of two hydrogen atoms and this suggests that benzyl alcohol and benzene 1,4-dimethanol act as *in situ* hydrogenation agents at high temperatures, similar to coal liquefaction reagents, resaturating olefinic double bonds as they are formed and interfering with the process of aromatization and subsequent formation of carbonaceous solids.

While the infrared studies performed to date have been rewarding, parallel NMR studies, which are the main focus of this preprint, were initiated to assist in the interpretation of the changes observed in the infrared spectra as a function of thermal stressing. NMR studies also provide additional information that is useful for the elucidation of the principal reaction pathways that lead to a retardation of carbonaceous solid formation.

EXPERIMENTAL

Samples for these studies were prepared from an essentially additive free Jet A-1 fuel supplied by the Air Force/WRDC Aero Propulsion Laboratory (No. 90-POSF-2747). Benzyl alcohol and benzene 1,4-dimethanol were purchased from Aldrich Chemical Company and used without further purification.

Thermal stressing was performed on 10 ml samples at 425°C in 15 ml type 316 stainless steel micro reactors[2] under 100 psi of air. The micro reactor containing the sample was purged

* To whom correspondence should be addressed.

with UHP-grade N_2 five times at 1000 psi to minimize the presence of dissolved oxygen and finally pressurized with 100 psi of air. It was then placed in a preheated sand bath at 425°C for the required reaction time, followed by quenching into cold water and depressurization to remove head space gases.

Samples for NMR analyses were prepared as 15 wt % solutions in deuterated chloroform. The spectra were recorded on a Brucker WP200 instrument at a field strength of 200 MHz.

RESULTS AND DISCUSSION

1. Thermal Stressing of Neat Jet A-1 Fuel at 425°C.

The physical appearance of the neat Jet A-1 fuel after thermal stressing at 425°C under 100 psi of air, changes from a clear, colorless, transparent liquid to a transparent, light yellow liquid after 1h, a slightly turbid, light brown liquid after 3h and a black liquid after 6h. Between 6 and 24h the black liquid becomes progressively more turbid and there is an obvious increasing presence of black carbonaceous solids (color pictures are shown in ref. 2). Changes observed in the infrared spectra of neat Jet A-1 fuel as a function of thermal stressing time led us to consider hydrogen donors as potential stabilizers. Prominent bands at approximately 1642 /1652 and 890 / 910 cm^{-1} in the spectra were assigned to C=C stretching vibrations resulting from the formation of olefins during thermal stressing. Between 6 and 18h these bands decrease in intensity and are barely detected after 12h in air at 425°C. Other relatively broad bands are observed at approximately 880 and 675 cm^{-1} and these become increasingly prominent in spectra of the samples after reaction times exceed 6h. These bands were attributed to substituted aromatics and their presence correlates well with the observation of the black carbonaceous material in the thermally stressed fuel at long reaction times.

Figure 1 shows ^1H NMR spectra (0-10 ppm) recorded at room temperature of Jet A-1 fuel samples thermally stressed under air after time periods of 0, 1, 3, 6, 12, 18 and 24h at 425°C. The NMR spectrum of the neat unstressed fuel is representative of a typical complex hydrocarbon mixture[4] with prominent lines attributed to paraffinic methyl and γ-methyl protons (0.5-1.05 ppm); paraffinic methylene, γ-methylene, β-methyl and β-methylene protons (1.05-2.0 ppm); α-methyl protons (Ar-CH_3*; 2.0-2.6 ppm); α-methylene protons (Ar-CH_2*-R; 2.6-3.4 ppm); α-methylene protons (Ar-CH_2*-Ar; 3.4-4.5 ppm) and aromatic protons (6.0-9.0 ppm). For completeness, olefinic protons, which are not detected at this scale expansion, resonate between 4.5-6.0 ppm. Upon thermal stressing at 425°C the distribution of aliphatic to aromatic moieties changes in favor of the latter. Systematic increases in the intensity of α-methyl, α-methylene and aromatic protons with corresponding decreases in the intensity of paraffinic methyl and methylene groups are observed. Figure 2 shows ^1H NMR spectra of the same samples (figure 1) scale expanded in the olefinic proton region (4.5-6.0 ppm). In the unstressed Jet A-1 fuel olefinic protons are not detected. However, in the spectra obtained after the sample had been thermally stressed for 1 and 3h there is the obvious presence of NMR resonances that may be attributed to internal and external olefins. In common with the infrared results[2], the concentration of olefins appears to maximize between 3 and 6h. Thus the NMR results obtained on the thermally stressed neat Jet A-1 corroborate the infrared spectroscopic findings.

2. Thermal Stressing of Jet A-1 Fuel Containing 5% Benzyl Alcohol at 425°C.

As we have demonstrated previously[2] the addition of 5% benzyl alcohol to Jet A-1 fuel results in a significant improvement in the thermal stability at 425°C, as confirmed by the retardation of carbonaceous solids formation by some 3h. Infrared spectroscopic analysis was informative. A band at 1720 cm^{-1}, assigned to the carbonyl stretching vibration of benzaldehyde was observed to increase in intensity to a maximum after approximately 3h of thermal stressing, decrease somewhat at 6h and was essentially absent at 12h of thermal stressing. Concomitant with these observations bands assigned to C=C stretching vibrations are detected at 1h, rise to a maximum at about 6h and are barely detected at 12h of thermal stressing. Significantly, after 12h of thermal stressing bands assigned to substituted aromatics are present and this again correlates

well with the observation of the black carbonaceous material in the thermally stressed fuel. The interpretation of these results was as follows. Benzyl alcohol and similar molecules *slowly* transform over a period of hours in the jet fuel to aldehydes with the loss of two hydrogen atoms. We believe that they act as *in situ* hydrogenation agents at high temperatures, similar to coal liquefaction reagents, resaturating olefinic double bonds as they are formed and interfering with the process of aromatization and subsequent formation of carbonaceous solids.

Figure 3 shows ^{1}H NMR spectra (0-10 ppm) recorded at room temperature of Jet A-1 fuel samples containing 5% benzyl alcohol and thermally stressed under air after time periods of 0, 10, 60, 180, 360, and 720 min. at 425°C. A comparison of the spectra of the unstressed Jet A-1 fuel with (figure 3) and without (figure 1) the additive, reveals that benzyl alcohol has a convenient characteristic resonance at 4.74 ppm attributable to the hydroxyl proton of the methalol group. Figure 4 shows ^{1}H NMR spectra of the same samples (figure 3) scale expanded in the olefinic proton region (4.5-6.0 ppm). In the unstressed sample there is no evidence of resonances attributable to olefinic protons and the spectrum is dominated by the intense line associated with the methalol group of benzyl alcohol at 4.74 ppm. It is significant that the intensity of this line at 4.74 ppm decreases as a function of thermal stressing, but is still present in the spectrum recorded after 6h at 425°C. This implies that benzyl alcohol gradually transforms to benzyladehyde (see infrared results[2]) in the Jet A-1 fuel over a period in excess of 6h under air at 425°C. At the same time, the olefinic resonances are clearly observed in the sample thermally stressed for 6h which is consistent with the infrared results and lends support for the *in situ* hydrogenation hypothesis.

ACKNOWLEDGMENTS

This project was jointly supported by the US Department of Energy, Pittsburgh Energy Technology Center and the U. S. Air Force WRDC/Aero Propulsion Laboratory, Wright-Patterson AFB. Funding was provided by the US DOE at Sandia National Laboratories under contract DE-AC04-76DP00789. We also wish to thank Mr. W.E.Harrison III of WRDC, Dr. E. Klavetter of SNL, Professor H. H. Schobert, and Dr. C. Song of PSU for their encouragement and many helpful discussions.

REFERENCES

(1) Selvaraj, L., Sobkowiak, M. and Coleman, M. M., ACS *Division of Petroleum Chemistry Preprints*, 37(2), 451 (1992).
(2) Coleman, M.M., Selvaraj, L., Sobkowiak, M. and Yoon, E., *Energy and Fuels*, submitted.
(3) Sivy, G.T., Gordon, B. and Coleman, M.M., *Carbon*, 21, 573 (1983).
(4) Song, C. et al., Compositional Factors Affecting Thermal Degradation of Jet Fuels Annual Report, Report for period July 1990 to July 1991, The Pennsylvania State University.

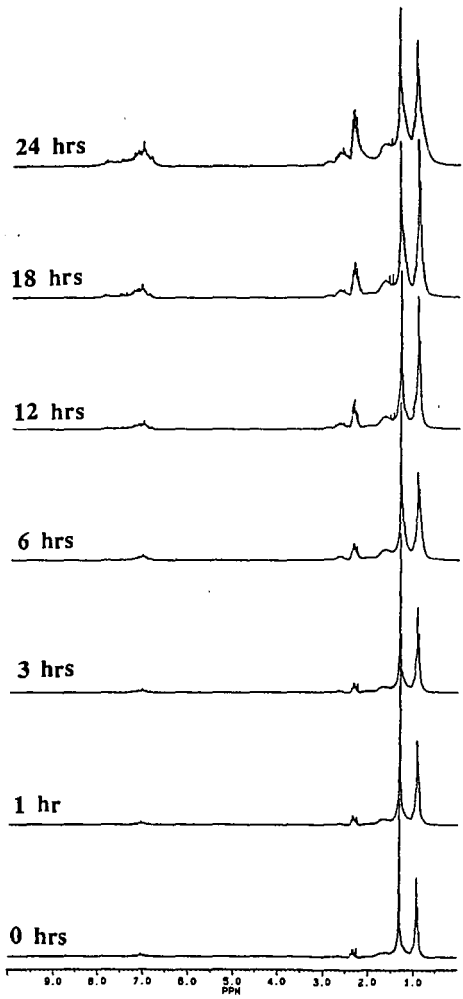

Figure 1. ^{1}H NMR spectra of neat Jet A-1 fuel thermally stressed for the times indicated over air at 425°C.

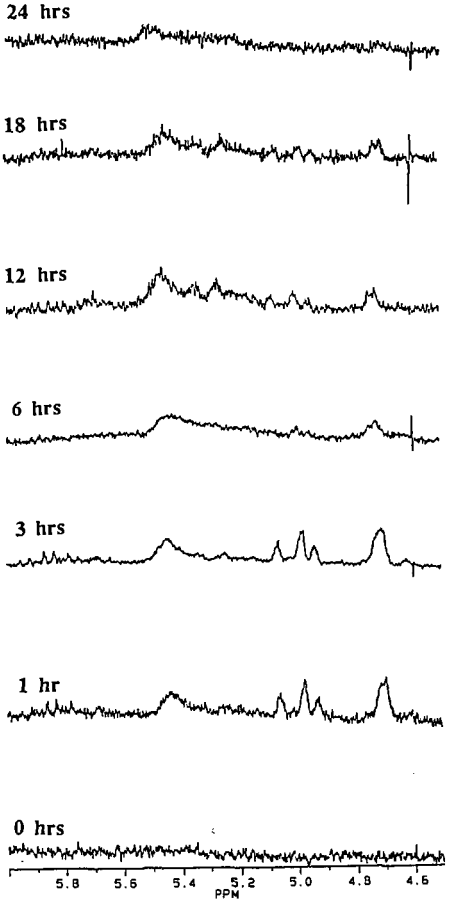

Figure 2. Scale expanded ^{1}H NMR spectra in the olefinic region of neat Jet A-1 fuel thermally stressed for the times indicated over air at 425°C.

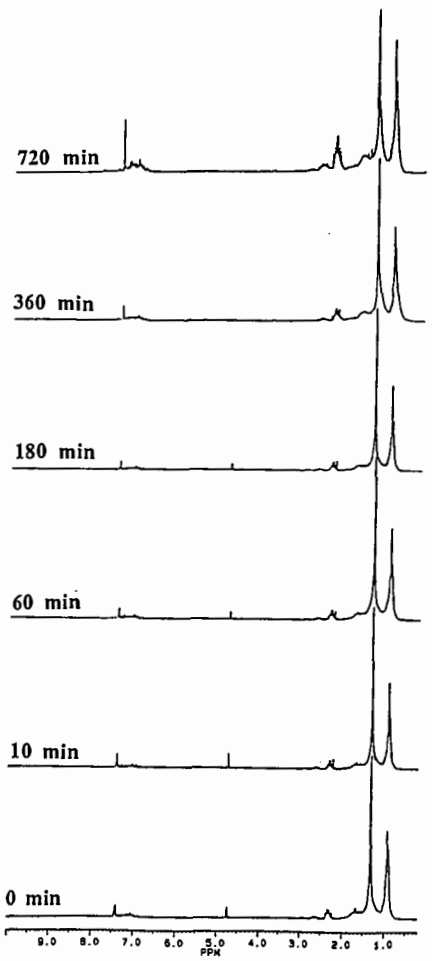

Figure 3. ^{1}H NMR spectra of Jet A-1 fuel containing 5% benzyl alcohol thermally stressed for the times indicated over air at 425°C.

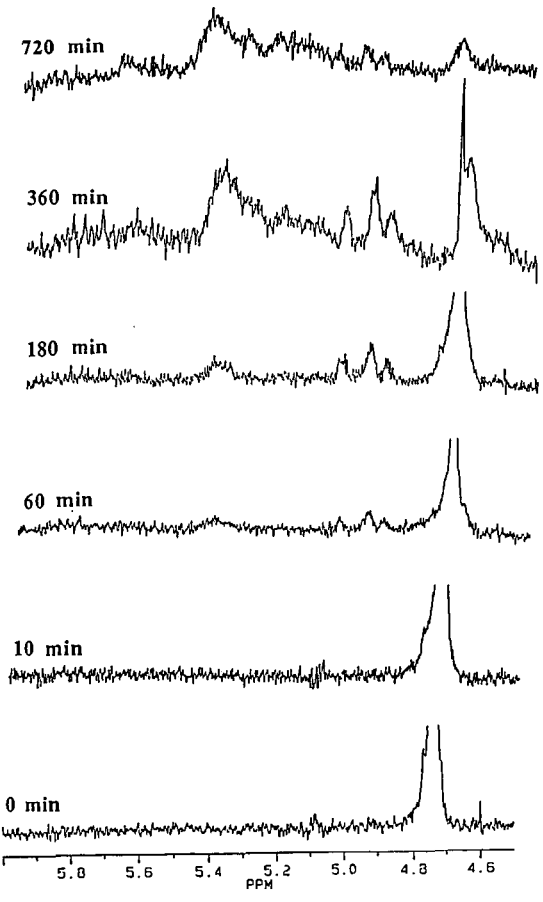

Figure 4. Scale expanded ^{1}H NMR spectra in the olefinic region of Jet A-1 fuel containing 5% benzyl alcohol thermally stressed for the times indicated over air at 425°C.

PYROLYTIC DEGRADATION OF COAL- AND PETROLEUM-DERIVED AVIATION JET FUELS AND MIDDLE DISTILLATES

Wei-Chuan Lai, Chunshan Song, Harold H. Schobert, and Rathnamala Arumugam
Fuel Science Program
Department of Materials Science and Engineering
209 Academic Projects Building
The Pennsylvania State University
University Park, PA 16802

Keywords: pyrolysis, jet fuels, middle distillates, thermal stability

INTRODUCTION

The thermal stability of jet fuels plays an important role in the design and development of future hypersonic aircraft. It was reported that the fuel in these new hypersonic aircraft may reach temperatures higher than 500°C. The temperatures are much higher than the current maximum operating temperature for the conventional aviation jet fuels. When the fuels are exposed to such high temperatures, serious pyrolytic degradation of the fuels will occur and will result in the formation of solid deposits on critical aircraft systems such as fuel pipeline, filter, and engine parts (Roquermore et al., 1989). This means that advanced jet fuels are required for hypersonic aircraft. The development of such fuels warrants detailed study of pyrolytic degradation of hydrocarbon fuels.

The ultimate goal of our research project is to develop advanced jet fuels that are thermally stable at high temperatures. The objectives of this work are to rank the thermal stability of current fuels, to identify thermally stable compounds in fuels, to clarify the chemistry of pyrolytic degradation and mechanisms of solid formation, and to enhance the intrinsic stability of jet fuels by optimizing fuel composition. The future fuels might derive not only from petroleum, but also from hydrocarbon resources such as coal, tar sands, and oil shale. The scope of this paper will concentrate on the thermal stability study of ten fuels including four coal-derived fuels and six petroleum-derived military and commercial jet fuels. The results concerning the effects of hydrogen-donors on the fuel stability are presented in Song et al. (1992b). In this study, the relative thermal stabilities of the fuels have been elucidated by their chemical composition.

EXPERIMENTAL

Apparatus and Procedures

Thermal stressing of the jet fuels and middle distillates were studied in tubing bomb reactors at 450°C for a heating period of 0-8 hours under 0.69 MPa UHP-N_2. The tubing bomb reactors were described in detail elsewhere (Eser et al., 1990). A 5 ml sample was confined in a leak-tested reactor. The sample was deoxygenated through repetitive (6 times) pressurization to 6.9 MPa with UHP-N_2 and purging to remove oxygen/air in the reactor or dissolved in the sample. The reactor was pressurized to the desired starting pressure of 0.69 MPa with UHP-N_2 before being immersed into a fluidized sand bath which has been preheated to 450°C. After the experiment was started, the reaction pressure was closely monitored. The experiment was ended after the desired stressing time by removing the reactor from the fluidized sand bath and immediately quenching in a cool water bath. The headspace gas was collected in a gas sampling bag.

Product Chemical Analysis

The gas samples were analyzed for their compositions and quantities by using a Perkin-Elmer Autosystem gas chromatograph (GC). Two detectors, a thermal conductivity detector (TCD) and a flame ionization detector (FID), were used to analyze the gas composition. The TCD was used to determine CH_4, C_2H_2, C_2H_4, and C_2H_6 as well as non-hydrocarbon gases such as H_2, CO, and CO_2. The FID was used to detect hydrocarbon gases from C_1 to C_6. The GC columns used were a 10 feet long, 1/8 inch diameter stainless steel column packed with 100/120 Carbosieve SII (Supelco) for TCD and a 6 feet long, 1/8 inch diameter stainless steel column packed with 80/100 Chemipack C 18 for FID. There are two liquid samples collected from each experiment: one is the liquid residue directly collected

from the reactor and the other is washed from the reactor wall with pentane. The compounds in the liquid products were identified by a HP 5890 Series II GC coupled with HP 5971A Mass Selective Detector (MSD) and quantified by a Perkin-Elmer GC 8500. The column used was a 30 m, 0.25 mm i.d., DB-17 Fused Silica Capillary Column (50% phenyl, 50% methyl silicone) with a film thickness of 0.25 μm. The solid deposits are operationally defined as the materials which are not soluble in the resulting liquid co-products and pentane (washing solvent). The solid deposits are to be analyzed by Fourier transform infra-red spectroscopy and NMR spectroscopy.

Samples

Ten jet fuels and middle distillates were studied. Four coal-derived fuels include JP-8C from hydrotreating of liquids produced from the Great Plains Gasification plant, and middle distillates derived either from direct coal liquefaction (WI-MD from Wilsonville plant and HRI-MD from HRI) or from indirect coal liquefaction (FT-MD from Fischer-Tropsch synthesis). Six petroleum-derived military and commercial jet fuels include JPTS (thermally stable jet fuel), JP7, JP-8P, JP-8P2, Jet A, and Jet A-1. The basic information of these fuels is presented in Table 1, and the properties of the samples are discussed in the following section.

RESULTS AND DISCUSSION

Properties of Samples

The fuel densities range from 0.76 g/cm^3 (FT-MD) to 0.96 g/cm^3 (WI-MD) with most falling in a smaller range of 0.79 to 0.81 g/cm^3 (JPTS, JP-7, JP-8P, Jet A, Jet A-1, and JP-8P2). The densities of JP-8C and HRI-MD are 0.84 and 0.92 g/cm^3, respectively. All the fuels were analyzed by GC and GC-MS before and after thermal stressing, and they are all complex mixtures of hundreds of compounds. Because of the large number of compounds in the fuels, one way to visualize their compositions is employing the total ion chromatograms (TIC) and specific ion chromatograms (SIC) of GC-MS analysis. Figure 1 presents the TIC and SIC (ions of m/z 57, 83, 91, 105, and 142) of JP-8P2. The fragment ions of m/z 57, 83, and 142 are characteristics of long-chain paraffins, alkylcyclohexanes, and alkylnaphthalenes, respectively. The ions of 91 and 105 imply the presence of alkylbenzenes. From the resemblance between TIC and SIC of m/z 57, we can find that the dominant constituents in JP-8P2 are the long-chain paraffins with carbon-number ranging from C_8 to C_{17} with most falling between C_{10} to C_{15}. The alkylbenzenes (C_2- ~ C_6-, mainly C_3- ~ C_5-) content is about 20 percent. JP-8P2 also includes 5% alkylcyclohexanes (C_3- ~ C_8-) and low concentrations of tetralin, alkylindan, and alkylnaphthalenes.

JP-8P, Jet A, JP-7, FT-MD, JPTS, and Jet A-1 are also paraffinic fuels derived from petroleum with long-chain paraffins as the dominant constituents, but the overall compositions and paraffins distributions are somewhat different. Figure 2 shows the SIC (m/z 57) for six of the seven paraffinic fuels. We can see that JP-8P and Jet A are quite similar to JP-8P2 in terms of the long-chain paraffins distributions. Jet A-1 has a narrower band from C_{10} to C_{14} with most falling between C_{11} and C_{12}. JPTS has a band from C_9 to C_{15}. JP-7 has a band from C_{11} to C_{16} with an average carbon number of 12. FT-MD is also a paraffinic fuel, although derived from coal, having almost exclusively paraffins (C_9 ~ C_{21}) with very low concentration of cycloparaffins. Table 2 summarizes the approximate compositions of the seven paraffinic fuels based on the three major hydrocarbon types found in fuels (paraffins, alkylbenzenes, alkylcyclohexanes) and others (such as alkylnaphthalenes, alkylindans, etc).

JP-8C, WI-MD, and HRI-MD are all coal-derived fuels, but their compositions are quite different from petroleum-derived paraffinic fuels. JP-8C is composed mainly of monocyclic and bicyclic alkanes, and two-ring hydroaromatic compounds. The major components are alkyl-substituted cyclohexanes (about 45%), decalin (6.3%), C_1-decalin (4%), and tetralin (3.9%). There are also about 10% alkylbenzenes. HRI-MD is a heavy fuel, i.e., with many high molecular-weight components compared with the paraffinic fuels and JP-8C. HRI-MD consists of (alkyl) bicyclic alkanes, alkyl two-ring aromatic compounds and some alkylbenzenes. There are about 15% alkyl-substituted (mainly, C_0- ~ C_3-) cyclohexanes and only 8% long-chain paraffins. There are also some (C_0- ~ C_2-) 3-ring or 4-ring aromatics. Regarding WI-MD, it is heavier (with carbon number ≥12) than the other nine fuels with few light molecular weight compounds. It has very high content of aromatics (with ring size not less than 2). The most abundant peaks are pyrene (4%) and multi-hydropyrenes (total about 8%), and less than 10% paraffins (C_{14} ~ C_{25}).

Degradation Product Distributions and Stability Comparison

The relative thermal stabilities of hydrocarbons in fuels as well as the whole fuels themselves were identified based on the overall reaction products (gas, liquid, and solid) distributions and GC/GC-MS analysis of the liquid products. For the hydrocarbons in fuels, it was found that at 450°C long-chain n- and iso-paraffins ($\geq C_{11}$), and n-alkylbenzenes (alkyl$\geq C_3$-) are some of the unstable compounds. Some compounds that are relatively more stable compounds include long-chain paraffins ($\leq C_8$), long-chain paraffins (C_9 and C_{10}, up to 4 hr), C_0- to C_3-cycloalkanes, and C_0- to C_2-benzenes. One example is shown in Figure 3, which presents the total ion chromatograms of the neat sample of, and the liquid products from, FT-MD after thermal stressing at 450°C for 1-8 hours. Recall that FT-MD is a paraffinic fuel which has paraffins ranging from C_9 to C_{21}. We can clearly find that long-chain paraffins of C_{11} through C_{21} decompose quickly; the decomposition rate increases with increasing chain size. Quantitative results from GC and qualitative results from GC-MS indicate that the main reactions occurring in the first 2.5 hours include cracking of the paraffins into lower alkanes and olefins, and cyclization to form alkylcyclic alkanes and olefins. The alkylcyclic compounds were then subjected to dehydrogenation to form alkylbenzenes. This observation is consistent with the mechanisms proposed by Song et al. (1992a). A quantitative presentation of how the paraffins content changes with time is shown in Figure 4 for the same sample. The paraffins were divided into 12 groups based on the carbon numbers; each group consists of straight and branched alkanes with the same carbon number. Figure 4 shows that at 450°C long-chain paraffins with carbon number no less than 11 (i.e., C_n, $n \geq 11$) are unstable. C_{15} through C_{21} decompose completely by 2.5 hours. Notice that the content of C_9 increases from the initial 0.5% to 5.7% at 1 hour and then decreases to 3.1% after 2.5 hours. The initial increase is contributed from cracking yield from longer chain paraffins, and the C_9 later decomposes and results in the C_9 fraction decreasing with increasing time.

The yields of the gas components from JP-8P thermally stressed at 450°C for 1-8 hours are presented in Figure 5. Methane is always the most abundant gaseous product (in mmole) followed by ethane and propane over the stressing range; this is also true for all other nine fuels studied. Another common characteristic for the fuels is that the paraffinic gases (CH_4, C_2H_6, C_3H_8, and C_4H_{10}) increase with increasing time but the olefinic gases (C_2H_4, C_3H_6, C_4H_8) increase initially then decrease with increasing time. Continuous cracking accounts for the progressive increase of paraffinic gases and the initial increase of olefinin gases. Olefins are known to be less stable and highly reactive because of unsaturation; this results in the later decrease of olefinic gases.

The decomposition extents of the ten fuels are significantly affected by their compositions. Figure 6 shows the gas yields from the ten fuels stressed for 1-8 hours. The figure indicates that the three coal-derived non-paraffinic fuels, i.e., JP-8C, HRI-MD, and WI-MD, are more stable than the other seven paraffinic fuels in terms of less gas formation. The difference in stability in terms of the gas formation is attributed to the composition difference. Paraffinic fuels produce more gases because the major reaction for long-chain paraffins is cracking into lighter gases of alkanes and olefins. On the other hand, the compositions of the three coal-derived non-paraffinic fuels are quite different from the paraffinic fuels; they have low fraction of paraffins but are rich in cyclic alkanes and hydroaromatics. Thus the major reaction for them is dehydrogenation to form alkylbenzenes (liquid yields) instead of the formation of low molecular-weight gases. It can be seen that HRI-MD and FT-MD produce the gas the least and the most, respectively. For example, the gas yields for HRI-MD and FT-MD are respectively 3.3% and 17% at 1 hour, 10% and 33% at 4 hours, and 16% and 52% at 8 hours. The six petroleum-derived paraffinic fuels (JP-8P, Jet A, JP-7, FT-MD, JPTS, and Jet A-1) have similar gas yields (ranging from 37% to 40%) for 8-hour stressing. However, for 1- ~ 4-hour stressing, Jet A-1 has the lowest or second to the lowest gas yields; this is consistent with the fact that among the paraffinic fuels, Jet A-1 has the lowest paraffin content and the narrowest paraffin band (from C_{10} to C_{14}, with most falling between C_{11} and C_{12}).

The solid yields from the ten fuels stressed for 1-8 hours are presented in Figure 7. The figure shows that there is no solid formed after 1-hour stressing for all the ten fuels, and the solid starts to form between 1 and 2.5 hours. The induction time, which is the time period needed for the formation of solid precursors (such as polyaromatics) from reactive intermediates, differs for each fuel. It was found that fuels rich in hydrogen-donors (such as cyclic alkanes) have longer induction period and tend to have better stability. The hydrogen abstracted from hydrogen-donors stabilizes the reactive radicals; this in consequence inhibits the secondary radical reactions and suppresses solid formation (Song et al., 1992b). Two of the three coal-derived non-paraffinic fuels, JP-8C and HRI-MD, have much better stability than other fuels in terms of much less solid formation. This is again attributed to the composition

difference and the fact that JP-8C and HRI-MD have high concentration of hydrogen donors. Figure 7 also shows that JP-7 and JPTS have higher stability among the seven paraffinic fuels in terms of less solid formation. This is also attributed to their lower aromatics content and higher hydrogen-donor compounds (alkylcyclohexanes).

WI-MD, on the other hand, does not have good stability in the long run, judging from its high solid formation at 8-hour stressing. Figure 8 presents the total ion chromatograms of the neat sample of, and the liquid products from, WI-MD after thermal stressing at 450°C for 1-8 hours. It can be seen that WI-MD has very high content of aromatics and hydroaromatics. The hydroaromatics decomposed quickly to form saturated aromatics through dehydrogenation, and these aromatic compounds subsequently form more polycyclic aromatic hydrocarbons and solid deposits. WI-MD seems to be stable in terms of low gas formation; however, GC-MS analysis of the liquid products shows that in fact WI-MD is quite unstable and decomposes quickly to form aromatics and precursors to solid. In short, WI-MD tends to form more solid than other fuels due to its high aromatic content nature, and it can not be a good jet fuel.

CONCLUSIONS

The thermal stability of the fuels is significantly affected by their chemical composition. Pyrolysis of ten jet fuels and middle distillates has been studied in a tubing bomb reactor. The compositions of the stressed as well as neat fuels were all qualitatively and quantitatively characterized by GC and GC-MS. This information is useful in explaining and evaluating the thermal stability of fuels. The relative thermal stabilities of hydrocarbons in fuels as well as the whole fuels themselves were identified. The fuels with higher contents of 1-3 ring cycloalkanes and/or hydroaromatics are more stable than those with higher contents of long-chain paraffins in terms of less gas formation. The former includes JP-8C, HRI-MD and WI-MD, and the latter covers the remaining 7 fuels including six petroleum-derived paraffinic fuels and one paraffinic fuel from indirect coal liquefaction. Among the paraffinic fuels, higher stability in terms of less gas formation was observed for those fuels having narrower distribution of paraffins with relatively shorter chain, e.g., Jet A-1; those with lower aromatics content and higher hydrogen-donor compounds exhibits less solid formation. Overall, coal-derived JP-8C and HRI-MD have the best thermal stability among the ten fuels studied either in terms of less gas or solid formation.

ACKNOWLEDGMENTS

This project was jointly supported by the U.S. Department of Energy, Pittsburgh Energy Technology Center and the Air Force WRDC/Aero Propulsion Laboratory, Wright-Patterson AFB. Funding was provided by the U.S. DOE at Sandia National Laboratories under contract DE-AC04-76DP00789. We are pleased to thank Drs. W.E. Harrison III, D.M. Storch and S.D. Anderson of WRDC for providing technical advice, support and jet fuel samples, Drs. E. Klavetter of SNL and S. Rogers of PETC for their support and helpful discussions, and Drs. G. Stigel and R. Hickey of PETC and Dr. P. Zhou of Burns & Roe Service Co. for the WI-MD and FT-MD samples. We also wish to thank Dr. P.G. Hatcher of PSU for instrumental support to the maintenance of analytical equipments for the jet fuel project.

REFERENCES

Eser, S., Song, C., Schobert, H. H., Hatcher, P. G. et al., "Advanced Thermally Stable Jet Fuels Development Program Annual Report", Volume II, Interim Report for period July 1989 to June 1990, WRDC-TR-90-2079, Vol. II, September 1990.

Roquemore, W. M., Pearce, J. A., Harrison III, W. E., Krazinski, J. L., and Vanka, S. P., *Preprints, American Chemical Society, Division of Petroleum Chemistry*, 34(4), *1989*, 841.

Song, C., Peng, Y., Jiang, H., and Schobert, H. H., "On the Mechanisms of PAH and Solid Formation during Thermal Degradation of Jet Fuels", *Preprints, American Chemical Society, Division of Petroleum Chemistry*, 37(2), *1992a*, 484-492.

Song, C., Lai, W.-C., and Schobert, H. H., "Hydrogen-Transferring Pyrolysis of Cyclic and Straight-Chain Hydrocarbons. Enhancing High Temperature Thermal Stability of Aviation Jet Fuels by Hydrogen-Donors", Paper to be presented at the 204th ACS National Meeting, Washington, D.C., August 23-28, *1992b*.

Table 1. Coal- and Petroleum-Derived Jet Fuels and Middle Distillates

Fuel	Description	Received	Supplier/Source	Sample No.
Coal-Derived Fuels				
1) JP-8C	Hydrotreated JP-8	5-30-89	WPAFB	89-POSF-2685 ?
2) WI-MD	Middle distillates from coal liquefaction at Wilsonville	4-20-90	DOE PETC	259E MD
3) FT-MD	Middle distillates from Fischer-Tropsch Synthesis	8-16-91	DOE PETC	PETC F-T
4) HRI-MD	Middle distillates from coal liquefaction at HRI	11-26-91	WPAFB	83-POSF-0849
Petroleum-Derived Jet Fuels				
5) JP-8P	Petroleum-Derived JP-8	5-30-89	WPAFB	
6) JP-8P2	Petroleum-Derived JP-8	5-31-90	WPAFB/Tank S-15	
7) JP-7	Petroleum-Derived JP-7	5-31-90	WPAFB/Tank S-16	
8) Jet A-1	Commercial jet fuel	8-16-91	WPAFB/Tank S-7	90-POSF-2747
9) JPTS	Thermally stable jet fuel	8-16-91	WPAFB	91-POSF-2799
10) Jet A	Commercial jet fuel	8-16-91	WPAFB	90-POSF-2827

Table 2. Approximate Compositions of Paraffinic Fuels

Fuel	Weight %			
	Paraffins	Alkylbenzenes	Alkylcyclohexanes	Others
JP-8P2	~ 70%	~ 20% (C_2- ~ C_6-)	~ 5% (C_3- ~ C_8-)	
JP-8P	~ 75%	~ 12% (C_2- ~ C_4-)	~ 8% (C_3- ~ C_7-)	
Jet A	~ 80%	~ 10% (C_2- ~ C_4-)	~ 6% (C_1- ~ C_6-)	
JP-7	~ 90%	very low	~ 10% (C_5- ~ C_8-)	
FT-MD	~ 100%		low	
JPTS	~ 70%	~ 8% (C_2- ~ C_4-)	~ 13% (C_1- ~ C_7-)	
Jet A-1	~ 65%	~ 26% (C_3- ~ C_5-)	~ 6% (C_4- ~ C_5-)	

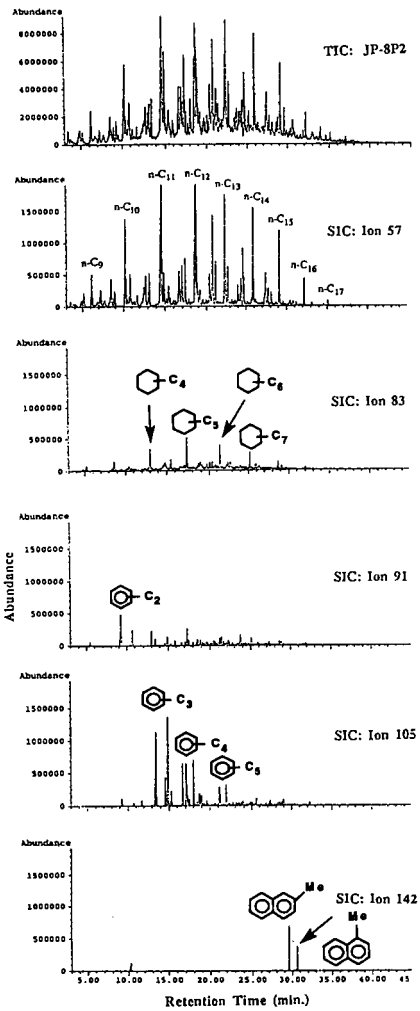

Figure 1. Total and specific ion chromatograms (ions of m/z 57, 83, 91, 105, and 142) of JP-8P2 from GC-MS analysis.

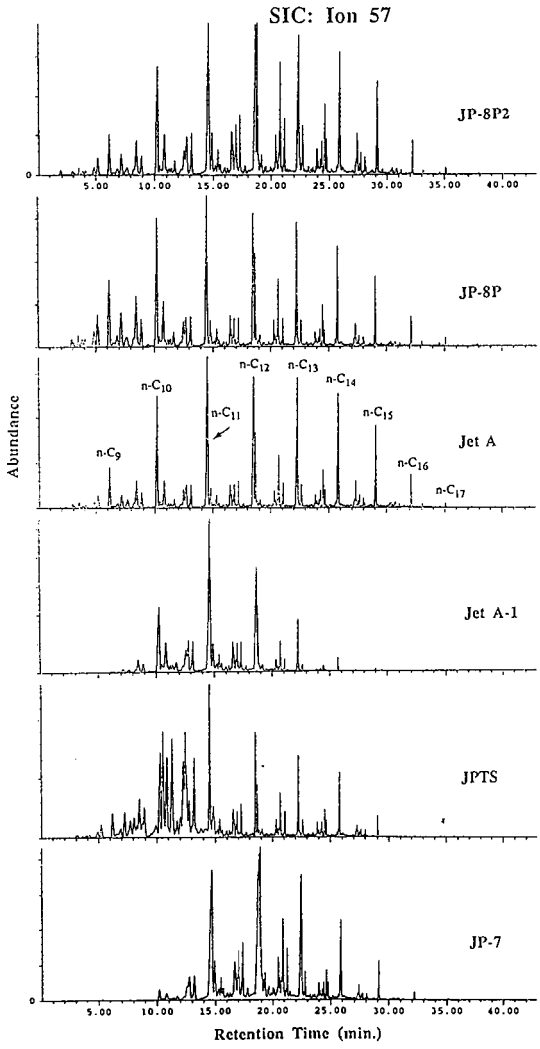

Figure 2. Specific ion chromatograms (ion of m/z 57) of six paraffinic fuels.

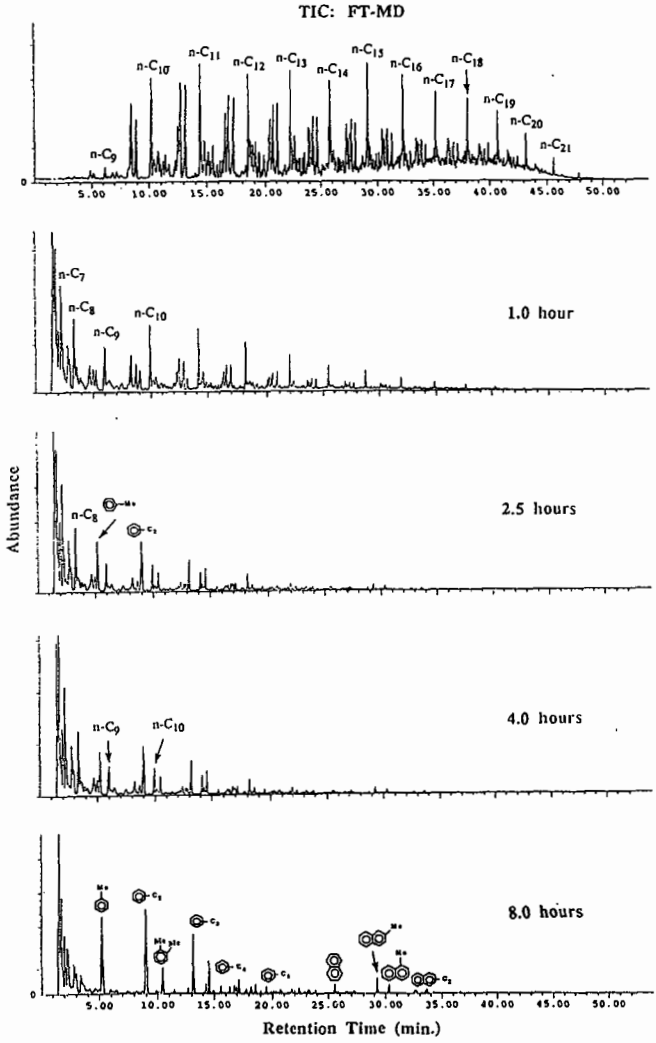

Figure 3. Total ion chromatograms of the neat sample of, and the liquid products from, FT-MD after thermal stressing at 450°C for 1-8 hours.

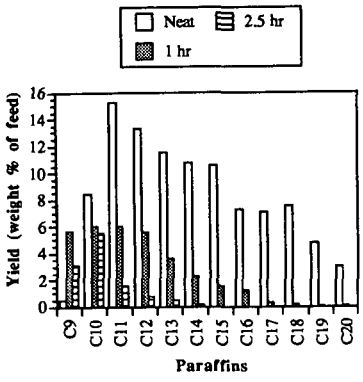

Figure 4. Paraffins distribution of liquids from FT-MD

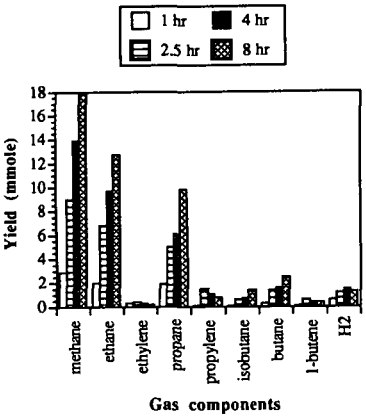

Figure 5. Yields of H_2 and $C_1 \sim C_4$ gases from JP-8P

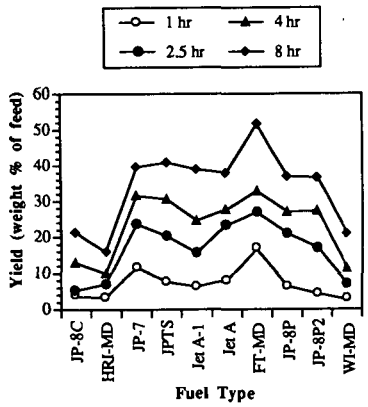

Figure 6. Yields of gases at 450°C

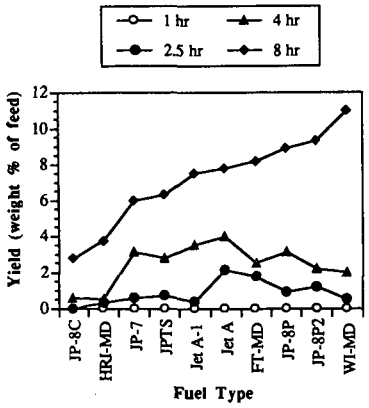

Figure 7. Yields of solid deposits at 450°C

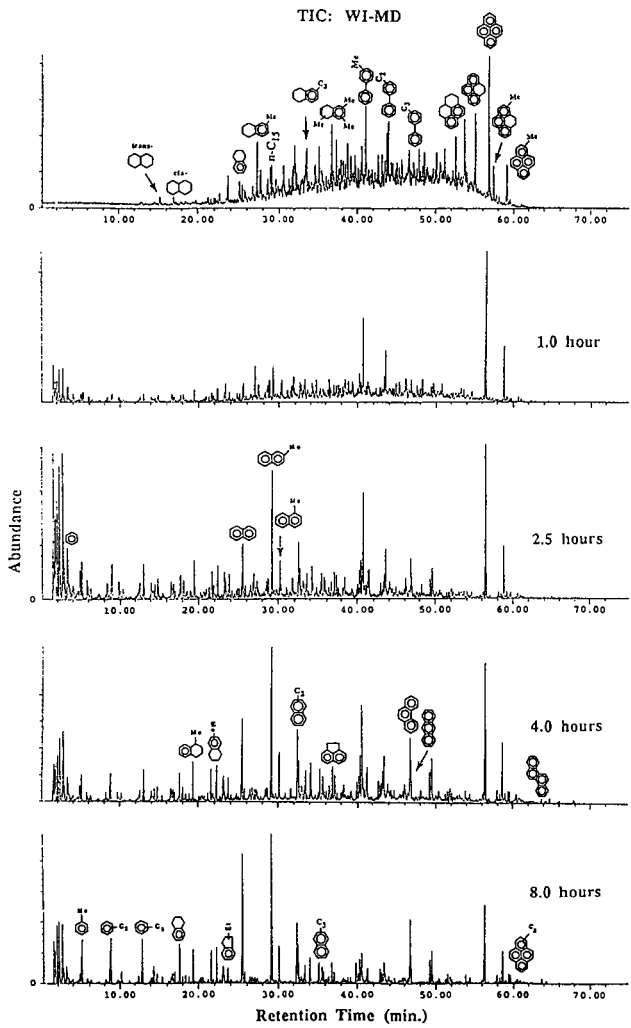

Figure 8. Total ion chromatograms of the neat sample of, and the liquid products from, WI-MD after thermal stressing at 450°C for 1-8 hours.

HYDROUS PYROLYSIS OF FOUR ARGONNE PREMIUM COALS

Michael A. Serio, Erik Kroo, Sylvie Charpenay, and Peter R. Solomon

Advanced Fuel Research, Inc.
87 Church Street
East Hartford, CT 06108

Keywords: Hydrous Pyrolysis, Pretreatment, Argonne Premium Coals

ABSTRACT

Pretreatment experiments were done under hydrous pyrolysis conditions with four Argonne Premium coals (Zap lignite, Wyodak subbituminous, Illinois bituminous, Pittsburgh bituminous) over a range of temperatures (250 -350 °C) and pressures (1000 - 4000 psig). The residues from these experiments were further studied by programmed pyrolysis in a TG-FTIR system. The yields of pyrolysis tar were found to increase sharply at short pretreatment times (< 60 min at 350 °C) and decline slowly at longer times. The yields of pyrolysis methane increase monotonically with pretreatment time, while the yields of pyrolysis CO_2 decline monotonically. All of these trends are in agreement with the contention that hydrous pyrolysis is similar to an accelerated geological aging of the coal. The results for CO evolution were somewhat contrary in that there was usually an initial increase followed by a decline. It is believed that this CO results from decomposition of hydroxy and dihydroxy structures which are created by the hydrous pyrolysis process.

INTRODUCTION

Hydrous pyrolysis (hydrothermal treatment) of coal has been studied previously as a pretreatment step to increase the yields of liquid products from extraction (1-5), pyrolysis (3-7), or liquefaction (8-11) of coal. However, the mechanisms of this process and the applications to coals of a wide range of ranks are still a subject of considerable debate. The similarity between the effects of steam or water pretreatment and accelerated geological aging of coal has recently been noted by several authors (8-11). Landais, Monthioux and coworkers have also discussed the analogy between pyrolysis in confined systems and accelerated geological aging (12-16), otherwise known as "artificial" maturation.

Siskin and Katritzky (17) have recently reviewed the reactivity of organic compounds in hot water, including a consideration of the geochemical implications. Their review indicates that, under conditions where conventional wisdom suggests that water is inert, it may be acting as a catalyst, reactant, and/or solvent. Based on work with model compounds with linkages and functional groups corresponding to those found in coals and shale kerogens, it was concluded that water has important effects on the conversion of plant and animal material into organic fuels under geological conditions of time, heat, and pressure. Much of their work was done in the range of 250 to 350 °C which is the temperature range of interest for hydrothermal treatment of coal. Because of significant changes in the physical and chemical properties of water with increasing temperature, it becomes more likely to react with organic compounds. For example, in the presence of water, ether and ester crosslinks can be readily broken by hydrolysis at relatively low temperatures (17).

The principal conclusions of their work as it relates to hydrothermal treatment of coal are: 1) it

is the ionic chemistry of water that is important under the pretreatment conditions; 2) that reactions in water systems are often "autocatalyzed" by water soluble organic reaction products; 3) aqueous chemistry provides cleavage pathways for major oxygen crosslinks which are too stable to cleave thermally; 4) water can act as a highly effective acidic or basic catalyst or even as an acid-base bicatalyst 5) reactions of water with organics can be catalyzed by clays. Siskin and coworkers (17-19) have demonstrated that there are plausible pathways for water to remove or reduce oxygen functional groups (e.g., conversion of alcohols to methyl groups) under conditions which are relevant to water pretreatment of coal.

EXPERIMENTAL

Sample Selection - The selection of coal samples was made from the Argonne Premium Sample Bank (20). The coals used were the Zap Lignite, the Wyodak subbituminous and the Illinois No. 6 bituminous. Selected experiments were also done with the Pittsburgh Seam bituminous coal from the same sample bank.

Steam/Water Pretreatment Experiments - A new reactor system was designed to carry out high pressure (up to 6000 psig), high temperature (up to ~ 400°C) hydrothermal treatment of coal in a closed bomb (20 ml) reactor. After 1-3 g coal is fed into the bomb and the reactor head is screwed on to get a gas tight seal, the system is purged with N_2 or evacuated, the high temperature, high pressure valve on the reactor base is closed, and the water is injected directly into the coal through the capillary tube with a ~ 0.1-1.0 ml/min rate. Deaerated and deionized water is used throughout the reaction.

Simultaneously with the water injection, the reactor is immersed into the fluidized sand bath held at the required temperature. The pressure is measured in the water feed capillary tubing directly after the pump. The amount of water pumped in and the temperature determines whether steam and/or water pretreatment is done. The results described in the current paper are for pretreatment with subcritical water at 350°C, 4000 psig and pretreatment times from 10 to 1200 minutes. Additional details of the experiments have been provided previously (11).

Product Analyses - The residues from the water pretreatment experiments with the four coals were subjected to analysis by programmed pyrolysis (TG-FTIR), solvent extraction, FT-IR, SEM/x-ray analysis and liquefaction experiments in a donor solvent. The liquefaction and solvent extraction experiments have been discussed previously (11). The current paper focuses primarily on the results from TG-FTIR (21) and FT-IR (22,23) analysis of the residues.

RESULTS AND DISCUSSION

Experimental Results - Figure 1 compares the TG-FTIR results for raw, water pretreated and demineralized Wyodak samples. Figures 1a, 1d, and 1g show the time-temperature profile, the TGA balance (lower curve) and the sum of gases (by FT-IR). Figures 1b, 1e, and 1h show the differential and integrated evolution curves for tar, while Figures 1c, 1f, and 1i show the same curves for CO_2. In addition, Figures 1f and 1i have the differential curves for the raw coal superimposed as dashed lines for comparison. The water pretreatment was done at 350 °C, 4000 psig for 20 minutes.

The results in Fig. 1 show that both hydrothermal treatment and demineralization lend to increases in the pyrolysis tar yield and a reduction in the pyrolysis CO_2 yield. These results are consistent with previous work which has suggested that crosslinking is associated with CO_2 evolution, i.e., the increase in tar is a result of a reduction in crosslinking (24,25). In the case of demineralization, the removal of divalent cations which act as crosslinks in the structure is

believed to be responsible for the observed result (25). In the case of hydrothermal treatment, the divalent cation content is essentially unchanged (10), so a different mechanism must be important.

A variety of explanations for the effects of hydrothermal treatment have been proposed:

- Hydrothermal treatment adds hydrogen (which can stabilize reactive fragments) and removes oxygen groups (which cause retrogressive reactions).

- Hydrothermal treatment partially depolymerizes the coal structure by breaking covalent bonds and disrupting hydrogen bonds.

Evidence for the former comes primarily from spectroscopic and elemental analysis (6-11) while evidence for the latter comes primarily from data on pyridine extractability (1-5,10,11). The relative importance of each mechanism is likely a function of coal type. Both are consistent with work that has been reported in the organic geochemistry literature on the artificial and natural maturation of organic matter (12-17). Landais and coworkers (12-16) conclude that pyrolysis in confined systems, such as occurs in hydrothermal treatment, can mimic the natural maturation process for coal and other organic matter. However, they also conclude that the presence of water may not be as important as close confinement of the sample with the products of primary pyrolysis. Of course, for low rank coals one of the principal primary pyrolysis products is water. The work of Siskin and Katritzky (17) would suggest more prominent role for water as a reactant species and in providing a medium in which ionic reactions can occur (based on an extensive series of studies with model compounds). However, they also agree that the artificial maturation reactions are auto-catalyzed, i.e., the products of the initial reactions become reactants in subsequent reactions.

Figure 2 shows a comparison of evolution curves from TG-FTIR analyses of (a-d) water pretreated Zap lignite residues (350 °C, 4000 psig) and (e-h) four Argonne premium coals of a range of rank. This figure shows four sets of plots of the differential evolution rate curves for tar, CH_4, CO_2, and CO. In the case of tar, the results in Fig. 2a indicate a sharp increase in tar yield at short pretreatment times followed by a gradual decline at long pretreatment times. This trend is consistent with the observed trend in the rank series shown in Fig. 2e. It is also true that the T_{max} values for tar increase with increasing pretreatment time, which is again consistent with the observed rank variation. As discussed above, the initial increase in the tar yield could be due to loss of crosslinking agents (oxygen functional groups) and/or depolymerization of the coal structure. The decline in tar yield at long pretreatment time could be due to an increase in the aromatic cluster size of the average repeating unit which would lend to lower volatility and/or a loss of aliphatic hydrogen which can stabilize reactive fragments (26). There is also evidence from recent solvent swelling measurements done at Advanced Fuel Research that short time water pretreatment loosens up the coal structure, while long time pretreatment makes it more compact.

The results for the CH_4 evolution rate with increasing pretreatment time (Fig. 2b) also shows the same trend that is observed in the rank series (Fig. 2f). A major source of CH_4 gas evolution is believed to be methyl groups. These can be created by rupture and stabilization of CH_2 - CH_2 bridges or CH_2 - O bridges. The latter groups are known to be reactive under hydrothermal treatment conditions. Katritzky et al. (19) have also shown that benzyl alcohols can react under these conditions to form toluene as a major product.

Figure 2c indicates significant reductions in the CO_2 yield with increasing pretreatment time which also parallel the changes with increasing rank (Fig. 2g). The removal of carboxyl groups by

hydrothermal treatment has been demonstrated by FT-IR analysis of pretreated samples (7,11,14). Siskin et al. (18) have shown that hydrothermal treatment at 343 °C of 1-naphthoic acid yielded only naphthalene.

The results for the change in CO evolution with hydrothermal treatment (Fig. 2d) are interesting in that they do not directly follow the trend of decreasing CO with increasing rank (Fig. 2h), i.e., there is an initial increase in CO evolution. The evolution of CO can occur from the decomposition of hydroxy or dihydroxy functionalities. Evidence from FIMS (27) and FT-IR analysis (6,11) of water pretreated coal residues shows an initial increase in the formation of phenols and catechols during water pretreatment which is consistent with the initial increase in pyrolytic CO formation. Siskin et al. (18) have shown from model compound studies that certain diaryl ethers could be readily converted to phenols under hydrothermal treatment conditions. An examination of proposed structures for low rank coals (28) would reveal several ether and hydroxyether structures where this type of chemistry could occur.

The results in Figs. 3-5 show the integral yields of tar, CH_4, CO_2, and CO from water pretreatment of Zap, Wyodak, and Illinois No.6 coals for a range of pretreatment times. The trends for Zap, shown in Fig. 3, are consistent with the more limited set of data shown in Figs. 2a-d. The results for the Wyodak coal shown in Fig. 4, are similar to those of the Zap. The results for the Illinois coal, shown in Fig. 5, appear to depend on the "freshness" of the coal sample. The freshly opened samples (indicated by the darkened circles) appear to follow the same trends as the two lower rank coals, except for the CO_2 yield. The results for samples which were opened and stored in a nitrogen purged glove box are more scattered, but appear to follow similar trends, except for the CH_4 yields. This sensitivity of the Illinois coal to aging at ambient conditions has been reported previously (29,30) and is probably related to catalytic activity of the pyrite.

Quatititative Modeling - Work was begun on using the AFR FG-DVC pyrolysis model (26) to simulate the results of the water pretreatment experiments with Zap lignite. It was decided to use the Zap data from pretreatment at 350°C for short pretreatment times, since it appears that the behavior at long pretreatment times is more complex. The pyrolysis version of the FG-DVC model was successful at predicting the increase in pyrolysis tar yield based on the lower amounts of CO_2 and the higher amounts of extractables and CH_4, which are inputs into the model (26). A comparison of the measured (*-*) and predicted (---) pyrolysis yields is given in Fig. 6 for the raw and water pretreated coals.

In Fig. 7, a plot is shown of a van Krevelen diagram for the Argonne coals. The simulation of the standard FG-DVC model for maturation conditions is shown as a solid line. The simulation of a modified FG-DVC model for maturation in which CO and CO_2 are removed with a higher rate process is shown as a dashed line. This work is discussed in more detail by Solomon et al. (31). The results for the gas yields (discussed above) and FT-IR analysis of the water pretreated residues indicate that hydrothermal pretreatment more closely follows the dashed line than the solid line, since oxygen is removed faster than hydrogen. This is especially true for the two low rank coals (Zap, Wyodak). The total hydrogen and the sum of ether and hydroxyl oxygen amounts determined by FT-IR analysis of the water pretreated residues from four coals are shown in Table 1, below. Previous work has shown that FT-IR analysis provides a good estimate of the total hydrogen content when compared to standard elemental analysis (32). It also provides a measure of the sum of ether and hydroxyl oxygen which correlates with the total oxygen content. This will be confirmed by doing elemental analysis of the residues.

TABLE 1

FT-IR ANALYSIS OF WATER PRETREATED RESIDUES FROM FOUR COALS

COAL	PRETREATMENT TIME (mins. at 350°C, 4000 psig)	H_{TOTAL}	O_{SUM}
ZAP	- - - -	3.9	10.5
	20	4.9	9.7
	180	4.4	8.2
	1080	4.5	6.7
WYODAK	- - - -	5.1	10.2
	20	5.4	8.8
	180	5.0	8.0
	1080	4.0	7.0
ILLINOIS #6	- - - -	5.7	6.0
	20	4.4	5.4
	300	4.3	5.1
	1080	3.4	4.5
PITT	- - - -	5.8	4.4
	20	5.9	6.3
	180	5.3	5.0
	1200	4.7	4.1

CONCLUSIONS

The conclusions can be summarized as follows:

1. The analysis of pyrolysis data from water pretreated Zap lignite and Wyodak subbituminous coal (reduction in CO_2 yield, maximum in tar yield, increase in CH_4 yield) shows a strong similarity of hydrothermal treatment to an accelerated geological aging process. The results for the Illinois and Pittsburgh bituminous coals were generally similar, though less dramatic.

2. The geological aging analogy is also consistent with results that were obtained in the literature on hydrothermal treatment, since it explains why the treatment is effective in increasing pyrolysis yields for low rank coals and is ineffective or reduces pyrolysis yields for high rank coals. However, there are certain trends, such as the fact that the CO yield appears to follow the tar yield (goes through a maximum along with the tar) which do not agree completely with this analogy.

3. The FT-IR data indicate a rapid reduction of oxygen groups during water pretreatment for low rank coals, although there is an initial increase in hydroxy functionalities, and a slower loss of hydrogen after an initial increase.

ACKNOWLEDGEMENTS

The support of this work by the U.S. DOE Pittsburgh Energy Technology Center under Contract No. DE-AC22-89PC89878 is gratefully acknowledged.

REFERENCES

1. Bienkowski, P.R., Narayan, R., Greenkorn, R.A., Choa, K.W., IEC Res., **26**, 202, (1987).
2. Bienkowski, P.R., Narayan, R., Greenkorn, R.A., and Choa, K.C., Ind. Eng. Chem. Res. **26**, 206, (1987).
3. Graff, R.A. and Brandes, S.D., Proceed. of the New Fuel Forms Workshop, U.S. DOE Fossil Energy, p. 35, (1986).
4. Graff, R.A. and Brandes, S.D., Energy & Fuels, **1**, 84, (1987).
5. Zhou, P. and Brandes, S.P., "Steam Conditioning of Coal for Synfuels Production", 7th Annual Gsaification Contractors Review Meeting, (June 16-19, 1987).
6. Brandes, S.D., Graff, R.A., Gorbaty, M.L., and Siskin, M., Energy & Fuels, **3**, 494, (1989).
7. Khan, M.R., Chen, W.-Y., and Suuberg, E.M., Energy & Fuels, **3**, 223, (1989).
8. Ross, D.S. and Hirschon, A., ACS Div. of Fuel Chem. Prepr., **35**(1), 37, (1990).
9. Ross, D.S., Hirschon, A., Tse, D.S., and Loo, B.H., ACS Div. of Fuel Chem. Prepr., **35**(2), 352, (1990).
10. Serio, M.A., Solomon, P.R., Kroo, E., and Charpenay, S., ACS Div. of Fuel Chem. Prepr., **36** (1), 7, (1991).
11. Serio, M.A., Kroo, E., and Solomon, P.R., ACS Div. of Fuel Chem. Prepr., 37 (432), (1992)
12. Landais, P., Michaels, R., and Poty, B., and Appl. Pyrol., **16**, 103, (1989).
13. Landais, P., Monin, J.C., Monthioux, M., Poty, B., and Zaugg, P., C.R. Acad. Sci., Paris, t, **308**, Serie II, p. 1161, (1989).
14. Monthioux, M., and Landais, P., Energy & Fuels, **2**, 794, (1988).
15. Landais, P., and Monthioux, M., Fuel Proc. Tech., 20, 123, (1988).
16. Monthioux, M., Fuel, 67, 843, (1988).
17. Siskin, M., and Katritzky, A.R., Science **254**, 231 (1991).
18. Siskin, M., Brons, G., Vaugh, S.N., Katritzky, A.R., and Balasubramanian, M., Energy & Fuel, **4**, (5), 488, (1990).
19. Katritzky, A.R., Balasubramanian, M., and Siskin, M., Energy & Fuel, **4**, (5), 499, (1990).
20. Vorres, K.S., Energy & Fuels, **4**, (5), 420, (1990).
21. Solomon, P.R., Serio, M.A., Carangelo, R.M., Bassilakis, R., Gravel, D., Baillargeon, M., Baudais, F., and Vail, G., Energy & Fuels, **4**, (3), 319, (1990).
22. Solomon, P.R., and Carangelo, R.M., Fuel, **61**, 663 (1982).
23. Solomon, P.R., and Carangelo, R.M., Fuel, **67**, 949 (1988).
24. Solomon, P.R., Serio, M.A., Deshande, G.V., and Kroo, E. Energy & Fuels **4**, (1), 42, (1990).
25. Serio, M.A., Solomon, P.R., Kroo, E., Bassilakis, R., Malhotra, R., and McMillen, D., ACS Div. of Fuel Chem. Prep., **35**, (1), 61, (1990)
26. Solomon, P.R., Hamblen, D.G., Carangelo, R.M., Serio, M.A., and Deshpande, G.V., Energy & Fuels, **2**, 405, (1988).
27. Ross, D.S., Hirschon, A., Tse, D.S., and Loo, B.H., Fuel, **70**, 289 (1991).
28. Hatcher, P.G., Org. Geochem., 16, 959, (1990).
29. Gethner, J.S., Fuel, **66**, 1091, (1987).
30. Kelemen, S.R., Freund, H., Energy & Fuels, **3**, 498-505, (1989).
31. Solomon, P.R., Serio, M.A., Carangelo, R.M., Bassilakis, R., Yu, Z.Z., Charpenay, S., and Whelan, J., Paper, Anal.. App. Pyrolysis, 19, 1, (1991).
32. Teng, H., Serio, M.A., Bassilakis, R., Knight, K.S., Bates, S.C., and Solomon, P.R., Paper to be Presented at ACS Washington Meeting, (1992).

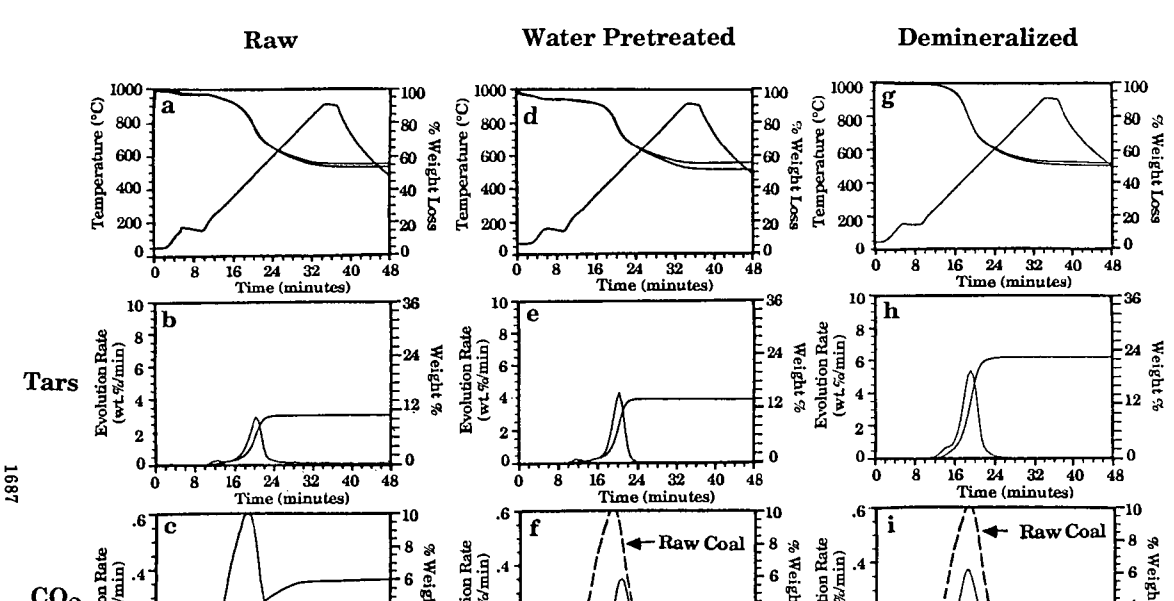

Figure 1. Product Evolution Curves for Raw, Water Pretreated and Demineralized Wyodak Subbituminous Coal. a,d,g) Weight Loss and Temperature Profile; b,e,h) Tar Evolution and Weight Loss; c,f,i) CO_2 Evolution and Weight Loss. Raw Coal Evolution Curve is Indicated in (f) and (i) as a Dashed Line for Comparison. The Water Pretreatment was done at 350°C, 4000 psig for 20 min.

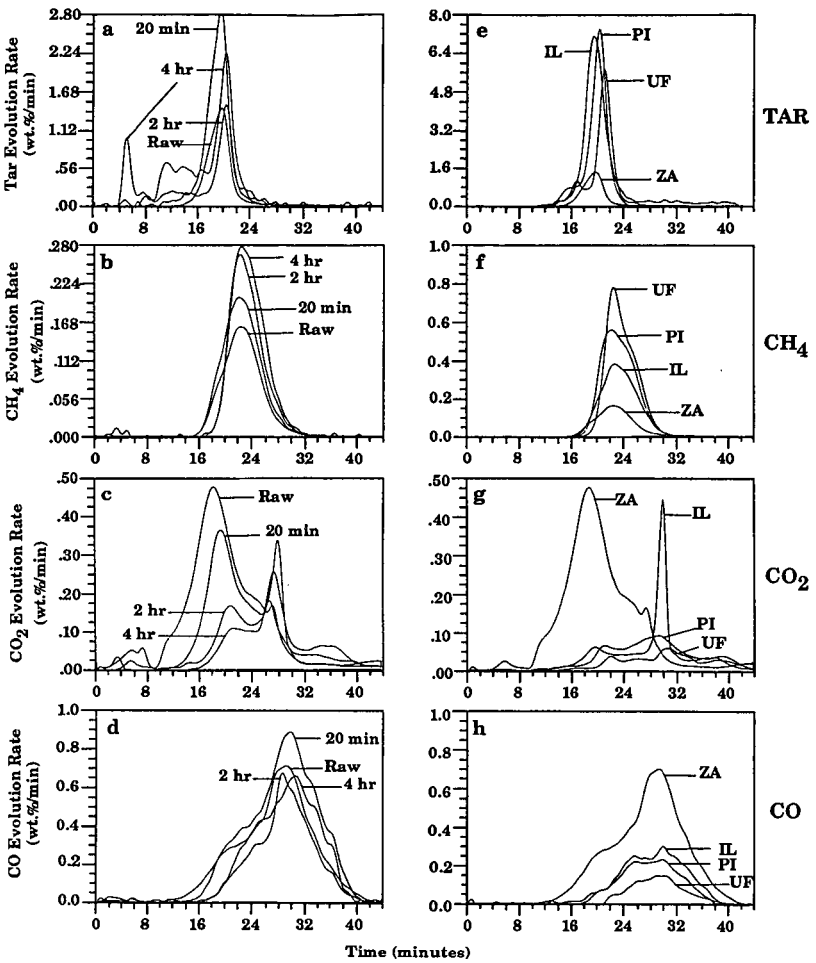

Figure 2. Comparison of Evolution Curves from TG-FTIR Analysis of a-d) Water Pretreated Zap Lignite Residues (350°C, 4000 psig) and e-h) Four Argonne Premium Coal Samples. The Evolution Rates are Given on an As-Received Basis. For the Water Pretreated Samples, the Rates are Normalized to the Moisture Content of the Raw Coal. The Samples are Heated to 150°C for Drying and then at 30°C/min to 900°C (starting at about 10 minutes).

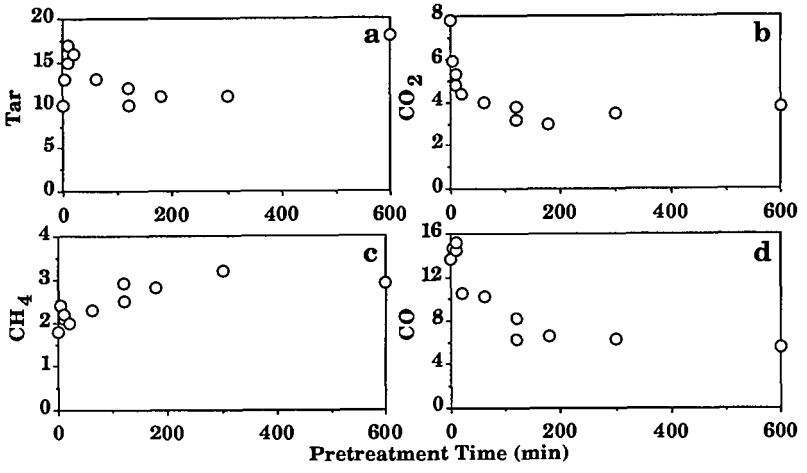

Figure 3. Results from TG-FTIR Analysis of Zap Residues Produced by Water Pretreatment at 350°C, 4000 psig for a Range of Pretreatment Times. All Results are Given on a DAF Basis.

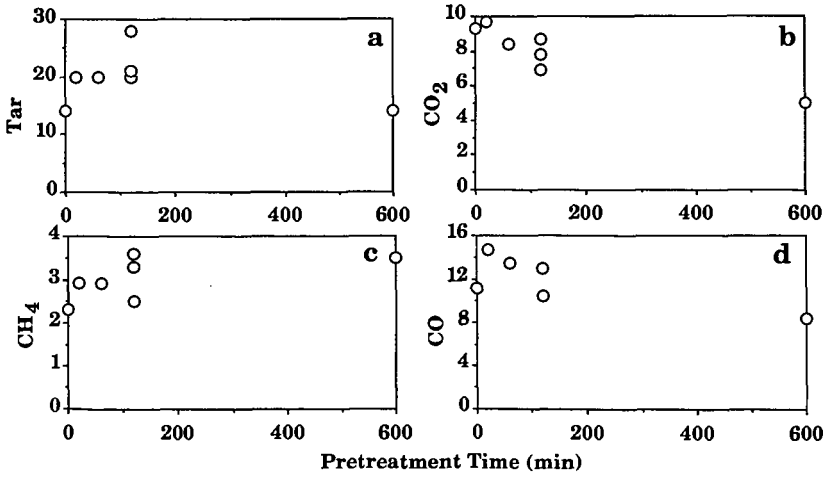

Figure 4. Results from TG-FTIR Analysis of Wyodak Residues Produced by Water Pretreatment at 350°C, 4000 psig for a Range of Pretreatment Times. All Results are Given on a DAF Basis.

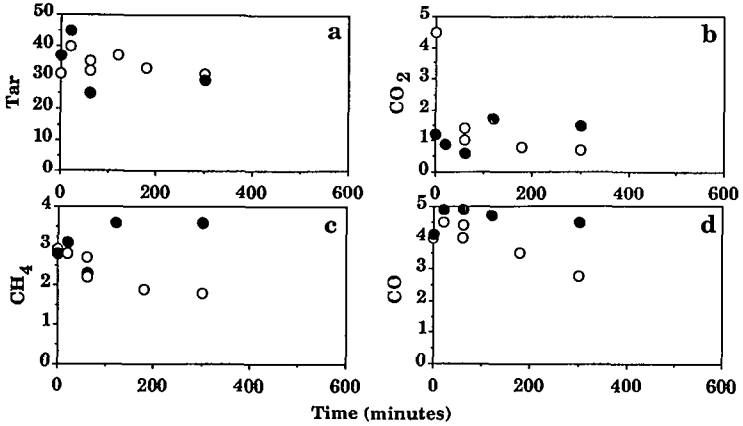

Figure 5. Results from TG-FTIR Analysis of Illinois Residues Produced by Water Pretreatment at 350°C, 4000 psig for a Range of Pretreatment Times. All Results are Given on a DAF Basis. Solid Circles are for Freshly Opened Samples. Open Circles are for Samples which had been Previously Open.

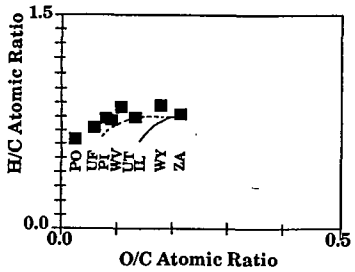

Figure 7. Maturation of Coal. Comparison of Predictions for FG-DVC Pyrolysis Model (solid line), FG-DVC Maturation Model (dashed line) and the Data for the Argonne Coals (symbols).

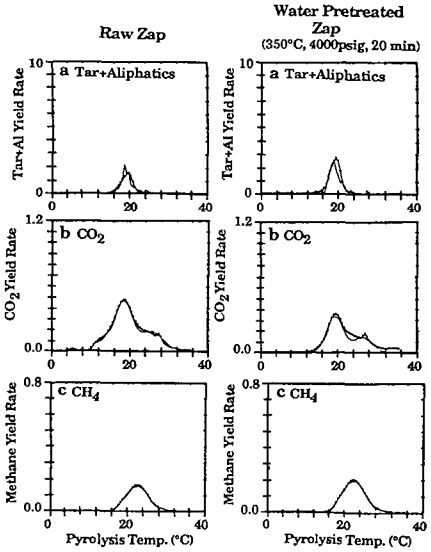

Figure 6. Comparison of Measured and Predicted Yields from Pyrolysis of Raw Zap and Water Pretreated Zap Lignites.

PYROLYSIS AND HYDROPYROLYSIS OF DIPHENYLMETHANE AND SULPHUR-CONTAINING COMPOUNDS IMMOBILISED ON SILICA

Stuart C. Mitchell[1], Christopher J. Lafferty[1], Roberto Garcia[1], Khudzir Ismail[1], Colin E. Snape[1], A.C. Buchanan III[2], Phillip F. Britt[2] and Elmer Klavetter[3]

[1] University of Strathclyde, Dept. of Pure & Applied Chemistry, Glasgow G1 1XL, UK.

[2] Chemistry Division, Oak Ridge National Laboratory, P.O. Box 2008, Oak Ridge, Tennessee 37831, USA

[3] Sandia National Laboratories, Albuquerque, NM 87185,USA

Keywords: Immobilised substrates, pyrolysis, hydropyrolysis, temperature programmed reduction.

ABSTRACT

The use of high pressures and dispersed catalysts, such as sulphided molybdenum (Mo) in fixed-bed hydropyrolysis of coals give rise to increased tar yields. In order to improve our understanding of these phenomena, particularly in relation to cleavage of C-C and C-S bonds, experiments have been conducted on samples of silica-immobilised benzene, diphenylmethane, thioanisole and dibenzothiophene (DBT). These model substrates have the inherent advantage that they do not soften and thus stay in the reactor. Moreover, for the surface-immobilised benzene, the SiO-C bond linking the substrate to the surface is reasonably stable and does not show significant cleavage until 550°C (peak maximum) with a high yield of benzene being achieved at 150 bar hydrogen pressure. For the diphenylmethane substrate, the use of 150 bar hydrogen pressure and the Mo catalyst both reduced the peak evolution temperatures for benzene and toluene clearly demonstrating their separate contributions to promoting C-C bond cleavage. Desulphurisation of the DBT substrate occurred only in hydrogen and the thermal decomposition of the thioanisole substrate was altered markedly by the Mo catalyst.

INTRODUCTION

Diphenylalkanes have been extensively used as model substrates to probe the free radical mechanisms involved in C-C bond cleavage reactions in coal liquefaction [1]. However, the fact that the macromolecular structure in coals is undoubtedly subject to highly restricted motion suggests intuitively that free radical pathways are likely to be somewhat different from those encountered in the vapour phase. Indeed, this has been confirmed by the use of silica-immobilised substrates where bimolecular reaction steps are significantly perturbed in the cases of diphenylethane, propane and butane compared to the corresponding vapour phase reactions [2-4]. Thus far, immobilised diphenylalkanes have only been studied at temperatures close to 400°C, but the fact that silicas do not melt below *ca* 1000°C means that the immobilised substrates also have considerable potential for probing coal and oil shale pyrolysis mechanisms at temperatures in the range 500-600°C which are generally used to maximise tar yields in both fluidised-beds and well-

swept fixed-beds [5-7]. The maximum temperature at which the substrates can be used will clearly be dictated by the cleavage of the C-O bond between the immobilised species and the silica. However, there are a number phenomena related to coal pyrolysis, particularly under hydrogen pressure (hydropyrolysis), which cannot be adequately modelled using model compounds in the vapour phase [8]. For example, the use of hydrogen pressure increases tar yields but without a concomitant increase in hydrocarbon gas yields at relatively low temperatures (< 600°C) where char hydrogasification would not appear to occur to a significant extent [5]. Secondary reactions of volatiles in coal pyrolysis are often implicated to explain reduced tar yields but, again, these are difficult to model, for example, with respect to non-thiophenic sulphur forms where C-S bonds are inherently weak but readily inter-convert to thiophenes [9].

In this study, pyrolysis and hydropyrolysis experiments have been conducted on silica-immobilised samples of benzene, diphenylmethane, thioanisole and dibenzothiophene (DBT) to begin to quantify the effects of hydrogen pressure and dispersed catalysts on C-C and C-S bond cleavage. The sulphur-containing substrates are also particularly useful in relation to temperature programmed reduction (TPR) where the authors from University of Strathclyde have devised a well-swept high pressure reactor [10] to enable virtually all the organic sulphur in coals to be released as hydrogen sulphide and, to a much lesser extent, as thiophenic compounds in tars. The only model substrates which can be possibly used to determine standard reduction temperatures in this regime for different organic sulphur forms are those which do not soften below the decomposition temperatures of the C-S bonds.

EXPERIMENTAL

The silica-immobilised benzene, diphenylmethane, thioanisole and DBT substrates were prepared as described previously [2-4] from the appropriate phenol. In the case of the sulphur-containing substrates, commercially available thioanisole and 3-hydroxyDBT synthesised from the corresponding bromo derivative were used [11]. The purity and loadings for the substrates as determined by base hydrolysis and subsequent gas chromatographic analysis of the silylated products were as follows. For DBT, GC/MS indicated that the remainder of the substrate appears to be derived from dihydroxyDBTs in the starting material.

	Loading, mmol g^{-1}	purity, %
Benzene	0.36	98.4
Diphenylmethane	0.45	99.5
Thioanisole	0.60	99.9
Dibenzothiophene	0.60	94.7

The sulphided Mo catalyst was prepared from ammonium dioxydithiomolybdate as previously described [12,13] which was loaded onto the substrates in methanol to give nominal Mo loadings of 2 or 5% w/w substrate. This helped to agglomerate the fine silica particles but there is the possibility that hydrolysis may have occurred to a limited extent. However, little difference was observed in the volatile evolution profiles without catalyst for the thioanisole substrate when the sample was contacted with methanol as a control experiment.

The high pressure apparatus used here is the same as that used recently for TPR [10]. The reactor tube was smaller but otherwise identical to that used previously in fixed-bed hydropyrolysis

studies (18" c.f. 42" both with 9/16" o.d., Incoloy) [12,13]. Between 0.2 and 0.5 g of sample (<75 μ) mixed with sand (up to 1:5 mass ratio, 75-250 μ sand to limit pressure drop across the reactor) was loaded into the reactor and held in place with steel wool plugs. The reactor tube was heated resistively up to 600°C at either 2 or 5°C min^{-1}. Hydrogen and nitrogen pressures of 30 and 150 bar were used with superficial gas velocities in the range 0.2-0.5 m s^{-1}. After pressure let-down through either a metering valve or a mass flow controller, the gas stream was sampled through a 1.8 m length of heated capillary tubing at a rate of 25 cm^3 min^{-1} into a quadrupole mass spectrometer (VG Monitorr, 0-100 a.m.u.). The signal from the control thermocouple situated in the coal bed was also fed to the mass spectrometer facilitating the construction of direct plots of evolved gas concentrations against temperature. The evolution profiles for the various species monitored can be fitted using the Redhead equation [14] to derive activation energies assuming first-order kinetics are operative.

RESULTS AND DISCUSSION

Benzene

The evolution profiles for benzene in 150 bar nitrogen and 150 bar hydrogen with and without catalyst and those for benzene, methane and toluene in 150 bar hydrogen are shown in Figures 1 and 2, respectively. In both nitrogen and hydrogen, the peak maxima for benzene are close to 550°C although, in nitrogen, there is also a peak at 500°C. However, much less benzene evolves in nitrogen and it is estimated that the amount is below 20% of that obtained with hydrogen at 150 bar. This is to be expected because the only source of hydrogen is the coupling of two molecules of surface-attached benzene. Indeed, the samples recovered from the nitrogen pyrolysis experiments were black qualitatively confirming that much less benzene had been released than in hydrogen where a small amount of methane and a trace of toluene were also observed at *ca* 570-600°C suggesting that hydrogasification is beginning to occur. No methane and toluene were observed with nitrogen confirming that hydrogasification does not occur under these conditions. Further, no phenol was detected indicating that the Si-O bond is unaffected. Benzene pyrolysis in fluid phases is a complicated process that follows an incompletely understood pathway [1] but it is interesting to note that the pyrolysis of benzene to give diphenyl and hydrogen begins to occur at reasonable rates at *ca* 550°C, the same temperature found here for benzene formation.

Catalyst addition at 150 bar hydrogen pressure vastly reduced the amount of benzene released. Further, the peak evolution temperature for the relatively small amount evolved was close to *ca* 500°C which is significantly lower than without catalyst (Figure 1). However, ions corresponding to methane and a number of alkene species including C_4H_8 and C_5H_8 were also observed suggesting that the benzene released above *ca* 500°C had been hydrocracked to a siginificant degree.

Diphenylmethane

The peak evolution temperatures for benzene and toluene formation are both 550°C with nitrogen (Figure 3) and the recovered sample was coloured indicating that some char must be formed on the substrate. Taking into account the response factors (benzene/toluene = *ca* 1.3 for the ions monitored), it is evident that more toluene is released than benzene (Figure 3, mass ratio being *ca* 2.5). Activation energies for fluid diphenylmethane have been found to be highly dependent on reaction conditions [1]. At low pressures, they are governed by dissociation of the weakest bonds (C-C and C-H are comparable at *ca* 82 kcal mol^{-1}) and hence temperatures in excess of 700°C are

required. However, at higher pressures (18-62 bar in diphenyl diluent), the activation energy is 66 kcal mol^{-1} in the temperature range 550-600°C [1] and this is close to the value of 63 kcal mol^{-1} derived from the evolution profile of benzene with nitrogen. The reaction mechanism in nitrogen is not well-understood but the hydrogen must come from the diphenylmethane itself probably through cyclisation to fluorene. Hence, it is possible that surface-immobilisation and the *para*-silyloxy substituent are lowering the activation energy for toluene release in some unknown fashion.

In hydrogen (without catalyst), roughly equal amounts of benzene and toluene evolve (Figure 4) with the white colour of the residue suggesting qualitatively that the char yield is small. Indeed, comparing the peak areas for benzene and toluene with those in the traces for the nitrogen runs, it is evident that, as anticipated, the amounts evolved are greater (*ca* 60 % more toluene and 4 times as much benzene). However, both evolution profiles would appear to be comprised of two components. The higher temperature one (550-580°C) is consistent with that anticipated for cleavage of the SiO-C bond in surface-immobilised benzene and toluene is similarly formed following the prior hydrogenolysis of the C-C linkages in diphenylmethane according to the reaction scheme below.

$$-SiOPhCH_2Ph + 2H_2 \text{ -------> } SiOPhH + PhCH_3 + -SiOPhCH_3 + PhH$$

Interestingly, the peak evolution temperature from C-C bond cleavage for toluene (495°C) is lower than that for benzene (530°C). The peak areas in the evolution profiles for the run with catalyst are lower than with hydrogen pressure alone (Figure 5) even allowing for the fact that less sample was used. The peak evolution temperatures for benzene and toluene are in the range 430-450°C and are significantly lower than those without catalyst. Further, with catalyst, no high temperature components in the evolution profiles of benzene and toluene are evident presumably because hydrocracking has occurred in a similar manner to the immobilised benzene (see above). The results clearly demonstrate that the use of hydrogen pressure and then the catalyst vastly reduce the activation energies for the disociation of the C-C linkages in the immobilsed diphenylmethane .

Thioanisole

Without catalyst at 150 bar hydrogen pressure, a H_2S peak with a maximum at *ca* 360°C is observed between 320-480°C (Figure 6) but there is no detectable CH_3SH. The methane profile comprises two components and the lower temperature one would appear to match the H_2S peak. Benzene, and to a lesser extent toluene, evolve from 380°C with the bulk evolving between 480 and 600°C probably from cleavage of the SiO-C bond as found for the benzene substrate (Figure 2). Further, the high temperature component of the CH_4 peak between 520 and 600°C broadly corresponds to the tail off in toluene concentration.

With catalyst, a low temperature CH_3SH peak is observed (Figure 7) with only a small amount of H_2S and a hint of methane being evolved at this stage. Some of the H_2S is undoubtedly from the thermal decomposition of the ammonium dioxydithiomolybdate but the overall H_2S concentration is considerably lower with catalyst which might be partly attributable to chemisorption of H_2S on the sulphided Mo (see below for DBT). The component of the methane peak at 350°C observed without catalyst has almost disappeared. Again, high temperature benzene and toluene peaks are observed from SiO-C bond cleavage but the ratio of benzene to toluene is much higher than without catalyst due to more sulphur being eliminated as CH_3SH. These experiments clearly

demonstrate the catalyst markedly affects the desulphurisation pathways of the immobilised thioanisole favouring cleavage of the phenyl-SCH_3 bond.

Dibenzothiophene

No detectable H_2S is evolved in nitrogen from the DBT substrate but, as anticipated from previous TPR and pyrolytic experiments on coals [10] , significant quantities are released with hydrogen pressures of 30 and 150 bar (Figure 8). The peak evolution temperature of *ca* 500°C (slighty lower at the higher pressure) is close to those in the range 450-500°C found in high pressure TPR for a number of coals [10] confirming that the dominant peaks arise from thiophenes; lower temperature peaks between 300 and 400°C, attributed to non-thiophenic forms are also observed for low-rank coals.

Catalyst addition to the DBT substrate vastly reduces the amount of H_2S evolved at 150 bar (Figure 8). This is thought to arise from chemisorption of of H_2S on the sulphided Mo catalyst as the mole ratio of Mo to evolved sulphur is relatively high (*ca* 0.4). The peak maximum of *ca* 430°C is again similar to those observed thus far for coals in TPR [10]. However, because the mole ratio of Mo to evolved H_2S was much lower for the coals, no loss of intensity was observed upon catalyst addition.

CONCLUSIONS

The benzene results have demonstrated that immobilised model compounds are stable enough to be used in the type of pyrolysis and hydropyrolysis regimes used here. It has been shown using the diphenylmethane substrate that dispersed sulphided Mo catalyses the hydrocracking of C-C bonds in the solid-state. The thioanisole and DBT samples have demonstrated the promise of using immobilised sulphur compounds as standards in TPR.

ACKNOWLEDGEMENTS

The research was supported at the (i) University of Strathclyde by the Science & Engineering Research Council (Grant No. GR/G/26600) (ii) Oak Ridge National Laboratory by the Division of Chemical Sciences, Office of Basic Energy Sciences, US DoE under contract DE-AC05-840R21400 with Martin Marietta Energy Systems, Inc. and (iii) Sandia National Laboratories by the US DoE.

REFERENCES

1. M.L. Poutsma, *Energy & Fuels*, **4(2)**, 113 (1990) and references therein.
2. A.C. Buchanan III and C.A. Biggs, *J. Org. Chem.*, **54**, 517 (1989).
3. A.C. Buchanan III, P.F. Britt and M.L. Poutsma, *Prepr. Am. Chem .Soc. Div. Fuel Chem.*, **35(1)**, 217 (1990).
4. P.F. Britt and A.C. Buchanan III, *J. Org. Chem.*, **56**, 6132 (1991).
5. C.E. Snape, *Fuel*, **70**, 285 (1991) and references therein.
6. Z.S. Gonenc, J.R. Gibbins, I.E. Katheklakis and R. Kandiyoti, *Fuel*, **69**, 383 (1990).
7. A.M. Ruben and T.T. Coburn, *Proc. 1981 Eastern US Oil Shale Symp.*, 21.
8. R. Cypres, C. Braekman-Danheux and A. Progneaux, *Fuel*, **65**, 1299 (1986).

9. M.L. Gorbaty, S.R. Kelemen, G.N. George, P.J. Kwiatek and M. Sansome, *Fuel*, **70**, 396 (1991) and references therein.
10. C.J. Lafferty, S.C. Mitchell, R. Garcia and C.E. Snape, *Fuel*, accepted for publication and C.J. Lafferty, C.E. Snape, R. Garcia and S.R. Moinelo, *Prepr. Am. Chem. Soc. Div. Fuel Chem.*, **36(3)**, 877 (1991).
11. M. Gates and W.G. Webb, *J. Am. Chem. Soc.*, **80**, 1186 (1957).
12. C.E. Snape and C.J. Lafferty, *Prepr. Am. Chem. Soc. Div. Fuel Chem.*, **35(1)**, 1 (1990).
13. C.E. Snape, C.J. Lafferty, S. Mitchell, F. Donald, C. A. McArthur, G. Eglinton, N. Robinson and R. Collier, *Final Report, EC Project EN3V-0048-UK(H)* (1991).
14. P.A. Redhead, *Vacuum*, **12**, 203 (1962).

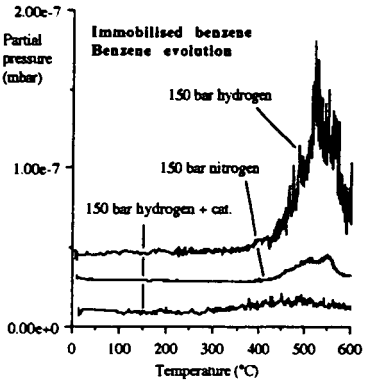

Figure 1. Evolution profiles of benzene from immobilised benzene.

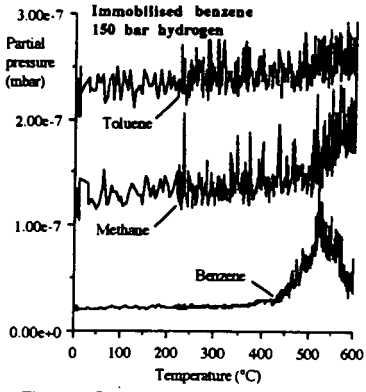

Figure 2. Evolution profiles of benzene, methane and toluene from immobilised benzene in 150 bar hydrogen.

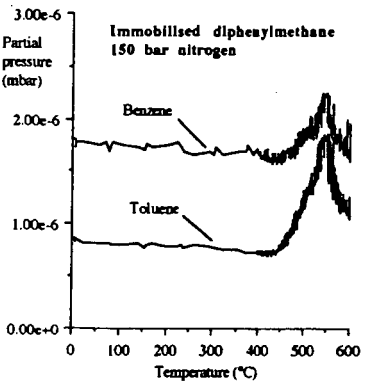

Figure 3. Evolution profiles of benzene and toluene from immobilised diphenylmethane in 150 bar nitrogen.

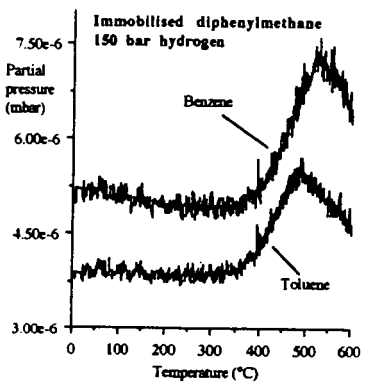

Figure 4. Evolution profiles of benzene and toluene from immobilised diphenylmethane in 150 bar hydrogen.

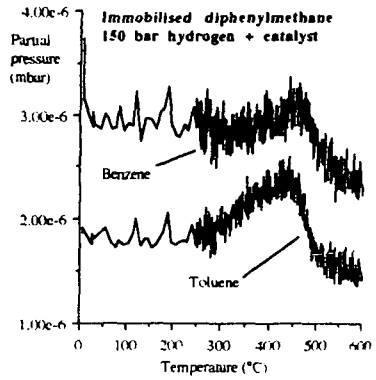

Figure 5. Evolution profiles of benzene and toluene from immobilised diphenylmethane in 150 bar hydrogen with the Mo catalyst.

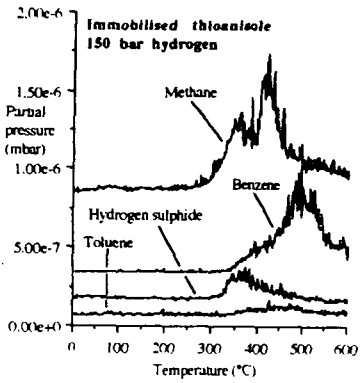

Figure 6. Evolution profiles of hydrogen sulphide, methane, benzene and toluene from immobilised thioanisole in 150 bar hydrogen.

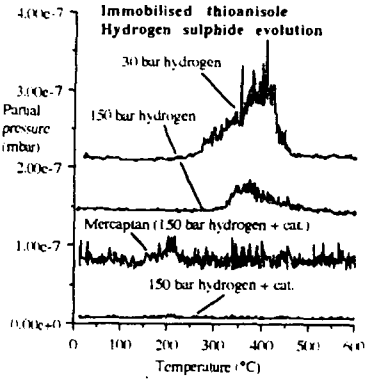

Figure 7. Evolution profiles of hydrogen sulphide and mercaptan from immobilised thioanisole.

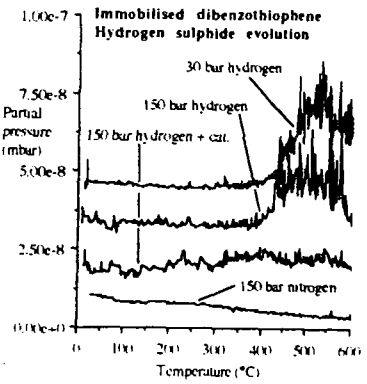

Figure 8. Evolution profiles of hydrogen sulphide from immobilised dibenzothiophene.

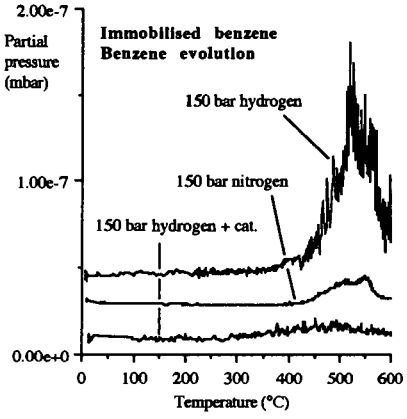

Figure 1. Evolution profiles of benzene from immobilised benzene.

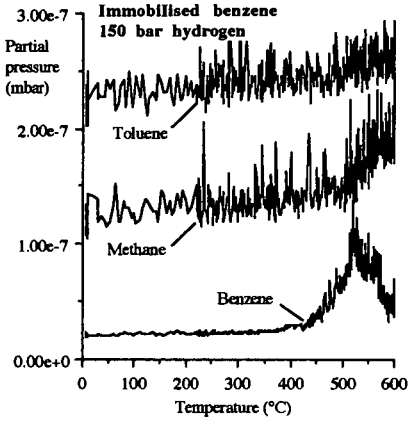

Figure 2. Evolution profiles of benzene, methane and toluene from immobilised benzene in 150 bar hydrogen.

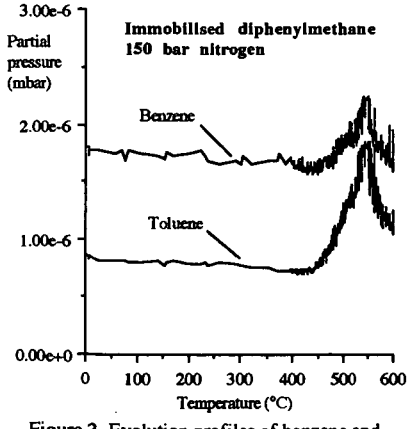

Figure 3. Evolution profiles of benzene and toluene from immobilised diphenylmethane in 150 bar nitrogen.

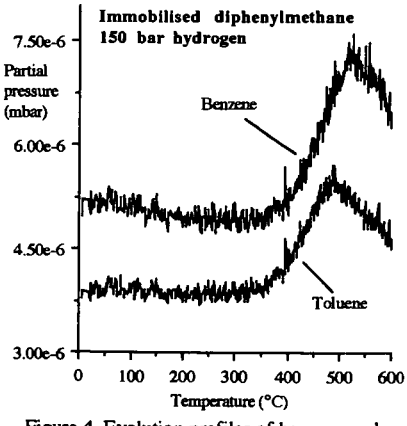

Figure 4. Evolution profiles of benzene and toluene from immobilised diphenylmethane in 150 bar hydrogen.

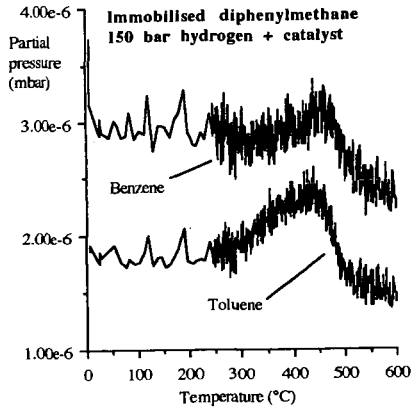

Figure 5. Evolution profiles of benzene and toluene from immobilised diphenylmethane in 150 bar hydrogen with the Mo catalyst.

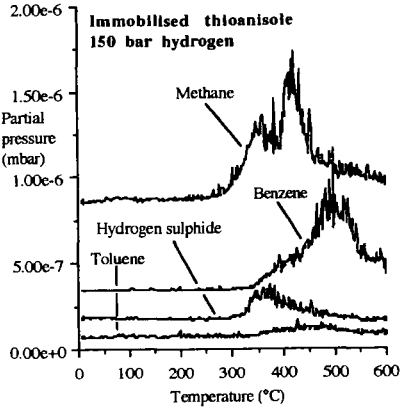

Figure 6. Evolution profiles of hydrogen sulphide, methane, benzene and toluene from immobilised thioanisole in 150 bar hydrogen.

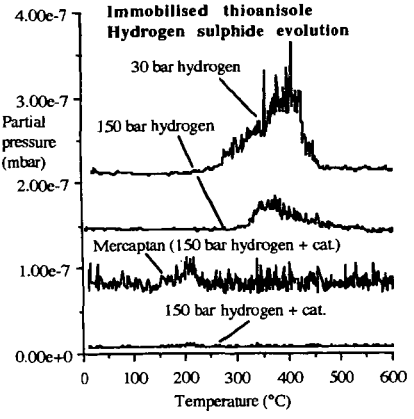

Figure 7. Evolution profiles of hydrogen sulphide and mercaptan from immobilised thioanisole.

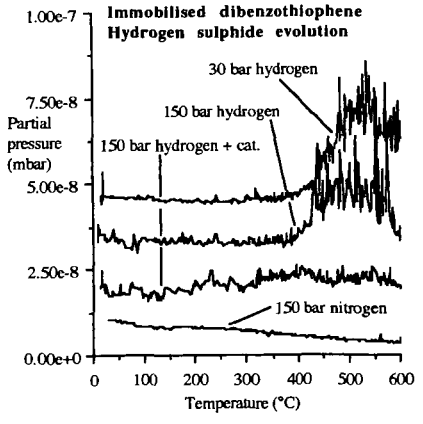

Figure 8. Evolution profiles of hydrogen sulphide from immobilised dibenzothiophene.

A ROLE OF DEVELOPING PORES FOR ORGANIC SULFUR RELEASE IN HYDROPYROLYSIS OF COAL

T. Sugawara and K. Sugawara

Division of Materials Process Engineering, Mining College
Akita University, Akita 010 Japan

Key words: hydrodesulfurization, sulfur form, rapid hydropyrolysis

INTRODUCTION

In our previous papers [1-4] , we examined the dynamic behavior of sulfur forms during hydropyrolysis of coal, changing heating rates from 40 K/min (fixed bed pyrolyzer, 1 atm hydrogen pressure) and 10 K/min (fixed bed pyrolyzer,30 atm hydrogen pressure) to 6000 K/s (free fall pyrolyzer, 1 atm hydrogen pressure). The desulfurization feature was characterized by a kinetic model as shown later, and the simulation of observed results was successful by applying the volume reaction model. We noticed that the extent of sulfur release from solid depended on the operating hydrogen pressure and on the heating rate. As for the organic sulfur in solid, it efficiently decreased when a rapid pyrolysis condition was adopted [4] . We pointed out that the release rate of volatile organic sulfur to tar and gas increased with increasing the release rate of volatile matter and with increasing the internal surface area at an initial stage of heating. The purpose of the present paper is to elucidate a role of developing pores which facilitate the organic sulfur release during rapid hydropyrolysis of coal.

EXPERIMENTAL

Table 1 shows the proximate, ultimate (daf basis), and sulfur form (% of total sulfur) analyses of sample coals: PSOC-830 (Indiana), Rosebud (Montana). A schematic diagram of the free fall pyrolyzer is shown in Fig.1. Coal particles (ca. 0.5 mm) were supplied from the hopper into the reactor at a feed rate of 0.2 g/min. The heating section length was controlled by changing the number of heating blocks from one to five as seen in the figure. Hydrogen gas flowing upwards (2.0 l NTP/min) encountered the coal particles and flowed out with gaseous products and tar. Volatile matter was determined by the difference of the weight of coal supplied and that of char received at the bottom of reactor. Hydrogen sulfide in gaseous products, the sulfur forms in coal and char were analyzed quantitatively [4] . The internal surface areas of the coal and char were measured by applying the Dubinin-Polanyi equation to CO_2 adsorption isotherms at 273 K.

KINETIC MODEL FOR DYNAMIC BEHAVIOR OF SULFUR FORMS

We proposed a kinetic model as illustrated in Fig. 2 where C and D were assumed firstly [2] to be present in void and later [4] in pores. Based on the Dusty Gas Model [5] , we assume here that C represents organic sulfur in tar in macropores and D hydrogen sulfide in gaseous products also in macropores. Micropores would play an important role for the surface reaction of reactants in solid. Decomposition of organic sulfur in coal, A into C and D, occurs at an initial stage of heating with volatile matter release. C and D in macropores could be reattached to solid phase, however, pressure increase in macropores with the evolution of volatile matter would facilitate the release of C and D to outside of a particle. As a consequence, we assume that only D forms refractory organic sulfur B at a later stage of heating where the remarkable evolution of volatile matter almost ends. Rate constants are the 1st order for k_1 - k_3, k_6 - k_8, the 0.5th order for k_4, and the 2nd order for k_5. Further reduction of iron sulfide F is negligible in the atmospheric treatment [4] . The release rates of C and D from macropores to outside of a particle are assumed to be the 1st order to their concentrations in macropores and the rate constants to be equal to the observed 1st order rate constant k for volatile matter release [4] .

EXPERIMENTAL RESULTS AND DISCUSSION

The top section of Fig. 3 shows a calculated curve of particle temperature Tc for PSOC-830 coal along with the distance from the coal hopper X. A set of simultaneous differential equations derived from the momentum, heat, and material balances for a particle were solved iteratively to give the relations of Tc and X and particle residence time t_R. Details of the calculation method are the same as in the reference [4] . A vertical dashed line denotes the point where the temperature begins to rise: particle residence time t_R was set to be 0 at X = 56 cm. Another calculation was also conducted for Rosebud coal which kept a larger apparent density in the pyrolyzer. The particle residence times t_Rs were 0.17, 0.25, 0.33, 0.41, 0.49 s for PSOC-830 coal, and 0.16, 0.24, 0.30, 0.36, 0.42 s for Rosebud coal , respectively, with the heating section lengths of 30 (X=116), 60 (146), 90 (176), 120 (206), 150 (236) cm. The middle section demonstrates change in internal surface area: a drastic change for PSOC-830 coal and a moderate increase for Rosebud coal. It should be noticed that the dynamic feature was quite different within the order of 100 ms even if the final value attained nearly the same. The bottom section of Fig. 3 represents the observed relation between volatile matter released V and the distance from the hopper X. Dashed lines are the calculated values with Eqs. (1) and (2):

$$dV/dt_R = k_0 \cdot \exp(-E/RTc) \cdot (V^* - V) \quad (1)$$

$$V = 0 \text{ at } t_R = 0 \quad (2)$$

where V^* means the ultimate value. A smaller value of the activation energy for PSOC-830 coal, 18 kcal/mol, would relate to the rapid development of micropores, compared with a larger value of 30 kcal/mol for Rosebud coal.
Figures 4 and 5 are observed changes in the sulfur forms distribution with X or t_R for PSOC-830 and Rosebud coals, respectively. Simulation curves are also drawn with one boldfaced and three lightfaced lines in each figure. The part below the boldfaced line in the figure indicates inorganic and organic sulfurs in solid. One can see that the organic sulfur content in solid in PSOC-830 coal decreases more rapidly and efficiently than Rosebud coal. When we concentrate our attention on the sulfur behavior at an initial stage of heating, i.e. t_R<0.2 s, we can evaluate the reaction characteristics of organic sulfur in solid with the rate constants, k_1 - k_3. The simulated values at 1233 K are as follows:

	k_1 [1/s]	k_2 [1/s]	k_3 [1/s]	k [1/s]
PSOC-830	10.1	12.6	25.2	27.7
Rosebud	6.9	4.0	10.1	19.2

Calculated values of the rate constants for volatile matter release with Eq.(1) and (2) are also included. The data suggest that the role of developing micropores is very important for efficient release of organic sulfur from solid.

ACKNOWLEDGEMENTS

This work was supported by Grant in Aid for Scientific Research, Ministry of Education, Science and Culture, Japan, Project no. N16B-01 (03453122). The Pennsylvania State University and Montana College of MineralScience and Technology are appreciated for the supply of coal samples.

REFERENCES

1. Sugawara, T., Sugawara, K., the late Ohashi, H., *Fuel* **67** 1263 (1988).
2. idem, *ibid* **68** 1005 (1989).
3. Sugawara, T., Sugawara, K., Sato, S., Chambers, A. K., Kovacik, G., Ungarian, D., *i bid* **69** 1177 (1990).
4. Sugawara, T., Sugawara, K., Nishiyama, Y., Sholes, M.A., *ibid* **70** 1091 (1991).
5. Bliek, A., van Poelje, W. M., van Swaaij, W. P. M., van Beckum, F. P. H., *AlChE J.* **31** 1666 (1985); Mason, E. A., Malinauskas, A. P., Evans III, R. B., *J. Chem. Phys.* **46** 199 (1967).

Table 1 Ultimate, proximate and sulfur form analyses

Sample	C	H	N	S	Diff.	VM(daf)	FC(daf)	Ash(dry)	FeS_2	SO_4^{2-}	Organic
PSOC 830	71.0	4.4	1.1	1.3	22.2	40.7	59.3	5.6	13	7	80
Rosebud	72.9	4.5	0.9	0.9	20.8	44.3	55.7	10.2	32	3	65

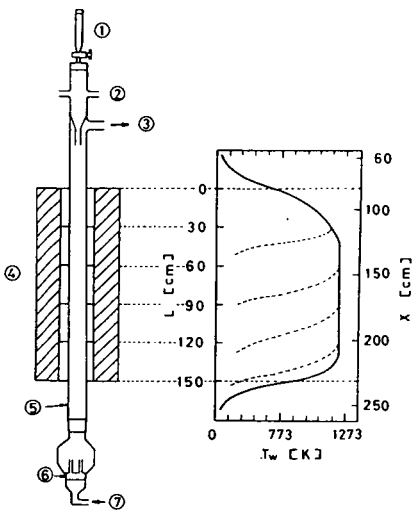

Fig.1 Schematic diagram of free fall pyrolyzer and longitudinal wall temperature profiles of reactor.

1, coal hopper
2, entrained gas inlet
3, gas outlet
4, furnace(5 blocks, 30 cm per block)
5, reactor (fused silica tube, 36 mm i.d.)
6, glass filter
7, gas inlet
L, length of furnace
X, distance from coal hopper

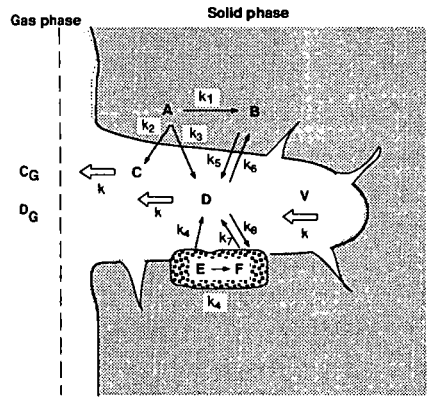

Fig.2 Image of desulfurization of coal.

A : (S_{org})coal
B : (S_{org})char
C : (S_{org})tar
D : S_{H_2S}
E : S_{FeS_2}
F : S_{FeS}
V : Volatile matter

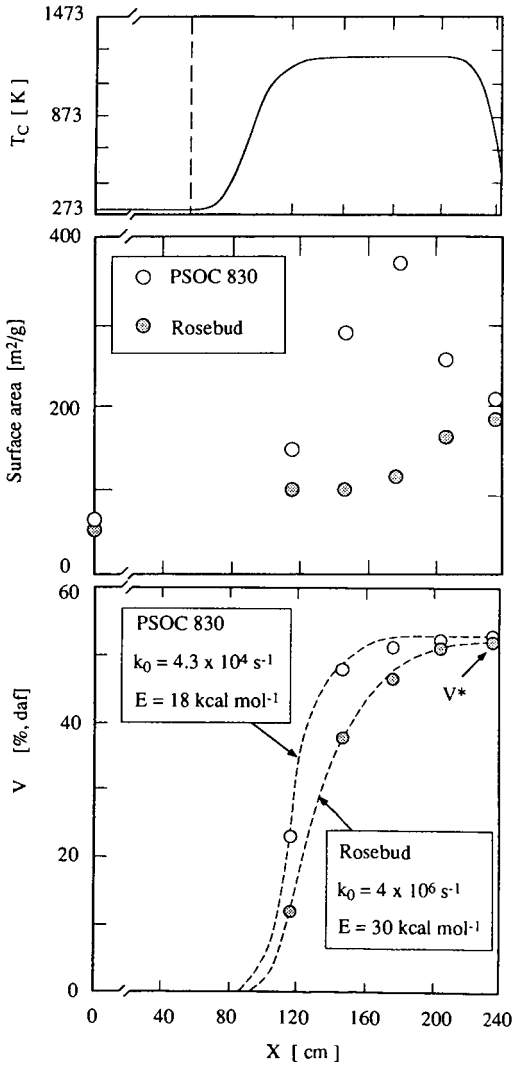

Fig.3 Estimated particle temperature T_c, internal surface area observed and volatile matter released V with simulation curve along with distance from coal hopper X.

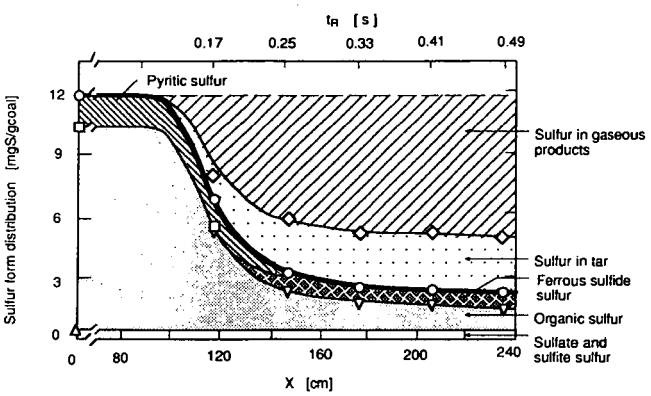

Fig.4 Change in sulfur form distribution with distance X from coal hopper or with particle residence time t_R for PSOC-830 coal.

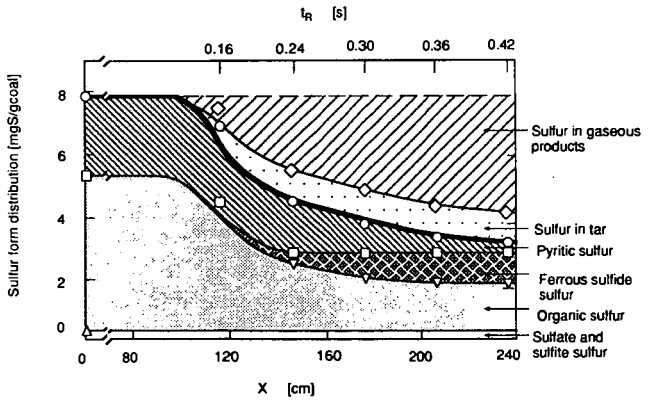

Fig.5 Change in sulfur form distribution with distance X from coal hopper or with particle residence time t_R for Rosebud coal.

CHANGES IN ORGANIC OXYGEN CONTENTS OF ILLINOIS #6 COAL DURING COAL LIQUEFACTION

Bongjin Jung, W. D. Provine, W. H. Calkins*, and M. T. Klein
Center for Catalytic Science and Technology
Department of Chemical Engineering
University of Delaware
Newark, DE 19716

Charles Scouten
Amoco Oil Company
Naperville, IL 60566

INTRODUCTION

The initial stage of direct coal liquefaction is generally presumed to involve the cleavage of the weak bonds in coal. While these weak bonds have not been identified, it appeared possible that they are ether oxygen bonds, and probably benzylic ether bonds because of their low bond strength, and the low activation energies observed in coal liquefaction (1). This view has been strengthened by the observation that coal liquefaction products frequently contain more phenolic components than do the coals from which they were derived (2), suggesting the cleavage of ethers to form phenols. To check this hypothesis, it would be of interest to follow the oxygen content of coal at very low liquefaction conversions, even before much of the coal actually becomes liquid. To do this requires a liquefaction reactor system capable of sampling at very short contact times and low conversions. This system must be such that temperatures and pressures are carefully controlled, and reaction times and reaction time distributions are known. Such a liquefaction reactor has been constructed in our laboratory (3). A preliminary report of the aromaticity of such low conversion products have already been reported (4). In this paper, we present a preliminary report on the total organic oxygen and organic oxygen species in these low conversion solid products.

EXPERIMENTAL

Reactor and Sampling System. The reactor system used is a 1 liter CSTR (continuous stirred tank reactor) described previously (3). A constant flow of tetralin (7 liters/hour) is maintained in a 900 psig nitrogen atmosphere (450 sccm nitrogen) at a temperature of 390°C. 50 gram charges of coal in a tetralin slurry (1:2 coal to solvent) are injected through a rupture disk almost instantaneously by diverting solvent into the charging bomb. Product samples taken in an automated sampling manifold (in this study at 2, 23, 55, 87, 119, and 151 seconds) after injection are quenched to 150°C with a countercurrent water heat exchanger. The system was tested with samples of dibenzylether to check the behavior of a compound with well-known kinetics in the system (5).

Sample Work-Up. The solids were filtered and washed with methylene chloride at room temperature, to remove residual tetralin and coal liquids, and dried in a vacuum oven.

Conversion. Conversion of the coal was determined by measuring the low-temperature ash content of the solid residue and comparing it to that of the unreacted coal (6). A low-temperature asher (LFE Corporation, LTA-302) was operated at 100 watts. The oxygen flow rate was kept at 100 cc/min. Samples were ashed to constant weight.

Organic Oxygen Content. Fast neutron activation analysis (FNAA) was used to determine the oxygen content of the dried reactor sample and the derived low temperature ash. The total

organic oxygen content was determined by correcting the FNAA value of the dried reactor sample for the oxygen content of the mineral matter in the ash (7,8).

Organic Oxygen Speciation. The organic oxygen species (carboxyl, hydroxyl and carbonyl) in the dried reactor samples were determined by the chemical methods of Blom and Schafer (9,10). The organic ether contents of the samples were determined by the difference of the total organic oxygen by FNAA and the oxygen species determined by the chemical methods mentioned above.

Coal Sample. The coal studied was Illinois #6 obtained from AMOCO Corporation. The entire sample was finer than 200 mesh. The analysis of this coal is summarized in Table 1.

RESULTS AND DISCUSSION

The changes in the solid coal at various reaction times are shown in Table 2.

It is apparent from the kinetics of coal conversion (Fig. 1) that a portion of the coal is liquefied more rapidly than the bulk of the coal. That this is not due to the conversion of a particularly reactive maceral is shown by the petrographic analysis summarized in Table 3. Fusinite and semifusinite are generally less reactive than vitrinite (11).

Moreover, these differences are not likely due to particle size effect since the entire sample was extremely fine. In short, a portion of the vitrinite appears to be more reactive than other parts of the vitrinite.

The data gathered thus far suggest that only a relatively small change in the total organic oxygen content occurred (perhaps 10%), even though up to 20% of the coal went into solution. The carboxyl or carbonyl contents of the solid coal are very low to begin with and show little or no change. On the other hand, the hydroxyl content dropped significantly (30–35%) and the ether groups, determined by difference, therefore increased. The explanation for the change in hydroxyl is not clear at this point. However, these results are consistent with the condensation of phenolic groups within the coal to form furane type ring structures (12).

SUMMARY AND CONCLUSIONS

Previous NMR results (4) and the present experiments show clearly that chemical changes occur in solid coal before it becomes a liquid. Further and more extensive measurements will be required before the details of these changes can be resolved. These experiments also show significant conversion of solid to liquid 390°C even at very short contact times. If the formation of these liquid products occurs by cleavage of benzyl ether bonds, they must have occurred in components of the coal having quite different reactivities than the rest of the coal, and to represent only a small proportion of the original ether groups present.

ACKNOWLEDGEMENTS

This research was sponsored in part by Amoco Oil Company and in part by the State of Delaware as authorized by the State Budget Act of Fiscal Year 1988. We also acknowledge the Radioanalytical Services of the University of Kentucky for doing the FNAA and Prof. John Crelling of Southern Illinois University for the petrographic analysis.

REFERENCES

1. Szladow, A. J. and Given, P. H. Ind. Eng. Chem., Process Des Dev. 1981, 20, 27-30.

2. Wachowska, H. and Pawlak, W. Fuel 56, 422 (1977).

3. Provine, W. D.; Poro, N. D.; LaMarca, C.; Foley, H.C.; Bischoff, K. B.; Scouten, C. G.; Cronauer, D. C.; Tait, A. M.; Klein, M. T. "Development of a Pulse Injection CSTR COal Liquefaction Flow Reactor" presented at the AIChE National Meeting, Chicago, IL, Nov. 1991.

4. Provine, W. D.; Jacintha, M. A.; Klein, M. T.; Calkins, W. H.; Dybowski, C. ACS Fuel Div. Preprints 37 (2), 670 (1992).

5. Cronauer, D. C.; Jewell, D. M.; Shah, Y. T.; Modi, R. S. Ind. Eng. Chem. Fund. 1979, 18, 153.

6. Shou, J. K. and Pitts, W. Fuel 1977, 54, 343.

7. James, W. D.; Ehmann, W. D.; Hamrin, C. E.; and Chyi, L. L. J. Radioanal. Chem. 32, 195, (1976).

8. Volborth, A.; Miller, C. E.; Garner, C. K. and Jerabek, P. A. Fuel 56, 204 (1977).

9. Blom, L.; Edelhausen, L. and van Krevelen, D. W. Fuel 36, 135 (1957).

10. Shafer, H. N. S. Fuel 49, 147 (1970).

11. Given, P. H.; Cronauer, D. C.; Spackman, W.; Lovell, H. L.; Davis, A. and Biswas, B. Fuel 54, 40 (1975).

12. Poutsma, M. L. and Dyer C. W. J. Org. Chem. 47, 3317 (1982).

Table 1. Elemental Analysis of Illinois #6 Coal Used.

Carbon	67.18	
Hydrogen	5.00	
Nitrogen	0.98	
Sulfur	3.63	
Chlorine	0.19	
Oxygen (by diff)	12.34	
Ash (ASTM D3174)	10.68	(High Temperature)

Table 2. Total Organic Oxygen Content and Oxygen Functional Groups in the Coal Liquefaction Residues as a Function of Reaction Time at 390°C.

Reaction Time (sec)	0	23	55	87	119	155
% Conversion	0	9.5	16.4	19.5	17.6	20.1
% Organic Oxygen	10.5	10.0	9.6	9.1	10.3	
% Oxygen as Hydroxyl	7.5	5.3		4.7		
% Oxygen as Carboxyl	0.6	0.4		.5	0.65	
% Oxygen as Carbonyl	0.6	0.9		0.6	0.7	
% Oxygen as Ether	2.1	3.3		3.4		

Table 3. Petrographic Analysis of Illinois #6 (AMOCO)

maceral	Volume %	
	Southern Ill. Univ.	Argonne National Laboratory
Vitrinite	86	85
Semifusinite	10.4	10
Fusinite	2.0	
Liptinite	1.6	5

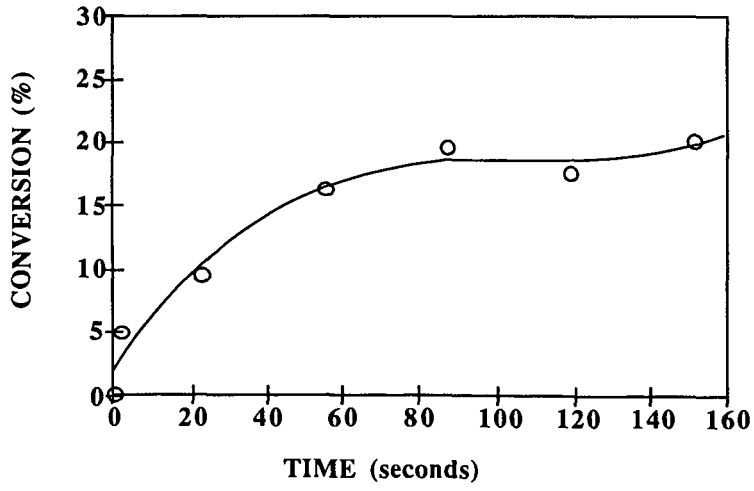

Figure 1. Conversion vs. Time

SULFUR AND NITROGEN EVOLUTION IN THE ARGONNE COALS

R. Bassilakis, M.A. Serio, and P.R. Solomon
Advanced Fuel Research, Inc., 87 Church Street, East Hartford, CT 06108

Keywords: Argonne Premium Coals, Sulfur, Nitrogen

INTRODUCTION

In a previous study (1), the major volatile products evolving from the Argonne Premium coals were investigated using TG-FTIR temperature programmed pyrolysis and combustion. The focus of this study is on the evolutions of two minor volatile products, sulfur and nitrogen, using the same TG-FTIR technique. Although sulfur and nitrogen are small contributors to the mass loss from coal during pyrolysis, their oxides are a major cause of environmental pollutants during coal combustion.

EXPERIMENTAL APPARATUS

Details on the TG-FTIR system appear elsewhere (1,2,3). Its components are as follows: a DuPont 951 TGA, a hardware interface, an Infrared Analysis 16 pass gas cell with transfer optics, and a Michelson 110 FT-IR (resolution, 4 cm^{-1}; detector, MCT). A helium sweep gas (250 cm^3/min) is employed to bring evolved products from the TGA directly into the gas cell. The system is operated at atmospheric pressure.

PROCEDURE

A 50 mg sample loaded in the platinum sample pan of the DuPont 951 is taken on a 30°C/min temperature excursion in helium first to 150°C to dry for 4 minutes and then to 900°C at 30°C/min for pyrolysis. Upon reaching 900°C and holding the temperature for 3 minutes, the sample is immediately cooled to 250°C over a 20 minute period. After cooling, a small flow of O_2 (20 cm^3/min) is added to the helium sweep gas and the temperature is ramped to 900°C in order to combust the remaining char. Infrared spectra are obtained once every 41 seconds.

A post-oxidation method was employed to collectively study sulfur evolution. In this procedure, heat (approximately 900°C) and oxygen (10 cm^3/min) is added to the volatile product stream after the furnace but before the analysis cell. This added step allows detection of H_2S, a very weak infrared absorber; elemental sulfur; and tar sulfur by monitoring SO_2 evolution rate. Details of this post-oxidation method appear elsewhere (1).

RESULTS AND DISCUSSION

Sulfur Evolution - The total sulfur evolution from pyrolysis of the Argonne Premium coals is presented in Figure 1. Sulfur was studied collectively by post-oxidizing the pyrolysis products and monitoring the SO_2 evolution rate. The SO_2 evolution curves exhibit two main evolution peaks. For each peak, the temperature of the maximum evolution rate (T_{max}) increases with increasing rank. Similar rank dependance has been reported by Kelemen et al. (4) and Oh et al.(5). Furthermore, the low temperature SO_2 evolution peak coincides with the coal's tar evolution peak.

To determine the pyritic sulfur contributions to the SO_2 evolutions, Illinois #6 and Pittsburgh #8 coals were subjected to ASTM D-2492 (6) under a nitrogen atmosphere. In this method, sulfate sulfur is extracted from the coal with dilute hydrochloric acid and pyrites (FeS_2) are removed using dilute nitric acid. Results from temperature programmed pyrolysis and combustion of raw and ASTM D-2492 modified Illinois #6 coal are presented in Figures 2 and 3 respectively. Figures 2a and 3a are the balance and thermocouple curves and Figures 2b and 3b are the SO_2 evolution and weight curves. The tar evolution curve for the raw Illinois #6 coal (obtained with out the post-oxidizer in line) is included in Figure 2a to demonstrate how the tar peak overlays the low temperature SO_2 peak. The ASTM D-2492 procedure removed a substantial amount of the low temperature SO_2 peak, the entire high temperature SO_2 peak and the "sharp" portion of the combustion cycle SO_2 peak. These results indicate that pyritic sulfur evolves during the low and the high temperature SO_2 peak, an observation that has been reported by others (5,7). Temperature programmed pyrolysis and combustion of raw and ASTM D-2492 modified Pittsburgh #8 coal showed similar trends as the Illinois #6 coal.

Table 1 compares the TG-FTIR's pyritic and organic sulfur values with those provided by Argonne National Laboratory (8) and also gives the pyrolysis and oxidation contributions to the pyritic and organic sulfur amounts. For Illinois #6 coal, 53 percent of the pyritic sulfur and 62 percent of the organic sulfur along with 47 (ash-free) weight percent of the volatiles evolved during pyrolysis while for Pittsburgh #8 coal, 64 percent of the pyritic sulfur and 48 percent of the organic sulfur along with 43 (ash-free) weight percent of the volatiles evolved during pyrolysis. Consequently, both coals are preferentially evolving sulfur during pyrolysis.

To compare coal pyrite with pure pyrite, a pure pyrite sample from Custer, South Dakota was subjected to temperature programmed pyrolysis and combustion and the evolution curve is presented in Figure 4. The pyrite sample shows no low temperature SO_2 and has a high temperature SO_2 T_{max} (609°C) slightly higher than that of Illinois #6 coal in Figure 2b (578°C).

What causes the low temperature pyrite decomposition in coals during pyrolysis? Since for each Argonne Premium coal the tar evolution and the low temperature SO_2 evolution have similar T_{max}'s, it is feasible that the tars are responsible for the low temperature pyrite decomposition in coal. In support of this possibility, presented in Figures 5a and b are Arrhenius plots comparing the mean reaction rates (r) for tar evolution and low temperature SO_2 evolution for Illinois #6 and Pittsburgh #8 coals respectively. The Arrhenius parameters were generated using the method of evaluating the T_{max} shift with heating rate as described by Braun et al. (9). In this method, a plot of $\ln H_i/T_{max}^2$ versus $1/T_{max}$, where H_i is the experimental heating rate, produces a line with the slope equal to $-(E_a/R)$. The Arrhenius plots show that the mean tar and low temperature SO_2 reaction rates differ by a factor of 4 for the Illinois #6 coal and are virtually identical for the Pittsburgh #8 coal.

As noted from Figure 1, the high temperature SO_2 T_{max} which is a result of pyrite decomposition demonstrates rank dependence. The SO_2 T_{max} increases from 564°C in the case of Zap coal, to 674°C in the case of Upper Freeport coal. It is unclear as to why pyrite in coal is rank dependent. Pyrolysis experiments are presently being done with pyrite/model compound mixtures and with pyrite in the presence of various gases added to the helium sweep gas in an attempt to address this issue.

Nitrogen Evolution - The NH_3 and HCN evolutions from pyrolysis of the Argonne Premium coals are presented in Figures 6 and 7. The NH_3 evolution curves exhibit two main evolution peaks.

For each peak, the T_{max} increases with increasing rank although the majority of the shift in T_{max} for the high temperature NH_3 peak occurs between Wyodak and Illinois #6 coals. The HCN evolution curves exhibit only one main evolution peak and, with the exception of Zap and Wyodak coals, the HCN evolution curves overlay the high temperature NH_3 evolution curve suggesting that a common source is responsible for their formation. In the cases of Zap and Wyodak coals, HCN evolves at a lower temperature than the high temperature NH_3 evolves.

Table 2 compares that TG-FTIR weight percents for NH_3 and HCN to previously obtained values generated during rapid heating rate pyrolysis in an entrained flow reactor (EFR) (10). For each coal, the total amount of nitrogen evolved in of the each pyrolysis systems is similar. The ratio of HCN to NH_3, however, differs significantly. The dominant product during slow heating rate pyrolysis in the TG-FTIR is NH_3 while the only product during rapid pyrolysis in the EFR is HCN. These results can be explained by the following possibilities: 1) A competitive reaction process leads to the formation of NH_3 at the expense of HCN at low pyrolysis heating rates; 2) In the entrained flow reactor, secondary pyrolysis reactions especially tar cracking, lead to the formation of HCN and the destruction of NH_3; 3) NH_3 is removed in the collection system in the entrained flow reactor (e.g., dissolution into water which condenses on the walls of the gas collection bag).

In an attempt to increase the tar cracking in a slow heating rate pyrolysis run, Utah Blind Canyon coal was pyrolyzed in the TG-FTIR and the pyrolysis products were passed through a hot quartz tube heated to approximately 900°C just prior the gas analysis cell. This post-pyrolysis method utilizes the same apparatus as the post-oxidization method; however, helium is added to the sample stream rather than oxygen. The post-pyrolysis results are presented in Figure 8. Figure 8a displays the HCN evolution curves while Figure 8b shows the NH_3 evolution curves. In the post-pyrolysis experiment, the HCN evolution peak at the 20 minute mark indicates a significant increase in tar cracking. This supports item 2 in the latter paragraph although post-pyrolysis does not show significant reductions in NH_3 evolution.

SUMMARY AND CONCLUSIONS

Sulfur Evolution - The total sulfur evolution during pyrolysis measured by post-oxidation of volatile products demonstrated two main evolution peaks which had consistent rank variations. The first SO_2 peak is from organic and pyritic sulfur while the second SO_2 peak is from pyritic sulfur only. Arrhenius plots showed that tar evolution and low temperature SO_2 evolution had similar mean reactions rates. And, sulfur was found to be preferentially released during pyrolysis.

Nitrogen Evolution - NH_3 evolution exhibited two main peaks whose T_{max}'s showed rank dependence although the majority of the shift in the high temperature NH_3 peak occurred between Wyodak and Illinois #6 coals. HCN evolution curves coincided with the high temperature NH_3 evolutions except in the cases of Wyodak and Zap coals where lower HCN T_{max}'s were observed. Finally, the dominant product during slow heating rate pyrolysis was NH_3 while during rapid heating rate pyrolysis HCN was the only product.

ACKNOWLEDGEMENTS

This work was supported by the Morgantown Energy Technology Center of the United States Department of Energy under contract DE-AC21-86MC23075. We wish to acknowledge the useful discussions with Erik Kroo of Advanced Fuel Research and Professor Eric Suuberg of Brown

University. We also thank Jean Whelan of Woods Hole Oceanographic Institute for supplying the pyrite sample.

REFERENCES

1. Solomon,, P.R., Serio, M.A., Carangelo, R.M., Bassilakis, R., Gravel, D., Bailargeon, M., Baudais, F., and Vail, G., Energy & Fuels, (1990).

2. Carangelo, R.M., Solomon, P.R., and Gerson, D.J., Fuel, **66**, 960 (1987).

3. Whelan, J.K., Solomon, P.R., Deshpande, G.V., and Carangelo, R.M., Energy & Fuels, **2**, 65 (1988).

4. Kelemen, S.R., Gorbaty, M.L., Vaughn, S.N., and George, G., "Transformation Kinetics of Organic Sulfur Forms in Argonne Premium Coals During Pyrolysis," Preprint, Am. Chem. Soc., Div. of Fuel Chem., **36** (3) pp.1225-1232 (1991).

5. Oh, M.S., Burnham, A.K., and Crawford, R.W., Preprints, Div. Fuel Chem., Am. Chem. Soc., **33** (1), 274 (1988).

6. Annual Book of ASTIM Standards, Sec. 5 Petroleum Products, Lubricants, and Fossil Fuels, Vol. 05.05 Gaseous Fuels; Coal and Coke, pp. 356-360, (1985)

7. Khan, M.R., Fuel, **68**, 1439 (1989)

8. Vorres, K.S., "Users Handbook for the Argonne Coal Sample Program," (1989).

9. Braun, R.L., and Burnham, A.K., Energy & Fuels **1** (2) pp.153-161 (1987)

10. Solomon, P.R., Hamblen, D.G., Carangelo, R.M., and Krause, J.L., "Coal Thermal Decomposition in an Entrained Flow Reactor: Experiments and Theory," 19th Symposium (International) on Combustion/The Combustion Institute, pp. 1139-1149 (1982)

Table 1. TG-FTIR and Argonne Values for Pyritic and Organic Sulfur in Illinois No. 6 and Pittsburgh No. 8.

	TG-FTIR (AF Wt.%)						Argonne Values (AF Wt.%)	
	Pyritic			Organic			Pyritic	Organic
	Pyrolysis	Oxid.	Total	Pyrolysis	Oxid.	Total	Total	Total
Illinois	1.73	1.53	3.26	1.17	0.73	1.90	3.02	2.16
Pittsburgh	1.12	0.64	1.76	0.42	0.46	0.88	1.48	0.88

Table 2. NH_3 and HCN Weight Percents from Pyrolysis in TG-FTIR and Entrained Flow Reactor.

	TG-FTIR (as-received wt.%)		EFR 1100°C, 24" (ash free wt.%)	
	HCN	NH_3	HCN	NH_3
Pocahontas	0.034	0.27	0.28	0
Upper Freeport	0.028	0.42	0.78	0
Pittsburgh	0.038	0.47	0.84	0
Stockton	0.051	0.45	0.55	0
Utah Blind Canyon	0.101	0.53	1.21	0
Illinois	0.065	0.45	---	---
Wyodak	0.035	0.28	0.60	0
Zap	0.082	0.40	---	---

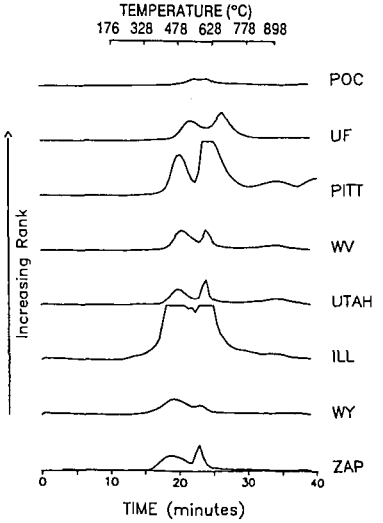

Figure 1. SO_2 Evolution Curves from Pyrolysis of the Argonne Coals with Post-Oxidation of Volatile Products.

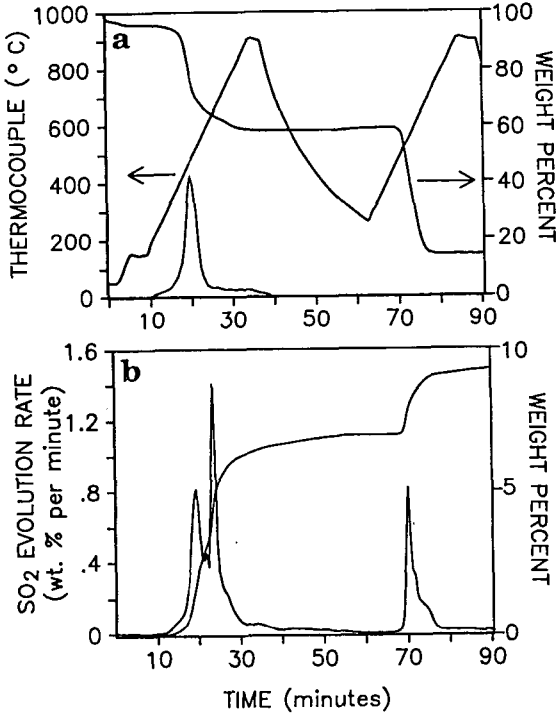

Figure 2. Results from Pyrolysis of Illinois No. 6 Coal with Post-Oxidation of Volatile Products. a) Balance, Thermocouple and Tar Evolution Curves and b) SO_2 Evolution and Weight Curves.

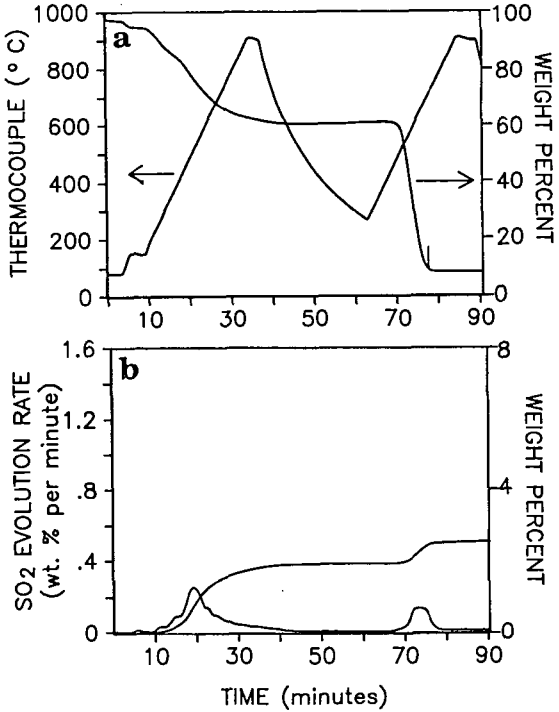

Figure 3. Results from Pyrolysis of ASTM D-2492 Modified Illinois No. 6 with Post-Oxidation of Volatile Products. a) Balance and Thermocouple Curves and b) SO_2 Evolution and Weight Curves.

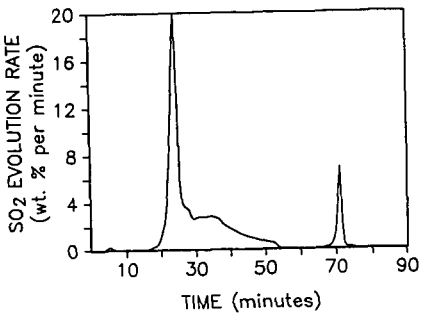

Figure 4. SO_2 Evolution Curve from Pyrolysis of Pyrite with Post-Oxidation of Volatile Products.

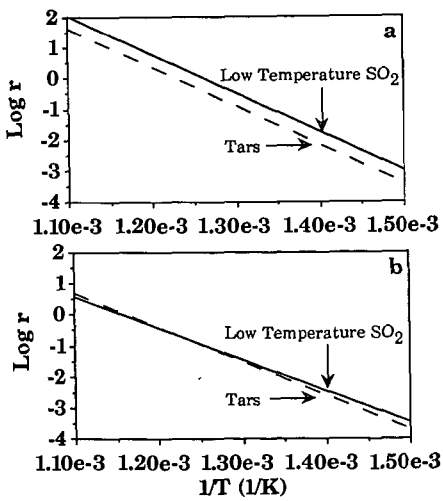

Figure 5. Arrhenius Plots Comparing Mean Reaction Rate (r) of Tar Evolution and Low Temperature SO_2 Evolution for a) Illinois No. 6 and b) Pittsburgh No. 8.

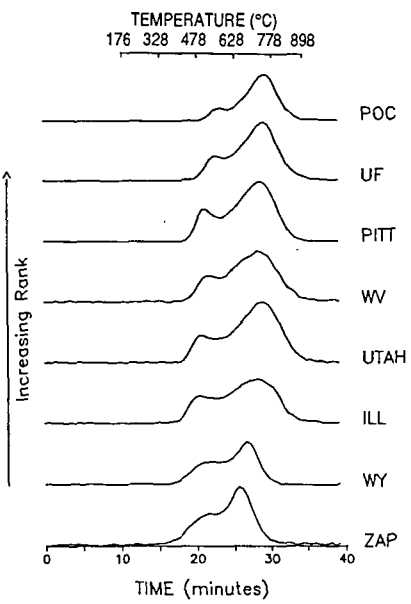

Figure 6. NH_3 Evolution Curves from Pyrolysis of the Argonne Coals.

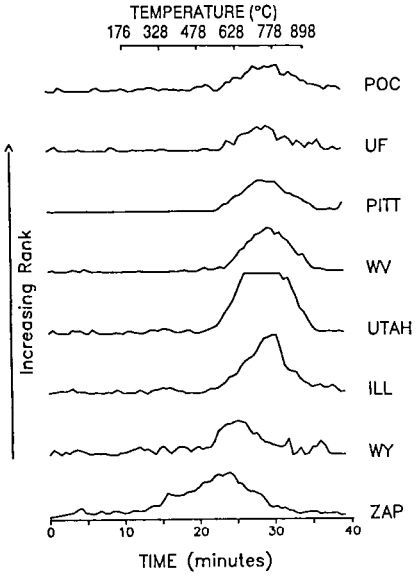

Figure 7. HCN Evolution Curves from Pyrolysis of the Argonne Coals.

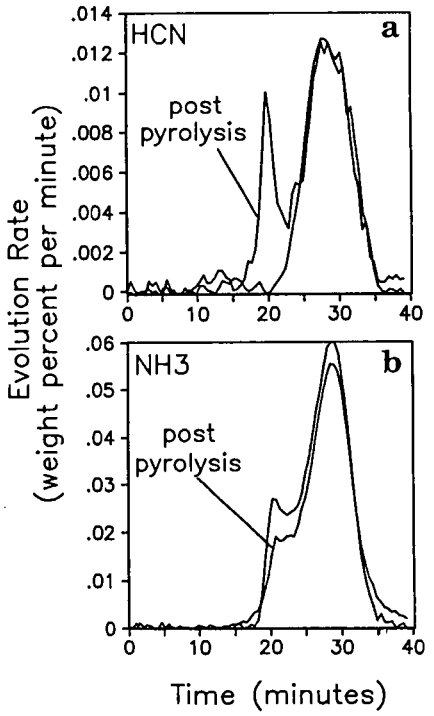

Figure 8. Results from Pyrolysis and Post-Pyrolysis of Utah Blind Canyon. a) HCN Evolution Curves and b) NH_3 Evolution Curves.

DECARBOXYLATION AND COUPLING REACTIONS OF COAL STRUCTURES

Jeffrey A. Manion, Donald F. McMillen, and Ripudaman Malhotra
Molecular Physics Laboratory, SRI International
333 Ravenswood Ave., Menlo Park, Calif. 94025

Keywords: Decarboxylation, cross-linking, retrograde reaction, liquefaction

ABSTRACT

Coupling reactions resulting from decarboxylation have long been associated with the retrograde reactions that hinder the pyrolysis and liquefaction of low-rank coals. The precise chemistry responsible for the coupling has not been proposed, beyond the suggestion that radical recombination or addition must be involved. We have performed a series of decarboxylation/coupling experiments in monomeric benzoic acid systems under liquefaction-relevant, but homogeneous, reaction conditions. The principal findings whose implications will be discussed are: (1) coupling as a result of decarboxylation tends to be very minor (generally < 10%); (2) under strongly oxidizing conditions, namely the absence of scavengers and the presence of one-electron oxidants (which may pertain to the interior of coal particles during the early part of liquefaction), coupling can be as much as 50% of the decarboxylations; (3) amine bases tend to promote decarboxylation but either inhibit or do not affect coupling; (4) H-donors inhibit coupling and, in some circumstances, decarboxylation induced by one-electron oxidants. The limited coupling associated with decarboxylation under most of these liquefaction-related conditions suggests that coupling associated with phenols may be more important.

INTRODUCTION AND OBJECTIVES

It has become increasingly clear in recent years not only that retrograde reactions substantially hinder the liquefaction of low-rank coals, but also that oxygen functional groups in the coal structure are major actors in these retrograde reactions. Carboxyl functions have been implicated in the crosslinking of coals during heating at relatively low temperatures,[1,2] and Serio et al.[3] have been able to model the pyrolytic loss of solvent swelling by including one additional crosslink in the network for every CO_2 evolved. Moreover, pretreatments that have been found to be effective in promoting liquefaction have also shown a corresponding decrease in the early CO_2 evolution.[4] Thus, although crosslinking is correlated with the evolution of CO_2 and H_2O and it therefore seems that carboxyl and/or phenolic groups are involved, we do not know exactly how or why. In order to best mitigate the retrograde reactions it is necessary to better understand their mechanisms—i.e., to know what factors promote and inhibit them.

A recent study by Siskin and coworkers[5] showed that decarboxylation of naphthoic acid under hydrothermal conditions was attended by formation of some binaphthyl, but the coupling aspect was not elaborated in that paper. As a prelude to studies with polymeric compounds, we have carried out and report here on a series of experiments with coal-related monomeric carboxylic acids. We have examined rates of decarboxylation and coupling to see if crosslinking results directly from decarboxylation, as well as how crosslinking is affected by ion exchange, the presence of a hydrothermal environment, and other conditions relevant to pretreatment.

EXPERIMENTAL

Procedures. Experiments on decarboxylation and coupling of monomeric carboxylic acids were carried out in fused silica ampoules. Samples were degassed and sealed under vacuum, with each sample filling approximately one-half of the tube at room temperature. The sealed tube and an appropriate quantity of solvent for pressure equalization was placed in an outer jacket of stainless steel tubing capped with compression fittings. The reaction vessel was then immersed in a temperature-controlled molten-salt bath for the desired time, the tube removed and quenched in water. After cooling in liquid nitrogen to condense CO_2 and volatile organics, the ampoule was opened and the sample removed by pipet and repeated washing of the tube with solvent. An internal standard was

added and the sample analyzed by gas chromatographic analysis using a flame ionization or mass selective detector. Product quantitation was obtained using the FID analyses, with molar responses determined separately for those compounds for which we had authentic samples and estimated by comparison with similar species when no sample was available. Generally, at least three split injections of each sample were performed using an autoinjector. For most species the reproducibility was within ± 2% and we estimate the overall analytical accuracy to be within ± 5%. An exception pertains to the highly polar carboxylic acids, which exhibited excessive peak tailing in the gas chromatograms. These compounds showed much less reproducibility both from injection to injection and in the day-to-day variation in the molar response. For these species we estimate the overall analytical accuracy to be ± 12%.

Chemicals. Benzoic acid (99+% by GC analysis), o-Anisic acid (2-Methoxybenzoic acid, Aldrich, 99%), 3,4-Dimethoxybenzoic acid (Aldrich 99+%), 3-Methoxy-4-hydroxybenzoic acid (Aldrich 97%), m-Hydroxybenzoic acid (Aldrich 99%), Phenylacetic acid (99+% by GC analysis), Cupric acetate monohydrate [$Cu(CH_3CO_2)_2 \cdot H_2O$, Fisher scientific] and Fe_3O_4 powder (supplier unknown, particle size ~ 0.2 μm) were used without further purification.

RESULTS

The Decarboxylation of Activated and Unactivated Benzoic Acids. Table 1 shows the results obtained for a series of benzoic acids under typical "liquefaction" conditions, i.e., 400 °C in tetralin, sometimes with small amounts of other additives such as base.

Data in this table demonstrate that the decarboxylation of benzoic acid itself is slow at 400°C in tetralin (3-5% in 1 hr), unless a fairly strong base or other decarboxylation promoter is present. The substituted but unactivated substrate 3-hydroxybenzoic acid gives a similar degree of decarboxylation. Surprisingly, the decarboxylation of calcium benzoate in tetralin is no faster than that of the free acid. None of these compounds gave significant coupling, either with the starting acid, benzene, tetralin, or naphthalene. In cases where species with hydroxyl groups, e.g. naphthol, were present, there was a small amount (up to several percent) of esterification together with small amounts of the rearranged product of this ester. Since esters will not survive liquefaction conditions when water is present, as it typically is in coal liquefaction, we currently do not consider these "non-permanent" linkages to be of great importance with regard to retrograde reactions.

The near-absence of coupling, together with the slow decarboxylation of benzoic acid itself at 400°C, would make it appear that unactivated aromatic carboxylic acids do not represent the acid species that undergo facile decarboxylation between 250° and 350°C during the heating of low-rank coals. Therefore, we performed additional experiments to examine the behavior of benzoic acid derivatives known[6,7] to be activated toward decarboxylation via electrophilic attack. For all of these, except for meta hydroxy benzoic acid and veratric acid (3,4-dimethoxy benzoic acid, last row in Table 1), decarboxylation in tetralin was almost complete in one hour at 400°C. Again however, there was no substantial level of coupling products. (In some cases there were small chromatographic peaks, as yet unidentified, at higher retention times. We cannot rule out the possibility that these result from some type of coupling associated with decarboxylation, but in any case they amount to less than 5% at most of the decarboxylated acid.)

Perhaps the most interesting result with the activated acids is that obtained with veratric acid. This acid did *not* undergo complete decarboxylation, but was recovered in ca. 25% yield after 1 hour in tetralin at 400°C, in contrast to the analog containing a free -OH in the para position, which underwent complete decarboxylation. Because p-OMe is generally just as activating toward electrophilic attack as p-OH, the above difference indicates that the rate-determining step cannot simply involve attack on the starting material itself. That is, this result suggests that the principal mode of decarboxylation by electrophilic attack either involves reaction of the phenoxy anion or the keto form of the phenolic acid, which is accessible only through the free phenol. One possibility it that the keto form of the acid simply undergoes thermal unimolecular bond cleavage (homolysis) to yield a stabilized radical (phenoxy) and the radical $\cdot CO_2H$, in exact analogy to the thermal cleavage of benzyl and phenoxy

phenols that has been previously elucidated.[8] This possibility, however, is ruled out by the estimated enthalpy requirement for the reaction, which dictates that the decarboxylation would have a half-life of no less than 1000 hours at 400°C.

The Effect of Electron-Transfer Agents and the Acceptor/Scavenger Ratio. Having seen very little coupling resulting from decarboxylation of any of the acids tested thus far, we have broadened the range of reaction conditions under which these acids are being heated, in an attempt to bring about more coupling and perhaps approximate more closely conditions encountered in the thermal processing of low rank coals. Essentially this means reaction in more oxidizing systems, i.e. systems with potential oxidants for carboxylate ions, and with little or no hydro- or alkyl-aromatic. During the early stages of coal liquefaction, such relatively oxidizing conditions might be expected to arise in the interior portions of the coal which are not directly surrounded by the liquefaction solvent. Furthermore, under these conditions, literature data for the reactions of phenyl- and other aryl radicals[11-13] lead us to expect that any phenyl radicals formed will add very readily to essentially any aromatic system, displacing hydrogen to form biaryl linkages. For these experiments we used mixtures of benzoic acid and naphthalene as the basic system and then added various combinations of the reagents that were found from our previous studies to affect decarboxylation, particularly base (pyridine) and the electron transfer agents Fe_3O_4 and $Cu(OAc)_2$.

Table 2 shows the effects of the 1-electon oxidants Fe_3O_4 and $Cu(OAc)_2$ and the solvent H-donating ability on the decarboxylation of benzoic acid. Both electron transfer agents markedly increase decarboxylation (from 3-5% as shown in Table 1 to at least ~50% as seen in Table 2). This increase is qualitatively in accord with the literature data on copper/amine-promoted decarboxylation.[6,7] Decarboxylation is at least ten times faster with $Cu(OAc)_2$ than with Fe_3O_4, but the generation of coupling products is about ten times faster in the presence of Fe_3O_4. In contrast to the experiments reported in Table 1, three main coupling products, phenylnaphthalenes, pyridinylnaphthalenes, and binaphthyls are now observed when either of the electron-transfer agents are present. The similarity of the products suggests that qualitatively similar chemistry is contributing in both systems. However, we still see only relatively low levels of coupling products, particularly in the $Cu(OAc)_2$ system.

The effect of the hydrogen donors on coupling and decarboxylation of benzoic acid can be seen by comparing the latter two experiments in Table 2. In these experiments with cupric acetate, the amount of coupling is decreased by 70% when naphthalene is replaced by a tetralin/1-methylnaphthalene/ naphthol mixture. Both the decarboxylation rate and the ratio of coupling to decarboxylation decrease significantly. This result is suggestive that the primary mode of coupling involves aryl radicals, which are readily scavenged by any of the three new components. The most likely mode of aryl radical production is from $C_6H_5CO_2\bullet$, which should rapidly decompose to $C_6H_5\bullet$ and CO_2. Interestingly, decarboxylation itself is also markedly slowed when an H-donor solvent is used, decreasing from ≥ 83% to about 47%. The reason for this is uncertain. Presuming decarboxylation involves $C_6H_5CO_2\bullet$, thermochemical kinetic analysis indicates that the $C_6H_5CO_2\bullet$ radical should decarboxylate much more rapidly than it could abstract hydrogen from e.g. tetralin. It appears, therefore, that the H-donor must be interfering in some other manner with the activity of the electron transfer agent. (For example, a redox reaction within a cupric acetate molecule to produce curpous acetate and $C_6H_5CO_2\bullet$ might possibly be interfered with by tetralin, which, as an added reducing agent might compete with the internal reducing agent, carboxylate anion.)

Coupling Product Distribution. A more detailed breakdown of products from benzoic acid under various conditions is provided in Table 3. The nature and distribution of the coupling products themselves may provide an indication of the factors limiting coupling under the above reaction conditions. GC/MS analysis has allowed us to identify the coupling products 1- and 2-phenylnaphthalene, two isomers of pyridinylnaphthalene, and the 1,1', 1,2', and 2,2'-binaphthyls, as listed in Table 3.

Typically the 1-phenylnaphthalene is two to three times more abundant than the 2-phenylnaphthalene, consistent with a radical mechanism and the relative rates of radical addition and H-transfer to naphthalene that have been reported in the literature.[14,15] In the case of the binaphthyls, the ratio of

1,2'-, 1,1'-, and 2,2'-binaphthyl is typically 3:2:1. This product distribution is consistent with a statistical preference for the 1,2' isomer, a rather small (1-2 kcal/mol) preference for abstraction of the naphthalene 1-hydrogens,[16] and very little kinetic preference for the highly exothermic addition of an aryl radical to the favored[14,15] 1-position of another naphthalene. The least abundant isomer (2,2'-) represents addition of the least favored aryl radical to the least favored position for addition. The isomer distribution reported by Stein,[16] who studied binaphthyl formation starting from the pure hydrocarbons, differs slightly from our product distribution; he reported the 2,2' isomer to be slightly more favored than the 1,1' binaphthyl.

In the case of the pyridinylnaphthalenes, the point of connection of the pyridine to the naphthalene ring is inferred from the phenylnaphthalenes, but the connections to the pyridine ring are unknown. The pyridinyl- and naphthylnaphthalene isomer distributions are generally consistent with those expected from H-abstraction from either pyridine or naphthalene by the initially produced phenyl radical, followed by addition of the new aryl radical to naphthalene. However, the formation of similar amounts of pyridinylnaphthalenes and naphthylnaphthalenes (binaphthyls) is surprising in view of the fact that the reaction mixture contains seven times as much naphthalene as pyridine. In order to check our inference that these products result directly or indirectly from decarboxylation, we performed control experiments with mixtures of benzene, pyridine, and naphthalene in the presence of Fe_3O_4. Although no significant quantity of phenylnaphthalenes were formed, we surprisingly did find pyridinylnaphthalenes and binaphthyls. Their amounts indicate that perhaps 30-40% of the *secondary* coupling products could arise from mechanisms not involving decarboxylation as the original radical source. However, the *primary* coupling products (i.e., those between phenyl and naphthalene) are almost entirely due to decarboxylation.

Rates of Decarboxylation and Coupling. As would be anticipated from the data of Tables 1 and 2, the addition of 10 m% of pyridine to the naphthalene/benzoic acid mixture (Condition 1 to Condition 2) should increase decarboxylation, and it does increase it about a factor of four (to 19%). It does not, however, substantially affect the coupling to decarboxylation ratio, which drops slightly from 0.027 to 0.023. However, if 10 m% of Fe_3O_4 is added instead of pyridine (Condition 1 to Condition 3), decarboxylation is increased by a factor of only two, while the coupling to decarboxylation ratio rises dramatically to 0.49. Apparently, the absence of a reducing agent such as tetralin *and* the presence of a 1-electron oxidant is necessary before coupling reactions become substantial. Finally, if pyridine is added along with the Fe_3O_4, decarboxylation is increased to $\geq$ 58%, but the ratio of coupling/decarboxylation ratio is reduced by two-thirds when compared to the Fe_3O_4-only case. Thus, although pyridine/Fe_3O_4 synergistically promote decarboxylation, the base leads to an interruption or circumvention of the pathway responsible for coupling.

Mechanistic implications. Although there seem to be relatively few definitive mechanistic investigations of the decarboxylation unactivated acids, decarboxylations have been major synthetic reactions for many years, and the phenomenology is extremely varied, including what appear to be anionic, free radical, and molecular routes.[5-7,9,10] The decarboxylation products we have observed at high temperatures (>300°C) in more oxidizing systems (no donor solvent present, and with an added electron-transfer agent) tend to support one of the traditionally anticipated routes, outlined below, whereby the benzoic acid is converted to benzoate by the base (R1) and the benzoate anion to the radical by the electron transfer agent (R2). The carboxyl radical then decomposes to CO_2 and phenyl radical (R3). Phenylnaphthalenes result from net displacement of a naphthyl hydrogen by phenyl radical (R4). Alternatively, the phenyl radical can abstract hydrogen from pyridine or naphthalene prior to successful addition, resulting in pyridinyl and naphthyl radicals. Attack of these secondary radicals on naphthalene can then explain the formation of pyridinylnaphthalenes and binaphthalenes, as briefly indicated above. The important conclusion is that appearance of these secondary coupling products and the impact of tetralin described above suggest that any radical scavenger should be able to substantially prevent this mode of coupling.

$$C_6H_5CO_2H + C_5H_5N \rightarrow C_6H_5CO_2^- + C_5H_5NH^+ \qquad (R1)$$

$$C_6H_5CO_2^- + Fe_3O_4 \rightarrow C_6H_5CO_2\bullet + Fe_3O_4^- \qquad (R2)$$

$$C_6H_5CO_2\bullet \rightarrow C_6H_5\bullet + CO_2 \qquad (R3)$$

$$C_6H_5\bullet + C_8H_{10} \rightarrow\rightarrow C_6H_5\text{–}C_8H_{10} + H\bullet \quad (R4)$$

It is interesting that a mechanism for the widely used copper/quinoline-promoted decarboxylation of aromatic acids was not published until 1970,[7a] and is still not entirely clear. It is thought to involve the formation of cuprous benzoate as a key intermediate, which then decomposes *without* the formation of a free aryl radical. Since reduction of cupric benzoate to cuprous benzoate can be accomplished by electron transfer from one of the benzoate moieties to the cupric ion, potentially releasing CO_2 and a phenyl radical, both radical and non-radical pathways may be accessible to different degrees and/or under different conditions (copper-quinoline promoted decarboxylations are usually carried out well below 300°C). Thus the scheme in Reactions 1 through 5 is almost certainly simplified and there is very likely more than one mechanism for transition-metal catalyzed decarboxylations operative for different substrates under different conditions.[7,10] In current experiments we are examining the behavior of some activated benzoic acids in the presence of iron oxide, as well as that for a prototypical aliphatic acid.

SUMMARY

The rates of decarboxylation of benzoic acids range from a few percent in 1 hour at 400 °C for unactivated acids to > 98% for species activated in the ortho, para positions. Rates of decarboxylation can be increased by the addition of amine base and/or 1-electron oxidants, but our experiments demonstrate that coupling reactions of activated and unactivated monomeric carboxylic acids are generally *not* important under coal liquefaction conditions in the absence of electron transfer agents. The decarboxylation of the calcium salt of benzoic acid is not significantly faster than that of benzoic acid itself. This is in apparent contrast to the fact the calcium or magnesium forms of low-rank coals produce more CO_2 and show more evidence of crosslinking on heating.[3,17,18] Decarboxylation and coupling reactions of benzoic acid are induced by the electron transfer agents $Cu(OAc)_2$ and Fe_3O_4, and under some highly oxidative conditions one coupling reaction can occur for every two decarboxylations. The rate of coupling in the presence of electron oxidants is greatly reduced by both base and H-donors such as tetralin. The overall conclusion is that, to the extent that monomeric species are representative of coal structures, rather selective conditions are necessary for decarboxylation to result in coupling during coal liquefaction. This suggests either that other mechanisms may be substantially responsible for the retrograde reactions associated with CO_2 evolution, or, if decarboxylation is involved, that it ought to be possible to interrupt these reactions by appropriate control of the conditions.

REFERENCES

1. Suuberg, E. M.; Lee, D.; Larsen, J. W., *Fuel* **1985**, *64*, 1668.
2. Serio, M. A.; Hamblen, D. A.; Markham, J. R.; Solomon, P. R., *Energy Fuels* **1987**, *1*, 138.
3. Solomon, P. R.; Serio, M. A.; Deshpande, G. V.; Kroo, E., *Energy Fuels* **1990**, *4*, 42.
4. Serio, M. A.; Solomon, P. R.; G. V.; Kroo, E.; Bassilakis, R.; Malhotra, R.; McMillen, D.F., *Am. Chem. Soc. Div Fuel Chem. Preprints* **1990**, *35(1)*, 61.
5. Siskin, M., private communication, 1991.
6. March, J., "Advanced Organic Chemistry, 3rd Edition" John Wiley and Sons, New York, 1985, p 507, 562, 653, 842, 928.
7. a. Cohen, T.; Schambach, *J. Am. Chem. Soc.* **1970**, *92*, 3189.
   b. Cairncross, A.; Roland, J. R.; Henderson, R. M.; Sheppard, W. A., *J. Am. Chem. Soc.* **1970**, *92*, 3187
   c. Kaeding, W. W.; Kerlinger, H. O.; Collins, G. R., *J. Org.Chem.* **1965**, *30*, 3754.
   d. Winter, K; Barton, D., *Can. J. Chem.*, **1970**, *48*, 3797.
8. McMillen, D. F.; Ogier, W. C.; Ross, D. S., *J. Org. Chem.* **1981**,*46*, 3322.
9. a. Friedel, C., *Justus Liebigs Ann. Chem.* **1858**, *108*, 122.
   b. Hites, R. A., Biemann, K., *J. Am. Chem. Soc.* **1972**, *94*, 5772.

10. Trahanovsky, W. S.; Cramer, J.; Brixius, D. W., *Am. Chem. Soc.* **1974**, *96*, 1077.
11. Fahr, A.; Stein, S. E., *J. Phys. Chem.* **1988**, *92*, 4951.
12. Fahr, A.; Mallard, W. G.; Stein, S. E., *21st Symposium International On Combusion: The Combustion Institute* **1986**, 825.
13. Chen, R. H.; Kafafi, S. A.; Stein, S. E., *Am. Chem. Soc.* **1989**, *111*, 1418.
14. Herndon, W. C., *J. Org. Chem.* **1981**, *46*, 2119.
15. McMillen, D. F.; Malhotra, R.; Chang, S. -J.; Fleming, R. H.; Ogier, W. C.; Nigenda, S. E., *Fuel* **1987**, *66*, 1611.
16. Stein, S. E.; Griffith, L. L.; Billmers, R.; Chen, R. H., *J. Org. Chem.* **1987**, *52*, 1582.
17. Schafer, H. N. S.*Fuel* **1979**, *58*, 667.
18. Chatterjee, K.; Bal, B.; Stock, L. M.; Zabransky, R. F., *Energy Fuels* **1989**, *3*, 427.

Table 1. Decarboxylation of activated and unactivated benzoic acids.

Acid Structure	Solvent System[d]	Concentration m%	Reaction Time Hrs	% Decarboxylation	% Coupling[a]
$PhCO_2H$ [b,c]	Tet/THQ 75/20	5	1	4	<20
	Tet/THQ/H_2O 55/20/20	5	1	5	<20
	Tet/PipPy 75/20	5	0.5	77	<3
	Tet/THQ/$Zn(OAc)_2$ 75/20	5	1	75	<5
	Tet/1-Naphthol 80/10	10	1	3	<2[e]
$Ca(PhCO_2)_2$	Tet/1-Naphthol 80/10	10	1	3	<2
4-OH-$PhCO_2H$	Tet	20	1	>98	<3
3-OH-$PhCO_2H$	Tet	10	1	2	-
2-OMe-$PhCO_2H$	Tet	10	1	>98	<3
	Tet	20	1	>99	<3
	Tet/Pyrene	10	1	>99	<3
3-OMe-4-OH-$PhCO_2H$	Tet	10	1	>99	<2
3-OMe-4-OMe-$PhCO_2H$	Tet	10	1	~75	<3

a. This figure should be considered an upper limit; it represents the sum of small unidentified high retention time peaks that are potential coupling products, given as a percent of decarboxylation. Thus larger values listed for cases where there is limited decarboxylation do not generally reflect larger absolute amounts of possible coupling products.
b. The first four sets of data for benzoic acid itself are taken from previous work.
c. For economy of space, the symbol "Ph" is used here to represent a single phenyl ring, regardless of whether there are 3, 4 or 5 unsubstituted positions on the ring.
d. "THQ" represents 1,2,3,4-tetrahydroquinoline, "Tet" is tetralin, and "PipPy" is the strong organic base/nucleophile 4-piperidinopyridine.
e. Does not include formation of naphthylbenzoate ester or rearranged product of this ester.

Table 2. Effects of different 1-electron oxidants and solvent H-donating ability on coupling and decarboxylation of benzoic acid[a]

BA (m%)[b]	Solvent System (m%)[b]	Results			
		%Rec. Acid	% Coupling[c]	% Decarbox.[d]	%(Coup/Decarb)
11.3	Naph/Pyridine/Fe_3O_4 68.8/9.8/10.1	19.5	9.34	57.6	16.2
10.4	Naph/Pyridine/Cu Acetate 70.4/8.9/10.3	<0.1	2.96	83.4	3.5
9.8	Tet/MN/Naphthol/Cu Acetate 29.9/29.9/12.2/9.6/9.7	45.9	0.51[e]	46.5	1.1

a. After reaction at 400°C for 1 hr.
b. BA = benzoic acid; Naph. = naphthalene; Tet = tetralin; MN = 1-methylnaphthalene; Naphthol = 1-naphthol; Cu Acet. = cupric acetate monohydrate [$Cu(CH_3CO_2)_2 \cdot H_2O$].
c. As mol% of benzoic acid; refers to all peaks in the "coupling" region of the chromatogram.
d. Based on identified decarboxylation products including benzene and phenyl-containing coupling products.
e. This figure does not include 1% formation of naphthyl benzoate from benzoic acid and naphthol.

Table 3. Effect of Fe_3O_4 and pyridine on decarboxylation and coupling of Benzoic acid during reaction in naphthalene at 400°c for 1 hour

Reactants	Condition 1 mol%	Condition 2 mol%	Condition 3 mol%	Condition 4 mol%
Benzoic Acid	9.57	10.00	10.13	11.26
Naphthalene	90.43	80.23	79.49	68.80
Pyridine	—	9.77	—	9.82
Fe_3O_4	—	—	10.38	10.11
Products				
Benzoic Acid	102.19	92.58	99.74	19.48
Naphthalene	99.80	99.89	98.38	96.08
Pyridine	—	78.88	—	87.54
Benzene	4.26	18.07	6.47	54.11
Naphthalene Impurities	0.77	0.76	0.75	0.76
Biphenyl[a]	< 0.004	< 0.004	< 0.004	0.14
1-Phenylnaphthalene[a]	0.058	0.23	2.36	2.20
2-Phenylnaphthalene[a]	0.055	0.20	1.02	0.99
1-Pyridinylnaphthalene[a]	—	< 0.004	—	2.45
2-Pyridinylnaphthalene[a]	—	< 0.004	—	0.90
1,1'-Binaphthalene[a]	< 0.004	< 0.004	0.91	0.79
1,2'-Binaphthalene[a]	< 0.004	< 0.004	1.44	1.44
2,2'-Binaphthalene[a]	< 0.004	< 0.004	0.44	0.43
% Decarboxylation[b]	4.4	18.5	9.9	57.6
% (Coupling/Decarbox.)[b,c]	2.7	2.3	48.5	16.2

a. Mol percentages are based on the benzoic acid reactant.
b. Based on identified products.
c. For the purposes of this table it is assumed that pyridinylnaphthalenes and binaphthyls are coupling products that stem from decarboxylation after a shift of the radical center from the initial phenyl radical to either pyridine or naphthalene (see text).

CATALYTIC HYDROCRACKING REACTION OF NASCENT COAL VOLATILE MATTER UNDER HIGH PRESSURE IN A TWO-STAGE REACTOR

Hiromi YAMASHITA, Metta CHAREONPANICH, Takayuki TAKEDA, and Akira TOMITA
Institute for Chemical Reaction Science,
Tohoku University, Katahira, Sendai 980, JAPAN.

Keywords: Coal Pyrolysis, Catalytic Hydrocracking, Two-stage reactor

INTRODUCTION

Various products are generated in coal pyrolysis. Usually, the yield of useful chemicals such as benzene, toluene, and xylenes (BTX) is low. If it can be increased to a considerable degree, a combination of flash pyrolysis of coal and gasification/combustion of residual char can become an efficient way to utilize coal. Coal pyrolysis consists of two steps. In the first step, radical species are generated and stabilized. In the second step, the secondary reaction of nascent products occurs in the char pore, in the gas-phase and/or on the char or catalyst surface. In our previous studies [1-4], the modification of the distribution of final products has been tried under the conditions where the primary reaction and the secondary reaction are separated as far as possible. From these studies, it was found that the product yield could be modified by controlling the secondary reaction in which the utilization of catalyst was quite effective.

Previous studies on the utilization of catalyst in coal pyrolysis can be classified into two types: i) hydrocracking of coal volatiles over catalysts added directly on coal [4-6], ii) hydrocracking of volatiles over catalysts placed separately from coal [3, 7, 8]. The results of these studies suggested that the yield of chemicals, such as BTX, can be increased by the following two factors: high H_2 pressure and effective catalyst. However, the coal pyrolysis under high pressure with subsequent catalytic hydrocracking of nascent volatile has not been examined extensively.

In the present study, a two-stage reactor which can be operated under high pressure was made. Using this reactor, coal was pyrolyzed under high pressure of hydrogen in the first stage and the coal volatiles was hydrocracked over sulfided Mo-based catalyst in the second stage. In order to design the distribution of final products, the effects of gas pressure, catalyst, coal type, and reaction temperature on the coal pyrolysis and post-cracking have been clarified.

EXPERIMENTAL

Apparatus and procedure. The schematic diagram of the two-stage reactor used in this study is shown in Fig. 1. The reactor is a SUS-316 tube (i.d. 7.6 mm). H_2 or He at pressure of 0.1-5 MPa was used (200 ml(NTP) min^{-1}). A coal sample (10 mg) was placed in a small quartz boat and was pyrolyzed in the first-stage by heating with an infrared furnace at a rate of 10 K s^{-1} up to a temperature (T_1)

ranging 500-800°C and held there for 2 min. The evolved volatile matter was introduced into the second-stage where the catalyst (800 mg) was packed and the temperature (T_2) was controlled at 400-700°C by another electric furnace. The final products were collected in a cold trap packed with Porapak P. After depressurization, the collected products were allowed to desorb from the trap and subjected to g.c. analysis.

Coal sample and catalyst. Five coals from Australia were used: one bituminous coal; Liddell (C, 83.5 % daf), two subbituminous coals; Wandoan (C, 78.5 %), Millmerran (C, 76.9 %) and two brown coals; Morwell (C, 67.4 %), Loy Yang (C, 66.7 %). Particle size of the coal sample was <100 μm. The sample was dried in N_2 at 107°C for 1 h before use. Ni/Mo/Al_2O_3 (NiO: 2.8 wt%, MoO_3: 10.3 wt%) from Harshow and Co/Mo/Al_2O_3 (CoO: 3.9 wt%, MoO_3: 10.8 wt%) from American Cyanamid were used as catalysts. Catalyst pellets were crushed to 32-60 mesh. Prior to each series of experiments, the catalyst was calcined in oxygen for 0.5 h, and treatment with hydrogen sulfide (H_2S, 4 %; H_2, balance) was carried out at 500°C for 0.5 h, followed by further treatment with hydrogen for 0.5 h. Ni/Mo/S and Co/Mo/S stand for the sulfided catalysts.

RESULTS AND DISCUSSION

Effect of gas pressure in the first-stage. The effect of gas pressure on the coal pyrolysis in the first-stage was investigated without catalyst in the second-stage (Table 1). The amount of volatile (weight loss) increased with increasing pressure of H_2 and with decreasing pressure of He. Hydrogen stabilizes the radical generated in the primary reaction, increasing the amount of volatile. The BTX yield increased with pressure in both gases. The increase of BTX yield observed in H_2 was larger than that in He. The secondary reaction of volatiles in char pore might be responsible for the pressure effect observed in the inert atmosphere of He.

Effect of catalyst and H_2 pressure in the second-stage. The effects of catalyst and H_2 pressure on the distribution of final products were studied by using several catalysts. The results obtained using Liddell coal at the temperature of T_1=600°C and T_2=500°C are shown in Table 2. Al_2O_3 was not effective to increase BTX yield which was similar to that without catalyst under a high H_2 pressure. On the other hand, Co/Mo/S and Ni/Mo/S catalysts were effective for the secondary reaction even under atmospheric pressure. A high pressure remarkably increased the yields of BTX and hydrocarbons, especially the yield of benzene and methane. Ni/Mo/S catalyst was more effective.

Effect of reaction temperature. Effect of reaction temperature of the first- or the second-stage was investigated with Millmerran coal, Ni/Mo/S, and 5 MPa H_2 (Table 3). With a constant T_2 of 500°C, the BTX yield increased with increasing T_1. On the other hand, at T_1 of 600°C, the maximum yields for BTX and hydrocarbon were obtained at a moderate T_2 (600°C). Using the two-stage reactor, the optimum temperatures for the first- and the second-stage can be selected independently.

Effect of coal types. Effect of coal type on the yield of final products is shown in Table 4. For all the coals, the amount of volatiles increased with H_2 pressure. However, the product distribution pattern was different among coals. Under high H_2 pressure, the highest BTX yield (6.2 %) were observed with Millmerran coal, while the highest C_2-C_7 yield (17.1 %) were obtained with Wandoan coal. The present BTX yields were compared with those obtained using Curie-point pyrolyzer (CPP) under atmospheric pressure of argon without catalyst [1] (Fig. 2). The two-stage reaction with Ni/Mo/S catalyst leads to a large increase in BTX yield. The values obtained under atmospheric pressure were twice and those obtained under high pressure were five times larger than those obtained with CPP. A higher BTX yield was obtained by using coal with higher H/C ratio. This is because the coal with higher H/C ratio generates a larger amount of tar during the primary pyrolysis [1], and BTX is produced by the secondary reaction (hydrocracking) of primary tar over catalyst. It can be concluded that the secondary reaction over Ni/Mo/S catalyst under high H_2 pressure is effective for producing valuable materials.

CONCLUSION

The yield of useful chemicals could be increased to a considerable extent by using catalyst under high H_2 pressure in a two-stage reactor. Coal with higher H/C ratio and operation under higher H_2 pressure are preferable for a high BTX yield. The type of catalyst is also an important factor. The Ni/Mo/S catalyst is the most effective. The higher reaction temperature in the first-stage was preferable and the moderate temperature of the second-stage was suitable for a high BTX yield. In the present study, the highest BTX yield (7.6 %) was observed under the following conditions: Millmerran coal, Ni/Mo/S catalyst, T_1=800°C, T_2=500°C, 5 MPa of H_2

REFERENCES

1. Xu, W. C.; Tomita, A. *Fuel* 1987, **66**, 627.
2. Xu, W. C.; Tomita, A. *Fuel Process. Technol.* 1989, **21**, 25.
3. Xu, W. C.; Yamashita, H.; Tomita, A. *Fuel* 1990, **69**, 1007.
4. Yamashita, H.; Xu, W. C.; Jinoka, T.; Shrotri, V.; Hajima, M.; Tomita, A. *J. Jpn. Inst. Energy* 1992, **71**, 189.
5. Bolton, C.; Riemer, C.; Snape, C. E.; Derbyshire, F. J.; Terrer, M. T. *Fuel* 1988, **67**, 901.
6. Sulimma, A.; Leonhardt, P.; van Heek, K. H.; Juentgen, H. *Fuel* 1986, **65**, 1457.
7. Nelson, P. F.; Tyler, R. J. *Energy Fuels* 1989, **3**, 488.
8. Krabiell, K.; Wanzl, W.; Juentgen, H. *Inter. Conf. Coal Sci.* 1987, pp. 687, Maastricht.

Table 1 Effect of Gas Pressure on Coal Pyrolysis.

Gas	Press. (MPa)	Weight loss (%, daf)	Yield (%, daf)					
			CO_x	CH_4	C_2-C_7	BTX	PCX	Tar
He	0.1	34	5.4	2.4	2.4	0.6	0.9	22.3
	2.0	30	4.6	3.3	3.4	1.0	0.5	17.2
	5.0	28	6.4	3.3	3.2	1.0	0.6	13.5
H_2	0.1	34	4.3	2.7	3.4	0.7	0.8	22.1
	2.0	36	4.7	5.2	3.8	2.1	0.7	19.5
	5.0	39	8.3	7.2	5.6	3.2	0.8	13.9

T_1-T_2: 600-500°C. Coal: Liddell. Catalyst: None.

Table 2 Effect of Catalyst and H_2 Pressure on Product Yields from Secondary Reaction of Volatiles.

Catalyst	H_2 press. (MPa)	Yield (%, daf)				
		CO_x	CH_4	C_2-C_7	BTX	PCX
None	0.1	4.3	2.7	3.3	0.7	0.8
	5.0	8.3	7.2	5.6	3.2	0.8
Al_2O_3	0.1	11.3	1.8	3.7	0.7	0.9
	5.0	10.2	5.0	11.3	2.9	0.9
Co/Mo/S	0.1	7.5	1.7	2.6	2.1	0.8
	5.0	2.0	4.4	7.4	4.7	0.8
Ni/Mo/S	0.1	4.3	4.4	4.3	2.1	0.9
	5.0	0.7	10.8	10.9	5.1	0.8

T_1-T_2: 600-500°C. Coal: Liddell.

Table 3 Effect of T_1 and T_2 on Product Yields from Secondary Reaction of Volatiles.

T_1-T_2 (°C)	Weight loss (%, daf)	Yield (%, daf)			
		CH_4	C_2-C_7	BTX	PCX
500-500	40	5.5	11.6	3.9	0.9
600-500	57	12.4	15.2	6.2	0.9
700-500	60	18.8	18.6	7.0	2.2
800-500	66	18.8	8.3	7.6	1.5
600-400	57	11.0	11.9	5.5	1.5
600-500	57	12.4	15.2	6.2	0.9
600-600	57	16.4	21.6	7.0	0.4
600-700	57	36.4	0.7	4.5	0.1

Catalyst: Ni/Mo/S. Coal: Millmerran.

Table 4 Effect of Coal Types and H_2 Pressure on Product Yields from Secondary Reaction of Volatiles.

Coal	H_2 press. (MPa)	Weight loss (%, daf)	Yield (%, daf)					
			CO_x	CH_4	C_2-C_7	BTX	PCX	Tar
Liddell	0.1	36	4.3	4.4	4.3	2.1	0.9	20.0
	5.0	42	0.7	10.8	10.9	5.1	0.8	13.7
Wandoan	0.1	46	8.8	4.5	6.7	2.5	1.1	22.4
	5.0	56	3.3	13.8	17.1	5.1	1.1	15.6
Millmerran	0.1	53	5.8	4.8	7.4	3.0	1.3	30.7
	5.0	57	1.2	12.4	15.2	6.2	0.9	21.1
Morwell	0.1	50	24.7	3.5	4.8	2.1	1.0	13.9
	5.0	64	2.3	11.4	9.9	5.2	0.8	34.4
Loy Yang	0.1	48	27.1	2.7	3.2	2.0	0.7	12.3
	5.0	56	3.7	14.7	10.8	3.4	0.6	22.8

T_1-T_2: 600-500°C. Catalyst: Ni/Mo/S .

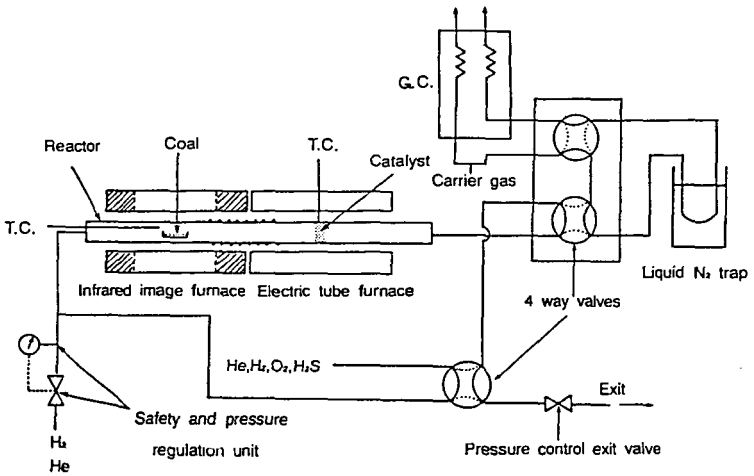

Fig. 1 Schematic diagram of a high pressure two-stage reactor.

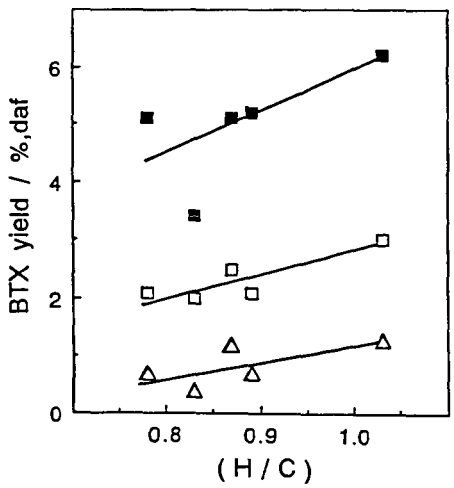

Fig. 2 Effect of H/C ratio of coal on BTX yields obtained in various reaction systems. (■) Two-stage reactor, Ni/Mo/S, 5 MPa H_2; (□) two-stage reactor, Ni/Mo/S, 0.1 MPa H_2; (△) CPP, none catalyst, 0.1 MPa Ar.

Effects of the Structure of the Side Chain on the Pyrolysis of Alkylbenzenes

Ying PENG, Harold H. SCHOBERT, Chunshan SONG
and Patrick G. HATCHER

Fuel Science Program
Department of Materials Science and Engineering
The Pennsylvania State University
University Park, PA 16802

Keywords: Pyrolysis, butylbenzenes

INTRODUCTION

The formation of solids from jet fuels under pyrolytic conditions is a subject of intensive research in the years. The deposit formation is attributed to the thermal breakdown of hydrocarbons at temperatures higher than 350°C (1). Petroleum-derived jet fuels generally consist of about 85% paraffins and less than 10% alkylaromatics (2). When paraffins are subjected to pyrolysis, the formation of unsaturated rings is related to the Diels-Alder type reactions of conjugated alkenes and olefins (3). Upon further heat treatment, these unsaturated rings may undergo dehydrogenation reactions to form alkylbenzenes and solid products. Large amounts of alkylbenzenes are detected in the pyrolysis of long chain paraffins such as decane, dodecane and tetradecane (4). These results suggest that alkylbenzenes are the "precursors" of carbonaceous solid products during the pyrolysis of jet fuels.

The thermal chemistry of alkylbenzenes has been extensively studied, but most of the efforts are directed towards primary products obtained on pyrolysis. The length and types of the alkyl side chains can significantly affect the thermal reactions of alkylbenzenes. As the length of the side chain increases, the reactivity also increases. For instance, the activation energy for the pyrolysis reaction of toluene is higher than that of n-butylbenzene (5). Also t-butylbenzene is found to have a much lower thermal reactivity than its isomer n-butylbenzene (6). Another notable feature is that long-chain alkylbenzenes on pyrolysis exhibit pronounced characteristics of paraffins, i.e., cracking reactions (β-bond scission) become more important (7).

Understanding the secondary reactions that lead to the formation of solid deposit is equally crucial in studying the high-temperature thermal degradation process of jet fuels in an aircraft. This objective is achieved in the following study by using high pressure microautoclave reactors to simulate the situation of the fuel line and fuel nozzles in an aircraft. Preliminary pyrolysis reactions have been performed on four isomeric alkylbenzenes (n-, iso-, sec- and t-butylbenzenes) at 450°C and 0.7 MPa nitrogen over pressure. Solid formation tendencies of these compounds have been compared. Fundamental behavior of these alkylbenzenes that lead to their degradation and the formation of solid deposit have been studied.

EXPERIMENTAL

The experimental apparatus, procedures and product work-up were described in the previous paper (6). All chemicals were obtained commercially and used as received. n-, iso- and sec-butylbenzenes (>99% purity) were purchased from Aldrich Chemical Company. t-Butylbenzene (98% purity) was purchased from TCI America.

RESULTS AND DISCUSSION

1. General Scheme in the High Pressure Microautoclave Reactor

Experiments were carried out in the microautoclave reactors (tubing bombs) at 450°C under 100 psi using ultra-high purity (UHP) N_2. Under this condition, the pyrolysis reactions are extremely complex. In a conventional flow reactor, the dominant reactions are scission of β-bonds, while in microautoclave reactors, this reaction is suppressed and secondary reactions are favored. For jet fuels and related model compounds, generally, three groups of compounds are formed in the quenched tubing bomb reactors. They are: (i) low molecular weight gaseous hydrocarbons with the carbon chain length varying from C_1 to C_4, (ii) liquid products of a wide range of molecular weight, and (iii) carbonaceous solid products. As a result of thermal treatment, the reactions proceed to a thermodynamically stable state. If the treatment is severe, a three-phase thermodynamic equilibrium among gaseous, liquid and solid products can be reached. This appears to be the reason for the changes of the color of the liquid products from white to light yellow to brown to dark brown to light brown. The change of color the from dark brown to light brown after long reaction times seems to be an indication of the achievement of equilibrium state.

2. Substrate Disappearance and Solid Product Formation

Figures 1 and 2 show the rate of disappearance of model compounds and the yield of solid products formed, respectively. Over a time period from 15 min. to 8 h, n-butylbenzene is quickly converted and t-butylbenzene is the most stable isomer, as shown in Figure 1. As the substrate compounds disappear, carbonaceous solids have been observed to form in the reactors. It can be seen from Figure 2 that each compound has a different induction period for the formation of solid products. The induction period reflects the ability of the compound to resist the formation of carbonaceous solid products. The order for the induction time of the four compounds is: n-<sec-<iso-<tert-butylbenzene. The order is the same as that of the rate of their disappearance. The amount of the solids formed increases with the reaction time for sec-, iso- and t-butylbenzene. This behavior is similar to that of jet fuels, which also exhibit a monotonic increase in the amount of solid products (8). Surprisingly, although solid products are quickly formed in the pyrolysis of n-butylbenzene after a short induction period, the amounts leveled off to an asymptotic value at around 5 h. As a result, the least amounts of solids is formed from the reaction of n-butylbenzene after 8 h at 450°C. The unique behavior of n-butylbenzene will be discussed in the following sections.

3. Major Substrate Consumption Pathways

Major substrate consumption pathways are studied in this paper by pyrolyzing the model compounds at very short residence times where little or no solid products are formed, and examining the compositions of the initial gaseous and liquid products.

(1) n-Butylbenzene (n-BB)

The pyrolysis of n-BB for 15 min. at 450°C indicates that ethane is present in the gas phase as a major product and toluene and styrene are major species present in liquid products. These results suggest that the major pathway of consumption n-BB is by breaking C_α-C_β bonds in the side chain (6).

(2) t-Butylbenzene (t-BB)

Although the initiation of t-BB is similar to that of n-BB (C_α-C_β bond cleavage), its initiation process is significantly retarded as shown in Figure 1. This can be explained by the following two reasons. Firstly, the C_α-C_β dissociation energy for t-BB is 73.7±1.5 kcal/mol, which is higher than that for n-BB, 70.0±1 kcal/mol (9). Secondly, the H-abstraction reaction by $C_6H_5C(CH_3)_2$ radicals formed by the homolysis of t-BB is expected to be much slower simply because of the relatively high stability of $C_6H_5C(CH_3)_2$ radicals and the poor stability of $C_6H_5C(CH_3)_2CH_2$ radicals produced. As a result, the

pyrolysis of t-BB is mainly carried out by isomerization reaction to form i-BB and s-BB (6).

(3) s-Butylbenzene (s-BB)

The composition of gaseous products for the reaction of s-BB are shown in Table 1. The major gaseous products after the initial period are methane, ethane and ethylene. As the reaction time increases, the concentration of ethylene decreases. Major liquid products identified include ethylbenzene (0.72 wt%), styrene (0.11 wt%), α-methylstyrene (0.10 wt%), trans-β-methylstyrene (0.70 wt%) and α-ethylstyrene (0.16 wt%). According to these results, removing a CH_3 radical from s-BB appears to be a dominant initiation process:

$$C_6H_5CH(CH_3)CH_2CH_3 \longrightarrow C_6H_5\dot{C}HCH_2CH_3 + CH_3\bullet$$

The presence of C_2 species in relatively high concentration in the gas phase indicates that removing a CH_3CH_2 radical also exists as another initiation process:

$$C_6H_5CH(CH_3)CH_2CH_3 \longrightarrow C_6H_5\dot{C}HCH_3 + C_2H_5\bullet$$

(4) i-Butylbenzene (i-BB)

The composition of gaseous products for i-BB is also shown in Table 1. Methane and propylene are two major gaseous products. Toluene (1.47 wt%) and trans-β-methylstyrene (2.80 wt%) are the major liquid products in the initial period. These data suggest that the following initiation reaction exists in the pyrolysis of i-BB.

$$C_6H_5CH_2CH(CH_3)CH_3 \longrightarrow C_6H_5CH_2\bullet + CH_3\dot{C}CH_3$$

4. Major Liquid Product Selectivities

Liquid products consist mostly of cracking products (4), the molecular weights of which are less than the substrate compounds. Cracking products include mainly benzene, toluene, ethylbenzene, i-propylbenzene and n-propylbenzene. Figures 3, 4 and 5 show the plot of selectivities of benzene, toluene and ethylbenzene from the pyrolysis of butylbenzenes. t-BB has the highest selectivity for benzene as shown in Figure 3. This appears to suggest that the aryl-alkyl bonds in t-BB are weakened by the presence of bulky t-butyl groups. The formation of benzene may also due to the attack of H to the ipso position of t-BB. In Figure 4, the concentration of toluene increases almost linearly with the increase of conversion except that the slope is lower for s-BB. Since β-bond scission to form benzyl radicals is the only initiation process in n-BB and it is easy for the benzyl radicals to abstract H from other species in the reaction system, n-BB has the highest selectivity to form toluene. In contrast, i-BB has two initiation pathways, only one of which forms benzyl radicals that lead to the formation of toluene. This lowers its toluene production. t-BB has been known to pyrolyze mainly by isomerization reactions to form i-BB (and s-BB to a lesser extent). The formation of toluene from t-BB might be attributed to the further dissociation of i-BB. It is obvious that direct decomposition of s-BB does not form toluene. Figure 5 shows the ethylbenzene selectivities. Similar behavior is observed in n-BB, s-BB and i-BB, t-BB. This could be understood from the discussion in the last section. It is possible that ethylbenzene can be formed as an initial reaction product for n-BB and s-BB, while i-BB and t-BB can only be formed between secondary reaction products.

5. Comparison of Solid Formation Tendencies

Compositions of liquid products seem to demonstrate that the reactivity of a model compound is governed by the initial reaction products. Generally there are two competing sets of reactions in the pyrolysis of all four model compounds at the initial stage, i.e.,

isomerizations and the characteristic breakdown for each specific compounds as shown below.

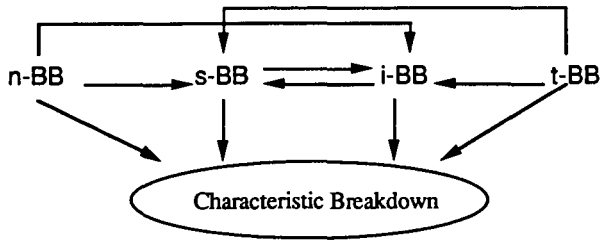

It is obvious from the previous discussion that for the pyrolysis of t-BB, the isomerization reaction to i-BB is more important than its characteristic breakdown. Therefore, the induction time for the solid formation from t-BB mainly depends on the isomerization reaction and the induction period of i-BB. This might account for its low reactivity and long induction period for solid formation (Figures 1 and 2). n-BB is the one that is most easily converted, but not the one that forms the highest amounts of solids. One reason for this is that it appears to be easy for n-BB to form cracking products such as toluene and ethylbenzene as shown in Figures 4 and 5, and stable high molecular weight compounds such as naphthalene as shown in Figure 6. The other reason is that fewer compounds of styrene-series were found in the liquid products of n-BB. In fact, only styrene is identified, and its concentration decreases rapidly as the reactions proceed. In the case of s-BB and i-BB, large amounts of compounds such as styrene, allylbenzene, α-methylstyrene, β-methylstyrene,and ethylstyrenes were present after the initial reaction period. This may constitute the reason for the formation of large amounts of solid products from the pyrolysis of s-BB and i-BB.

CONCLUSIONS

There is a significant effect of the structure of the side chains on the pyrolysis of alkylbenzenes. The rate of the disappearance or reactivity of an alkylbenzene depends on the ease of the dissociation energy of its initiation reactions. The order of reactivity or conversion of substrate was found to be n->sec->iso->tert-butylbenzenes. This indicates that, in general, branching seems to decrease the thermal reactivity of the alkybenzenes. The amount of solids produced is related to the stability of the intermediate products especially at the initial stage. It seems that styrene-series compounds formed at the early stage are responsible for the formation of large amounts of solid products during the pyrolysis of sec- and iso-butylbenzenes.

ACKNOWLEDGEMENTS

This project was jointly supported by the U. S. Department of Energy, Pittsburgh Energy Technology Center and Air Force WRDC/Aero Propulsion Laboratory, Wright-Patterson AFB. Funding was provided by the U. S. DOE at Sandia National Laboratories under contract DE-AC04-76DP00789. We wish to thank Mr. W.E. Harrison III of WRDC, Drs. E. Klavetter of SNL, and S. Lee, M. Baird and S. Rogers of PETC for their support and helpful discussions.

REFERENCES

(1). Frenkenfeld, J.W. and Taylor, W.F., Ind. Eng. Chem. Prod. Res. Dev., 19, 65, 1980

(2). Song, C. and Hatcher, P.G., Preprints, Div. Pet. Chem., ACS, 37(2), 529, 1992

(3). Nohara, D. and Sakai, T., Ind. Eng. Chem. Res., 31, 14, 1992
(4). Song, C., Eser, S., Schobert, H.H. and Hatcher, P.G. et. al., Advanced Thermally Stable Jet Fuels Development Program Annual Report, Volume II, Interim Report for Period July 1990 to July 1991
(5). Leigh, C. H. and Szwarc, M., J. Phys. Chem., 1952, 20, 844
(6). Peng, Y, Schobert. H.H, Song, C. and Hatcher, P.G., Preprints, Div. Pet. Chem., ACS, 37(2), 505, 1992
(7). Savage, P. E. and Korotney, D. J., Ind. Eng. Chem. Res., 1990, 29, 499
(8). Song, C., Peng, Y., Jiang, H. and Schobert, H.H., Preprints, Div. Pet. Chem., ACS, 37(2), 484, 1992
(9). Lide, D.R., CRC Handbook of Chemistry and Physics, CRC Press, 1990-1991

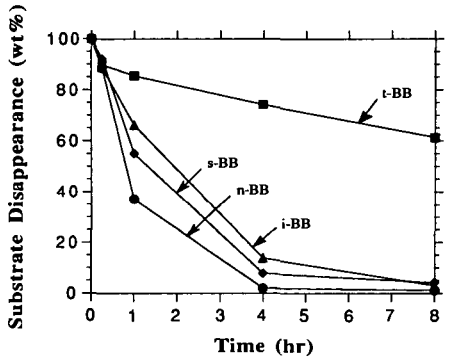

Figure 1. The disappearance of the substrate compounds at 450°C

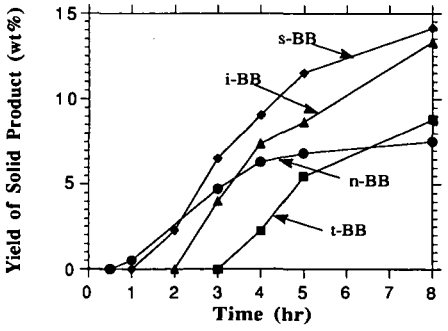

Figure 2. The formation of solid products at 450°C from the pyrolysis of butylbenzenes

Table 1. Composition of Gaseous Products from the Pyrolysis of sec- and iso-Butylbenzenes at 450°C

Time (hr)	CH_4 (mol%)		C_2H_4 (mol%)		C_2H_6 (mol%)		C_3H_8 (mol%)		C_3H_6 (mol%)		Volume (ml)	
	s-BB	i-BB	s-BB	i-BB	s-BB	i-BB	s-BB	i-BB	s-BB	i-BB	s-BB	i-BB
0.25	83.49	71.84	9.52	0.34	6.04	0.87	0.75	3.02	0.08	21.17	44	42
1.00	86.59	62.85	3.13	0.54	8.07	4.11	1.29	7.18	0.80	19.28	293	203
2.00	84.25	68.25	1.50	0.57	10.79	6.35	1.91	9.61	0.59	10.43	497	355
4.00	83.99	63.39	1.08	0.89	12.16	9.58	2.26	14.60	0.32	4.08	687	601
8.00	82.15	62.67	0.54	0.26	13.36	12.16	3.11	15.32	0.23	4.55	727	733

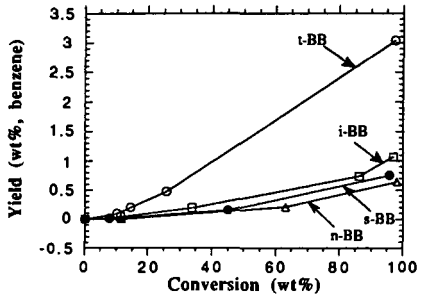

Figure 3. Selectivities of benzene in the pyrolysis of butylbenzenes

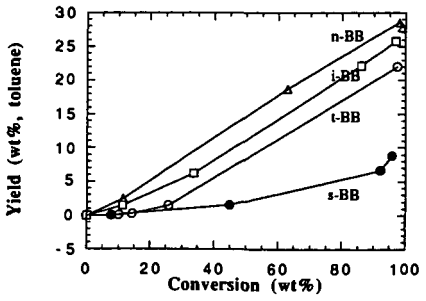

Figure 4. Selectivities of toluene in the pyrolysis of butylbenzenes

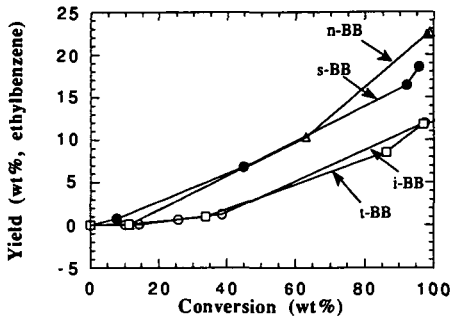

Figure 5. Selectivities of ethylbenzene in the pyrolysis of butylbenzenes

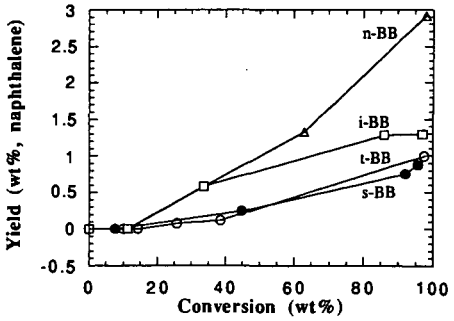

Figure 6. Selectivities of naphthalene in the pyrolysis of butylbenzenes

FORMATION OF POLYCYCLIC AROMATIC HYDROCARBONS AND ELIMINATION OF ALIPHATIC SUBSTITUENTS IN SECONDARY REACTION OF FLASH PYROLYSIS TAR

Jun-ichiro Hayashi, Tsutomu Kawakami, Tomohiro Taniguchi,
Katsuki Kusakabe and Shigeharu Morooka
Department of Chemical Science and Technology,
Kyushu University, Fukuoka 812, Japan

INTRODUCTION

Polycyclic aromatic hydrocarbons (PAHs) derived from coal tar and pitch are very useful for starting materials of various specialty chemicals. To produce PAHs, flash pyrolysis of coal is attractive because its tar yield is much higher than that of other carbonization processes with slow heating rates.[1] However, the quality of flash pyrolysis tar is rather inferior to that of slow pyrolysis tar.[2]

Coal pyrolysis consists of two reactions in series: the primary reaction of the macromolecular network of coal to tar; and the secondary reaction of tar in the gas phase.[3]

Division of reaction zones is indispensable for the quantitative examination of time- and temperature-dependent changes in molecular composition of tar, as indicated by Xu et al.[4] and Serio et al.[5] who separated these reaction zones by using the two-stage reactors comprising of a fixed bed of coal and a tubular reactor connected downstream.

In the present study, the two-stage concept is applied to the flash pyrolysis of a subbituminous coal with a fluidized-bed reactor divided into two zones: a dense bed for the primary reaction and a freeboard above the dense bed for the secondary reaction. Tar is processed in the freeboard at a temperature different from that in the dense bed. PAHs in the tar is characterized by FIMS and ^{1}H-NMR after the separation based on ring structure of molecule. The temperature dependence of the following features are determined: molar yield of homologues having the same ring structure; and number-based distribution of aliphatic carbons per molecule for each homologue.

EXPERIMENTAL

Flash pyrolysis

Wandoan subbituminous coal (C:76.2, H:5.77, N:1.03 in wt.%, daf) was employed for the experiment. The coal sample was pulverized, sized to 0.37-0.74 mm and dried in vacuo at 100°C. The fluidized-bed reactor was divided into dense and freeboard zones, and they were heated separately with external furnaces whose temperatures were independently controlled. The temperature was set in the range of 600-900°C for the freeboard and fixed at 600°C for the dense bed. Coal particles were introduced into the dense bed at a constant rate of 4.2 mg/s. The total gas flow rate was 33.3 ml/s at 20°C. The total residence time of tar vapor was 4.0-4.5 s.

Separation and characterization of tar samples

The tar was separated into benzene-soluble (asphaltene) and insoluble (preasphaltene) portions. The asphaltene was further fractionated into saturates, aromatic hydrocarbons, nitrogen-containing compounds, hydroxylic compounds and the uneluted components by the elution chromatography with neutral alumina.[6] The yield of the uneluted component was added to that of the preasphaltene.

The aromatic hydrocarbons was further separated by HPLC on the basis of ring structure with a semipreparative NH_2 column (Hiber Column, Merck) with n-heptane as the mobile phase.[7] By this method, aromatics were classified by number of double bonds per molecule (d.b.) into 3 (monocyclic), 5 (dicyclic), 6 (dicyclic), 7 (tri-cyclic), 8 (tetracyclic), 9 (tetracyclic), 10 (pentacyclic), 11 and 12 (pentacyclic and greater PAHs). Each double-bond fractions were analyzed by ^{1}H-NMR and FIMS.

RESULTS AND DISCUSSION

Temperature dependence of yield and chemical composition of tar

Figure 1(a) shows the effect of freeboard temperature on the tar yield. When fine coal particles were fed into the dense bed, most particles were entrained by the gas flow. When coal particles were in the size range of 0.21-0.42 mm, however, entrainment hardly occurred. The tar yield by the pyrolysis of the 0.21-0.42 mm particles was virtually identical to that shown in Figure 1. Thus the tar evolution was completed in a short period compared with the residence time of gas in the freeboard.

Figure 1(b) shows yields of components normalized by total tar yield as a function of freeboard temperature. There are three patterns of temperature dependence. The yield of PAHs and nitrogen-containing compounds increases with increasing temperature and then attains ca. 80 wt.% of the total tar yield at 900°C, while that of saturates and preasphaltene decreases monotonously above 600°C. Ethers and hydroxylic compounds show their maximum yield at 700°C. It is clear that the increase in yield of PAHs is compensated by the decrease of the other components, and their roles as precursors of PAHs vary by component.

Yield and structural distribution of PAH component

The FIMS analysis reveals that a PAH molecule has 5 to 12 double bonds. Figure 2 shows the FIMS spectra of the 6, 7 and 8 d.b. fractions separated from tar at 800°C. The spectra shown in Figure 2(a) consist of two series of signals appearing at the mass number 152+14n and 154+14n (n = integer). The former is attributed to the homologue of acenaphthylene (MW = 152) and fluorene (MW = 166), and the latter to that of biphenyl (MW = 154). These homologues have the same double-bond number of 6. Figure 2(b) and (c) show that the 7 and 8 d.b. fractions are composed of the homologues of phenanthrene (or anthracene) and pyrene (or fluoranthene) respectively. Each fraction is a mixture of compounds having the same number of aromatic rings and a different number of methylene units. Peaks with the smallest mass in the FIMS spectrum of each homologue are assigned to the PAHs listed in Table 1.

All the PAH homologues are composed of an unsubstituted PAH and its alkyl-derivatives. Since alkyl substituents are sensitive to the reaction temperature, the total mass of compounds is not a reliable indicator of the yield of homologue. Therefore, the mass of a substituted PAH having aliphatic carbons is converted to that of an

unsubstituted PAH. Figure 3 shows the yield of the 6-12 d.b. homologues. All of them monotonously increase with increasing temperature. This suggests that the formation of PAHs below 900°C is predominant over the soot formation that causes a decrease in the PAH yield. The homologues of 6, 7 and 8 d.b. are most abundant. Each of them comprises more than 1.0 wt% of coal on daf basis at 900°C. The temperature profile of PAH yield varies by homologue. The larger the d.b. number, the higher the temperature at which the slope changes steeply. The yields of the 11 and 12 d.b. homologues increase remarkably above 700°C in accord with the evo-lution of hydrogen gas. In this temperature range, a part of the 11 and 12 d.b. homologues is formed via condensation of smaller aromatic rings, and hydrogen gas is produced as a result.

Aliphatic carbons attached to aromatic ring

The number-based distribution of aliphatic carbons (methylene units) per molecule is shown in Figure 4 for the 8 and 9 d.b. homologues. The FIMS analysis combined with the HPLC separation allows the determination of the yield of molecules composed of a specific aromatic ring and a specific number of aliphatic carbons. The number of aliphatic carbons per molecule is distributed over the range of 0 to 9 at 600°C, where aliphatic carbons are most abundant. Teo and Watkinson[8] pyrolyzed coals in a spouted bed and characterized the molecular composition of tar by HPLC and GC-MS. They found that the number of aliphatic carbons was less than four for aromatic homologues with 1 to 4 rings. Our results, on the other hand, reveal that PAHs bearing more than four or five aliphatic carbons are abundant, particularly in low-temperature tars.

The distribution shown in Figure 4 moves toward the small-number side with increasing secondary reaction temperature. The mole fraction of unsubstituted PAHs is only ca. 5% in the homologues obtained at 600°C, but is ca. 50% at 900°C. The temperature dependence of the yield of substituted molecules varies with the number of aliphatic carbons. In the case of the 7 d.b. homologue, the yield of C_1 and C_2 derivatives shows a maximum at 800°C, while that of C_3 and C_4 derivatives at 700°C. The yield of molecules having more than five aliphatic carbons decreases monotonously over the temperature range tested.

Classification of aliphatic carbons

The NMR data of each d.b. fraction are analyzed by assuming the existence of only methyl-, ethyl- and propyl-chains. This is reasonable because the b-hydrogen content is at most half that of α-hydrogen even at 600°C, where the ratio of β- to α-hydrogen is the highest for all the fractions. The number of chains is given by the following equations.

$$N(\text{propyl}) = N(H_\gamma)/3 \quad (1)$$

$$N(\text{ethyl}) = [\, N(H_\beta) - 2N(\text{propyl}) \,]/3 \quad (2)$$

$$N(\text{methyl}) = [\, N(H_\alpha) - 2N(\text{ethyl}) - 2N(\text{propyl}) \,]/3 \quad (3)$$

$$N(\alpha,\alpha\text{-methylene}) = N(H\alpha,\alpha)/2 \quad (4)$$

where $N(H_\alpha)$, $N(H_\beta)$ and $N(H_\gamma)$ are respectively the number-based content of α-, β- and γ-hydrogen normalized by the total hydrogen content. The total number of aliphatic carbons is

$$C_{al} = N(\text{methyl}) + 2N(\text{ethyl}) + 3N(\text{propyl}) + N(\alpha,\alpha\text{-methylene}) \quad (5)$$

The sum of the number of protonated and alkylated aromatic carbons is

$$C_{pa} = N(\text{methyl}) + N(\text{ethyl}) + N(\text{propyl}) + N(H_{ar}) + 2N(\alpha,\alpha\text{-methylene}) \quad (6)$$

where $N(H_{ar})$ is the number-based content of aromatic hydrogens. The total number of aromatic carbons is given as

$$C_{ar} = C_{pa} + C_b \quad (7)$$

where C_b is the number of bridgehead carbons. The ratio of Cpa to Cb is determined from the ring structure. The value of C_{pa}/C_{ar} is calculated from the composition of PAHs by the FIMS analysis in all the fractions of different d.b., and is for instance 10/14 for the 7 d.b. homologue. The averaged number of aliphatic carbons per molecule is

$$N(CH_2) = C_{al}/(C_{ar}/ARC) \quad (8)$$

where ARC is the averaged number of aromatic carbons per molecule. The value of N(CH2) can also be determined by the FIMS data as shown in Figure 4. The values of $N(CH_2)$ calculated from Equation (8) are in agreement with those by the FIMS analysis within an error of 10%.

Figure 5 exhibits the composition of aliphatic carbons in the fractions of 8 and 9 d.b. The number of α-, β- and γ-carbons decreases with increasing temperature. The number of α,α-carbons is independent of temperature in the range of 600-800°C, while it decreases above 800°C.

Figure 6 shows the number of methyl and ethyl chains per molecule for the 8 and 9 d.b. fractions. The number of ethyl chains decreases by 65-85% in the range of 600-700°C, while that of methyl chains hardly changes. This result suggests that the decrease in the number of a-carbons at 600-700°C is due to detachment of ethyl and propyl chains by the selective bond cleavage at aryl-α positions.

REFERENCES

1. Peters, W.; Bertling, H. *Fuel* 1965, **44**, 317.
2. Khan, M.R. *Fuel* 1989, **68**, 1522.
3. Serio, M.A.; Hamblen, D.G.; Markham, J.R.; Solomon, P.R. *Energy and Fuels* 1987, **1**, 138.
4. Xu, W.-C.; Tomita, A. *Fuel Process. Tech.* 1989, **21**, 25.
5. Serio, M.A.; Peters, W.A.; Howard, J.B. *Ind. Eng. Chem. Res.* 1987, **26**, 1831.
6. Schiller, J.E.; Mathiason, D.R. *Anal. Chem.* 1977, **49**, 1225.
7. Boduszynski, M.M.; Hurtubise, R.J.; Allen, T.W.; Silver, H.F. *Anal. Chem.* 1983, **55**, 225.
8. Teo, K.C.; Watkinson, A.P. *Fuel* 1986, **65**, 949.

Table 1. Molecular mass of initial peaks in FIMS spectra of each d.b. homologue.

d.b.	Molecular mass
5	128 (naphthalene)
6	152 (acenaphthylene), 154 (biphenyl)
7	178 (anthracene, phenanthrene)
8	202 (pyrene and fluorenthene)
9	226, 228 (chrysene)
10	252 (benzo(a)pyrene, perylene), 254 (phenylphenenthrene)
11	276, 278 (picene, dibenzanthracene)
12	300 (coronene), 302 (dibenzpyrene), 304 (phenanthrenoanthracene)

[a] Compounds indicated in parenthesis are PAHs to which the peaks are assigned.

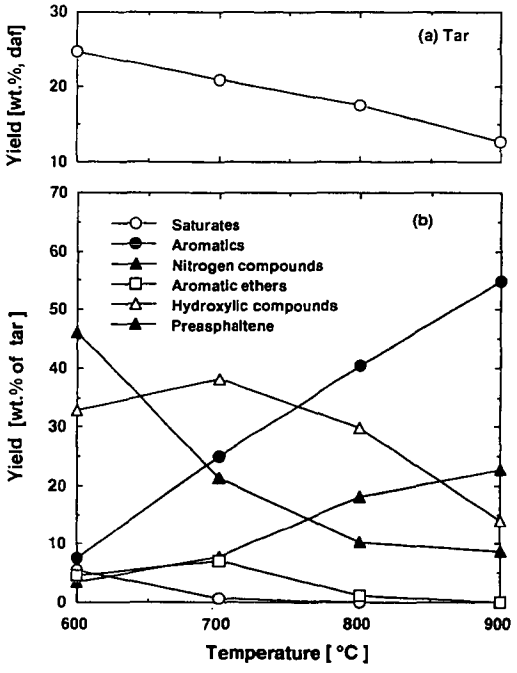

Figure 1. Temperature dependence of yield and composition of tar.

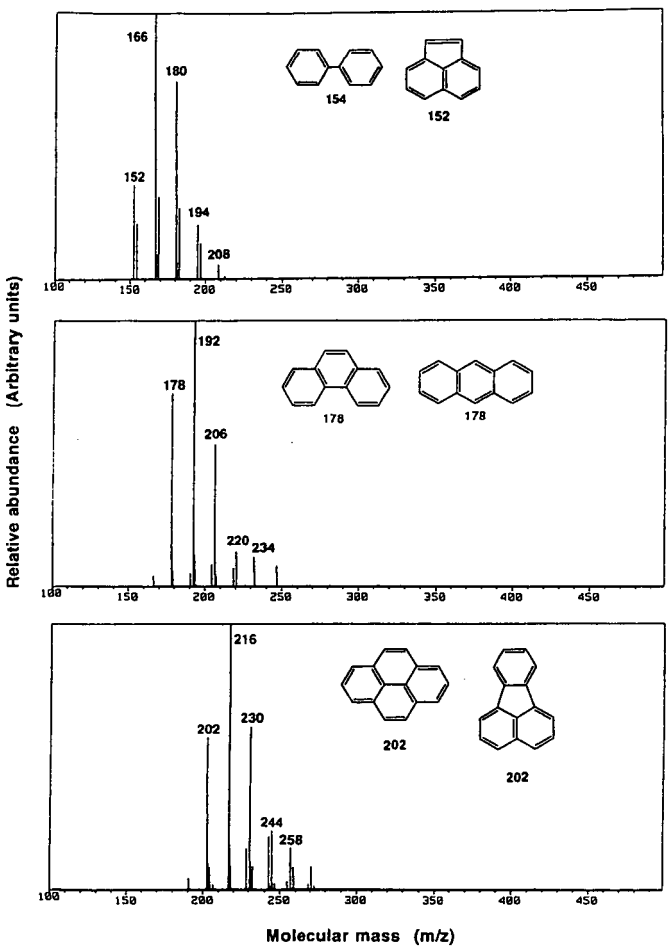

Figure 2. FIMS spectra of 6, 7 and 8 d.b. fractions at 800°C.

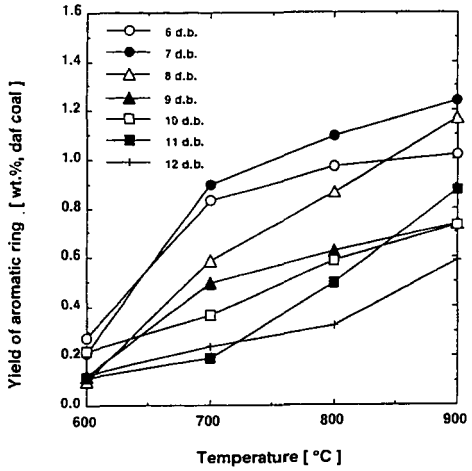

Figure 3. Yield of individual double-bond homologues converted into that of unsubstituted PAH.

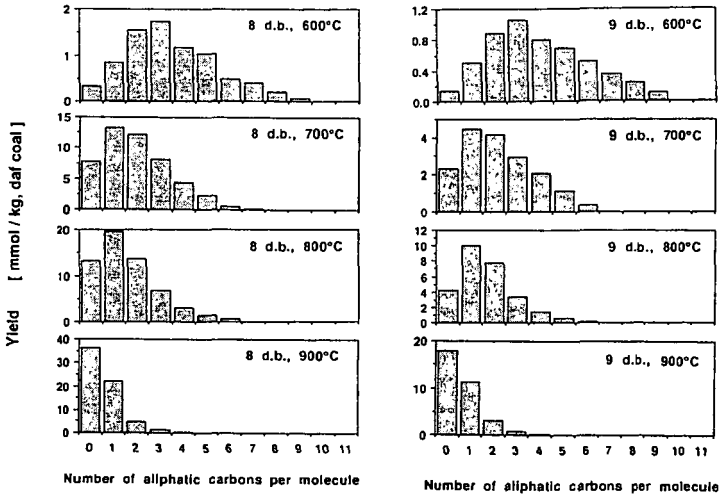

Figure 4. Distribution in number of aliphatic carbons per molecule for 8 and 9 d.b. homologues.

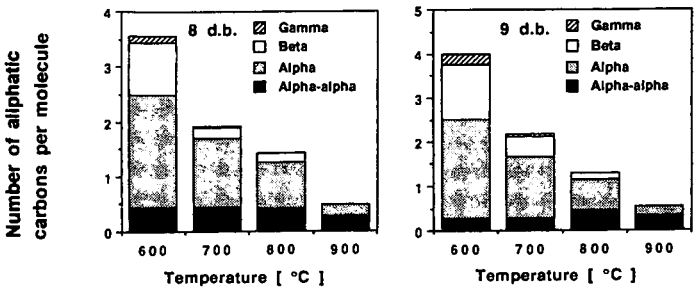

Figure 5. Composition of aliphatic carbons in 8 and 9 d.b. fractions.

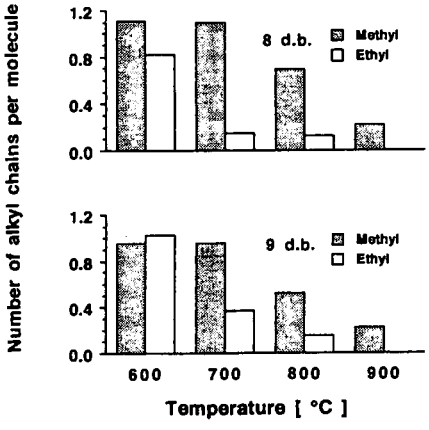

Figure 6. Number of methyl and ethyl chains per molecule for 8 and 9 d.b.fractions.

HYDROUS PYROLYSIS OF n-$C_{32}H_{66}$ IN THE PRESENCE AND ABSENCE OF INORGANIC COMPONENTS

Roald N. Leif[1], Bernd R. T. Simoneit[1] and Keith A. Kvenvolden[2]

[1] Petroleum Research Group, College of Oceanography, Oregon State University, Corvallis, OR 97331

[2] U. S. Geological Survey, 345 Middlefield Road, Menlo Park, CA 94025

Keywords : hydrocarbon cracking, n-alkanes, n-alkenes, n-alkanones

Introduction

There has been much research on catagenetic processes by laboratory simulations. These experiments are performed over short durations but at elevated temperatures to compensate for the lower temperature organic reactions which occur over geologic timescales. Experimental designs for achieving these reactions have been quite diverse. In addition to varying time and temperature, many different combinations of experimental parameters have been used including: vacuum or controlled atmosphere conditions, open or closed systems, different reaction vessel materials, aqueous or anhydrous conditions, varied mineral assemblages, and a wide range of organic source materials (e.g., 1-7). Hydrous pyrolysis is a closed system procedure of heating a sample which is submerged in water and not in contact with water vapor or supercritical water (8). It appears to be the most promising system since it most closely mimics the conditions found in nature, especially those found in hydrothermal systems (9). In this paper, the study of the aqueous high temperature organic chemistry of n-$C_{32}H_{66}$ in the presence or absence of several selected inorganic components is presented. The experiments were performed under nitrogen in a stainless steel reaction vessel, the only variable being the addition of inorganic species. The results of these experiments are relevant for hydrous pyrolysis studies of sedimentary source materials where large amounts of inorganic salts and minerals are present.

Experimental

A 250 mL stainless steel vessel (Parr Instrument T316SS) used for the reactions was equipped with a thermocouple for temperature control (± 2°C) and a gage block assembly for recovery of volatiles. Conditioning of the vessel prior to each experiment was done by heating it with 63.5 mL water at 350°C for 24 h. No effort was made to remove air from the system during the conditioning process. The experiments are summarized in Table 1. For each experiment 0.050 g of n-$C_{32}H_{66}$ and 63.5 mL of deoxygenated water alone or water and an equimolar amount of inorganic species were combined in the reaction vessel. The deoxygenated water was prepared by bubbling N_2 gas into distilled water for twenty minutes before each experiment. Assembly of the reaction vessel was done in a glove bag under a nitrogen atmosphere. The vessel was then placed in a heater and temperature maintained at 350°C for 72 h. In the case of the H_2O - n-$C_{32}H_{66}$ - sulfide system, the interior of the vessel was coated with a sulfide formed by heating the vessel with 0.5 g elemental sulfur and 63.5 mL water for 24 h. After cooling to room temperature, the excess sulfur was rinsed from the vessel leaving a uniform sulfide coating. Then under a N_2 atmosphere, 0.050 g of n-$C_{32}H_{66}$ and 63.5 mL of deoxygenated water were combined and allowed to react.

The vessel was cooled to room temperature before opening and contents transferred to a separatory funnel. The interior of the vessel was rinsed with methanol and methylene chloride, which were added to the separatory funnel, and the organic fraction was separated. The water was extracted with two additional 20 mL portions of methylene chloride. The organic fractions were combined and concentrated.

The products were fractionated by thin layer chromatography (20 x 20 cm, 250 microns Silica Gel G) into four fractions using heptane as developer. Hydrogenation of selected

samples was done by bubbling H_2 gas into the sample for 30 minutes in the presence of platinum (IV) oxide (Adams' catalyst).

Gas chromatography (GC) was performed using a Hewlett-Packard 5890 gas chromatograph equipped with a DB-5 open tubular column (30 m x 0.25 mm ID, 0.25 μm film) programmed from 65° (isothermal 2 min.) to 310°C at 4°C / min. (isothermal 30 min.). Compound identification was aided by comparison with authentic standards.

Results

Although a large amount of cracking occurred, there was no gas pressure in any of the heating experiments. Most of the unreacted starting material along with the cracking products was in the form of a wax disk floating on the water. The walls of the vessel were also coated with the wax which made it difficult to ensure that all of the organic material was completely transferred from the vessel for analysis.

The GC traces of the total extracts are shown in Fig. 1. They are characterized by a broad distribution of cracking products with a large amount of unreacted starting material. The cracking products range in carbon number from C_9 to C_{31}. The cracking products in all experiments maximized at C_{16}, half the carbon number of the starting material. The total extracts consisted primarily of a nonpolar fraction of n-alkanes and n-alkenes and a polar fraction made up of oxygenated compounds. A low amount of branched and aromatic compounds were formed under these conditions.

H_2O - n-$C_{32}H_{66}$. Chromatograms of the nonpolar fraction before and after catalytic hydrogenation confirms the presence of the n-alkene isomers (Fig. 2a and 2b). The n-alkanes were the major products of hydrocarbons with 16 or more carbon atoms. No particular series dominated in hydrocarbons less than C_{16}. The polar fraction consisted of homologous n-alkanal and n-alkan-2-one series in addition to other oxygenated species (Fig. 2c).

H_2O - n-$C_{32}H_{66}$ - NaCl. The nonpolar and polar fractions were similar to the H_2O - n-$C_{32}H_{66}$ system but the n-alkane predominance of the heavier hydrocarbons was not observed.

H_2O - n-$C_{32}H_{66}$ - HCl. The acidic conditions favored the formation of n-alkanes over n-alkenes. No significant differences in the polar fraction was observed.

H_2O - n-$C_{32}H_{66}$ - NaOH. A simple product distribution was generated which was composed primarily of terminal n-alkenes with a minor amount of n-alkanes. A similar distribution of polar compounds was generated in this experiment.

H_2O - n-$C_{32}H_{66}$ - NH_4Cl. The formation of n-alkanes over n-alkenes was slightly favored in this system when compared to the H_2O - n-$C_{32}H_{66}$ system but a similar distribution of polar compounds were formed.

H_2O - n-$C_{32}H_{66}$ - Na_2SO_4. Cracking products below C_{14} were low in this experiment. The nonpolar fraction consisted mainly of n-alkanes and terminal n-alkenes in approximately equal amounts for each carbon number.

H_2O - n-$C_{32}H_{66}$ - Elemental Sulfur. The formation of n-alkanes was favored by the addition of elemental sulfur. The n-alkan-2-ones were present but formed in lower amounts.

H_2O - n-$C_{32}H_{66}$ - Sulfide. This system greatly favored the formation of n-alkanes over any other products, and n-alkan-2-ones were the major series in the polar fraction (Fig. 3).

Discussion

These preliminary experiments were designed to study the effects that some selected inorganic components have on the aqueous pyrolysis of a representative n-alkane. The choice of systems was not comprehensive but does include some major components likely to be found when experimenting with sediments and whole rocks.

Hydrous pyrolysis of n-$C_{32}H_{66}$ results in the formation of alkanes, alkenes, and to a lesser extent oxygenated species. Relative amounts of the products were affected by the inorganic species present in the system. The formation of n-alkene isomers by these pyrolysis experiments confirms the results previously described where terminal n-alkenes and a range of internal n-alkenes, formed by double bond migration, were produced during aqueous pyrolysis of n-hexadecane at 317°C (10). Acid-catalyzed double bond migration was also observed in

the aqueous pyrolysis of 1-decene to form 2-, 3-, 4- and 5-decene (11). The low hydrogen ion concentration under alkaline conditions (H_2O - n-$C_{32}H_{66}$ - NaOH) did not permit much double bond migration. This lack of secondary double bond migration resulted in terminal n-alkenes as the major products, preserving the original cracking products formed by the homolytic bond cleavage of n-$C_{32}H_{66}$. The increase in the hydrogen ion concentration in the NH_4Cl and HCl systems favored a higher alkane to alkene ratio relative to the H_2O - n-$C_{32}H_{66}$ system, indicating an enhancement of hydrogenation occurred under acid conditions. This result may be due to the interaction with the stainless steel vessel to alter the hydrogenation capacity of the reaction system. The corrosion of the stainless steel reaction vessel by the following reaction has been proposed to account for a change in pH observed in some experiments (12) :

$$Fe + 2H^+ \longrightarrow Fe^{2+} + H_2$$

The increased hydrogen ion concentration in the acidic systems could drive this reaction to the right, producing a larger amount of hydrogen gas. This could provide the increased hydrogenation capacity necessary to result in the observed increases in the alkane to alkene ratios. The alkaline conditions of the NaOH system resulted in a greatly diminished hydrogenation capacity to produce a low alkane to alkene ratio. The role of the initial oxidation state of the sulfur species can be seen by comparing the sulfate, elemental sulfur and sulfide systems. The distribution of n-alkanes and terminal n-alkenes as primary products of the H_2O - n-$C_{32}H_{66}$ - Na_2SO_4 system suggests that aqueous sulfate consumes hydrogen ions to decrease both the acid-catalyzed double bond isomerization and the hydrogenation capacity of the system, resulting in a nonpolar fraction similar to the alkaline H_2O - n-$C_{32}H_{66}$ - NaOH system. Both elemental sulfur and sulfide generate acidic systems but the lack of n-alkenes indicates a strongly hydrogenating system. The polar fraction of the sulfide system consisted mainly of n-alkan-2-ones. The n-alkan-2-ones are one of several series of polar compounds commonly found in oils collected from interiors of high temperature hydrothermal vents of the Guaymas Basin hydrothermal system (13). The results of these laboratory experiments suggest that these oxygenated compounds may be formed entirely by thermogenic processes.

Conclusions

The products generated by the heating experiments appear to be the result of primary cracking of n-$C_{32}H_{66}$ to form alkenes followed by secondary reactions of these cracking products. The main findings are listed below :

1. Primary cracking of n-$C_{32}H_{66}$ produced a homologous series of terminal n-alkenes.
2. Specific acid-catalyzed double bond isomerization of the terminal alkenes occurred where a sufficient hydrogen ion concentration existed.
3. The extent of alkene hydrogenation was affected by the hydrogen ion concentration, possibly by corrosion of the stainless steel reaction vessel.
4. The initial oxidation state of sulfur had a major effect on controlling the product distribution, with elemental sulfur and sulfide favoring n-alkane generation.

These experiments provide information on how some inorganic species influence the predominant chemical reactions which n-paraffins undergo under high temperature aqueous conditions. These preliminary results suggest that care should be taken when comparing the results from simple aqueous pyrolysis systems to whole rock and whole sediment pyrolyses where the mineral and salt contents are vastly different.

Acknowledgements

We thank the National Science Foundation, Division of Ocean Sciences (Grant OCE-9002366), the Donors of the Petroleum Research Fund administered by the American Chemical Society and the Gilbert Fellowship Program of the U. S. Geological Survey, for support of this research.

Literature Cited

(1) B. Horsfield and A. G. Douglas, *Geochim. Cosmochim. Acta* **44**, 1119 (1980).
(2) K. E. Peters, B. G. Rohrback and I. R. Kaplan, *Am. Assoc. Pet. Geol. Bull.* **65**, 688 (1981).
(3) M. D. Lewan, *Phil. Trans. R. Soc. Lond.* **A315**, 123 (1985).
(4) P. A. Comet, J. McEvoy, W. Giger and A. G. Douglas, *Org. Geochem.* **9**, 171 (1986).
(5) T. I. Eglinton, S. J. Rowland, C. D. Curtis and A. G. Douglas, in *Advances in Organic Geochemistry 1985*, D. Leythaeuser and J. Rullkötter, Eds., *Org. Geochem.* **10**, 1041 (1986).
(6) E. Tannenbaum, B. J. Huizinga and I. R. Kaplan, *Am. Assoc. Pet. Geol. Bull.* **70**, 1156 (1986).
(7) B. J. Huizinga, E. Tannenbaum and I. R. Kaplan, *Org. Geochem.* **11**, 591 (1987).
(8) M. D. Lewan, J. C. Winters and J. H. McDonald, *Science* **203**, 897 (1979).
(9) B. R. T. Simoneit, in *Productivity, Accumulation and Preservation of Organic Matter in Recent and Ancient Sediments*, J. K. Whelan and J. W. Farrington, Eds. (Columbia University Press, New York, 1992), pp. 368-402.
(10) O. Weres, A. S. Newton and L. Tsao, *Org. Geochem.* **12**, 433 (1988).
(11) M. Siskin, G. Brons, A. Katritzky and M. Balasubramanian, *Energy Fuels* **4**, 475 (1990).
(12) Y. K. Kharaka, W. W. Carothers and R. J. Rosenbauer, *Geochim. Cosmochim. Acta* **47**, 397 (1983).
(13) R. N. Leif and B. R. T. Simoneit, unpublished data.

Table 1. Summary of reaction systems performed in 63.5 mL H_2O at 350°C for 72 h.

Figure	System Description	Reactant Amounts
1a	H_2O - n-$C_{32}H_{66}$	0.050 g n-$C_{32}H_{66}$
1b	H_2O - n-$C_{32}H_{66}$ - NaCl	0.050 g n-$C_{32}H_{66}$ 0.111 mmol NaCl
1c	H_2O - n-$C_{32}H_{66}$ - HCl	0.050 g n-$C_{32}H_{66}$ 0.111 mmol HCl
1d	H_2O - n-$C_{32}H_{66}$ - NaOH	0.050 g n-$C_{32}H_{66}$ 0.111 mmol NaOH
1e	H_2O - n-$C_{32}H_{66}$ - NH_4Cl	0.050 g n-$C_{32}H_{66}$ 0.111 mmol NH_4Cl
1f	H_2O - n-$C_{32}H_{66}$ - Na_2SO_4	0.050 g n-$C_{32}H_{66}$ 0.111 mmol Na_2SO_4
1g	H_2O - n-$C_{32}H_{66}$ - Sulfur	0.050 g n-$C_{32}H_{66}$ 0.111 mmol Sulfur
1h	H_2O - n-$C_{32}H_{66}$ - Sulfide	0.050 g n-$C_{32}H_{66}$ Sulfide coated vessel

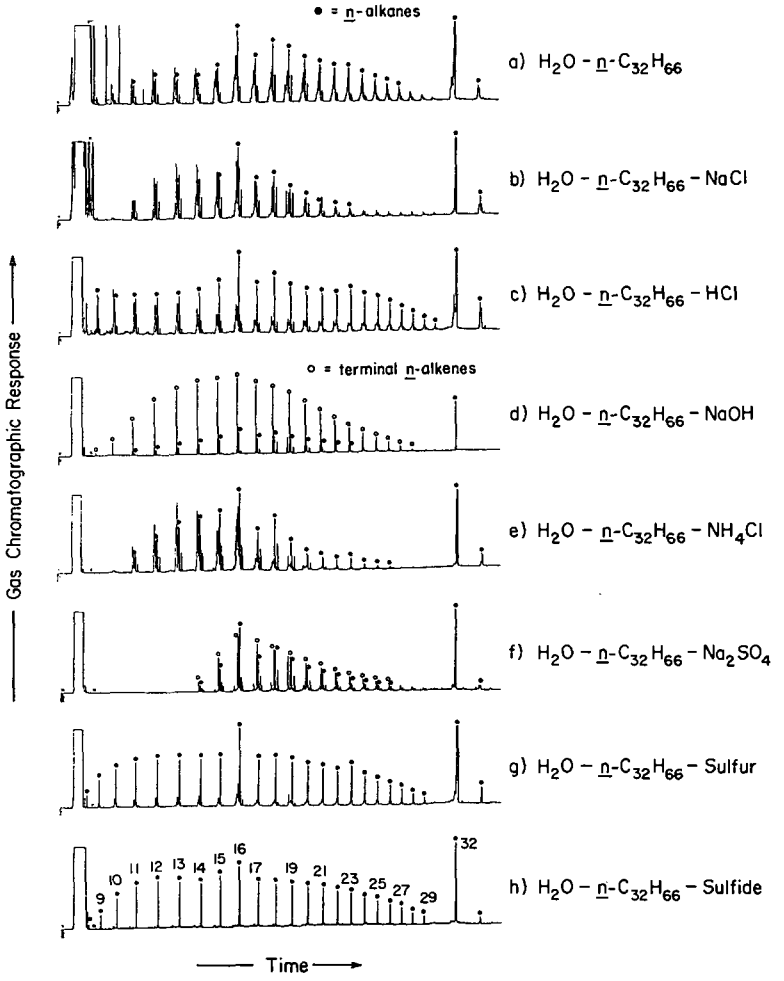

Fig. 1. Gas chromatograms of the total extracts from the hydrous pyrolysis experiments : a) H_2O - n-$C_{32}H_{66}$; b) H_2O - n-$C_{32}H_{66}$ - NaCl; c) H_2O - n-$C_{32}H_{66}$ - HCl; d) H_2O - n-$C_{32}H_{66}$ - NaOH; e) H_2O - n-$C_{32}H_{66}$ - NH_4Cl; f) H_2O - n-$C_{32}H_{66}$ - Na_2SO_4; g) H_2O - n-$C_{32}H_{66}$ - Sulfur; h) H_2O - n-$C_{32}H_{66}$ - Sulfide. [GC conditions : oven was temperature programmed from 65° (isothermal 2 min.) to 310°C at 4°C / min. (isothermal 30 min.)]. Numbers refer to carbon chain lengths of the n-alkanes.

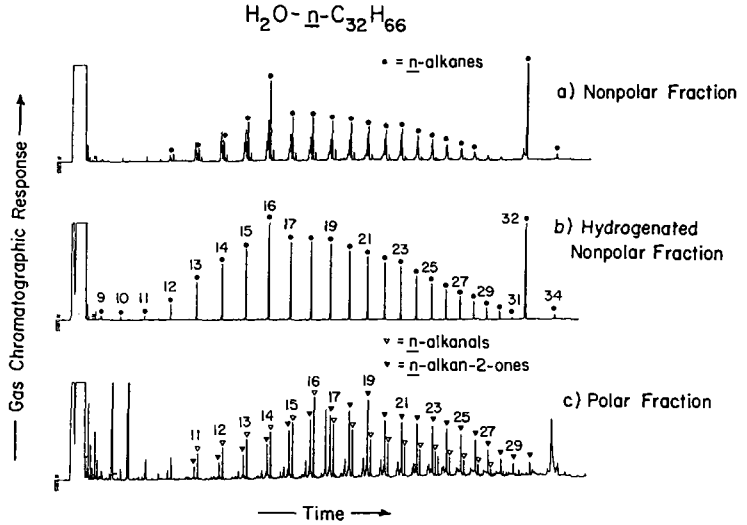

Fig. 2. Gas chromatograms of the H_2O - n-$C_{32}H_{66}$ system : a) nonpolar fraction before catalytic hydrogenation; b) nonpolar fraction after catalytic hydrogenation; c) polar fraction. Numbers refer to carbon chain lengths.

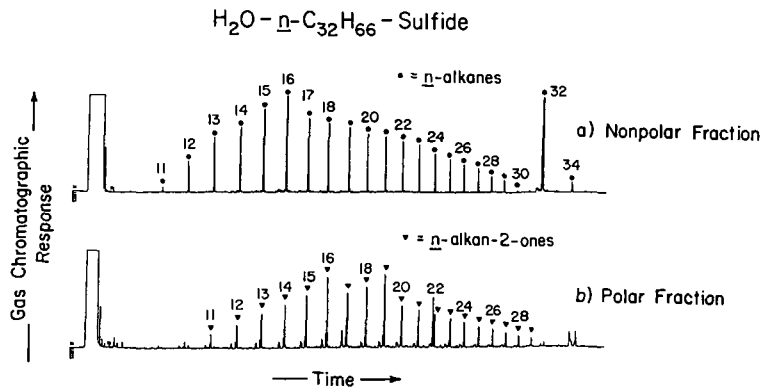

Fig. 3. Gas chromatograms of the H_2O - n-$C_{32}H_{66}$ - Sulfide system : a) nonpolar fraction; b) polar fraction. Numbers refer to carbon chain lengths.

THE EFFECT OF MINERALS ON TRACE ELEMENT DISTRIBUTIONS IN HYDROUS PYROLYSATES OF KEROGENS FROM THE NEW ALBANY SHALE

S. L. Fitzgerald and R. H. Filby
Department of Chemistry
Washington State University
Pullman, WA 99164-4630

Keywords: Minerals, Trace Elements, Pyrolysis

INTRODUCTION

Trace element complexes are present in most crude oils and source rock bitumens (1). Past studies have used trace element distributions in oil-oil (2-10) and to a lesser extent in oil-source rock correlation studies (11,12). Unfortunately, the use of trace element distributions in correlation studies is limited because, other than the nickel and vanadyl porphyrins, very little is known about the nature of these trace element complexes. Even less is known about the parameters controlling their distributions in oils and bitumens (1).

Mineral matter has been shown to play an important role during the catalytic alteration of kerogen to form petroleum (13-18). Kaplan and co-workers (13-15) demonstrated that, during kerogen pyrolysis, the presence of clays decreases the pyrolysate yield due to adsorption of polar constituents and the increase in gaseous products. Work by Rose et. al (19). also showed that while the addition of minerals did not increase the aromatization of the kerogen, they did alter the pyrolysate yields.

Considering the effect that minerals in the source rock have on the hydrocarbon distributions during petroleum formation, it seems reasonable that they also influence the trace element contents in crude oils. In order to study this influence, kerogen from the New Albany shale was subjected to hydrous pyrolysis in the presence and absence of added minerals. A comparison of the trace element abundances in the generated pyrolysates and in the whole shale bitumen indicates the extent to which minerals control the trace element contents in the New Albany bitumen.

EXPERIMENTAL

Kerogens were isolated from the New Albany shale as described previously (20). The bitumen-II was removed from the kerogen by soxhlet extraction (48 hrs.) using chloroform,

the kerogen was then separated into float/sink fractions by suspension in chloroform to remove residual minerals (mostly pyrite). The minerals added in the pyrolysis experiments were calcite, pyrite, Na-montmorillonite, kaolinite, and illite.

In a typical experiment, 30g of kerogen and 30g of mineral were mixed in a Pyrex "sleeve" with 130 mL deionized water. The "sleeve" was then placed in a 1L autoclave. The system was flushed with nitrogen, and heated for 5 hours at 300°C. Temperatures were monitored through a thermo-well placed directly into the sample. For comparative purposes, the bitumen-I extracted shale was pyrolysed under hydrous conditions (150g shale, 200 ml H_2O) for 5 hrs. at 300°C.

The pyrolysates were recovered after each pyrolysis by the same extraction method used to recover the bitumen-II. Pyrolysate yields were determined relative to the amount of kerogen originally pyrolysed and were not corrected for mineral content,mechanical sample loss, or losses due to formation of gaseous products. Trace element concentrations for all samples were determined by instrumental neutron activation analysis (INAA) using the method described previously (21).

RESULTS AND DISCUSSION

Pyrolysate yields. The pyrolysis of kerogen with calcite gave the lowest yield of all the runs (table 1). This is consistent with the observations of Huizinga et. al. (15) who noted (for short heating times) lower pyrolysate yields for kerogens with calcite during both dry (and to a lesser degree) hydrous pyrolysis. They attributed this decrease in yield to inefficient heating due to the large amount of mineral present. It seems more likely that this effect is the result of an interaction between the kerogen and the calcite, however, since similar results were obtained under the conditions of this study (i.e. lower kerogen to mineral ratio, hydrous conditions, and temperature measured from within the sample).

The decrease in pyrolysate products generated in the presence of montmorillonite, and illite also agreed with the findings of Huizinga et. al.(15). They demonstrated that these clays have high adsorptive capacities for the more polar components of the pyrolysate, and thermocatalyticly induce the formation of more gaseous products. These two effects cause a net reduction in pyrolysate yield. In contrast, however, the kerogen heated with kaolinite gave an increase in yield. This seems to indicate that kaolinite provides some thermocatalytic activity with a substantially lower adsorption capacity for pyrolysate products than illite or montmorillonite.

Trace Elements. The concentrations of twenty trace elements in the bitumens, kerogen, and related pyrolysates are

shown in Table 1. For the sake of brevity only the nickel and vanadium values and their ratios will be discussed here. As can be seen from the graph in Figure 1, the vanadium concentrations for the different kerogen pyrolysates are fairly constant. This indicates that the minerals used have very little if any affect on the abundance of vanadyl porphyrins in the pyrolysates. The nickel concentrations (Fig. 2), however, show substantial variation among the pyrolysates. The most noticeable trend is the increase in nickel concentrations from Na-montmorillonite to kaolinite to illite. One explanation for this trend could be the preferential adsorption of nickel porphyrin with montmorillonite being the strongest adsorbent and illite the weakest. However, this is inconsistent with the pyrolysis yield data which indicates that kaolinite is the least adsorbent of the three clays. Another explanation for this trend is that the clays are causing the preferential decomposition of the nickel porphyrins on the surface as a function of surface acidity (Na-montmorillonite being the most acidic).

The value for the nickel concentration from the kerogen-pyrite (KP) pyrolysis shows a dramatic drop which is comparable to the concentration from the montmorillonite run. It has been shown that at temperatures above 240 C, porphyrins in the presence of H_2S are partially decomposed. Also in the presence of H_2S and a Co-Mo catalyst, nickel and vanadyl porphyrins can be demetallated with nickel porphyrins having the higher demetallation rate (22). The generation of large amounts of H_2S during pyrolysis with pyrite could possibly explain the observed drop in the nickel concentration. The pyrolysis with calcite also shows a drop in nickel concentration similar to the value seen in the kaolinite run. It is uncertain at this time why calcite would have this effect on the nickel porphyrins and further investigation is needed to determine the cause of this effect.

A comparison of the Ni/V ratios for the bitumens, kerogen, and related pyrolysates is shown in Figure 3. It can be seen from this comparison that the Ni/V ratios are similar for the kerogen, and for the pyrolysates from the original kerogen, the kerogen float, and the whole shale. This is unsurprising since the kerogen is the source of the Ni and V complexes in these pyrolysates. Variations in the Ni/V ratio in pyrolysates generated in the presence of minerals reflect the variations in the nickel concentrations for the pyrolysates.

A comparison of the bitumen-II Ni/V ratio with that from the Na-montmorillonite pyrolysate shows the two have very similar values. This indicates that the Ni pophyrin in the bitumen-II, which is more intimately associated with the mineral component of the shale, may be decomposing due to interaction with clays.

CONCLUSIONS

The work presented here indicates that the mineral matrix of the shale plays an important role in determining the trace element distributions during petroleum formation. The data show variations in the Ni during pyrolysis of kerogen with clays and pyrite, whereas the V concentration remains essentially constant. Further investigation is needed to determine if this loss is due to the adsorption or the decomposition of the nickel complexes present.

ACKNOWLEDGMENTS

The authors thank Cathy Grimm and the Nuclear Radiation Center staff for their prompt aid during the instrumental neutron activation analysis.

REFERENCES

1. Branthaver, J.F. and Filby, R.H., in "Metal Complexes In Fossil Fuels", eds. Filby, R.H.and Branthaver, J.F., ACS Symposium Series No. 344, American Chemical Society: Washington, DC, 1987.
2. Hodgson, G.W., *Bull. Am. Assoc. petrol. geol.*, 1954, **38**, 2737-54.
3. Hodgson, G.W., Fiores, J., Baker, B.L. *Bull. Am. Assoc. Petrol. Geol.* 1959, **43**, 311-28.
4. Hitchon, B., Filby, R.H. *Alberta Research Council Open File Report* 1983-02, 144 p.
5. Hitchon, B., Filby, R.H. *Bull. Am. Assoc. Petrol. Geol.* 1984, **68**, 838-49.
6. Hyden, H.J., *U.S. Geol. Serv. Bull. 1100-B*, 1961.
7. Saban, M., Vitorovic, O. and Vitorovic, in "Symposium on Characterization of Heavy Crude Oils and Petroleum Residues", Editions Technip: Paris, 1984.
8. Al-Shahristani, H. and Al-Atyia, M.J., *Geochim. Et Cosmochim. Acta*, 1972,**36**, 929-37.
9. Curiale, J.A. In "Exploration for Heavy Oil and Bitumen"; Am. Assoc. Petrol. Geol. Research Conference, Santa Maria, Calif., Oct. 28-Nov. 2, 1984, Vol.1, pp.1-39.
10. Curiale, J.A., in "Metal Complexes in Fossil Fuels", eds. Filby, R.H. and Branthaver, J.F., ACS Symposium Series No. 344, American Chemical Society: Washington, DC, 1987.
11. Hirner, A.V., in "Metal Complexes in Fossil Fuels", eds. Filby, R.H. and Branthaver, J.F., ACS Symposium Series No. 344, American Chemical Society: Washington, DC, 1987.
12. Chakhmachkev, V.A., Lositskaya, I.F., Punanova, S.A.., Semenova, R.A. *Geokhimiya* 1985, 703-09.

13. Lu, S.-T., Kaplan, I.R. *Geochim.et Cosmochim. Acta*, 1985, **49**, 2589-2604.
14. Tannenbaum, E., Huizinga, B.J. and Kaplan, I.R. *Amer. Assoc. Petrol. Geol. Bull.*, 1986, **70**, 1156-1165.
15. Huizinga,B.J., Tannenbaum, E. and Kaplan, I.R. *Org. Geochem.*, 1987, **11**, 591-604.
16. Lu, S.-T., Ruth, E. and Kaplan, I.R. *Org. Geochem.*, 1989, **14**, 491-499.
17. Lu, S.-T. and Kaplan, I.R. *Org. Geochem.*, 1989, **14**, 501-510.
18. Espitalie, J., Makadi, K.S. and Tricket, J. *Org. Geochem.*, 1984, **6**, 365.
19. Rose, H.R., Smith, D.R., Hanna, J.B., Palmisano, A.J. and Wilson, M.A. *Fuel*, 1992, **71**, 355-360.
20. Mercer, G.E., Fitzgerald, S.L., Day, J.W. and Filby, R.H. *ACS Fuel Div. Preprints*, 1991, **36**, 1180-1189.
21. VanBerkel, G.J., Ph.D. Thesis, Department of Chemistry, Washington State University, 1987.
22. Rankel, L.A. *Preprints Div. Petrol. Chem.ACS*, 1981, **26**, 689.

Table 1. Trace element concentrations in kerogen pyrolysates(WK-KL), bitumens (BI, BII), shale pyrolysate (SP), and kerogen (KER).

	WK	K	KP	KC	KM	KK	KL	BI	SP	BII	KER
As (ppm)	18.1	3.07	32.0	1.54	1.76	4.43	3.24	1.78	4.36	120	89
Br (ppm)	14.0	17.6	14.6	12.0	6.73	12.1	10.1	32.1	30.6	102	12.6
Cl (ppm)	5920	12600	6210	6230	2200	9540	2620	617	1680	13500	59100
Co (ppm)	26.2	2.24	2.08	10.6	1.50	1.18	14.8	4.46	64.6	17.7	67.0
Cr (ppm)	22.2	34.5	95.0	0.866	0.396	21.4	2.28	0.794	<0.516	1.29	35.8
Cu (ppm)	232	269	42.2	<27.9	<35.9	96.6	53.3	<68.7	<71.3	308	<1070
Fe (ppm)	237	566	121	892	26.0	566	130	152	492	1600	33800
Ga (ppm)	31.5	20.5	13.2	4.43	4.40	15.8	23.6	0.498	2.82	14.4	27.6
Hg (ppm)	7.64	9.58	15.0	5.14	18.6	9.44	12.0	93.6	20.6	370	33.8
La (ppb)	496	254	193	104	60.3	130	432	38.4	<57.6	214	33000
Mn (ppb)	243	337	620	356	194	330	273	529	1180	602	27700
Mo (ppm)	4.79	7.94	7.26	1.27	1.46	5.47	3.98	4.35	3.72	101	1230
Na (ppm)	29.7	23.2	157	34.8	30.1	13.6	20.8	31.4	25.6	36.0	3280
Ni (ppm)	3290	2600	1560	1940	1600	1920	2700	2180	3460	2405	1830
Sb (ppb)	743	348	330	130	90.5	376	170	<89.4	130	23100	26000
Sc (ppb)	3.11	2.12	19.7	3.38	1.81	2.66	<3.74	1.68	<6.14	<8.26	4190
Se (ppm)	32.2	33.1	62.2	20.9	77.8	39.2	50.8	373	82.2	1510	136
Th (ppb)	24.6	<28.3	<31.8	<32.6	<23.3	<27.5	24.4	<35.6	65.6	<105	3560
V (ppm)	1430	1120	1040	1040	1200	1050	1160	2540	1560	2070	741
Zn (ppm)	36.6	24.0	274	20.3	2.95	14.4	9.10	11.0	56.6	61.8	570
Ni/V	*2.30*	*2.32*	*1.50*	*1.87*	*1.33*	*1.83*	*2.33*	*0.86*	*2.22*	*1.16*	*2.47*
Pyrolysate Yield	3.97%	4.84%	3.40%	2.87%	3.04%	5.59%	3.38%	n/a	0.97%	n/a	n/a

WK=untreated kerogen, K=kerogen float, KP=kerogen+pyrite, KC=kerogen+calcite, KM=kerogen+montmorillonite
KK=kerogen+kaolinite, KL=kerogen+illite, BI=bitumen I, SP=extracted shale pyrolysate, BII=bitumen II, KER.=kerogen

*Percentages refer to original kerogen mass (not corrected for mineral content), except for NAP which refers to extracted shale mass.

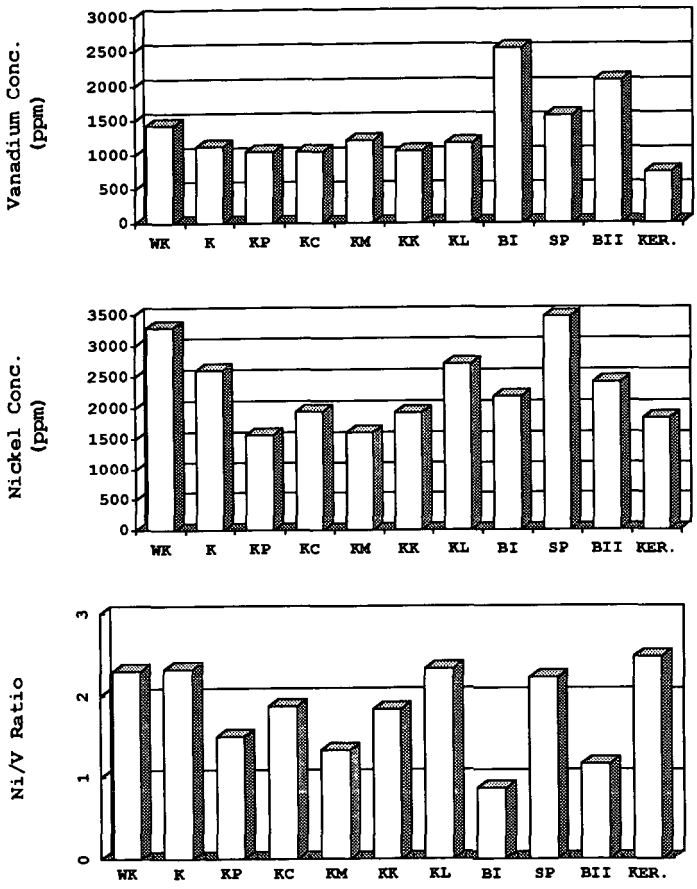

Figure 1 (upper); 2 (middle); 3 (lower) Vanadium, Nickel, and Nickel/Vanadium Ratios in New Albany Kerogen Pyrolysates.

WK=untreated kerogen, K=kerogen float, KP=kerogen+pyrite, KC=kerogen+calcite, KM=kerogen+montmorillonite, KK=kerogen+kaolinite, KL=kerogen+illite, BI=bitumen I, SP=extracted shale pyrolysate, BII=bitumen II, KER.=kerogen

TRACE ELEMENT DISTRIBUTIONS IN KEROGEN, BITUMENS AND PYROLYSATES ISOLATED FROM NEW ALBANY SHALE

Gregory E. Mercer Adam J. Regner, and Royston H. Filby

Department of Chemistry
Washington State University
Pullman, WA 99164-4630

Keywords: pyrolysis, metal complexes; oil-source rock correlation

INTRODUCTION

Although trace element distributions have been used to correlate oils (1-8), there have been few similar studies on oil-source rock correlations (9).

The bitumen, kerogen or a pyrolysate from a source rock may, in principle, be used to correlate a source rock to an oil. However, if trace element abundances are to be used for oil-source rock correlations, the bitumen, kerogen and the pyrolysates of a source rock should show correlation in their trace element distributions. For example, it has been shown (10) that the kerogen of the New Albany shale releases Ni(II) and VO(II) porphyrins during pyrolysis in amounts that are directly proportional to organically combined Ni and V, in the kerogen.

In this study trace element distributions were measured in the bitumen and kerogen from the New Albany shale and in pyrolysates generated from the shale under different conditions (i.e., dry, hydrous, toluene, toluene/methanol). Trace element distributions were also compared in chromatographic fractions of the bitumen and pyrolysates. Implications for oil-source rock correlation are discussed.

EXPERIMENTAL

Detailed geological information on New Albany shale (Clark County, Indiana) are reported elsewhere (11). The procedures for the extraction of the bitumen I and II and the isolation of kerogen by demineralization were similar to those of Mercer et al. (12). Boscan (Venezuela) crude oil was also analyzed for comparison.

Shale samples (150 g) were pyrolysed for 5 hours at 300°C in a 1L autoclave in toluene, toluene/methanol (7:3), or water (200 mL each) and without solvent ("dry" conditions) at initially 1 atm N_2. The pyrolysed shale samples were extracted as for the bitumen-I. The shale which was pyrolysed in toluene was re-pyrolysed four times in toluene and for a fifth time in toluene/methanol (7:3) under the same conditions.

Liquid chromatography (silica gel) was used to separate the bitumen and pyrolysate samples into fractions for analysis. The first fractions were eluted with a) hexanes (saturates), b) CH_2Cl_2 in hexanes (porphyrin aggregate), c) $CHCl_3$ (polar material), and d) 7:3 toluene/methanol followed by 100% methanol (asphaltenes plus other highly polar fractions).

Trace element concentrations were determined by instrumental neutron activation analysis (INAA) using the method published previously (12,13).

RESULTS

The concentrations of 13 elements in New Albany bitumens, kerogen and pyrolysates are listed in Tables 1 and 2.

The kerogen is the source of Ni and V complexes found in the pyrolysates (10) and, through maturation, of the complexes in the bitumen I and II. Hence, it might be expected that the pyrolysates should have similar Ni/V ratios as the kerogen (1.91 after accounting for inorganic Ni contributions, 12). The first toluene pyrolysate, however, has a Ni/V ratio similar to that of the bitumen-I (0.91 and 0.95, respectively) rather than that of the kerogen (1.91). Subsequent toluene pyrolysates, as well as the hydrous, dry, and toluene-methanol pyrolysates, have Ni/V ratios which are similar to that of the kerogen. Thus the first toluene pyrolysate may represent residual bitumen I but the subsequent pyrolysates reflect the Ni/V ratio of the kerogen. Previous electron microprobe work with the New Albany shale (14) indicates that the kerogen is intimately associated with the clay minerals present in the rock. Hence, the extraction of the bitumen-I by sonication in a solvent at 40°C is probably incomplete. Thus, the first heating in the presence of toluene may generate a pyrolysate which is predominantly an improved extraction of the remaining inherent bitumen in the bitumen-I extracted shale, while the subsequent pyrolysates are generated primarily from the breakdown of kerogen. A similar conclusion was reached by Van Berkel, et al (15) to explain the similarity of an initial toluene pyrolysate of the New Albany kerogen and the bitumen-II extracted from the kerogen.

The data in Tables 1 and 2 show that the solvent plays a role in determining the resultant Ni/V ratio of the pyrolysate. Variations of the Ni/V ratio are probably related to the composition of the pyrolysate (i.e., polar versus nonpolar material) which is dependent on the polarity of the solvent and possibly to solvent-mineral interactions. The composition of the bitumen-I and the pyrolysates can be compared using the relative abundances of nonpolar (fractions 1 plus 2) and polar material (fractions 3 plus 4) measured by the chromatographic separation. Table 3 shows the Ni/V values compared to the non-polar/polar ratio. The hydrous and toluene/methanol pyrolysates contain the highest proportion of asphaltic/polar material and have Ni/V ratios very similar to that of the kerogen. A possible explanation is that water and methanol (in the toluene/methanol pyrolysis) deactivate the clay mineral-bitumen-kerogen interface, thus reducing conversion of asphaltic material to nonpolar hydrocarbons. Similarly, Ni and V complexes released by the kerogen are poorly adsorbed by the deactivated mineral matrix and thus the Ni/V ratios are similar to that of the kerogen. The higher Ni/V ratio (relative to the hydrous and toluene/methanol pyrolysates and the kerogen) observed for the dry pyrolysate is probably due to the high yield of the nonpolar fraction resulting from catalytic action of the clays. The large amounts of nonpolar organic matter generated during pyrolysis may

act as a nonpolar solvent and preferentially extract more of the less-polar Ni(II) porphyrins than the polar VO(II) species, thereby producing a pyrolysate with a higher Ni/V ratio than that of the hydrous or toluene/methanol pyrolysates. Similarly, under non-hydrous conditions the active clay surfaces retain the more polar VO(II) species relative to the less polar Ni(II) species. The second and third toluene pyrolysates were also likely to be derived from the breakdown of kerogen in which the catalytic action of the clays is not inhibited, such that conditions are similar to those of the dry pyrolysis.

For elements other than Ni and V the data in Tables 1 and 2 indicate that considerable variations in concentration relative to the bitumen I are observed. None of the pyrolysis conditions produces a pyrolysate that contains trace element distributions identical to that of the bitumen I; the hydrous pyrolysate is closest.

Distribution of Trace Elements in Pyrolysate Fractions. The four chromatographic fractions of each pyrolysate and the bitumen I were analyzed for trace elements. Distributions of trace elements among these fractions (i.e., percentage of element in each fraction relative to original sample) were similar for all pyrolysates and the bitumen I. Data for Ni, V, Se, Cr, Co, Fe and As in the bitumen I and the hydrous pyrolysate are shown in Figure 1. Figure 1 shows that Ni, V, and Se (Fig. 1a,b) are distributed differently from Cr, Cu, Fe, and As (Fig. 1c,d). Data for Ga, Mo, Sb, Zn, and Mn show similar patterns to Cr, Fe, Co and As. Nickel and vanadium are present predominantly as metalloporphyrins in the bitumen and the hydrous pyrolysate (porphyrin aggregate plus the $CHCl_3$ fraction which contains Ni(II) and VO(II) porphyrins). Only minor amounts of Ni and V are present in the asphaltene-polar fraction (<17%) and part of this is probably porphyrinic because weak Soret peaks at 390-410 nm are observed in this fraction. Hence, greater than 80% of the Ni and V in the bitumen and in the hydrous pyrolysates is present as metalloporphyrins. The distribution of Se in the bitumen I and the hydrous pyrolysate is related to that of sulfur. The non-polar (hexanes) fraction contains elemental sulfur and analysis of this fraction of the bitumen-II shows that approximately 86% of the sample was elemental sulfur. The mass spectrum of some of the sulfur crystals (Figure 2) revealed that the sulfur occurs predominantly as S_8 and that Se substitutes for a S in the S_8 ring to give the S_7Se molecule. Therefore, the Se observed in the nonpolar fractions of the pyrolysates is associated with elemental sulfur. The elemental sulfur is probably formed by the breakdown of sulfides, primarily pyrite and marcasite (FeS_2), during pyrolysis. The data also suggests that there is a considerable amount of elemental S/Se in the bitumen-I. This "inherent" elemental sulfur could be derived from weathering, bacterial activity or exposure to any other conditions which are capable of oxidizing sulfide minerals and could have occurred at any point in the history of the rock.

The distributions of Cr, Co, Fe and As (and other elements not shown in Fig. 1) in the hydrous pyrolysate and the bitumen I are similar. These elements are concentrated in the polar fraction (asphaltenes) although mass balance calculations show some retention of the column of these elements, presumably associated with highly polar asphaltenes that did not elute.

The similarity in trace element distributions in the chromatographic fractions of the bitumen I and the hydrous pyrolysate (and other pyrolysates) of the shale indicate that metal species or complexes generated by the kerogen by maturation in the bitumen I and by pyrolysis are also similar. Differences in absolute concentrations among the pyrolysates and the bitumen are probably due to kerogen-mineral or metal species-mineral interactions during interaction of pyrolysis.

CONCLUSION

1. The trace element concentrations in the pyrolysates vary significantly. It is necessary, therefore, to be consistent when choosing pyrolysis conditions for comparative purposes or for correlation work. Hydrous pyrolysis appears to give trace element concentrations closest to those of the bitumen I.

2. The Ni/V ratios observed for the pyrolysates are significantly different from that of the bitumen-I, except for the first toluene pyrolysate which may be residual bitumen-I released during initial pyrolysis. Excluding the first toluene pyrolysate, the Ni/V ratio of the pyrolysates resembled that of the kerogen. The major factor controlling the Ni/V ratio in the pyrolysates appears to be the polarity of the pyrolysis solvent and its deactivating effect on clay catalysis and related adsorption of metal species on clays. Deactivation of clay surfaces by water or methanol (hydrous or toluene/methanol pyrolysis) results in a pyrolysate with a higher proportion of polar material and Ni/V ratios similar to that of the kerogen. Pyrolysis under dry conditions or in toluene (pyrolysates 2 and 3) results in higher proportions of nonpolar material and pyrolysates have higher Ni/V ratios than those generated under hydrous or toluene/methanol conditions.

3. The elemental S and Se in the bitumen II result from decomposition of sulfides (FeS_2) during demineralization and are present primarily as S_8 and S_7Se which elute in the nonpolar fraction. Thus, the S and/or Se content of the nonpolar fraction of pyrolysates may be related to the amount of sulfide mineral breakdown during pyrolysis.

ACKNOWLEDGEMENTS

The help of Cathy Grimm and the Nuclear Radiation Center staff in the INAA analysis is acknowledged.

LITERATURE CITED

1. Hodgson, G.W., Bull. Am. Assoc. Petrol. Geol., 1954, 38, 2737-54.

2. Hyden, H.J., U.S. Geol. Serv. Bull. 1100-B, 1961.

3. Al-Shahristani, H. and Al-Atyia, M.J., Geochim. et Cosmochim. Acta, 1972, 36, 929-37.

4. Saban, M., Vitorovic, O. and Vitorovic, in "Symposium on Characterization of Heavy Crude Oils and Petroleum Residues", Editions Technip: Paris, 1984.

5. Ellrich, J., Hirner, A.V. and Stark, H., Chem. Geol., 1985, 48, 313-23.

6. Abu-Elgheit, M., Khalil, S.O. and Barakat, A.O., Prepr. Div. Petrol. Chem. ACS, 1979, 24, 793-97.

7. Curiale, J.A., in "Metal Complexes in Fossil Fuels", eds. Filby, R.H. and Branthaver, J.F., ACS Symposium Series No. 344, American Chemical Society: Washington, DC, 1987.

8. Hitchon, B. and Filby, R.H., Bull. Am. Assoc. Petrol. Geol., 1984, 68, 838-49.

9. Hirner, A.V., in "Metal Complexes in Fossil Fuels", eds. Filby, R.H. and Branthaver, J.F., ACS Symposium Series No. 344, American Chemical Society: Washington, DC, 1987.

10. Van Berkel, G.J. and Filby, R.H., in "Metal Complexes in Fossil Fuels", eds. Filby, R.H. and Branthaver, J.F., ACS Symposium Series No. 344, American Chemical Society: Washington, DC, 1987.

11. Hasenmueller, N.R. and Woodward, G.S., "Studies of the New Albany Shale (Devonian and Mississippian) and equivalent strata in Indiana", Indiana Geological Survey Contract Report to U.S. Department of Energy, Contract DE-AC-21-76MC05204, 1981, 100.

12. Mercer, G.E., Fitzgerald, S.L., Day, J.W. and Filby, R.H., ACS Fuel Div. Preprints, 1991, 36, 1180-89.

13. Van Berkel, G.J., Ph.D. Thesis, Department of Chemistry, Washington State University, 1987.

14. Fitzgerald, S.L., Day, J.W. and Mercer, G.E., (unpublished data).

15. Van Berkel, G.J., Quirke, J.M.E., and Filby, R.H., Org. Geochem., 1989, 14, 119-128.

Table 1. Concentrations of trace elements in the kerogen, bitumens and pyrolysates of the New Albany shale and in Boscan crude oil.

Element	Elemental Concentration (μg/g)							
	Kerogen[1]	Bitumen I	Bitumen II	Dry Pyr.	H_2O Pyr.	Toluene Pyr.	Tol/MeOH Pyr.	Boscan Crude
As	36.4	75.8	89.1	86.3	64.5	536	406	0.320
Co	115	8.63	113	14.3	10.6	13.4	61.2	0.224
Cr	35.2	1.04	12.3	1.75	0.865	1.65	1.39	0.401
Fe	0 by defn.	353	3140	556	744	992	1180	15.9
Ga	11.0	7.93	32.6	2.30	4.77	6.78	7.12	0.147
Mn	0	0.32	1.24	0.62	0.43	0.53	0.59	0.109
Mo	2400	28.7	460	17.4	6.24	54.6	29.8	4.26
Na	1240	156	816	8.57	171	53.0	53.7	25.0
Ni	2160	2560	3710	896	2760	1710	2300	97.2
Sb	72.6	0.598	56.0	12.2	0.561	1.40	1.38	0.296
Se	175	79.5	3840	18.9	215	43.8	7.86	0.320
V	1130	2700	3400	365	1540	1880	1230	1200
Zn	71.9	65.7	252	10.5	66.5	53.6	67.3	0.608
Ni/V Ratio	1.91 ±0.25	0.95 ±0.02	1.09 ±0.03	2.45 ±0.17	1.80 ±0.06	0.91 ±0.03	1.87 ±0.13	0.081 ±0.006
Yield (%)	25%	1.4%	0.37%	3.6%	1.0%	1.0%	1.5%	--

[1] Corrected for inorganic contributions by the density fraction method described by Mercer et al. (22).

Table 2. Concentrations of trace elements in the sequential pyrolysates and residual bitumen (bitumen-III) from the pyrolysed New Albany shale.

Element	Elemental Concentration (μg/g)						
	Pyr.[1] #1	Pyr. #2	Pyr. #3	Pyr. #4	Pyr. #5	Pyr. #6	Bitumen III
As	536	85.1	80.0	290	77.7	8.74	118
Co	13.4	7.04	4.81	3.30	0.360	0.834	7.13
Cr	1.65	2.50	0.786	1.41	0.770	0.50	6.82
Fe	992	594	389	395	151	65.5	1405
Ga	6.78	2.77	2.65	5.87	0.815	0.579	21.6
Mn	0.53	1.18	0.380	0.546	0.42	0.48	0.61
Mo	54.6	17.3	25.9	45.3	17.6	14.1	344
Na	53.0	230	50.0	70.0	45.3	86.0	18.6
Ni	1713	1189	933	777	276	458	516
Sb	1.40	0.267	0.960	0.545	0.17	0.135	15.6
Se	43.8	80.1	51.1	169	131	18.0	956
V	1883	484	393	471	126	242	384
Zn	53.6	12.2	7.03	13.0	7.31	37.0	52.1
Ni/V Ratio	0.91 ±0.03	2.46 ±0.06	2.37 ±0.10	1.65 ±0.10	2.19 ±0.11	1.89 ±0.92	1.34 ±0.07
Yield (%)	1.0	0.54	1.3	0.29	0.16	0.22	0.33

[1] Pyrolysis runs 1-5 in toluene, run 6 in toluene/MeOH
[2] Bitumen-III = extractable organic material of shale after six pyrolyses and demineralization.

Table 3. Ni/V and Non-Polar/Polar Ratios.

Sample	Ni/V	Non-Polar/Polar*
Kerogen	1.91	--
Bitumen I	0.95	1.04
Toluene Pyr. 1	0.91	0.94
Toluene Pyr. 2	2.46	1.54
Toluene Pyr. 3	2.37	1.81
Dry Pyr.	2.45	1.64
Hydrous Pyr.	1.80	0.65
Toluene/MeOH Pyr	1.87	0.68

*Computed from fractional yields of fractions (1+2)/(3+4).

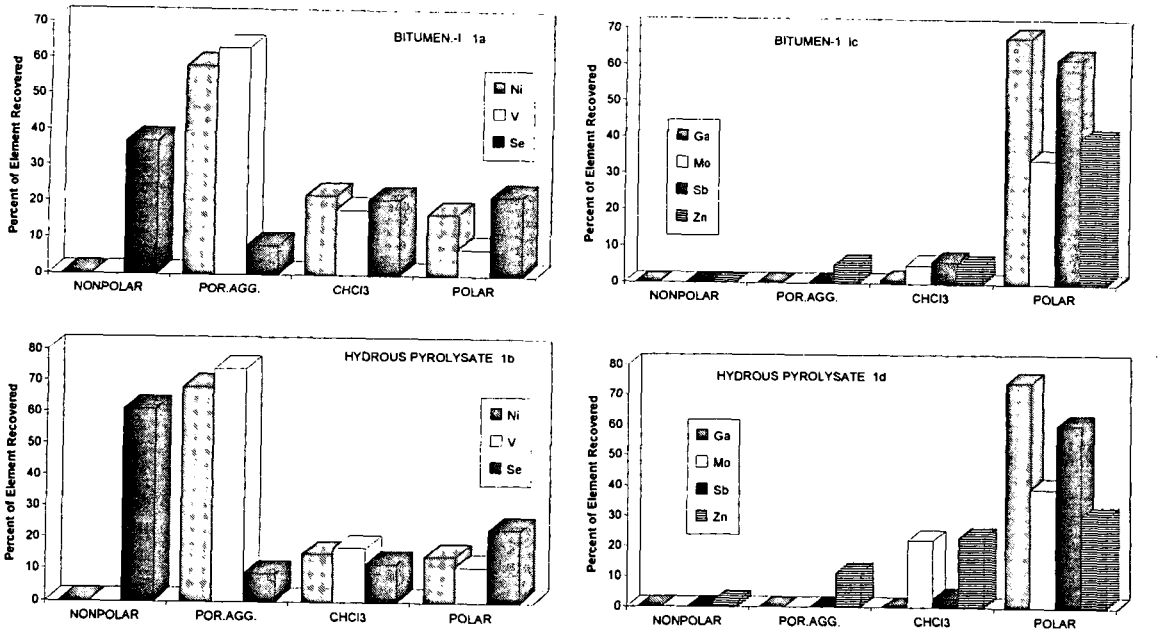

Figure 1: Comparison of elemental distributions in the bitumen I (a,c) and *the hydrous pyrolysate (b,d)*

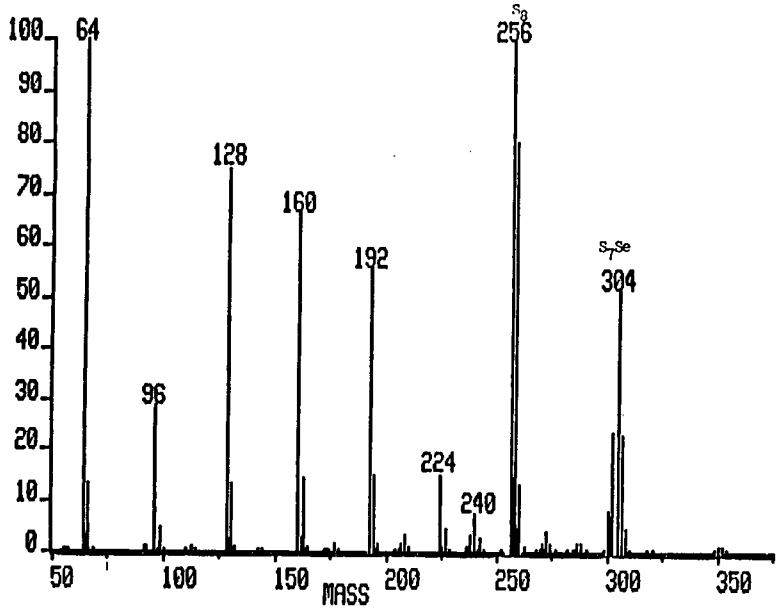

Figure 2: EI/MS spectrum of the non-polar fraction of the bitumen II of the Albany Shale